

# NASA CONTRACTOR REPORT



NASA CR-1

0060400



LOAN COPY: RETURN TO  
AFWL (WLIL-2)  
KIRTLAND AFB, N MEX

NASA CR-1094

## LUNAR ORBITER V

### Photography

*Prepared by*  
**THE BOEING COMPANY**  
Seattle, Wash.  
*for Langley Research Center*



## LUNAR ORBITER V

### Photography

Distribution of this report is provided in the interest of information exchange. Responsibility for the contents resides in the author or organization that prepared it.

Issued by Originator as Boeing Document D2-100755-2 (Vol. II)

Prepared under Contract No. NAS 1-3800 by  
THE BOEING COMPANY  
Seattle, Wash.

for Langley Research Center

NATIONAL AERONAUTICS AND SPACE ADMINISTRATION



# Contents

	Page
INTRODUCTION	
1.0 PHOTOGRAPHIC MISSION DESCRIPTION	1
1.1 Project Objectives	1
1.2 Mission V Objectives	1
2.0 PHOTOGRAPHIC MISSION DESIGN	3
2.1 Mission Tasks	3
2.1.1 Task 1	3
2.1.2 Task 2	4
2.1.3 Task 3	4
2.1.4 Tasks 4 and 5	4
2.2 Site Selection	4
2.3 Orbit Design	8
2.4 Film Management and Budgeting	11
2.4.1 Film Budget	11
2.4.2 Film Management	11
3.0 MISSION V PHOTO SUBSYSTEM CHARACTERISTICS	15
3.1 Photo Subsystem Description	15
3.1.1 Camera	15
3.1.2 Processor-Dryer	15
3.1.3 Photo Video Chain	15
3.1.4 Command Control and Programmer	16
3.1.5 Ground Reconstruction Electronics	16
3.2 Calibration	16
3.3 Film Characteristics	16
3.3.1 Gray-Scale Calibration of Flight Film	16
3.3.2 Reseau Pattern	17
4.0 PHOTOGRAPHS	19
4.1 Evaluation Methods	19
4.2 General Mission Characteristics	20
4.2.1 Exposure	20
4.2.2 Resolution	21
4.2.3 Spacecraft Film Processing	21
4.2.4 Readout and Reconstruction	23
4.2.5 Reassembly and Printing	23
4.3 Apollo Sites	24
4.3.1 General Characteristics	24
4.3.2 Individual Apollo Sites	25
4.3.2.1 Sites V-3.1, -6, -8a, -8b (Apollo Site IP-1)	25
4.3.2.2 Sites V-9.1, -11a, -11b (Apollo Site IIP-2)	27
4.3.2.3 Sites V-13, -16a, -16b (Apollo IIP-6)	28
4.3.2.4 Sites V-27a, -27b (Apollo Site IIP-8)	29
4.3.2.5 Sites V-41a, -42b (Apollo Site IIIP-11)	29
4.4 Science and Apollo Applications Program (AAP) Sites	30
4.4.1 General Characteristics	31
4.4.2 Individual Sites	31



## Contents (Cont.)

	Page
4.4.2.1 Site V-1, Petavius . . . . .	31
4.4.2.2 Site V-2.1, Petavius B . . . . .	32
4.4.2.3 Site V-4, Stevinus A . . . . .	32
4.4.2.4 Site V-5.1, Messier and Messier A . . . . .	35
4.4.2.5 Site V-10, Altai Scarp . . . . .	38
4.4.2.6 Site V-12, Censorinus . . . . .	43
4.4.2.7 Site V-14, Littrow Rilles . . . . .	43
4.4.2.8 Site V-15.1, Dawes . . . . .	46
4.4.2.9 Site V-18, Dionysius . . . . .	49
4.4.2.10 Site V-19, Abulfeda Crater Chain . . . . .	54
4.4.2.11 Site V-21, South of Alexander . . . . .	54
4.4.2.12 Site V-22, Sulpicius Gallus Rilles . . . . .	57
4.4.2.13 Site V-23.2, Hyginus Rilles . . . . .	60
4.4.2.14 Site V-24, Hipparchus . . . . .	63
4.4.2.15 Site V-25, Alpine Valley . . . . .	68
4.4.2.16 Site V-26.1, Hadley Rille . . . . .	71
4.4.2.17 Site V-28, Alphonsus . . . . .	71
4.4.2.18 Site V-29, Rima Bode II . . . . .	74
4.4.2.19 Site V-30, Tycho . . . . .	77
4.4.2.20 Site V-31, Sinuous Complex Rilles East of Plato . . . . .	80
4.4.2.21 Site V-32, Eratosthenes . . . . .	84
4.4.2.22 Site V-33, Area of Copernicus CD . . . . .	87
4.4.2.23 Site V-34, Fra Mauro . . . . .	90
4.4.2.24 Site V-35, Copernicus Secondaries . . . . .	90
4.4.2.25 Site V-36, Copernicus H . . . . .	96
4.4.2.26 Site V-37, Copernicus . . . . .	97
4.4.2.27 Site V-38, Imbrium Flows . . . . .	100
4.4.2.28 Site V-40, Dome Near Tobias Mayer . . . . .	105
4.4.2.29 Site V-41, Vitello . . . . .	107
4.4.2.30 Site V-43.2, Gassendi . . . . .	107
4.4.2.31 Site V-45.1, Domes Near Gruithuisen and Gruithuisen K. . . . .	111
4.4.2.32 Site V-46, Harbinger Mountains . . . . .	114
4.4.2.33 Site V-48, Aristarchus . . . . .	118
4.4.2.34 Site V-49, Cobra Head . . . . .	121
4.4.2.35 Site V-50, Aristarchus Plateau . . . . .	126
4.4.2.36 Site V-51, Marius Hills . . . . .	129
4.5 Farside Sites . . . . .	132
4.5.1 General Group Characteristics . . . . .	132
4.5.2 Photographs . . . . .	132
4.6 Earth Photograph . . . . .	140
4.6.1 Acquisition . . . . .	140
4.6.2 Photographic Results . . . . .	140
5.0 PHOTOGRAPHIC SUPPORTING DATA . . . . .	145
5.1 Input Data Summary . . . . .	145
5.1.1 Spacecraft Position and Velocity . . . . .	145
5.1.2 Spacecraft Attitude . . . . .	145
5.1.3 Camera-On Time . . . . .	145
5.1.4 Planetary Constants . . . . .	146

## Contents (Cont.)

	Page
5.2 Computational Procedure .....	146
5.3 Accuracy of Calculations .....	146
5.3.1 Error Sources .....	146
5.3.1.1 Timing Errors .....	146
5.3.1.2 Attitude Maneuver Errors .....	147
5.3.1.3 Uncertainty in State Vectors .....	149
5.3.1.4 Uncertainty in Site Elevation .....	149
5.3.2 Summation of Errors .....	150
5.4 Photographic Distortion .....	151
5.4.1 Photo System Distortions .....	151
5.4.2 Geometric Distortions .....	152
5.4.3 Lunar Characteristics .....	152
5.5 Photographic Supporting Data Tables .....	152
6.0 PHOTOGRAPHIC OPERATIONS .....	189
6.1 Mission Planning Summary .....	189
6.2 Mission Conduct .....	189
6.2.1 Initial Ellipse .....	189
6.2.2 Intermediate Ellipse .....	190
6.2.3 Final Ellipse .....	191
6.2.3.1 Photographic Coverage Design .....	191
6.2.3.2 Photographic Phase .....	191
6.2.3.3 Final Readout .....	194
6.3 Photographic Control .....	194
6.3.1 Exposure Control .....	194
6.3.2 Camera-On-Time Bias .....	197
6.4 Photo Subsystem Performance .....	197
6.4.1 Film Budget and Photo Data Summary .....	197
6.4.2 Camera .....	197
6.4.2.1 Camera Film Handling .....	197
6.4.2.2 V/H Ratio Deviation .....	211
6.4.2.3 Film Breakage During Rewind .....	212
6.4.3 Processor .....	212
6.4.3.1 White Level and Bimat Dryout .....	212
6.4.3.2 Processing Lace Defect .....	212
6.4.4 Readout .....	214
6.4.4.1 Video Dropout .....	214
6.4.4.2 Framelet Loss .....	214
7.0 PROGRAM SUMMARY .....	215
7.1 Photographic Objectives .....	215
7.2 Program Photographic Accomplishments .....	215
7.2.1 Landing Site Photography .....	215
7.2.2 Broad-Area Coverage .....	216
7.2.3 Scientific Photography .....	217
7.2.4 Surveyor and Ranger Location .....	219
7.2.5 Earth Photography .....	219

## Contents (Cont.)

	<b>Page</b>
7.3 Operational Summary .....	224
7.3.1 Photographic Problems .....	224
7.3.2 Program Statistics .....	226
7.4 Conclusion .....	229

# Figures

	Page
2-1 Location of Apollo Sites for Mission V Photography .....	7
2-2 Mission V Nearside Sites Designated for AAP .....	8
2-3 Mission V Nearside Science Sites .....	9
2-4 Static Resolution vs Spacecraft Latitude .....	11
2-5 Planned Photo Period Sequence of Events .....	13
3-1 Flight Film Density vs Log E Curve and Position of Gray-Scale Steps .....	17
3-2 Comparison of Lunar Orbiter V Test and Eastman Kodak Statistical Sensitometric Curves for Bimat-Processed SO-243 .....	17
3-3 Readout Density vs ASA Visual Density for Bimat-Processed SO-243 .....	17
3-4 Preexposed Reseau Mark Placement and Detail of Cross .....	18
4-1 Telephoto Resolution vs Line-of-Sight Distance; Near Apolune .....	20
4-2 Telephoto Resolution vs Line-of-Sight Distance; Near Perilune .....	20
4-3 Apolune Photography Field of View .....	22
4-4 Albedo Distribution for Apollo Site IP-1 .....	25
4-5 Site V-3.1, Apollo Site IP-1; Westerly Oblique .....	26
4-6 Albedo Distribution for Apollo Site IIP-2 .....	27
4-7 Albedo Distribution for Apollo Site IIP-6 .....	28
4-8 Albedo Distribution for Apollo Site IIP-8 .....	29
4-9 Albedo Distribution for Apollo Site IIIP-11 .....	30
4-10 Albedo Distribution for Site V-1, Petavius .....	32
4-11 Site V-1, Petavius; Wide Angle .....	33
4-12 Site V-1, Petavius; Telephoto .....	34
4-13 Albedo Distribution for Site V-2.1, Petavius B .....	35
4-14 Albedo Distribution for Site V-4, Stevinus A .....	35
4-15 Site V-4, Stevinus A; Wide Angle .....	36
4-16 Site V-4, Stevinus A; Telephoto Frame 40 .....	37
4-17 Site V-5.1, Messier; Wide Angle .....	39
4-18 Site V-5.1, Messier; Telephoto .....	40
4-19 Site V-10, Altai Scarp; Wide Angle .....	41
4-20 Site V-10, Altai Scarp; Telephoto .....	42
4-21 Albedo Distribution for Site V-12, Censorinus .....	43
4-22 Site V-12, Censorinus; Wide Angle .....	44
4-23 Site V-12, Censorinus; Telephoto .....	45
4-24 Albedo Distribution for Site V-14, Littrow Rilles .....	46
4-25 Site V-14, Littrow Rilles; Wide Angle .....	47
4-26 Site V-14, Littrow Rilles; Telephoto .....	48
4-27 Albedo Distribution for Site V-15.1, Dawes .....	46
4-28 Site V-15.1, Dawes; Wide Angle .....	50
4-29 Site V-15.1, Dawes; Telephoto .....	51
4-30 Albedo Distribution for Site V-18, Dionysius .....	49
4-31 Site V-18, Dionysius; Wide Angle .....	52
4-32 Site V-18, Dionysius; Telephoto .....	53
4-33 Albedo Distribution for Site V-19, Abulfeda Crater Chain .....	54
4-34 Site V-19, Abulfeda Crater Chain; Wide Angle .....	55
4-35 Site V-19, Abulfeda Crater Chain; Telephoto .....	56
4-36 Albedo Distribution for Site V-21; South of Alexander .....	57
4-37 Site V-21, South of Alexander; Wide Angle .....	58

## Figures (Cont.)

	Page
4-38 Site V-21, South of Alexander; Telephoto . . . . .	59
4-39 Albedo Distribution for Site V-22, Sulpicius Gallus Rilles . . . . .	60
4-40 Site V-22, Sulpicius Gallus Rilles, Wide Angle . . . . .	61
4-41 Site V-22, Sulpicius Gallus Rilles; Telephoto . . . . .	62
4-42 Albedo Distribution for Site V-23.2, Hyginus Rilles . . . . .	63
4-43 Site V-23.2, Hyginus Rille; Wide Angle . . . . .	64
4-44 Site V-23.2, Hyginus Rille; Telephoto . . . . .	65
4-45 Site V-23.2, Hyginus Rille; Enlarged Telephoto Image . . . . .	66
4-46 Site V-23.2, Hyginus Rille; Telephoto . . . . .	67
4-47 Albedo Distribution for Site V-23, Hipparchus . . . . .	63
4-48 Site V-24, Hipparchus; Telephoto . . . . .	69
4-49 Site V-25, Alpine Valley; Wide Angle . . . . .	70
4-50 Albedo Distribution for Site V-26.1, Hadley Rille . . . . .	71
4-51 Site V-26.1, Hadley Rille; Wide Angle . . . . .	72
4-52 Site V-26.1, Hadley Rille; Telephoto . . . . .	73
4-53 Albedo Distribution for Site V-28, Alphonsus . . . . .	74
4-54 Site V-28, Alphonsus; Wide Angle . . . . .	75
4-55 Site V-28, Alphonsus; Telephoto . . . . .	76
4-56 Albedo Distribution for Site V-29, Rima Bode II . . . . .	77
4-57 Site V-29, Rima Bode II; Wide Angle . . . . .	78
4-58 Site V-29, Rima Bode II; Telephoto . . . . .	79
4-59 Albedo Distribution for Site V-30, Tycho . . . . .	80
4-60 Site V-30, Tycho; Wide Angle . . . . .	81
4-61 Site V-30, Tycho Floor; Telephoto . . . . .	82
4-62 Site V-30, Tycho Rim; Telephoto . . . . .	83
4-63 Albedo Distribution for Site V-31, Sinuous Rille East of Plato . . . . .	84
4-64 Site V-31, Sinuous Rille East of Plato; Wide Angle . . . . .	85
4-65 Site V-31, Sinuous Rille East of Plato; Telephoto . . . . .	86
4-66 Albedo Distribution for Site V-32, Eratosthenes . . . . .	87
4-67 Site V-32, Eratosthenes; Wide Angle . . . . .	88
4-68 Site V-32, Eratosthenes; Telephoto . . . . .	89
4-69 Albedo Distribution for Site V-33, Area of Copernicus CD . . . . .	87
4-70 Site V-33, Area of Copernicus CD; Wide Angle . . . . .	91
4-71 Site V-33, Area of Copernicus CD; Telephoto . . . . .	92
4-72 Albedo Distribution for Site V-34, Fra Mauro . . . . .	90
4-73 Site V-34, Fra Mauro; Wide Angle . . . . .	93
4-74 Site V-34, Fra Mauro; Telephoto . . . . .	94
4-75 Site V-34, Fra Mauro; Telephoto . . . . .	95
4-76 Albedo Distribution for Site V-35, Copernicus Secondary Craters . . . . .	96
4-77 Albedo Distribution for Site V-36, Copernicus H . . . . .	97
4-78 Site V-36, Copernicus H; Wide Angle . . . . .	98
4-79 Site V-36, Copernicus H; Telephoto . . . . .	99
4-80 Albedo Distribution for Site V-37; Copernicus . . . . .	100
4-81 Site V-37, Copernicus; Wide Angle . . . . .	101
4-82 Site V-37, Copernicus; Wide Angle . . . . .	102
4-83 Site V-37, Copernicus; Telephoto . . . . .	103
4-84 Site V-37, Copernicus; Telephoto . . . . .	104
4-85 Albedo Distribution for Site V-38, Imbrium Flows . . . . .	105
4-86 Site V-38, Imbrium Flows; Wide Angle . . . . .	106

## Figures (Cont.)

	Page
4-87 Albedo Distribution for Site V-40, Tobias Mayer Dome .....	105
4-88 Site V-40, Dome Near Tobias Mayer; Wide Angle .....	108
4-89 Albedo Distribution for Site V-41; Vitello .....	107
4-90 Site V-41, Vitello; Wide Angle .....	109
4-91 Site V-41, Vitello; Telephoto .....	110
4-92 Albedo Distribution for Site V-43.2; Gassendi .....	111
4-93 Site V-43.2, Gassendi; Wide Angle .....	112
4-94 Site V-43.2, Gassendi; Telephoto .....	113
4-95 Albedo Distribution for Site V-45.1, Domes Near Gruithuisen and Gruithuisen K .....	114
4-96 Site V-45.1, Domes Near Gruithuisen and Gruithuisen K; Wide Angle .....	115
4-97 Site V-45.1, Domes Near Gruithuisen and Gruithuisen K; Telephoto .....	116
4-98 Site V-45.1, Domes Near Gruithuisen and Gruithuisen K; Telephoto .....	117
4-99 Albedo Distribution for Site V-46, Harbinger Mountains .....	118
4-100 Site V-46, Harbinger Mountains; Wide Angle .....	119
4-101 Site V-46, Harbinger Mountains; Telephoto .....	120
4-102 Albedo Distribution for Site V-48, Aristarchus .....	121
4-103 Site V-48, Aristarchus; Wide Angle .....	122
4-104 Site V-48, Aristarchus; Telephoto .....	123
4-105 Site V-48, Aristarchus; Telephoto .....	124
4-106 Site V-48, Aristarchus; Telephoto .....	125
4-107 Albedo Distribution for Site V-49; Cobra Head .....	126
4-108 Site V-49, Cobra Head; Wide Angle .....	127
4-109 Site V-49, Cobra Head; Telephoto .....	128
4-110 Albedo Distribution for Site V-50, Aristarchus Plateau .....	126
4-111 Site V-50, Aristarchus Plateau; Wide Angle .....	130
4-112 Site V-50, Aristarchus Plateau; Telephoto .....	131
4-113 Albedo Distribution for Site V-51, Marius Hills .....	129
4-114 Site V-51, Marius Hills; Wide Angle .....	133
4-115 Site V-51, Marius Hills; Telephoto .....	134
4-116 Site V-51, Marius Hills; Telephoto .....	135
4-117 Envelope of Photographs Comprising Mission V Farside Photographic Coverage .....	136
4-118 Site VA-21, Representative Wide-Angle Photograph of Farside .....	138
4-119 Site VA-21, Representative Telephoto Photograph of Farside .....	139
4-120 Site VA-9, Earth Photo Geometry .....	141
4-121 Site VA-9, Earth .....	142
4-122 Location Diagram for Earth Photograph .....	143
 5-1 Geometry of Photographic Parameters .....	 155
 6-1 Perilune Altitude vs Time .....	 192
6-2 Orbit Inclination vs Time .....	192
6-3 Argument of Perilune History .....	193
6-4 Ascending-Node Longitude History .....	193
6-5 Transfer Function Plot for Site V11a .....	195
6-6 Distribution of First Exposure Time Deviations .....	197
6-7 Mission V Priority Readout .....	210
6-8 Camera Film Advances .....	211

## Figures (Cont.)

	<b>Page</b>
6-9 White-Level Variation Showing Effect of Extended Bimat Dryout Period . . . .	.213
6-10 White-Level Variation Showing Effect of Normal Bimat Dryout Period . . . . .	.213
7-1 Lunar Farside Chart; Polar Areas . . . . .	.220
7-2 Lunar Farside Chart; Mercator . . . . .	.221

## Tables

	Page
2-1 Status of Apollo Landing Site Photography .....	3
2-2 Mission V Nearside Photographic Sites .....	4
2-3 Orbital Design Parameters .....	10
2-4 Mission Film Allocation .....	11
3-1 Log E and Densities of Edge-Data Gray Scale .....	16
4-1 Principal Parameters of Apollo Site IP-1 Photography .....	25
4-2 Apollo Site II P-2 Principal Photographic Parameters .....	27
4-3 Apollo Site II P-6 Principal Photographic Parameters .....	28
4-4 Apollo Site II P-8 Principal Photographic Parameters .....	29
4-5 Apollo Site III P-11 Principal Photographic Parameters .....	30
4-6 Farside Site Principal Photographic Parameters .....	137
5-1 Initial Condition Errors .....	148
5-2 Photo Maneuver Errors .....	148
5-3 Summation of Errors .....	150
5-4 Photographic Supporting Data .....	157
6-1 Primary Orbital Parameters — Lunar Orbiter Missions .....	189
6-2 Initial-Ellipse Photography .....	190
6-3 Comparison of Designed and Achieved Intermediate-Ellipse Elements .....	190
6-4 Intermediate-Ellipse Photography .....	190
6-5 Comparison of Designed and Achieved Final-Ellipse Elements .....	191
6-6 Exposure Control Data for QUAL Input .....	194
6-7 Mission V Predicted Spacecraft Film Densities .....	196
6-8 Actual Mission V Film Budget .....	198
6-9 Photography Operational Data Summary .....	201
7-1 Location of Landing Site Photography .....	215
7-2 Mission I Landing Site Photography .....	216
7-3 Mission II Landing Site Photography .....	217
7-4 Mission III Landing Site Photography .....	218
7-5 Mission V Landing Site Photography .....	219
7-6 Special Interest Areas Photographed on Missions I through III .....	223
7-7 Ellipse Parameters .....	227
7-8 Photographic Parameters .....	228





## Introduction

This Lunar Orbiter final report contains a description of Mission V planning, its conduct with respect to photography, and an evaluation of the photographic results. Data pertinent to analysis and interpretation of the photographs by the user are included. A detailed functional description of the spacecraft photo subsystem and the ground reconstruction may be found in *Lunar Orbiter Mission 1 Final Report*, NASA Document CR-847. Changes and modifications based on that and following missions are described in the respective final reports on photography for those missions. No modifications significant to the photographic results were made following Mission IV.

Mission V was basically similar to the first three missions but with two important differences: a highly inclined (85-degree) orbit was used (as for Mission IV), and the number of individual photographic sites was markedly increased. The number of frames used for farside photography was also increased.

Near-vertical, convergent telephoto stereo-

scopic, and oblique photography was used to obtain the desired data. Either single- or multiple-frame sequences were taken for coverage appropriate for the particular site. All photography planned for the mission was accomplished and the photographs were reconstructed. No major subsystem malfunctions or failures occurred.

Camera operation was satisfactory and high-quality photography was achieved. Photographic quality was somewhat degraded in certain frames by the occurrence of a defect in processing, and by occasional intermittent video dropout. The latter problem had only a very minor effect on information content of the photographs because it involved only a few scan lines each occurrence.

Mission photography began August 6, 1967, at 11:24 GMT, and ended August 18 at 21:40 GMT after 212 frames had been exposed. The photographic portion of the mission was terminated August 26, 1967, with the completion of final readout.

## 1.0 Photographic Mission Description

### 1.1 PROJECT OBJECTIVES

The Lunar Orbiter program primary objective is to provide information necessary to locate and to certify sites that meet the requirements for Apollo manned lunar landings. Secondary objectives are to provide lunar environmental data and data pertinent to selenodesy. These objectives and requirements have been stated explicitly in the Mission III final report on photography (NASA CR 984). Mission III essentially completed the original Lunar Orbiter task and permitted an extension of project objectives: to contribute directly to solving the problem of understanding the Moon as an entity. Mission IV is noted for the major accomplishment of near-vertical photography of virtually all of the nearside — most at a ground resolution of 60 to 80 meters. The success of Mission IV provided the opportunity for even further extension of Lunar Orbiter project objectives.

### 1.2 MISSION V OBJECTIVES

Mission V objectives have been stated in NASA LOTD-120-0:

**“Primary:**

To obtain from lunar orbit, photography of selected scientifically interesting areas on the front and far sides of the Moon, and supplemental photography of candidate Apollo sites.

**Secondary:**

To provide precision trajectory information for use in improving the definition of the lunar gravitational field.

To provide measurements of micro-meteoroid flux and radiation dose in the lunar environment, primarily for spacecraft performance analysis.

To provide a spacecraft which can be tracked in lunar orbit by the MSFN stations for the purpose of exercising and evaluating the tracking network and Apollo Orbit Determination Program.”



## 2.0 Photographic Mission Design

Five basic photographic tasks were defined to accomplish the primary mission objective.

- Provide additional photography for the Apollo program;
- Provide broad-survey photography of unphotographed areas of the farside;
- Provide photography of scientifically interesting Surveyor sites;
- Provide photography of scientifically interesting "landable" areas for the Apollo Application Program (AAP);
- Provide photography of scientifically interesting areas.

Accomplishment of each task results in scientifically interesting photography, but photography of the Apollo landing sites for their certification was directed more toward the problems associated with manned lunar landings than toward a particular scientific objective. Mission design was directed by the tasks to be done and by the constraints and requirements dictated by the spacecraft and photo subsystem.

### 2.1 MISSION TASKS

Although two basic types of photography – Apollo and science – are involved, each of the tasks are defined separately to facilitate understanding some of the unique photographic and site characteristics.

#### 2.1.1 Task 1

Eight candidate Apollo landing sites have been

selected from data obtained from Lunar Orbiters I, II, III, and Surveyor I. An additional potential site on the western edge of Mare Fecunditatis has been located on the basis of less data. Therefore, there are nine sites for which the Manned Spacecraft Center desired the following three types of photography which have been determined to be useful for Apollo landing site certification.

- Near-vertical, to provide the best ground resolution for identification of landing site characteristics and hazards, and for slope data within the landing area and part of the approach path.
- Convergent telephoto stereo, to provide additional slope data for the site and portions of the approach path.
- Oblique, to show a representative view of the site and approach path as will be seen by an astronaut during a manned lunar landing. This type is also to be used for landmark identification along the approach path and proximal to the site.

The Mission V task – to provide the additional photography needed to complete coverage of the selected sites – is summarized in Table 2-1. The sites are identified by the designation given on previous missions.

In addition to the above photography, an oblique

Table 2-1: Status of Apollo Landing Site Photography

Site*	Photographic Data Type		
	Near-Vertical	Convergent Telephoto Stereo	Oblique
IP-1	Required	Required	Required
IIP-2	Completed	Required	Required
IIP-6	Completed	Required	Required
IIP-8	Completed	Required	Completed
IIP-9	Completed	Completed	Completed
IIP-11	Completed	Completed	Completed
IIIP-11	Completed	Required	Completed
IIP-13	Completed	Completed	Completed
IIIP-12	Completed	Completed	Completed

\* Site number designated on prior Lunar Orbiter mission.

photograph including the zero-phase point to simulate a "worst case" view during an approach was to be obtained in Mare Fecunditatis.

### 2.1.2 Task 2

This task of Mission V is to photograph as much of the unphotographed farside as possible, with emphasis given to coverage of the equatorial gap remaining from previous missions.

### 2.1.3 Task 3

Lunar Orbiters I, II, and III photographed several areas to provide data for use in evaluating their potential as Surveyor landing sites. One of these was used for Surveyor III. Additional areas had been selected for future Surveyor missions, including Sinus Medii, in Mare Tranquillitatis, and Hipparchus. This Mission V task was to provide contiguous telephoto coverage of specific areas such as Hipparchus, so that if used as a Surveyor landing site, correlation of Lunar Orbiter and Surveyor photography can uniquely locate the Surveyor spacecraft as done for Surveyor III.

### 2.1.4 Tasks 4 and 5

One of the Mission V tasks was to screen potential sites for AAP in much the same manner as was done by Lunar Orbiters I and II for Apollo. The characteristics that a site must have to be "landable" by AAP are presently undefined; therefore, a judgment was employed

using Apollo requirements as a guide. The complete group of scientifically interesting sites that could be accommodated by Mission V were first selected and then reexamined to define those with landing potential for AAP.

Task 5 differs from Task 4 only in that the sites selected for photography as a part of Task 5 do not have AAP landing potential by the criteria used. The prime criteria for a Task 4 or 5 site were that Mission V photography must be expected to answer some additional questions that will contribute to scientific understanding of the Moon.

## 2.2 SITE SELECTION

Fifty sites were selected to satisfy the requirements defined by Tasks 1, 3, 4, and 5, and 24 on the farside to satisfy Task 2. In addition, a photograph of Earth with nearly full illumination was planned. The nearside sites are summarized in Table 2-2 and are shown plotted on a lunar mosaic in Figures 2-1, -2, and -3. Of the 50 nearside sites, 14 are in support of the Task 1 Apollo requirement.

To expedite planning, initial selection of Mission V sites was made prior to availability of Mission IV photographic data. When this data became available for additional evaluation of the initial site selections, a few sites were deleted and the location of others was modified to obtain more significant data.

**Table 2-2: Mission V Nearside Photographic Sites**

\*See "Notes" at end of table

<u>Site</u>	<u>Task*</u>	<u>Name</u>	<u>Coverage*</u>	<u>Type*</u>
V-1	5	Petavius	4 F	NV
V-2.1	5	Petavius B	1	NV
V-3.1	1	IP-1	1	WO (a)
V-4	5	Stevinus A	1	NV
V-5.1	5	Messier	1	CO (b)
V-6	1	IP-1	1	WO

Table 2-2 (Continued)

<u>Site</u>	<u>Task*</u>	<u>Name</u>	<u>Coverage*</u>	<u>Type*</u>
V-8a	1	IP-1	4 F	CTS
V-8b	1	IP-1	4 F	
V-9.1	1	IIP-2	1	WO
V-10	5	Altai Scarp	1	CO (c)
V-11a	1	IIP-2	4 F	CTS
V-11b	1	IIP-2	4 F	
V-12	5	Censorinus	1	NV
V-13	1	IIP-6	1	WO
V-14	4-5	Littrow	4 F	NV
V-15.1	4	Dawes	1	NV
V-16a	1	IIP-6	4 F	CTS
V-16b	1	IIP-6	4 F	
V-18	4	Dionysius	4 F	NV
V-19	5	Albufeda Crater Chain	1	NV
V-21	4-5	South of Alexander	4 F	NV
V-22	4	Sulpicius Gallus Rilles	4 F	NV
V-23.2	4	Hyginus Rilles	4 F	NV
V-24	3-5	Hipparchus	4F	NV
V-25	5	Alpine Valley	1	CO (c)
V-26.1	5	Hadley Rille	4 S	NV
V-27a	1	IIP-8	4 F	CTS
V-27b	1	IIP-8	4 F	
V-28	4-5	Alphonsus	4 F	NV
V-29	5	Rima Bode II	4 F	NV

**Table 2-2 (Continued)**

<u>Site</u>	<u>Task*</u>	<u>Name</u>	<u>Coverage*</u>	<u>Type*</u>
V-30	5	Tycho	4 F	NV
V-31	5	Sinuous Rille East of Plato	4 F	NV
V-32	5	Eratosthenes	4 F	NV
V-33	4-5	Area of Copernicus CD	1	NV
V-34	4-5	Fra Mauro	4 F	NV
V-35	4-5	Copernicus Secondaries	4 S	NV
V-36	5	Copernicus H	4 F	NV
V-37	4-5	Copernicus	8 F	NV
V-38	4-5	Imbrium Flows	4 F	NV
V-40	4-5	Tobias Mayer Dome	4 F	NV
V-41	5	Vitello	1	NV
V-42a	1	IIP-11	4 F	CTS
V-42b	1	IIP-11	4 F	
V-43.2	5	Gassendi	4 F	NV
V-45.1	5	Jura Domes	4 F	NV
V-46	5	Harbinger Mountains	8 F	NV
V-48	5	Aristarchus	8 F	NV
V-49	5	Cobra Head	4 F	NV
V-50	4-5	Aristarchus Plateau	4 F	NV
V-51	4-5	Marius Hills	4 F	NV

Notes

Coverage:

- Number of frames exposed and sequencing mode;
- F - fast mode contiguous telephoto coverage
- S - slow mode 50% wide-angle overlap



Table 2-2 Notes (Continued)

Tasks: 1 Apollo support  
3 Surveyor candidate site  
4 AAP candidate site  
5 Science site

Type:

NV Near-vertical

WO Westerly oblique

a) Includes zero-phase point

CO Conventional oblique

b) Westerly perpendicular to orbit

c) Southwesterly

CTS Convergent telephoto stereo

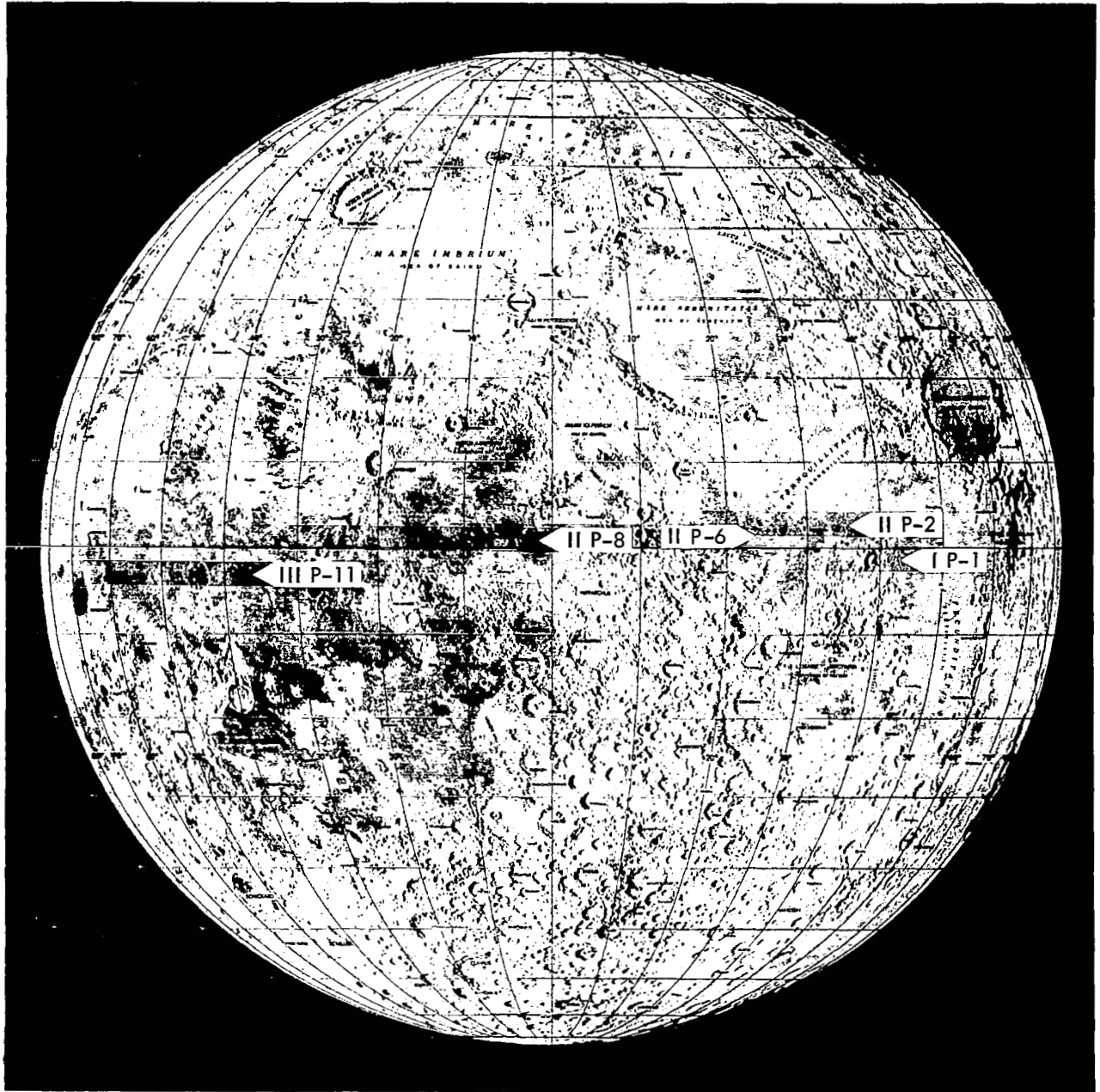
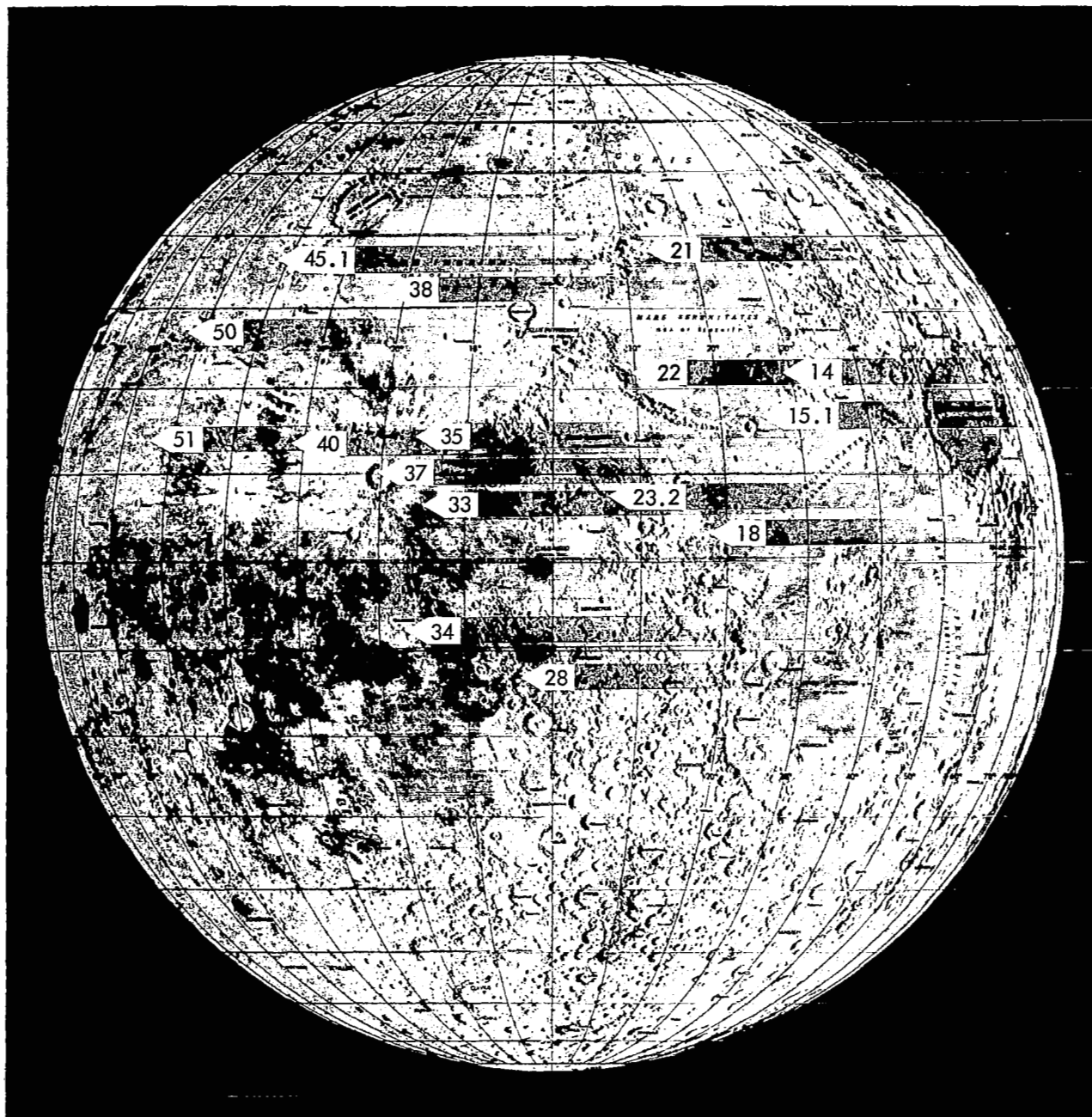


Figure 2-1: Location of Apollo Sites for Mission V Photography

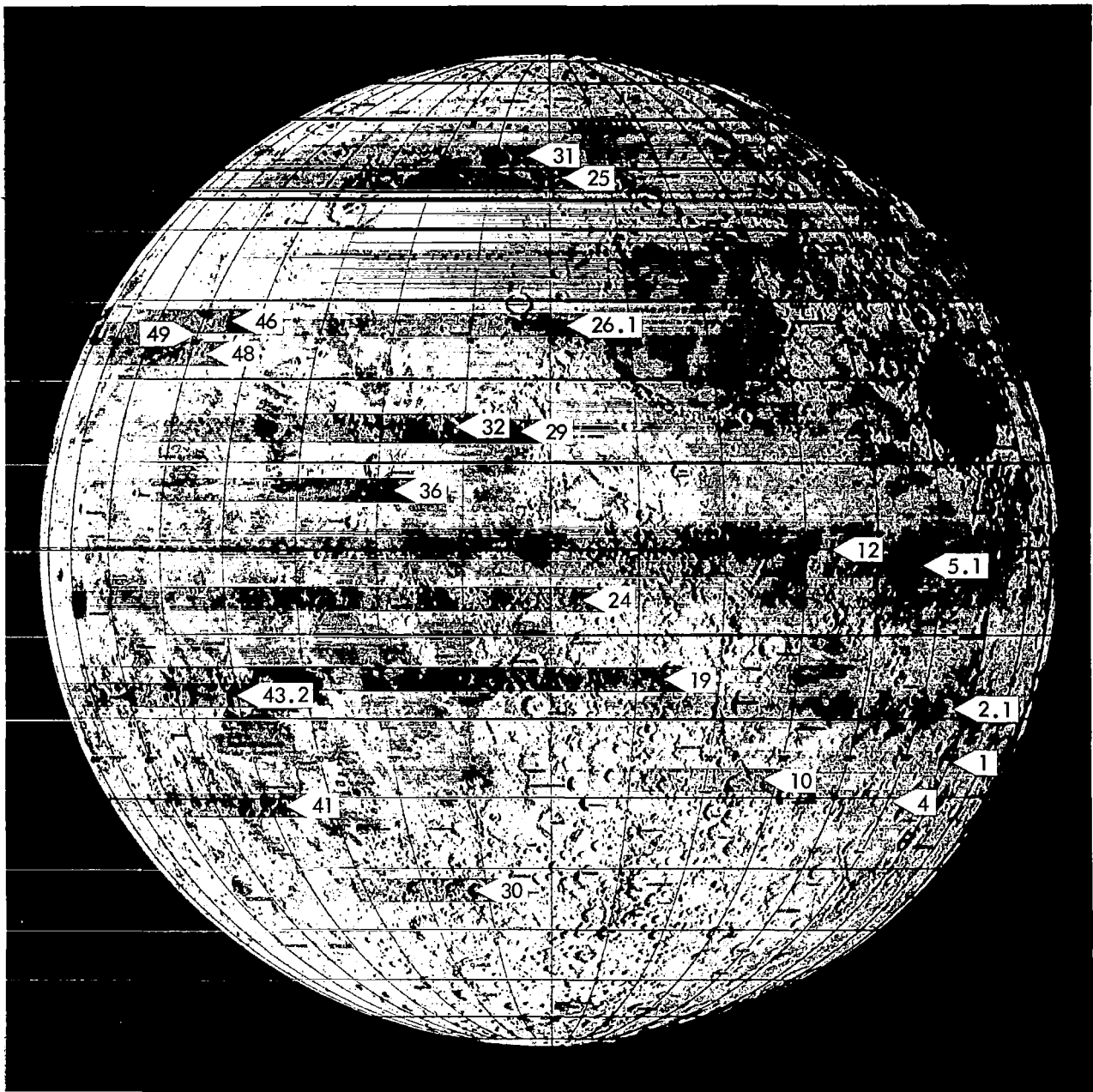


**Figure 2-2: Mission V Nearside Sites Designated for AAP**

### **2.3 ORBIT DESIGN**

Mission site locations and the type and extent of required coverage were major considerations in determining the most suitable mission orbital parameters. The combination of broad coverage of the farside, without using excessive tilt, and high resolution of nearside areas required a highly elliptical, 85-degree-inclination initial

orbit for part of the farside photography, followed by transfer to a lower orbit for nearside photography. To change from the initial highly elliptical orbit, having a 6,000-kilometer apolune and a 200-kilometer perilune, to the final desired orbit having a 1,500-kilometer apolune and a 100-kilometer perilune, an intermediate orbit was necessary. For the second or intermediate



**Figure 2-3: Mission V Nearside Science Sites**

orbit, perilune was lowered to 100 kilometers. The planned orbital parameters and reasons for their selection are summarized in Table 2-3.

With apolune of the initial orbit over the farside, the area could be photographed with the camera axis tilted toward the properly illuminated portion. The required tilt was not excessive,

since photography was accomplished from a high altitude. The photography planned from this initial orbit was similar to some Mission IV photography.

Following completion of operations in the initial orbit, transfer to a second, intermediate orbit was required before the orbit necessary for the

---

**Table 2-3: Orbital Design Parameters**


---

<u>Orbital Parameters</u>	<u>Reason</u>
Posigrade	Visibility of deboost from Earth
Ascending-node nearside photog-raphy	Preferred lighting conditions; Canopus update
Inclination 85 deg	Access to and proper lighting for high-latitude sites
Initial ellipse Period 8.4 hrs Perilune 200 km Apolune 6,000 km	To provide farside coverage. Impact hazard
Intermediate ellipse Period 8.3 hrs Perilune 100 km Apolune 6,000 km	Intermediate step to achieve final orbit
Final ellipse Period 3.2 hrs Perilune 100 km Apolune 1,500 km	Within IMC operating range at high latitudes, minimize cross- track tilt; acceptable photo resolu- tion and areal coverage, within $\Delta V$ capability

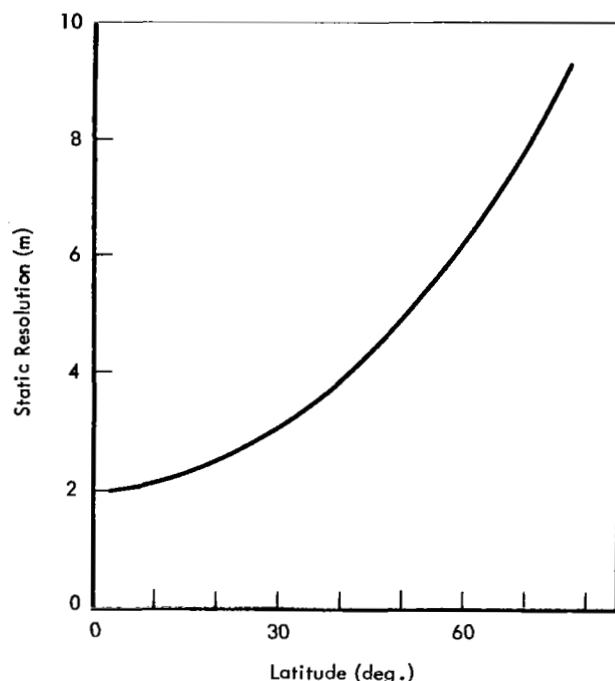
---

major portion of the mission photography could be achieved. For the intermediate orbit, perilune was changed from 200 to 100 kilometers. Additional farside photography was planned for the intermediate orbit. Photography from the intermediate orbit was similar to that from the initial orbit because apolune altitude remained unchanged from about 6,000 kilometers. The final maneuver sequence reduced apolune to 1,500 kilometers to place the spacecraft in the orbit desired for principal Mission V nearside photography.

Orbital parameters selected for the final orbit affected mission photography characteristics. The 100-kilometer perilune altitude was about twice that used in the first three missions; thus, the best resolution of the photographs would be about 2 meters for the telephoto lens and 16 meters for the wide-angle lens. This reduction in resolution was accepted to enable convergent telephoto stereo coverage without excessive camera tilt. The Manned Spacecraft Center has

defined the maximum useful cross-track tilt to be approximately 30 degrees, and the higher altitude reduced the required tilt. In addition, the area included in the coverage of a given photograph would be increased by a factor of four, allowing near-equatorial sites to be photographed with half the number of frames necessary on the first three missions; hence, a larger number of sites could be photographed.

Although perilune was nearly over the equator, the dispersion of sites over a wide latitude range resulted in a difference in photographic altitude dependent on the site latitude. This also resulted in a variation in static resolution approximately proportional to the latitude because of high inclination of the elliptical orbit. This relationship is shown in Figure 2-4, in which premission orbital parameters with perilune over the equator were used. Actual parameters differed slightly. Because of parameter changes caused by gravitational anomalies, some spacecraft altitude variation occurred at a given latitude.



**Figure 2-4: Static Resolution vs Spacecraft Latitude**

Actually, perilune did not occur directly over the equator but at about 2°N, thus affecting the altitude-latitude relation for north and south latitudes. Varying amounts of camera axis tilt were required to photograph the targets; therefore, actual static resolution should be related to slant range rather than to spacecraft altitude because resolution is proportional to the distance from camera to object. This data may be obtained for each photograph from Table 5-4.

## 2.4 FILM MANAGEMENT AND BUDGETING

### 2.4.1 Film Budget

Allocation of frames for photography of the planned sites was established on the basis of a number of requirements and system constraints, which include the following.

- Initially, 11 frames were required to move the leader-to-film splice off the supply roll and through the camera to place the fifth frame of SO-243 in position for the wide-angle photograph of the first site.
- The Bimat-stick restraint required two frames to be processed every 15 hours, but processing two frames less frequently than every 4 hours

promotes Bimat dryout that results in some processing degradation. Depending on the dispersion of sites and the resulting schedule for photography determined by orbit parameters, frames were required for necessary film movement.

- Film allocation for each site was governed by the type of photography required for that site (see Table 2-4).

**Table 2-4: Mission Film Allocation**

Ellipse	Photography			
	Farside		Nearside	
	Sites	Frames	Sites	Frames
Initial	5	19	0	0
Intermediate	7	7	0	0
Final	13	13	50	174
Photo Sequences	Farside		Nearside	
Single frames	23		14	
One four-frame	0		22	
Two four-frame	0		5	
One eight-frame	2		4	

Single frames were used for oblique photographs and for features that are relatively small and did not need broader coverage or forward wide-angle stereo. A single four-frame sequence was used where contiguous telephoto coverage was desired and the area or feature required four frames. In two instances, Sites V-26.1 and V-35, broader coverage was more desirable; thus, slow-mode sequencing was used for these two sites. At three sites – V-37, Copernicus; V-46, Harbinger mountains; and V-48, Aristarchus – broader coverage with contiguous telephoto coverage was desired and eight-frame sequences in the fast mode were used. Two four-frame sequences were scheduled for each of five sites where convergent telephoto stereo coverage was desired.

### 2.4.2 Film Management

Film management during the photographic portion of the mission was planned by a mission

event sequence and time-line analysis. This study established the relationships of photographic film utilization, processing, priority readout, and final readout. Basic to the study was consideration of such factors as:

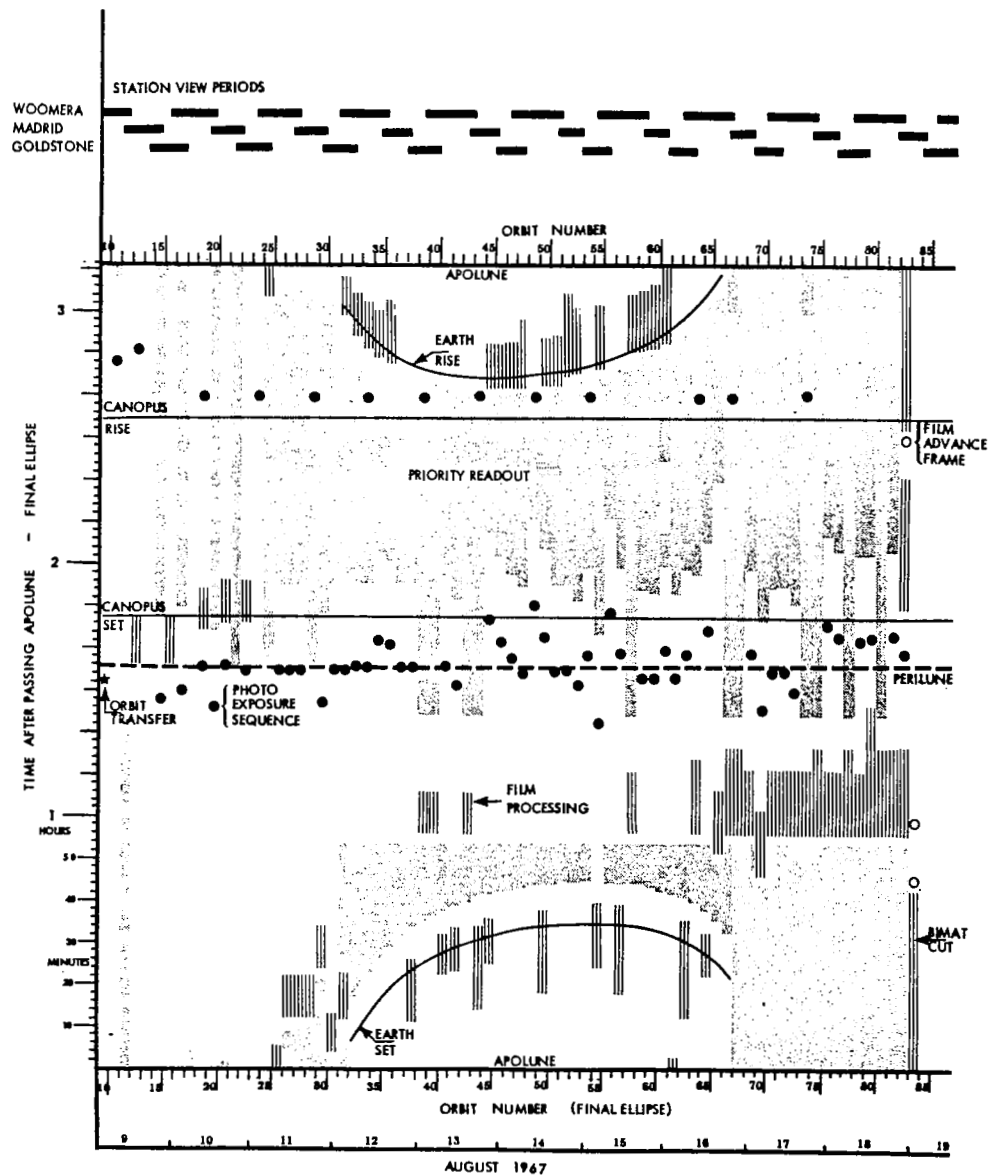
- Photo subsystem requirements and constraints established by Bimat-stick, Bimat dryout, film-set, thermal control, power requirements, and limitations on processing and readout;
- Target area illumination;
- Orbital parameters and environmental factors, including orbital period, times and duration of Sun and Earth occultation, and view periods of the Deep Space Network stations;
- Requirements for priority readout for operational evaluation and data recovery.

The relationship of photography, film processing, and readout sequences to Sun, Earth, and Canopus occultation times, orbital position, and DSIF station view periods is shown graphically in Figure 2-5. Start of photography was planned for 17.5 hours after injection into the initial orbit to enable photography of an area at 104°W before it was obscured by the terminator. Once begun, photography had to be maintained to provide contiguous farside coverage.

The plan indicates processing two frames at intervals varying from 6.5 to 15 hours from the beginning of photography until Orbit 25. Thereafter, at least two frames were to be processed

every 4 hours because these would be nearside photographs. Processing frequency requirements were relaxed during the early portion of the mission and reinstated for the prime nearside photographs. Processing two frames every 4 hours from the beginning of photography would have required expenditure of approximately 40 additional frames early in the mission. In addition, frames were conserved and priority readout was increased by relaxing the constraint requiring a minimum content of two frames in the camera loop to enable Bimat-cut in the event of an inoperable film advance. The last time the plan allowed the loop contents to go below two frames was in Orbit 30, since prior to that all photo data would have been read out. If Bimat-cut had not been possible, only lower-priority farside coverage would have been permanently lost.

After photographing Site V-51, 217 frames of film would have been used, including the four unexposed frames between the splice and the first wide-angle exposure. Then 6.3 frames were to be processed, leaving four in the loop. On the next orbit, the camera was to be advanced 16 frames and 16 frames processed, completing a total of 227 frames equivalent of wet Bimat. Following Bimat-cut, additional frames would have to be advanced to place the last frame of Site V-51 in readout position. After Frame 217 was advanced past the optical-mechanical scanner and Bimat was clear, final readout could start.



**Figure 2-5: Planned Photo Period Sequence of Events**





## 3.0 Mission V Photo Subsystem Characteristics

### 3.1 PHOTO SUBSYSTEM DESCRIPTION

The Lunar Orbiter photo subsystem includes five basic components: the dual-lens camera, film processor-dryer, photo-video chain, command-control-and-programmer, and ground equipment. No major changes were made in this subsystem following Mission III.

A brief description of the photo subsystem is presented below for those unfamiliar with the technique for acquiring the lunar photographs. A detailed description of the subsystem and its functions, together with the ground support equipment necessary for reconstruction of the photographs, has been included in *Lunar Orbiter Mission I Final Report*, NASA CR-847. Changes and modifications incorporated for Missions II and III will be found in the final reports for those missions, NASA CR 931 and CR 984 respectively. The same modifications were made on subsequent mission subsystems.

#### 3.1.1 Camera

The camera had two separate objective lenses, a 610-mm telephoto lens and an 80-mm wide-angle lens, both operated at a fixed aperture of  $f/5.6$ . A neutral-density filter having an optical density of 0.18 was attached to the 80-mm lens to balance its transmissivity with that of the 610-mm lens. Both lenses focused on the same roll of 70-mm SO-243 film, with the two images separated by a length of film equivalent to that of a wide-angle and a telephoto format. A folding mirror in the optical path of the telephoto lens was necessary for design requirements. Vacuum platens held the film during exposure. To compensate for image motion from the spacecraft motion, platen movement parallel to the flight direction, or the spacecraft X axis, is controlled by a velocity-to-height-ratio sensor (V/H sensor) that tracks a portion of the 610-mm lens image of the surface.

A focal-plane shutter was used with the telephoto lens and a between-the-lens shutter with the wide-angle lens. Exposure control was achieved by commanded selection of shutter speed. Three speeds — 0.04, 0.02, and 0.01 second — were available. Both shutters operat-

ed, at the same nominal speed, with actuation of the 80-mm shutter delayed 40 milliseconds after that of the focal-plane shutter. Operation of the 80-mm shutter activated a series of small lights that produce a binary time code on the film.

Photographs could be taken as single frames or sequences of 4, 8, or 16 frames. Multiple-frame sequences could be taken in the fast mode — which obtained contiguous telephoto coverage with 87% forward overlap of wide-angle coverage — or in the slow mode, which provided 50% forward overlap of wide-angle coverage.

#### 3.1.2 Processor - Dryer

The SO-243 film was processed by the Bimat processing method. In this process, the film is temporarily laminated to the Bimat and carried around a temperature-controlled drum while in contact. During the lamination period, a single-solution processing liquid, absorbed in the Bimat emulsion, diffused into the SO-243 emulsion to simultaneously develop and fix the photographic image. The SO-243 and Bimat were delaminated upon leaving the processor drum. The used Bimat was collected onto a takeup reel and the slightly moist SO-243 passed through a heated dryer. The moisture was absorbed by a desiccant.

#### 3.1.3 Photo Video Chain

Optical density variations of the negative photographic image were converted into analog electrical signals by the photo-video chain for transmission to Earth. A 6.5-micron-diameter image of an oscillating spot of light produced on the rotating anode of a line-scan tube was focused on the photographic film in the readout gate. The image moved longitudinally on the film a distance of 2.67 mm, and the scanner lens moved at right angles to the film following each scan. The result was a "framelet" having a raster of 16,359 lines across 57 mm of the 70-mm width. Following completion of one framelet, the film was moved 2.54 mm to begin scan of the next, moving across the film in the opposite direction.

The light passing through the film, modulated by the image density, was sensed by a photomultiplier tube through associated light collection optics. The resulting analog signal was amplified, timing and synchronization pulses were added to form the composite video signal, and the signal was transmitted to Earth by the spacecraft video transmitter.

#### 3.1.4 Command Control and Programmer

The command control and programmer (CCP) electronics provided the capability to accept real-time commands, store commands for later action, and store programmed commands. The CCP incorporated the logic to control the necessarily complex sequencing and limitations of the photo subsystem operation. This component provided the versatility of operational procedures that made possible the variety of photographic techniques used by Lunar Orbiter.

#### 3.1.5 Ground Reconstruction Electronics

The ground reconstruction electronics (GRE) provided the means of converting the received composite video signal back into a photographic image. The video portion of the signal was separated, displayed on a kinescope tube, and recorded on 35-mm film. In this process, the photographic image was enlarged by a factor of 7.2, resulting in each framelet being recorded on 425.76 mm of the 35-mm film with a width of 19.939 mm, including the overlap of 0.445 mm with the adjacent framelet. The GRE reconstructed the photograph as a positive image rather than a negative as on the spacecraft. The individual framelets were subsequently reassembled to form the complete photograph. Approximately 28 framelets are required for a wide-angle photograph and 96 for the telephoto.

### 3.2 CALIBRATION

Tests and calibrations performed on the photographic subsystem for Mission V were the same as those for previous missions and are described in *Lunar Orbiter 1 Final Report*, NASA CR 847. The tests and calibrations include lens-film characteristics, exposure calibration and control, image-motion compensation, camera alignment, readout quality, and photogrammetric distortion of the 80-mm lens.

The test and calibration data specific to Mission V have been submitted to NASA. These data, along with copies of the photographs obtained during the mission, can be obtained by interested scientists from the National Space Science Data Center of the Goddard Space Flight Center.

### 3.3 FILM CHARACTERISTICS

#### 3.3.1 Gray-Scale Calibration of Flight Film

Edge data gray-scale measurements for calibration of Mission V flight film were made using an Ansco Model 4 microdensitometer calibrated for ASA Visual density. The strip of SO-243 flight film was Bimat-processed in the preflight processor at the Eastern Test Range. Exposure values as Log E meter-candle-second (mcs) for each gray-scale step and the corresponding ASA Visual density are tabulated in Table 3-1.

The log E value for Step 1 should be used with caution, as the density was very near the measured minimum density of the film. The background density was measured as 0.42 Visual

**Table 3-1:**  
**Log E and Densities of Edge-Data Gray Scale**

Step Number	Log E (mcs)	Densities	
		ASA Visual	Readout
1	2.56	0.40	0.33
2	2.83	0.43	0.37
3	1.02	0.47	0.41
4	1.17	0.56	0.52
5	1.33	0.73	0.72
6	1.51	0.94	0.97
7	1.75	1.24	1.25
8	1.93	1.46	1.33 (Est.)
9	0.08	1.65	---

density. This corresponds to 0.35 Readout density, or just within the specification of  $0.30 \pm 0.05$ .

The measured D vs log E curve for the hand-processed test strip of flight film is shown in Figure 3-1. This curve is corrected for calibration of the EG&G sensitometer used at ETR. The location of the edge data gray-scale steps on the curve is shown. A comparison between the measured curve for the hand-processed film and the statistical average curve published by Eastman Kodak for SO-243 film with Bimat processing is shown in Figure 3-2. Very good agreement between these curves is seen. Figure 3-3 presents a conversion curve relating the ASA Visual and Readout densities.

### 3.3.2 Reseau Pattern

A resseau pattern of crosses, identical to that used for Missions III and IV, was preexposed on the flight film by Eastman Kodak coincident with the edge data. The pattern, with dimensions of the crosses and their placement on the spacecraft film, is shown in Figure 3-4. These dimensions must be increased by a factor of 7.2 when applied to the GRE reconstructed record.

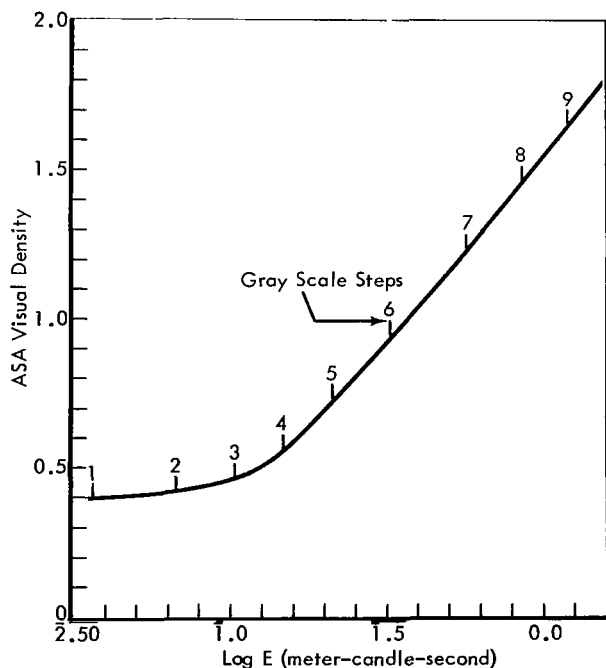


Figure 3-1: Flight Film Density vs Log E Curve and Position of Gray-Scale Steps

The resseau pattern provides a means of determining and correcting for any distortion of the photographic image that occurred subsequent to exposure, and does not reveal any optical distortions caused by the camera.

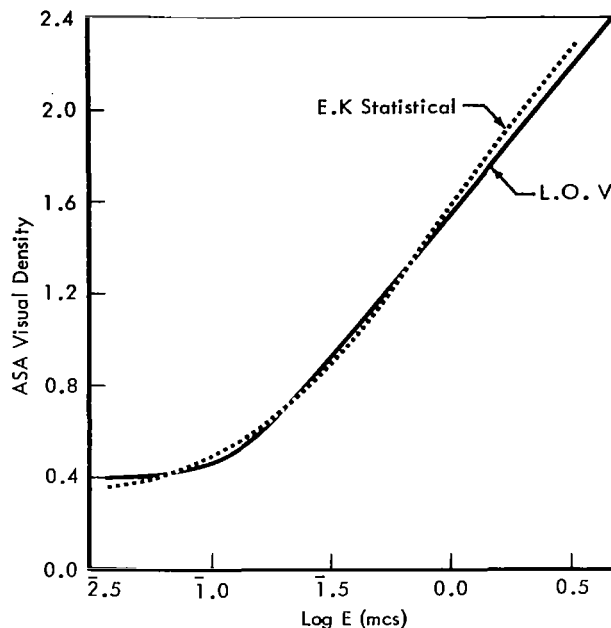


Figure 3-2: Comparison of Lunar Orbiter V Test and Eastman Kodak Statistical Sensitometric Curves for Bimat-Processed SO-243

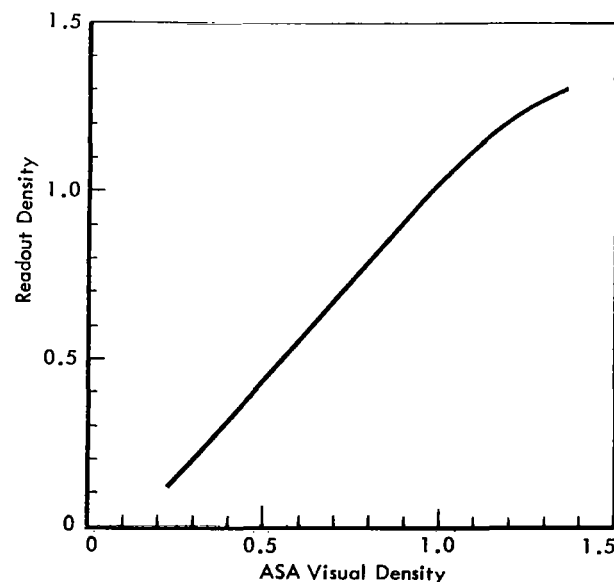
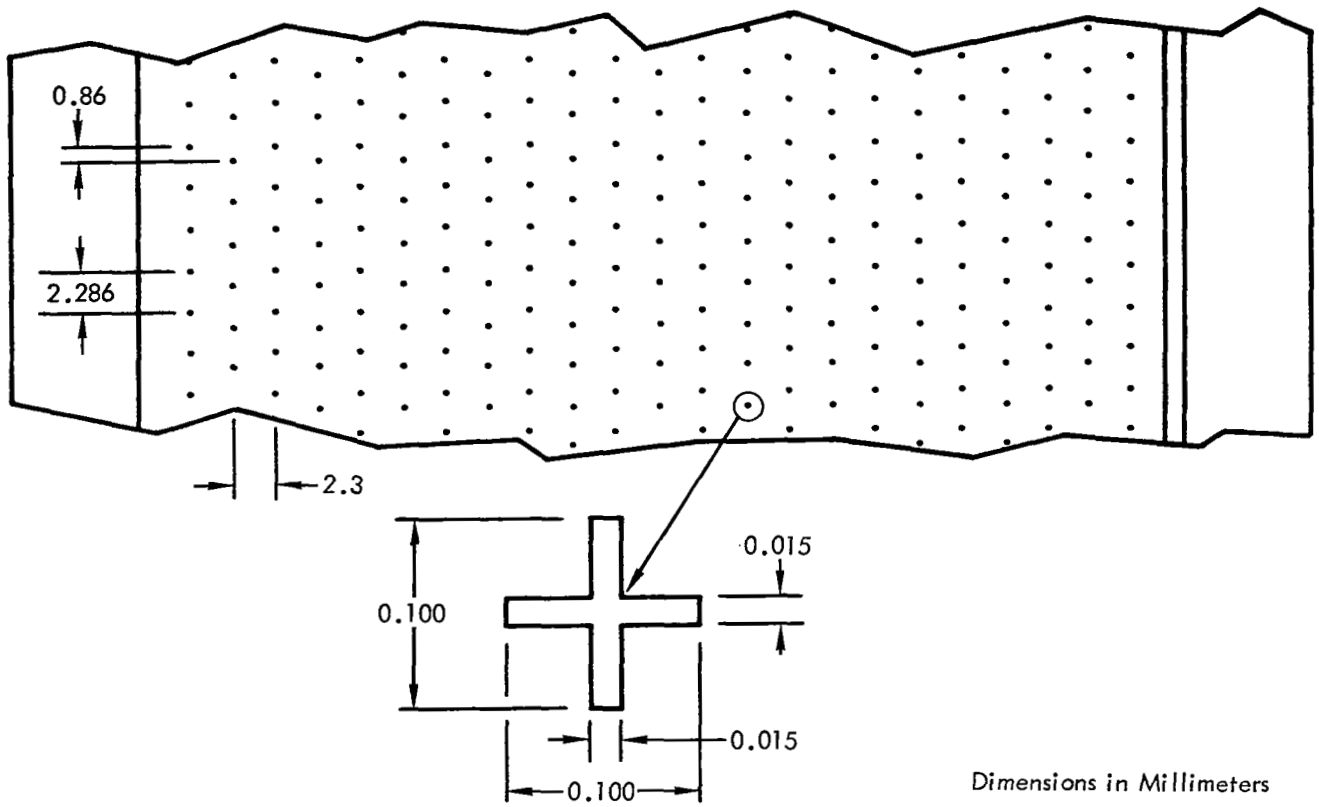


Figure 3-3: Readout Density vs ASA Visual Density for Bimat-Processed SO-243



**Figure 3-4: Preexposed Reseau Mark Placement and Detail of Cross**

## 4.0 Photographs

Lunar Orbiter Mission V was a completely different type of mission from those preceding it. In fulfilling the primary objective of science-site photography, a large number of individual areas was photographed. Considering the purpose of the mission, the variety of features and conditions of photography, and the great diversity of potential applications of the photographs, it was believed that mission photography evaluation should, wherever possible, treat the science sites individually. Apolune photographs and those of Apollo sites will be considered separately.

### 4.1 EVALUATION METHODS

Mission photography evaluation has been based on examination of a second-generation copy of the GRE-reconstructed record and reassembled photographic prints prepared by both the Army Map Service and Langley Research Center. Prints from the latter source were prepared from GRE records obtained by playback of the FR-900 magnetic-tape video signal recording. Primary source for the Army Map Service prints was copies of the DSN GRE record. Print image density and contrast control techniques were used by both agencies. In addition, Langley Research Center, using the magnetic-tape video recording, employed GRE gain adjustment as compensation for signal strength variation caused by spacecraft film exposure. This latter technique enabled usable image to be obtained in areas that, because of illumination or albedo characteristics, were exposed more than desirable, but at the expense of losing information in image areas of minimum exposure. However, preparation of multiple GRE reconstructions, each at different gain settings, resulted in a good-quality image extending over a significantly broader range of surface luminance than otherwise possible.

In evaluating mission photography on the basis of the paper prints, whether from the Army Map Service or Langley Research Center, these control techniques were taken into consideration. Use of the paper prints for evaluation was, therefore, mainly confined to assessing those

factors applicable to the photographs as a whole and to mission photography in general. Factors relating to full frames and to site sequences included:

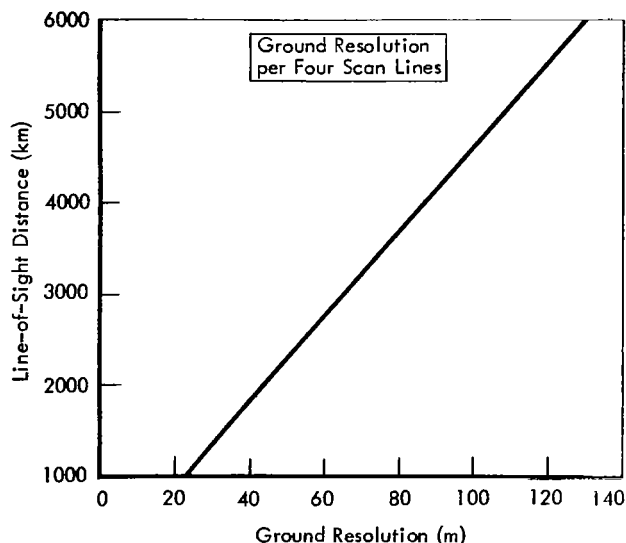
- Uniformity of exposure within the frame format;
- Relation or effect of terrain character on exposure and information content (apparent albedo range, presence of mountainous terrain or steep interior crater slopes, etc.);
- Coverage of the target feature.

Factors relating to overall mission photography, such as quality of processing (Bimat dryout, stop lines, and lace defect), were also considered.

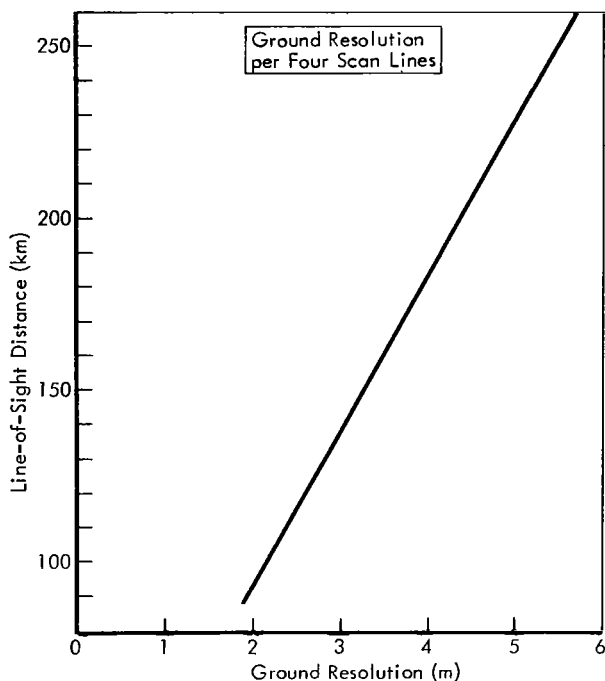
Estimation of photographic resolution was based entirely on visual examination of the GRE film at a magnification of up to about 20 diameters. Resolution was estimated by noting the smallest surface feature that could be distinguished and recognized — usually a crater — and recording its size in terms of scan lines spanned. Care was always taken to ensure that the object was in fact a lunar surface feature and not noise pattern or a small blemish.

The rationale for expressing resolution in this manner is discussed in *Lunar Orbiter III Final Report*, NASA CR 984, Section 2.3.1.2. Briefly, it provides a means for comparison of resolution related to the spacecraft film image independent of the altitude of photography. The specifications for photography require a resolution of about 76 lines per millimeter on the spacecraft film. This in turn corresponds to detection of a feature spanning approximately four scan lines of the optical-mechanical scanner. Ground resolution is proportional to the line-of-sight distance, as shown in Figures 4-1 and 4-2 in which the size of an object on the ground whose image spans four scan lines on the telephoto frame is given for a range of distances between camera and object. Two plots are presented, Figure 4-1 for distances applicable to the farside near-apolune photographs, and Figure 4-2 for nearside photography.

The above method of estimating resolution has been used as one means of assessing relative photographic quality. It is not considered nor intended to be a quantitative determination for use in determining compliance with mission specifications.



**Figure 4-1 : Telephoto Resolution vs Line-of-Sight Distance; Near Apolune**



**Figure 4-2 : Telephoto Resolution vs Line-of-Sight Distance; Near Perilune**

## 4.2 GENERAL MISSION CHARACTERISTICS

### 4.2.1 Exposure

Exposure control for the various nearside sites was accomplished, first, by mission planning which scheduled photography such that illumination was within the acceptable Sun angle range, as the spacecraft passed within sight of the target, without undesirable camera axis tilt. Second, exposure was controlled by selection of one of the three available camera shutter speeds (0.04, 0.02, or 0.01 second). The lens aperture was fixed at f/5.6. Because of a differential in transmissivity between the 610-mm telephoto optics and the 80-mm wide-angle lens, a 0.18-density neutral-density filter was installed on the 80-mm lens.

The neutral-density filter did not completely balance exposure of the wide-angle and telephoto frames. Throughout the mission, the former received slightly more exposure, resulting in average GRE film densities of 0.1 to 0.2 lower than the corresponding telephoto frames. The comparison can be only approximate because of the difficulty in obtaining density measurements on corresponding surface feature images in the two different photographs. The exposure differential was not enough to have serious consequences in photographic quality, with the exception of limited image areas near the extremes of the system limitations imposed by the photo-video chain, spacecraft film sensitivity, and GRE.

Throughout the mission, shutter speed selection was made on the basis of predicted spacecraft film densities computed by the Photo Quality Prediction (QUAL) program. This program considered the camera-film constants and the variables of illumination and observation geometry and site albedo that control apparent luminance of the target. Recommended albedo values for individual sites were provided by the USGS. For most sites, a histogram was shown giving the albedo distribution within the site area, and their recommended value. However, Lunar Orbiter operational experience from previous missions has shown that improved exposure was obtained by reducing the USGS recommended value by a factor of 1.3 for use

in the QUAL program providing data for exposure control (see Section 6.3.1). The histograms included in the discussion of individual site photography are shown as presented by the USGS. Their recommended albedo value and the corresponding value used in the QUAL program are noted in each figure. Exposure was sometimes modified, by direction of qualified NASA geologists, to optimize for characteristics of limited target area or specific features. Exposure was always optimized for the telephoto frame.

Overall, exposure of both wide-angle and telephoto frames was satisfactory. The exposure selection for each site is considered to have been correct. Because of the topographic characteristics of lunar terrain, effects of the lunar photometric function, and system limitations, almost all photographs include at least some areas of under or over exposure where information is lost because of the extreme luminance range of the surface. (This is frequently the case where steep slopes occur, but usually nearby or adjacent areas of the same or similar character are oriented with respect to the Sun so that surface detail representative of those areas is suitably shown and can be examined.)

Some exposure variation occurs within the frames because of variation in lens transmission with angular field of view. While present in both lenses, it is most apparent in telephoto frames, and results in some darkening (less exposure) in the corners of wide-angle frames and ends of telephoto frames. This is of consequence to interpretation of the photographs only where surface luminance for the site was near the lower limit of the system or exposure was optimized for brighter areas.

Farside photography presented additional problems. Photographs were always taken from a high altitude, thus including a large area. Further, photography was by PM illumination and it was necessary to tilt the camera toward the illuminated limb to bring the area of most suitable illumination within the telephoto field of view. Wide-angle frames cover the Moon from the bright limb to beyond the terminator;

thus, the image ranges from over exposure to complete lack of exposure. All, however, include a band where surface features are very well shown. The field of view for the farside photographs is illustrated in Figure 4-3.

#### 4.2.2 Resolution

Resolution of both wide-angle and telephoto photographs equaled or bettered that of previous missions. Resolution of between three and four scan lines (see Section 4.1) was observed consistently on nearly all frames, both wide-angle and telephoto, near the center of the frame. Of the 213 dual frames taken, only six individual frames were found to have resolution of lower quality — between five and seven scan lines. Two additional telephoto frames, Frames 38 and 54, were found to have a resolution of about 15 scan lines. These photographs were oblique with orientation such that image-motion compensation was not possible and the V/H sensor was off. As a result, a slight amount of image smear occurred. The degradation is not readily apparent without visual aid.

#### 4.2.3 Spacecraft Film Processing

Spacecraft film processing was accomplished without mechanical malfunction affecting image quality. As on previous missions, the requirement for intermittent processing resulted in formation of typical lines of degraded image each time the processing operation was stopped. These lines — the “processor-stop” and “Bimat pulloff” lines — have been described and explained in the final reports for Missions I and II, *Photography*.

Processing of Mission V photography was generally comparable with that of previous missions, although occurrence of the lace defect appeared to be more extensive. This defect appears as blemishes in the form of small, round spots, either light or dark; or elongated spots or loops. They occur commonly in bands aligned longitudinally on the spacecraft film, and in more isolated groups. The photographic image is absent within the area of the individual spots, but is unaffected between them; thus, the image is not totally obscured within the general lace areas. This defect has occurred on all missions

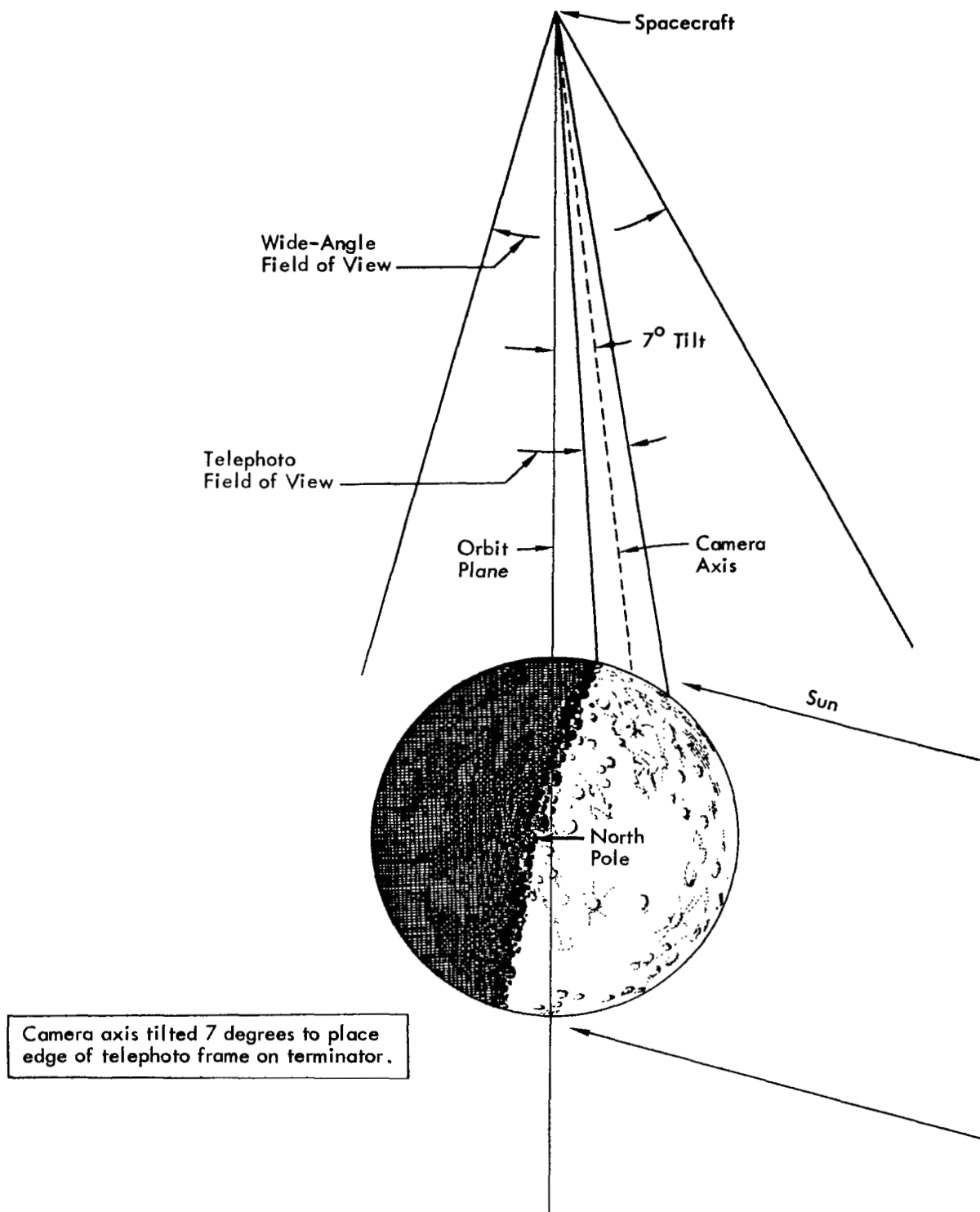


Figure 4-3: Apolune Photography Field of View



and, although the subject of extensive investigation, the cause has not been positively established. At present it is believed to be the result of improper lamination of the Bimat to the photographic film on the processor drum, possibly by occluded gas bubbles which prevent intimate contact and thus processing at those points.

#### **4.2.4 Readout and Reconstruction**

Readout of all mission photography was accomplished and was of satisfactory quality. Readout progressed normally and with proper operation of the scanning mechanism. No instances of incorrect film advance causing improper framelet overlap were noted. Because of the reliable operation, extended readout sequences were accomplished during final readout without affecting photographic quality.

Intermittent video dropout was the only problem related to readout that affected the photographs (see Section 6.4.4.1). Narrow white lines (in positive images) extending the width of individual framelets were produced. In each case, about six to eight scan lines were affected (each framelet is composed of over 16,000 scan lines), but because of the very short interval little information was lost by each occurrence. Further, because priority readout duplicates much of the mission photography, the data loss is not significant.

During both priority and final readouts, reconstructed records were made using two GRE's at each receiving DSIF site. One record was designated as prime and identified as "OP-1," the other, "OP-2." The record designated "OP-1" was whichever appeared to be best and included the record of the entire readout sequence. Judgment was based on on-site evaluation.

In addition to the GRE-reconstructed record, the video signal was recorded on magnetic tape by an FR-900 recorder. The magnetic-tape record was forwarded to the Langley Research Center, where it has been used in preparing additional GRE records that are the source of positive paper prints from that facility. Use of

the magnetic-tape record has made possible an image enhancement technique in which the GRE gain has been modified to bring out image detail lost in normal reconstruction because of system limitations in reproduction of image density range. Image detail otherwise degraded by exposure extremes can be recovered by in effect shifting the density range. In doing this, however, adjustment to enhance detail in highlights will result in some loss of shadow detail. The enhancement technique cannot compensate for gross exposure differences that exceed sensitivity limitations of the SO-243 film used in the spacecraft cameras.

#### **4.2.5 Reassembly and Printing**

All reassembly of Mission V photographs has been accomplished manually by both Langley Research Center and the Army Map Service. As for Mission IV, no machine reassembly of Mission V photographs was done by Eastman Kodak using their reassembly printer. Although reassembly by the Army Map Service and by Langley Research Center was done by hand, the procedure by which positive paper prints were prepared was different. Each technique resulted in characteristics of the prints that distinguished those from either facility.

The Army Map Service begins with a negative copy of the prime GRE record made by Eastman Kodak Co. They then prepare a positive contact print on a heavier-based film to avoid curl. This contact print is then cut along the fiducial lines to separate the individual framelets, which are then mounted on a transparent backing in the correct sequence and orientation. A film negative is then made by contact printing from the assembled framelets. During production of the final negative, a Fluoro-Dodger was used for density control where extreme density variation occurred over an appreciable area of a frame. The resulting negative was then used in making paper prints. The Army Map Service assembled complete wide-angle frames as a unit, and prepared telephoto frames in three sections.

While the control technique used by the Army Map Service may, in some circumstances, make interpretation of the photographs easier, it

destroys photometric relationships useful in slope determination, and frequently causes bright areas to print as a gray tone.

As mentioned in the previous section, Langley Research Center prepares GRE film records from playback of the magnetic-tape video record. These films are used for the hand reassembly from which negatives for print production are prepared. Dodging techniques such as the Fluoro-Dodger or LogEtronics printer are not used. Rather, the image enhancement method described in Section 4.2.4. is used since multiple records could be made to enhance either or both ends of the density range.

In general, the prints prepared by the Langley Research Center were considered to be of better photographic quality with respect to tonal gradations. There appeared to be no significant difference in resolution or sharpness of detail. Prints from both sources are characteristically of high contrast, which may well be related to the complete readout and reconstruction system.

### 4.3 APOLLO SITES

Five of the lunar areas that have been designated as potential landing sites for the Apollo program were selected for additional photography on Mission V as one of the specified tasks. The scheduled photography was planned to provide all three types of photography—vertical, oblique, and telephoto convergent stereo—at each of the eight candidate Apollo sites. Mission V was to complete the desired coverages.

Although each single- or multiple-frame sequence exposed on Mission V has been designated as a “site,” those pertaining to a single Apollo candidate landing site have been grouped together for the purpose of discussion and evaluation. Thus, in this section two to four Mission V sites are considered grouped with respect to the Apollo site covered.

#### 4.3.1 General Characteristics

As a whole, photography of the candidate Apollo sites on Mission V was satisfactory. Since the sites are within mare areas, the topography is generally quite flat with few large features that present photographic problems of large areas

having a wide luminance range due to the geometrical relationships. Luminance extremes are, however, present as a result of small-scale roughness, primarily smaller steep-walled craters. These craters contain hard shadow on one side and very bright slopes on the opposite sunward side. Detail is always lost in hard shadow and on bright slopes where the system luminance limitation is exceeded. However, although most interior detail is lost, the high contrast enhances small-crater definition and assists in evaluating small-scale surface roughness. Exposure of the photographs was selected on the basis of an assumed level surface; as a result, general exposure was satisfactory.

The oblique photographs, taken in a westerly direction to provide a view similar to that which the Apollo astronaut will have during his approach, presented a special problem. In each case, the wide-angle field of view included the zero-phase point, that point at which the Sun's rays and line-of-sight coincide. This point, corresponding to full Moon illumination, attains maximum luminance; thus, this point and the area within a few angular degrees surrounding it will invariably be overexposed. Further, also because of the dependence of luminance on the geometrical relationships of illumination, observation, and lunar photometric characteristics, the foreground areas will have lower luminance and thus tend toward underexposure. For the oblique photographs, the camera was oriented to place the zero-phase point closer to the frame edge so that the camera axis corresponded to the area of most suitable luminance for acceptable exposure. These considerations also affected choice of the photo orbit because the camera axis was to be directed at the target as well. Thus, it was inescapable that the oblique photographs would have areas overexposed and with no detail, and part of the wide-angle frame quite underexposed. The telephoto frames also show the effects of the luminance variation, but because of the narrower field of view, do not include the extremes. Consequently, while the exposure varies across the frame, surface detail is present in most, if not all, of the frame.

Resolution appeared to be uniformly good with

few exceptions. On the basis of GRE film sampling, resolution appeared to be well within system specifications, although precise measurements were not made.

A detailed analysis of the coverage obtained for the telephoto convergent stereo has not been made nor has an attempt been made to evaluate stereo quality.

#### 4.3.2 Individual Apollo Sites

Photography of each candidate Apollo landing site photographed on Mission V is discussed below. These sites and the corresponding Mission V site designations are:

Apollo Site	Mission V Sites
IP-1	V-3.1, -6, -8a, -8b
IIP-2	V-9.1, -11a, -11b
IIP-6	V-13, -16a, -16b
IIP-8	V-27a, -27b
IIIP-11	V-42a, -42b

##### 4.3.2.1 Sites V-3.1, -6, -8a, -8b (Apollo Site IP-1)

Photography of this Apollo site included two separate single-exposure obliques and two four-frame sequences to provide convergent telephoto stereo. Albedo distribution for the site, as provided by the USGS, is shown in Figure 4-4 plotted as a histogram in terms of percent of the site area for the albedo ranges shown. The albedo recommended for exposure prediction and the value used for QUAL computations of

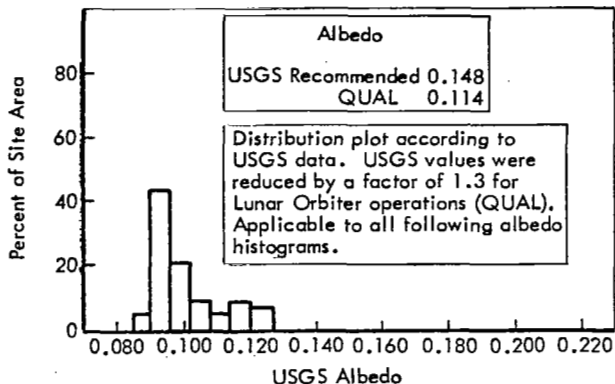


Figure 4-4: Albedo Distribution for Apollo Site IP-1

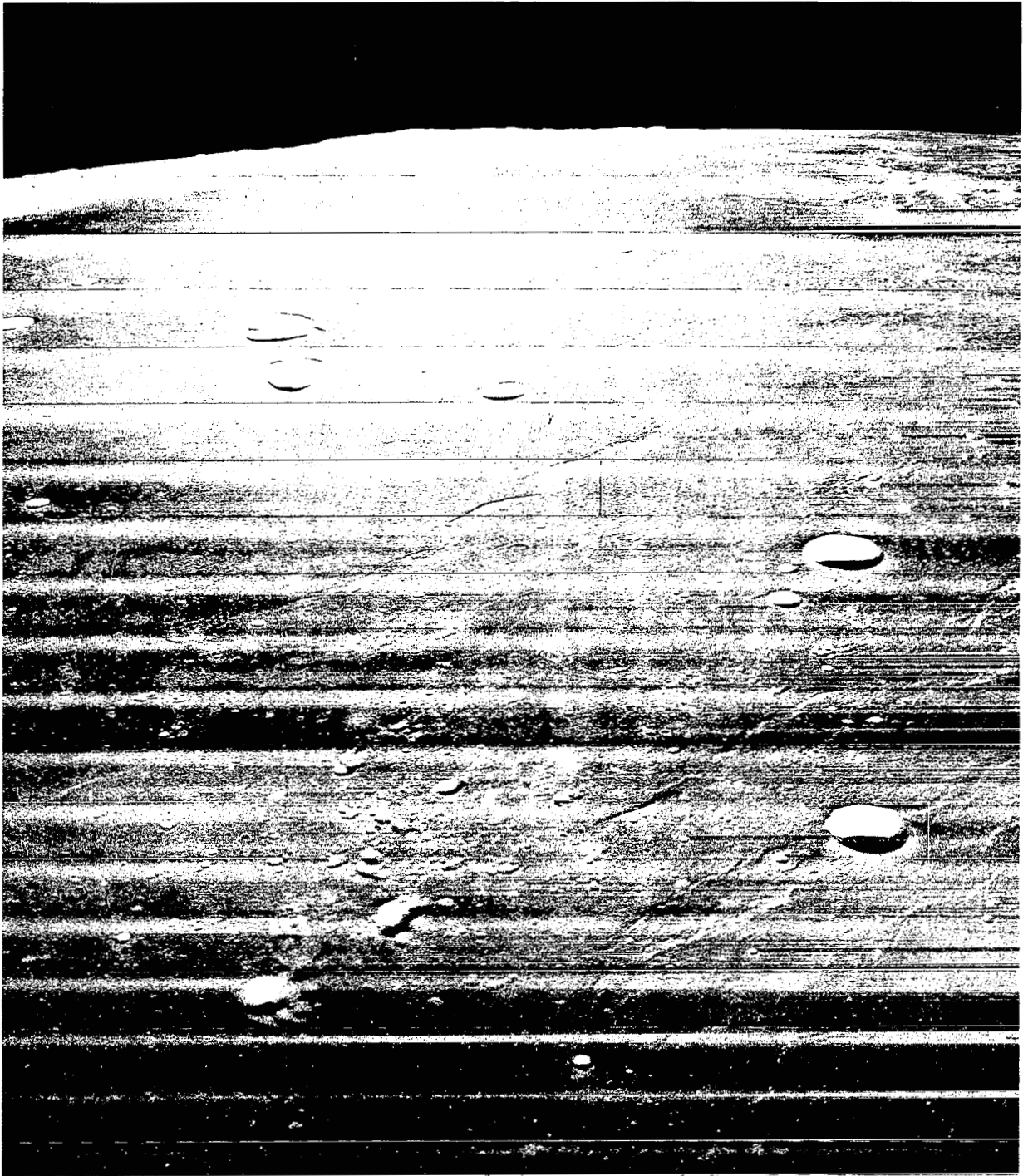
predicted image densities are shown. Additional photographic parameters are listed below in Table 4-1.

Both westerly obliques (Sites V-3.1 and V-6) include the zero-phase point with the camera oriented to place this point near the horizon so that the best illumination and exposure are near the principal point, as may be seen in Figure 4-5 showing the wide-angle frame of Site V-3.1. In each case overexposure occurs near zero-phase as expected. This effect is increased in the case of Site V-6, taken farther west than V-3.1, since the zero-phase is located in upland terrain having more sunward sloped areas and higher albedo. The zero-phase point is not included within the telephoto field of view, but the luminance variation within the frame is very apparent. Exposure of the central part is satisfactory.

Resolution of the Site V-3.1 telephoto frame appeared to be somewhat poorer than that of

Table 4-1: Principal Parameters of Apollo Site IP-1 Photography

Mission V Site No.	Frame Numbers	Phase Angle (deg)	$\alpha$ (deg)	Shutter Speed (sec)	Altitude (km)	Type
V-3.1	38	8.66	+64.6	0.01	98.9	W. Oblique
V-6	42	17.4	+54.7	0.01	96.5	W. Oblique
V-8a	44 - 47	62.9	+ 5.8	0.02	96.9	Stereo
V-8b	48 - 51	92.4	-25.3	0.04	96.8	Stereo



Wide-Angle Frame 38 showing effect of the lunar photometric characteristics on scene luminance.

**Figure 4-5: Site V-3.1, Apollo Site IP-1; Westerly Oblique**

V-6. However, the V/H sensor was not used for the former, so a slight image smear was inevitable. The wide-angle photograph was found to have a resolution of three to four scan lines.

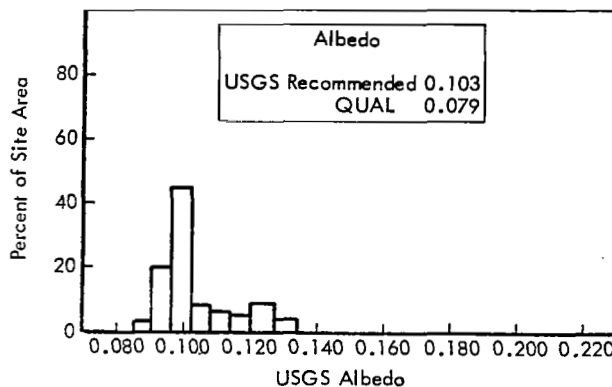
Site V-3.1 includes Messier in the wide-angle frame but not in the telephoto.

Sites V-8a and -8b were taken to provide convergent telephoto stereo coverage of the Apollo site. The two four-frame sequences were taken on successive orbits (Orbits 26 and 27). Exposure of both sequences is satisfactory and the photographs show very good detail. Evaluation of the GRE record indicated that exposure of V-8b was a little better than for V-8a. As seen in Table 4-1, the illumination and observation geometry for each sequence is quite different, but good photographs were obtained in each case. Resolution equivalent to three scan lines was observed. Excellent detail is present on the interior slope of a larger crater included in Telephoto Frame 50.

No attempt has been made to evaluate stereo quality because of limitations on time and availability of instruments.

**4.3.2.2 Sites V-9.1, -11a, -11b (Apollo Site IIP-2)**  
Photography of this potential Apollo landing site included a single westerly oblique and two four-frame sequences taken for convergent telephoto stereo coverage. The area previously was photographed on Missions II and III as Sites IIP-2 and IIP-1, respectively. The site is centered at approximately 34.2°E longitude, 2.5°N latitude.

Principal photographic parameters are listed in Table 4-2, and Figure 4-6 showing the albedo distribution.



**Figure 4-6: Albedo Distribution for Apollo Site IIP-2**

Site V-9.1 was taken as a westerly oblique providing a view similar to that which an astronaut will see during his approach to landing. The photographs thus present information regarding suitable landmarks for guidance and site recognition as they will appear during this critical period.

The wide-angle photograph of Site V-9.1 includes the zero-phase point and, as a consequence, includes a wide luminance range. However, the area of maximum luminance occurs near the horizon toward the edge of the frame. Exposure was optimized for the area near the camera axis; thus, because of the geometrically dependent luminance, the foreground appears underexposed and dark. The telephoto frame of the oblique shows generally satisfac-

**Table 4-2: Apollo Site IIP-2 Principal Photographic Parameters**

Mission V Site No.	Frame Numbers	Phase Angle (deg)	$\alpha$ (deg)	Shutter Speed (sec)	Altitude (km)	Type
V-9.1	52	16.9	+55.6	0.01	97	W. Oblique
V-11a	55 - 58	60.8	+ 8.1	0.02	96.8	Stereo
V-11b	59 - 62	91.4	-23.8	0.04	96.1	Stereo

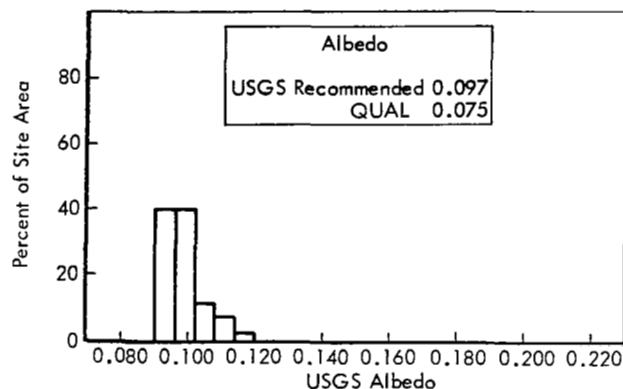
tory exposure although the unavoidable variation in luminance is apparent as an exposure difference over the frame length. Resolution of both wide-angle and telephoto frames was good. Surface feature details spanning as few as four scan lines were observed.

Sites V-11a and -11b provide contiguous telephoto convergent stereo coverage of the proposed Apollo landing site. Both sequences appear to be exposed satisfactorily, although slightly less than optimum. The GRE film record, particularly the telephoto frames of the first sequence, are a little more dense than optimum (density about 1.5 to 1.8). However, surface detail is shown very well in the reassembled prints. Because of the trend toward less than normal exposure, detail can be seen on some sunward crater interiors but without loss of detail on the general mare surface. The frames of the second sequence, V-11b, received more exposure than the first; hence, the GRE densities are less. Wide-angle average density was about 0.8; telephoto, about 1.1.

Resolution of both wide-angle and telephoto frames of both sequences was excellent. Detail spanning three to five scan lines was observed in frames of V-11a while resolution in photographs of V-11b were consistently about three scan lines.

**4.3.2.3 Sites V-13, -16a, -16b (Apollo Site IIP-6)**  
Photography of the potential Apollo landing site, Site IIP-6, was similar to that for Site IIP-2. A single westerly oblique and two four-frame sequences for contiguous convergent telephoto

stereo coverage were taken. This area, previously photographed as Sites IP-3, IIP-6, and IIIP-5, is located at approximately 23.8°E longitude, 0.6°N latitude. The principal photographic parameters are listed in Table 4-3 and Figure 4-7.



**Figure 4-7: Albedo Distribution for Apollo Site IIP-6**

The photographs taken as Site V-13 are typical of westerly obliques that include the zero-phase point. A very wide luminance range occurs within the wide-angle field of view, and the luminance range in the telephoto frame is very apparent. Good exposure occurs near the center of the frame, with greater exposure toward the zero-phase point and less exposure in the foreground. The telephoto frame of V-13 shows the luminance variation but the general exposure does not exceed system density limits, although the foreground approaches the minimum. Detail is good and resolution of about three scan lines was observed in the telephoto and five scan lines in the wide-angle photographs near the frame centers.

**Table 4-3: Apollo Site IIP-6 Principal Photographic Parameters**

Mission V Site No.	Frame Numbers	Phase Angle (deg)	$\alpha$ (deg)	Shutter Speed (sec)	Altitude (km)	Type
V-13	64	18.4	+55.0	0.01	96.4	W. Oblique
V-16a	71 - 74	66.5	+ 3.5	0.02	95.4	Stereo
V-16b	75 - 78	95.8	-27.5	0.04	95.9	Stereo

Photography of V-16a and -16b for convergent telephoto stereo is of satisfactory quality. The exposure for the first sequence appears to be less than optimum, although surface detail in the photographs is good. GRE film densities for this sequence were found to average about 1.4 for wide angle and about 1.7 for telephoto. The second sequence (V-16b) had more optimum exposure and is of better quality in this respect. GRE film densities averaged about 1.2 for telephoto frames and about 1.0 for wide angle. Resolution of both wide-angle and telephoto frames of both sequences was very good, with detail spanning three to four scan lines observed in all frames examined.

The photographs in this group were affected by lace processing defect to some extent. Both the wide-angle and telephoto frames of V-13 were significantly degraded by this defect.

#### 4.3.2.4 Sites V-27a and -27b (Apollo Site IIP-8)

This potential Apollo landing site was photographed during two successive orbits with four-frame sequences for contiguous telephoto convergent stereo coverage. The westerly oblique of this area was taken previously as Sites IP-5, IIP-8, and IIP-7. Principal parameters for Mission V photography are listed in Table 4-4 and Figure 4-8.

The area photographed is almost entirely mare-type but with some low hills. A wrinkle ridge and at least one low dome are within the site and there are clusters of secondary craters. Exposure of both sequences is satisfactory, but that for the second sequence is more nearly optimum than the first. GRE film densities of the first sequence averaged about 1.6 for the telephoto frames and about 1.4 for the wide angle. On the

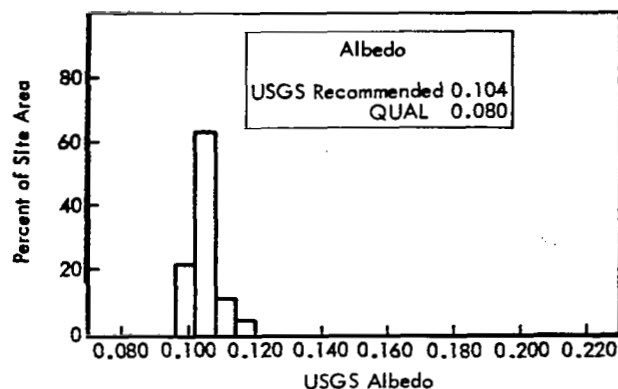


Figure 4-8: Albedo Distribution for Apollo Site IIP-8

second sequence, telephoto frames averaged about 1.1 density, the wide angle, 0.8. While the higher densities of the GRE record for the first sequence make examination of this film more difficult, good detail is present in the paper prints of reassembled photographs of both sequences. Resolution of photographs from both sequences is adequate to show details spanning three to four scan lines on all frames examined. No lace processing defects were present on the photographs of either sequence.

#### 4.3.2.5 Sites V-42a and -42b (Apollo Site IIP-11)

This potential Apollo landing site was also photographed by four-frame sequences on two successive orbits to provide contiguous telephoto convergent stereo coverage. The area, at approximately 36.2°W longitude, 3.5°S latitude, had been photographed previously as Site IP-8.1 as well as IIP-11, but telephoto convergent stereo had not been acquired.

The area is entirely within mare area, but includes a part of the prominent system of wrinkle

Table 4-4: Apollo Site IIP-8 Principal Photographic Parameters

Site Number	Frame Number	Phase Angle (deg)	$\alpha$ (deg)	Shutter Speed (sec)	Altitude (km)
V-27a	108 - 111	61.5	+10.7	0.02	97.5
V-27b	112 - 115	91.4	-20.8	0.04	96.6



ridges northwest of the Flamsteed region. In addition to the ridges, the mare surface has been modified by ray structure and clusters of secondary impact craters. The albedo range, however, is unusually narrow and of a low value as shown in Figure 4-9.

Principal photographic parameters for the site are listed in Table 4-5.

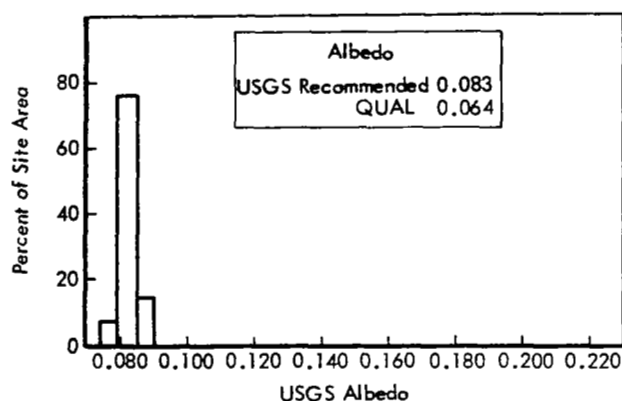


Figure 4-9: Albedo Distribution for Apollo Site IIP-11

Both the wide-angle and telephoto photographs are satisfactory. The paper prints show very good detail, although the GRE film density is slightly higher than optimum. The center-frame density averaged about 1.2 for the wide-angle and 1.4 for the telephoto frames of the first sequence (V-42a). On the second sequence, both telephoto and wide-angle frames appeared to average near 1.4. The photographs show the wrinkle ridges in excellent detail. The telephoto frames show detail on ridge slopes and the dome-like area associated with the ridges;

very few areas exceed the luminance range limit.

Resolution of all photographs of the two sequences appeared to be excellent, with features spanning only three to four scan lines observed. Detail is sharp and very small craters are well defined.

Some processing defects appear on photographs of both sequences, but since they are almost all of the small "freckle" type, little information is obscured.

Since both sequences were taken in the fast sequencing mode, stereo coverage was obtained by both forward overlap and convergent coverage in the wide-angle photographs.

#### 4.4 SCIENCE AND APOLLO APPLICATIONS PROGRAM (AAP) SITES

Mission V Tasks 4 and 5 required photography of scientifically interesting areas. Sites selected for each of these two tasks differed only in that those for Task 4 had, in addition, landing potential for AAP. Because of the basic similarity in type of subject—scientific interest—the sites for Tasks 4 and 5 have not been grouped separately for discussion. The nature of the target features or areas has injected a far greater diversity in the photography and in photographic problems presented than in any of the previous four missions. For this reason, and because of the potentially great variety of applications for the photographs, the individual sites are discussed. Each site is considered in the order of photography during the mission.

Among the sites in this section, the following were designated as AAP.

Table 4-5: Apollo Site IIP-11 Principal Photographic Parameters

Mission V Site No.	Frame Numbers	Phase Angle (deg)	$\alpha$ (deg)	Shutter Speed (sec)	Altitude (km)
V-42a	169 - 172	67.08	+ 8.05	0.04	103
V-42b	173 - 176	92.57	-18.90	0.04	103



V-14	Littrow rilles
V-15.1	Dawes
V-18	Dionysius
V-21	South of Alexander
V-22	Sulpicius Gallus rilles
V-23.2	Hyginus rilles
V-28	Alphonsus
V-33	Area of Copernicus CD
V-34	Fra Mauro
V-35	Copernicus secondary craters
V-37	Copernicus
V-38	Imbrium flows
V-40	Tobias Mayer dome
V-45.1	Gruithuisen K and domes near Gruithuisen
V-50	Aristarchus Plateau
V-51	Marius Hills

#### 4.4.1 General Characteristics

The principal characteristic of the science and AAP sites is, of course, the great variety of terrain and terrain features that were photographed. Such variety has a direct bearing on photographic quality because of the close relationship of topographic variation, surface properties, illumination, and characteristics of the complete photographic system, including both spacecraft and ground components. A photograph is, simply, a representation of luminance variations existing on a surface within the field of view of an optical system. Judgment of photographic quality basically is an assessment of the fidelity with which detail of those variations is presumed to be represented, consideration being given to known limitations.

Based on those factors specifically related to the individual sites, photography of this group is considered to be of overall high quality. As expected, luminance extremes ranging from very bright, steep, sunward slopes to hard shadow or deeply shaded areas — well beyond reproduction limitations of the system — occurred within most individual frames. However, areas within acceptable luminance range were satisfactorily represented. Where exposure was optimized for certain features, occasionally at the expense of others, the target was shown with acceptable quality.

Targeting of the photograph appeared to be very satisfactory, bringing critical target features

within the narrow telephoto field of view. Camera aiming precision is exemplified by the photography of Aristarchus, Site V-48, for which the spacecraft altitude was such that the crater image was very nearly the same size as the long axis of the telephoto frame. Virtually none of the crater rim was lost in the telephoto frames because of pointing error.

Because photographic quality is quite site-dependent, reference should be made to the discussion of individual sites.

#### 4.4.2 Individual Sites

Individual-site photography is discussed in the following sections. A brief description of each site and the reasons for its inclusion in the mission photography are given as a basis for judging photographic quality and success in fulfilling the assigned task.

##### 4.4.2.1 Site V-1, Petavius

*Location: 60.67°E longitude, 25.70°S latitude*

*Altitude: 142.4 km Frames: 33 to 36*

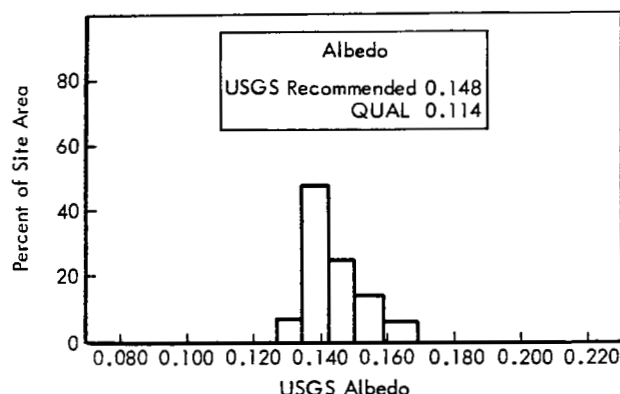
*Phase angle: 75.5 degrees Alpha: -3.70 degrees*

*QUAL Albedo: 0.114 Shutter speed: 0.02 second*

The target feature was the central peak of this relatively old crater. The floor of the crater and the central peak are intersected by rilles. The site was chosen to provide information on structure of the central peak—possibly deep strata—where it is intersected by the rille. It was thought that beds might be exposed in the rilles.

The site was photographed with a four-frame sequence taken in the fast mode, providing contiguous telephoto coverage. The sequence was well centered to cover the central part of the crater.

Exposure was based on a corrected albedo of 0.114, equivalent to a USGS value of 0.148 (see Figure 4-10), to optimize on the crater floor, with some bias toward the brighter slopes. GRE film densities over most of the area were well within the acceptable limits. However, the rather rugged nature of the central peak area resulted in a wide luminance range. Limited areas of steeper sunward slopes are overexposed and most detail is lost there (Figure 4-11).



**Figure 4-10: Albedo Distribution for Site V-1, Petavius**

The telephoto frames are of good quality, although hard shadows and some areas of steeper bright slopes on the central peaks have resulted in loss of information. The narrower field of view of the telephoto lens (thus, larger image) results in a greater proportion of the frames so affected.

Very good detail is shown in all areas where slopes have not produced luminance extremes. The location where the large rille intersects the central peak is partially obscured by hard shadow, but sections of the rille walls are well shown (Figure 4-12). The area shown in Figure 4-12 is outlined in Figure 4-11. Much information of geological significance is present.

Detail in the photographs is excellent. In all frames examined in the form of GRE-reconstructed record, surface details spanning only three lines were observed by microscope.

#### 4.4.2.2 Site V-2.1, Petavius B

*Location: 57.14°E longitude, 19.05°S latitude*

*Altitude: 122.8 km Frame: 37*

*Phase angle: 67.3 degrees Alpha: +3.58 degrees*

*QUAL Albedo: 0.105 Shutter speed: 0.02 second*

Petavius B is a crater approximately 33 kilometers in diameter located in terra bordering the eastern part of Mare Fecunditatis. Rays originating from this crater have a pie-shaped, occluded sector toward the north. One of the purposes of photographing this area was to provide information suitable for investigating the cause of occlusion in the ray pattern.

The site was photographed by a single frame. The camera axis was pointed approximately one crater radius (16 to 17 kilometers) north of the crater rim. With this positioning, the south rim of the crater was just out of the field of view of the wide-angle camera, but the north rim and the occluded sector of the ray pattern are included. The crater rim is out of the telephoto camera field of view, but part of the ejecta blanket on the outer rim is included.

Exposure selection appears to be very good. Areas more nearly level are well exposed. The northern interior slope of the crater and its floor are shown in good detail, but the western sunward slope had too high a luminance and is overexposed. The ejecta pattern on the outer rim, including the dune-like topography, is very well shown. The outer rim area included within the telephoto frame is relatively flat on a large scale, although some rounded hills are included within the western end of the frame; thus, there are no large areas of hard shadow. The eastern end of the telephoto frame includes part of a cluster of secondary craters possibly associated with Petavius B; here, there is more small-scale roughness and associated smaller areas of hard shadow and high luminance within the many small craters.

Exposure selection presented some problem because of the rather wide range of albedo resulting from inclusion of both mare area and the bright rays on terra. As may be seen in the albedo distribution histogram, Figure 4-13, there is no markedly predominant albedo. Exposure was therefore based on a near-average value for the site.

Resolution of both wide-angle and telephoto frames was excellent, with surface detail to only three scan lines observed.

#### 4.4.2.3 Site V-4 Stevinus A

*Location: 51.50°E longitude, 31.50°S latitude*

*Altitude: 162.0 km Frame: 40*

*Phase angle: 83.6 degrees Alpha: -10.1 degrees*

*QUAL Albedo: 0.158 Shutter speed: 0.02 second*

Crater Stevinus A, approximately 9 kilometers in diameter, is located in the southern highlands



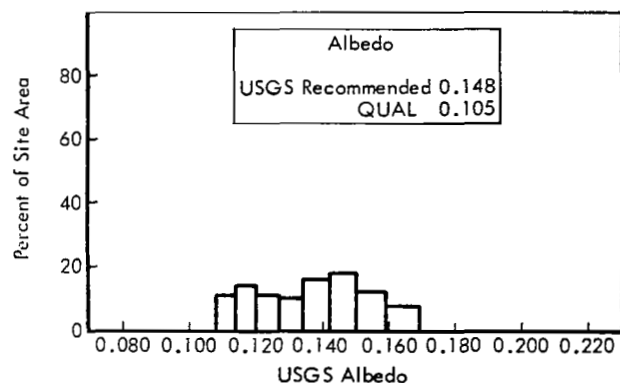
Wide-Angle Frame 35, third of a sequence of four, showing rille system of crater. Area outlined shown in Figure 4-12.

**Figure 4-11: Site V-1, Petavius; Wide Angle**



A portion of Telephoto Frame 34 showing detail of inner slope of rille intersecting central peaks. Tracks of rolling rocks can be seen. Reproduced at GRE film scale.

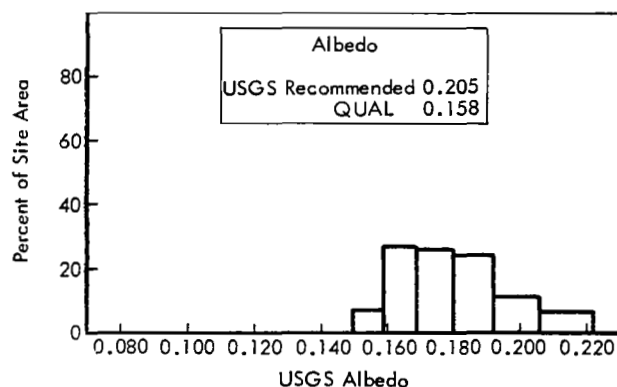
**Figure 4-12: Site V-1, Petavius; Telephoto**



**Figure 4-13: Albedo Distribution for Site V-2.1, Petavius B**

on the east limb, slightly west of the much larger crater Stevinus. The upland terrain in this region is heavily cratered. Stevinus A is considered to be relatively young because of its associated bright ray system. At eclipse, the crater displays a high thermal anomaly. Stevinus A was photographed to obtain additional information on the cratering process as well as differences in such a process that might be related to upland terrain. Possible characteristics that may be related to its thermally anomalous behavior were of additional interest.

An exposure time of 0.02 second was used for the single-frame photograph of this site. The exposure was made from an altitude of approximately 162 kilometers. Although the scene had a wide luminance range, the exposure produced good image quality in both the wide-angle and telephoto frames. A histogram of the albedo distribution for this site is shown in Figure 4-14.



**Figure 4-14: Albedo Distribution for Site V-4, Stevinus A**

Stevinus A appears in the southwest corner of the wide-angle photograph outside the telephoto lens field of view. Crater structure is well defined, and detail is particularly good where illumination and surface geometry were favorably combined for photography. The crater wall, which is very abrupt and topped by a sharply edged rim, is very well defined. Very fine detail is present in the ejecta blanket near the center of the photograph (Figure 4-15). Overall resolution is very good in the wide-angle frame. Craters spanning as few as three scan lines can be detected.

The telephoto frame first gives the impression of being smeared. However, closer examination reveals that the smeared appearance is caused by surface characteristics of the ejecta blanket which may be related to the blast effect at the time Stevinus A was formed. Inspection of diffused areas in the photograph reveals the presence of many small, well-defined craters, indicating satisfactory resolution. This is an excellent photographic record of ejecta characteristics and surface features associated with the formation of this crater. This may be seen in Figure 4-16.

#### 4.4.2.4 Site V-5.1, Messier and Messier A

*Location: 47.24°E longitude, 2.03°S latitude*

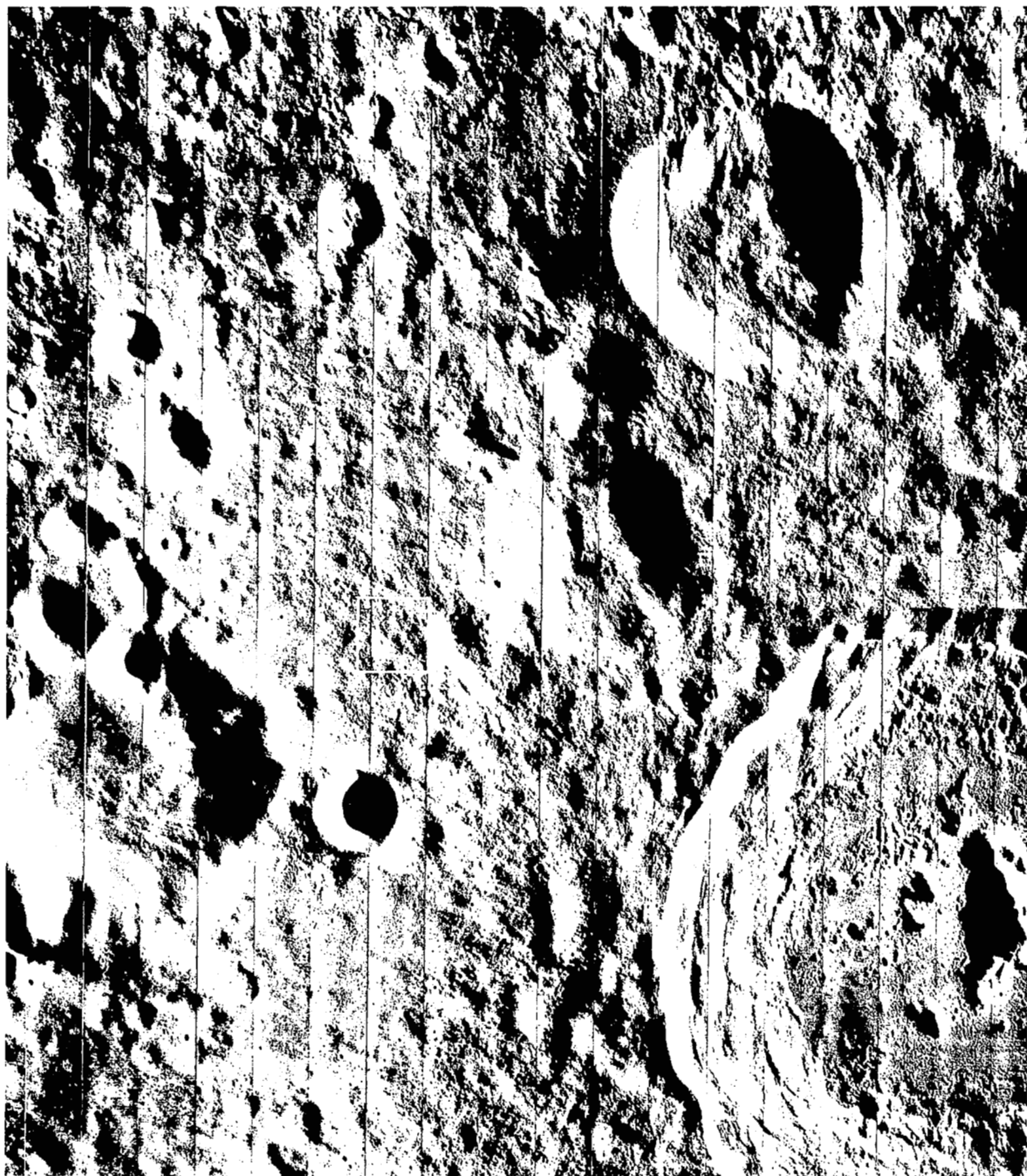
*Altitude: 98.3 km Frame: 41*

*Phase angle: 15.90 degrees*

*Alpha: +55.24 degrees QUAL Albedo: 0.077*

*Shutter speed: 0.01 second*

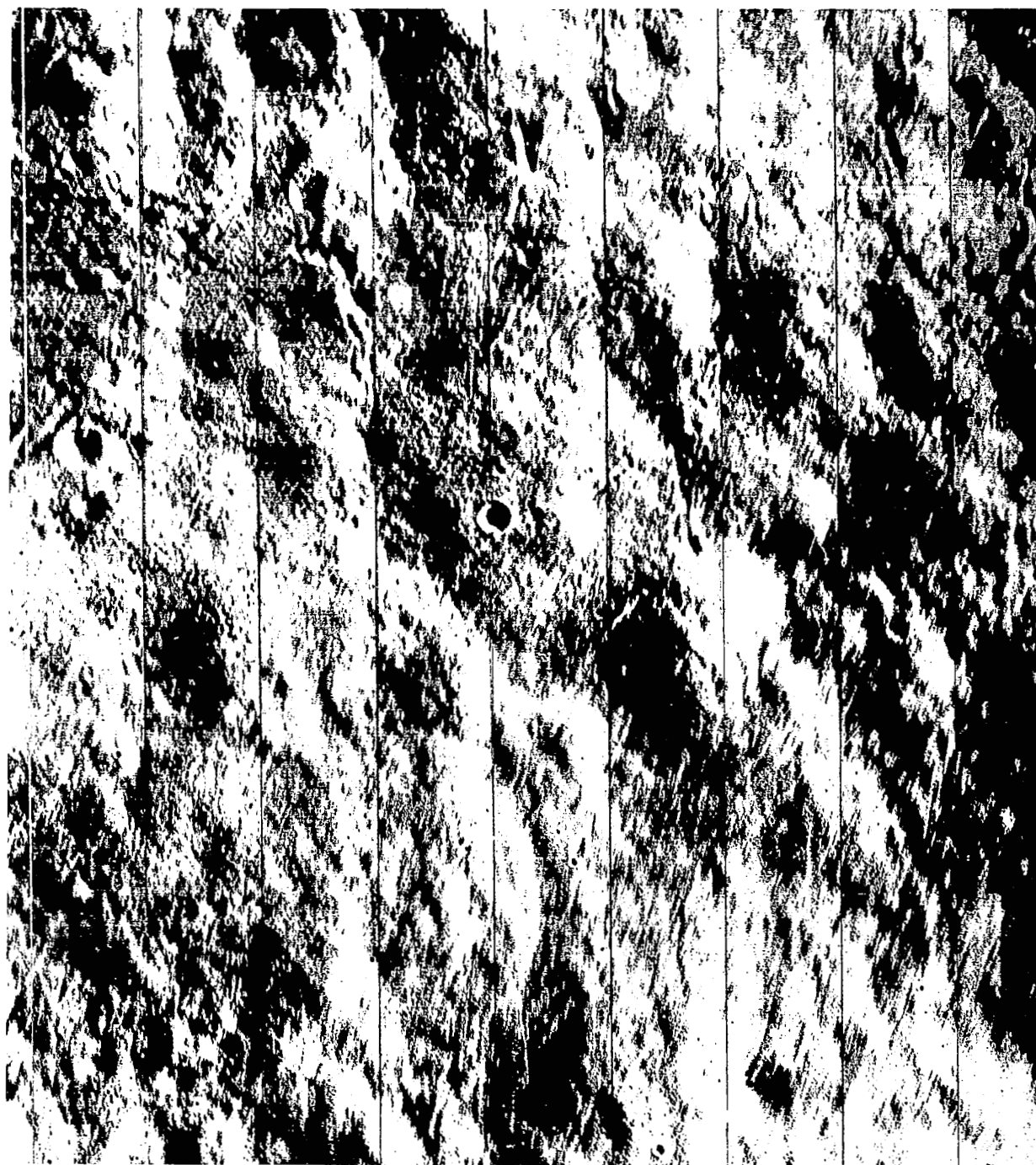
Site V-5.1 was selected to investigate these unusual—if not unique—craters. Messier has a nearly perfect elliptical outline and little evidence of a ray structure, although it does have a raised rim. Messier A just to the west appeared, by telescopic observation, to be a double crater. Mission IV photography revealed that Messier A was a round crater superimposed on another possibly originally elliptical crater such as Messier. Two long, well-defined rays extend west from Messier A. Mission IV also revealed unusual marking or streaks on the floor of Messier. Information leading to understanding of the origin of the craters and their unusual asymmetry was the objective of this site photography.



Frame 40 showing detail of ejecta pattern from crater. Area outlined shown in Figure 4-16.

**Figure 4-15: Site V-4, Stevinus A; Wide Angle**





Note that the surface texture caused by the ejecta makes the photograph appear smeared, but small craters are sharp.

**Figure 4-16: Site V-4, Stevinus A; Telephoto Frame 40**

Both wide-angle and telephoto photography of this site are of excellent quality. The camera axis was tilted to provide an oblique view toward the west. Target features are nicely centered in the wide-angle frame and show the double rays leading off toward the distant horizon (Figure 4-17). Although the zero-phase point is within the wide-angle field of view, it is slightly above the horizon. Consequently, overexposure occurs only at the horizon; virtually all the visible surface is shown in good detail. Accurate camera pointing placed both craters within the field of view of the telephoto camera so that both crater interiors and outer rims may be studied in detail.

Exposure (based on a corrected albedo of 0.077, typical of a mare surface) is very good, particularly in the vicinity of the target craters. The oblique angle of photography resulted in a wide variation of photographic geometry within the frames; thus, the density predictions derived from the QUAL computer program were invaluable in shutter-speed selection. Although hard shadow occurs within the craters, the westerly direction of the view minimized the relative frame area obscured. Although some of the interior sunward slopes are overexposed, significant detail of the western interior slope of Messier A is shown in the telephoto frame. The telephoto frame also reveals much detail of unusual streaks on the floor of Messier (Figure 4-18).

Resolution of both telephoto and wide-angle photographs is very good. As in the Petavius B photographs, detail spanning only three scan lines on the GRE film was observed.

#### *4.4.2.5 Site V-10, Altai Scarp*

*Location: 27.90°E longitude, 27.70°S latitude*

*Altitude: 130.9 km Frame: 54*

*Phase angle: 33.85 degrees Alpha: +35.2 degrees*

*QUAL Albedo: 0.110 Shutter speed: 0.01 second*

The target feature is a major scarp having a general northwest-southeast orientation, with the face of the scarp toward the northeast. It is peripheral to Mare Nectaris. The purpose of photography was to provide data for investigation of possible bedding by revealing exposed strata or outcrops. In addition, information

regarding downward movement of material on the extensive steep slopes was desired.

The site was photographed as an oblique view, with the western horizon within the wide-angle field of view. The section of the scarp selected for photography included a portion oriented in a more east-west direction to provide most suitable illumination. It was apparent that, where slopes faced the Sun more directly, surface luminance would exceed the limit imposed by the photo subsystem and the desired information would be lost by overexposure. Oblique photography was chosen to enhance interpretation of the generally rough topography.

Photography of the site appears to be quite satisfactory. The camera was properly oriented to place a well-lighted section of the scarp within the telephoto field of view. The best detail of the scarp is shown on a section along the eastern edge of Rothmann G. This is very close to the center of the wide-angle frame and is included in the telephoto frame (Figure 4-19). Exposure of the photographs (based on an albedo of 0.110, typical of much terra) was satisfactory, although the GRE densities indicated a slight underexposure of the more nearly level areas. Because of the many steeper slopes, and particularly because the sunward scarp face was of principal interest, the faster shutter speed was the most suitable. The telephoto frame is of good quality and shows detail on the bright slopes (Figure 4-20). Additional detail on these slopes may possibly be revealed by the enhancement techniques employed at Langley Research Center in which the GRE gain is increased when preparing reconstructed records from the magnetic-tape video record.

Resolution of the wide-angle frame is very good, with features spanning three scan lines observed on the GRE film record examined. For this frame, the V/H sensor was not used because of the combination of camera tilt and orientation with respect to flight path. The absence of image motion compensation, therefore, resulted in some degradation of telephoto resolution. The smallest detail observed was approximately 10 to 15 scan lines, and some streaking or elongation of small craters could be detected.





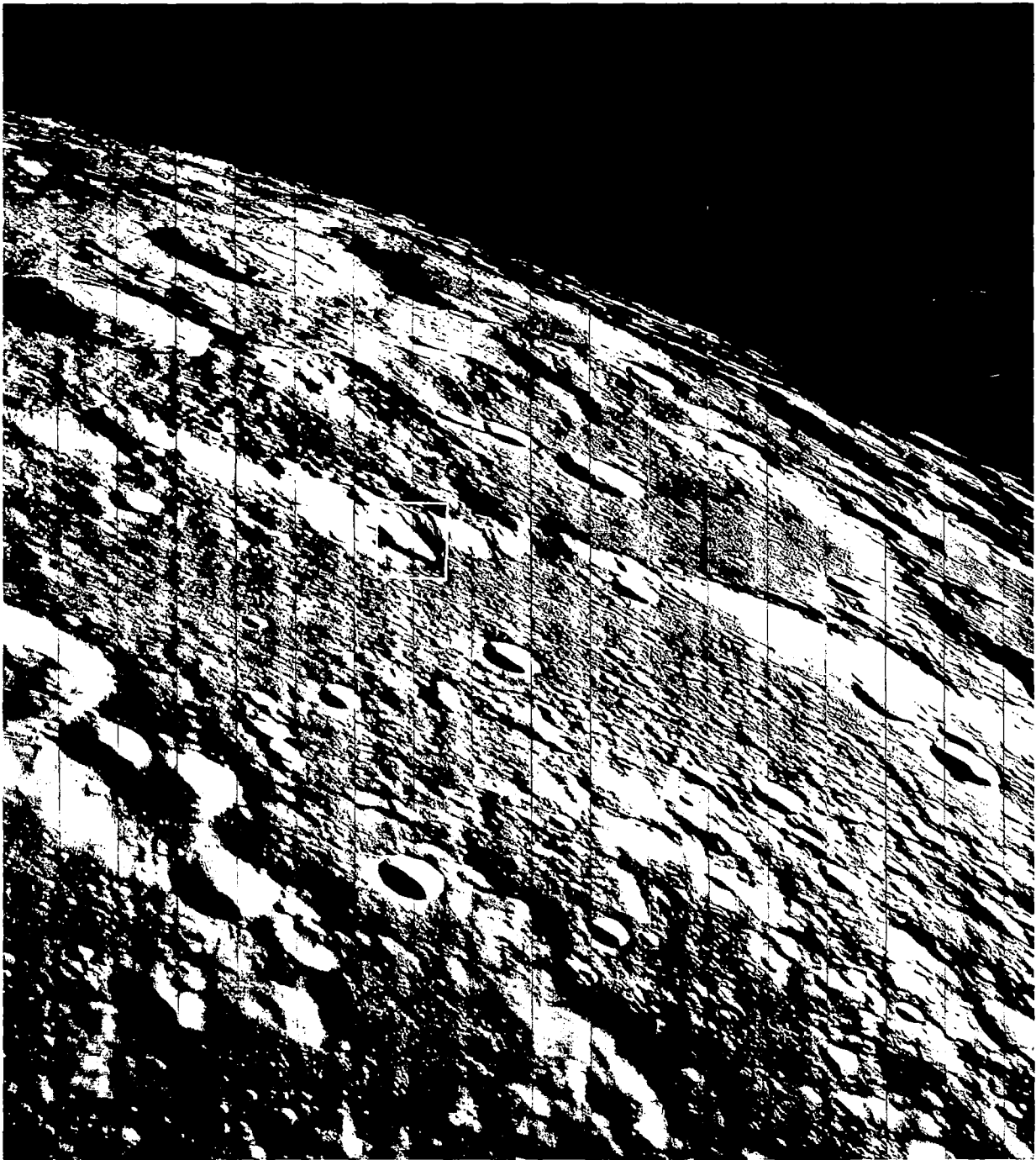
A portion of Wide Angle Frame 41, reproduced at GRE scale, showing Messier, Messier A, and the double rays. Oblique view toward west.

**Figure 4-17: Site V-5.1, Messier; Wide Angle**



A portion of the telephoto frame, reproduced at GRE scale, showing detail of crater floor and wall.

**Figure 4-18: Site V-5.1, Messier; Telephoto**



This is an oblique photograph looking southwest.

**Figure 4-19; Site V-10, Altai Scarp; Wide Angle**



This is a portion of **Frame 54** showing the area outlined in **Figure 4-19**. Note slope detail where orientation provides more nearly grazing illumination.

**Figure 4-20: Site V-10, Altai Scarp; Telephoto**

#### 4.4.2.6 Site V-12, Censorinus

*Location: 32.75°E longitude, 0.43°S latitude*

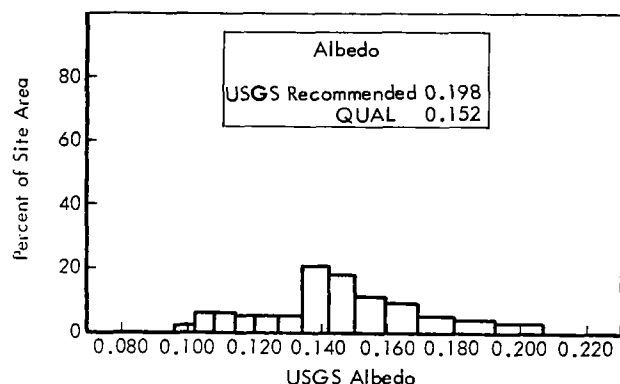
*Altitude: 95.9 km Frame: 63*

*Phase angle: 98.5 degrees Alpha: -31.0 degrees*

*QUAL Albedo: 0.152 Shutter speed: 0.02 second*

Censorinus is a small, bright crater located near the equator in upland terrain that is bordered by the Maria Nectaris, Tranquillitatis, and Fecunditatis. The crater is situated on a plateau of relatively uncratered material which extends to nearby Mare Tranquillitatis. Additional photographs of this site were desired to assist in establishing the feasibility of sampling exposed material in the Censorinus area by future ground missions. The geologic structure of this site is also of interest because of the thermal anomaly exhibited during eclipse.

The exposure selected for this site resulted in satisfactory photographs, although the high albedo of the crater and its associated bright rays together with shadow areas resulted in a wide luminance range. A histogram of the albedo characteristics is shown in Figure 4-21.



**Figure 4-21: Albedo Distribution for Site V-12, Censorinus**

Some loss of detail occurred in highlighted slopes and in deep shadows because the luminance range exceeded system limits (Figure 4-22). However, in both wide-angle and telephoto frames, considerable detail was recorded in the more subdued bright slopes. Very good detail was obtained for most of the site area.

Definition of small surface features is very good in the wide-angle and telephoto frames.

Small craters, rocks, and surface projections spanning as few as three scan lines may be discerned. Details of secondary craters and ejecta blanket are excellent in the 610-mm photograph, although some overexposure of the bright surface features near the crater was apparent (see Figure 4-23). Some loss of detail occurred because of processing lace; however, the lace does not seriously impair the significant portions of principal features in the photographs. The frames were well centered on the target. A few scattered video dropouts are noticeable in the telephoto frame. Spacecraft altitude for photography of this site was approximately 95.9 kilometers.

#### 4.4.2.7 Site V-14, Littrow Rilles

*Location: 29.31°E longitude, 21.78°N latitude*

*Altitude: 121.5 km. Frames: 66-69*

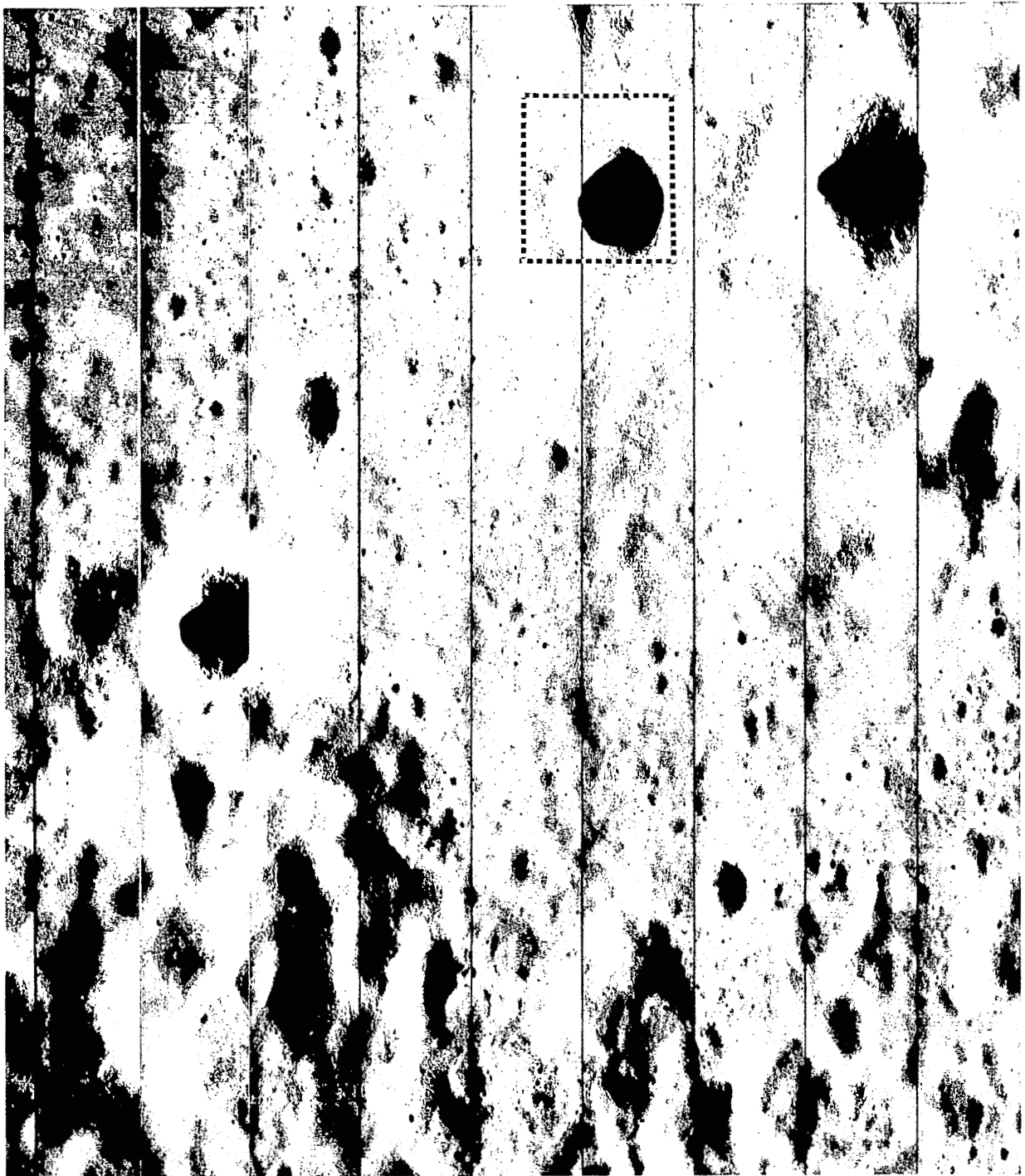
*Phase angle: 68.38 degrees Alpha: +0.37 degree*

*QUAL Albedo: 0.066 Shutter speed: 0.02 second*

The target area, one of the AAP sites, includes a complex of rilles that appears to be a part of the concentric system around the periphery of Mare Serenitatis. The Littrow rilles occur within an area of dark mare material but transect a small, brighter area of terra-like character. The mare area appears to be of two distinct domains differentiated by both albedo and density of small craters. In some places the border between the two mare regions is defined by an elevation change apparent by shadowing. A small but conspicuous braided wrinkle ridge is also present.

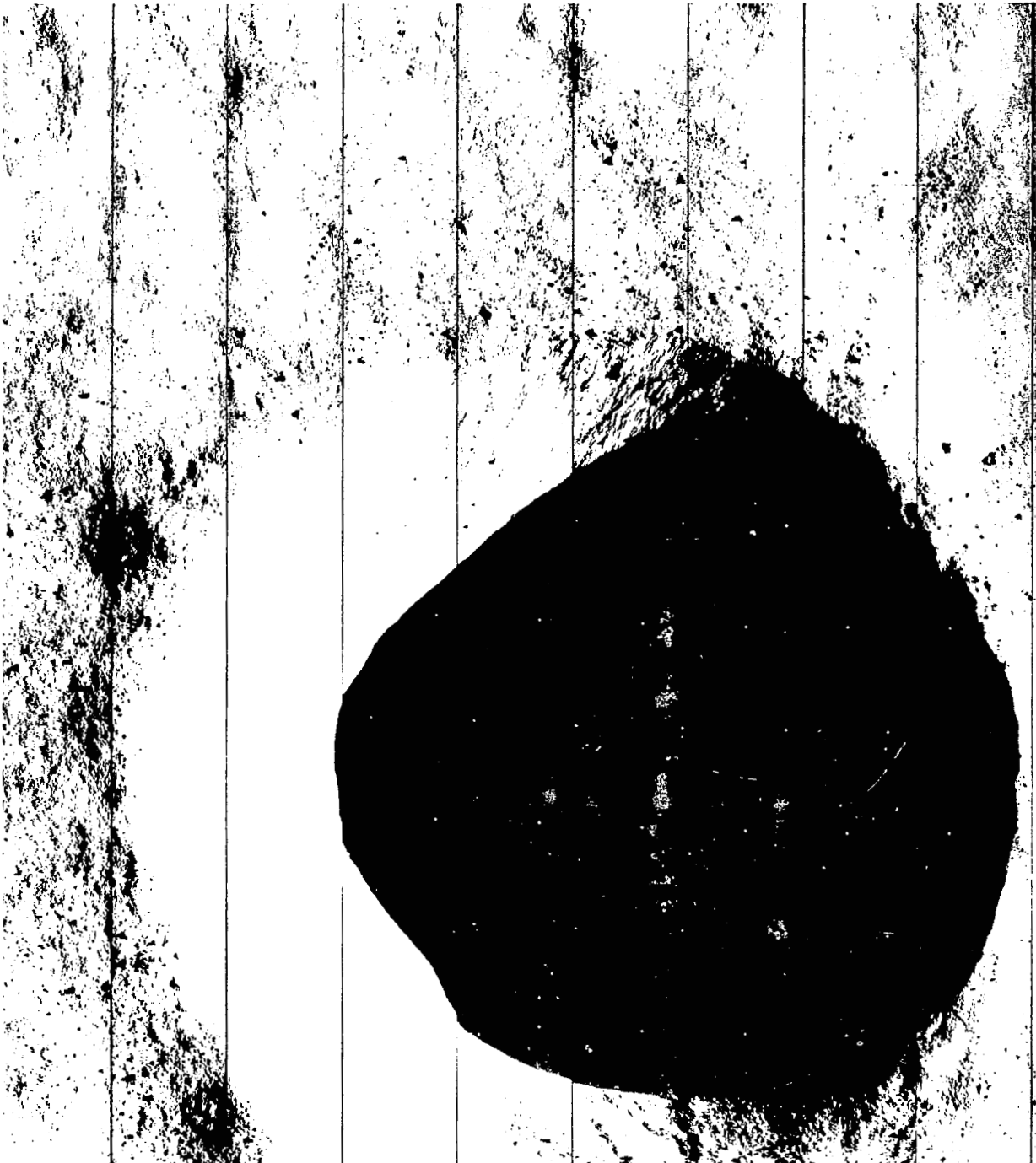
The two types of mare surface and the possible exposure of bedding by the rilles was of interest here, as well as investigation of the light-haloed craters (Littrow BA) just north of Littrow B. There has been some conjecture that Littrow BA was of volcanic origin which, if correct, would be very unusual for a light-haloed crater.

The target area was photographed by a four-frame sequence taken in the fast mode to provide contiguous telephoto coverage. Exposure was based on a corrected albedo of 0.066 to favor the darker mare surface (Figure 4-24) and rilles. Some overexposure of the area



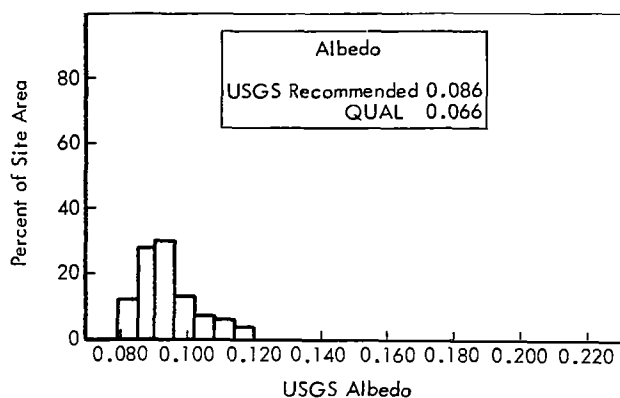
Portion of Wide-Angle Frame 63 including bright crater and ejecta pattern. Reproduced at GRE scale.

**Figure 4-22: Site V-12, Censorinus; Wide Angle**



Portion of Telephoto Frame 63 covering area outlined in Figure 4-22. This shows a very rare instance where light reflected from the sunward crater wall provides sufficient illumination to show detail on shadowed side.

**Figure 4-23: Site V-12, Censorinus; Telephoto**



**Figure 4-24: Albedo Distribution for Site V-14, Littrow Rilles**

around Littrow BA was anticipated.

Site photography quality was good to fair. Detail in the dark mare is well shown in the wide-angle photographs, although the density of the GRE film was slightly higher than desirable (Figure 4-25). The mare area in the telephoto frames was more underexposed, although detail is present in most areas of the darker mare. Good detail is present in the bright area surrounding Littrow BA, and on many of the illuminated inner slopes of the rilles (Figure 4-26). However, some of the slopes are overexposed, indicating a very large luminance range within the area.

Resolution near the center of both telephoto and wide-angle photographs was found to be good in spite of the general underexposure. Detail spanning three to four scan lines was observed on the GRE film.

The photographs of this sequence have been degraded by lace processing defects. Because of forward overlap of the wide-angle photographs, the processing defects do not obscure information derivable from these frames. Where processing defects occur on the telephoto frames, lack of overlap prevents recovery of data in the limited areas affected. Since the defect is mostly of the "freckle" type, the individual spots are small. The occurrence of defective processing may make interpretation and use of the photographs more difficult.

#### 4.4.2.8 Site V-15.1, Dawes

*Location: 26.36°E longitude, 17.19°N latitude*

*Altitude: 110.9 km Frame: 70*

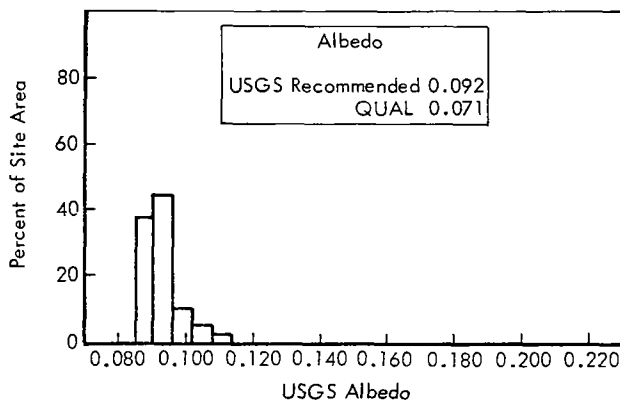
*Phase angle: 57.13 degrees*

*Alpha: +12.40 degrees QUAL Albedo: 0.071*

*Shutter speed: 0.02 second*

This site is included in the AAP group. Dawes, a crater about 18 kilometers in diameter, is of interest because of several unusual characteristics. It has one of the greatest thermal anomalies at eclipse observed by Shorthill and Saari, and although Mission IV photography showed it to have characteristics of a fresh crater, it does not have the bright rays typical of fresh craters and those having a thermal anomaly. A high thermal anomaly and no bright rays seems inconsistent. More detailed information suitable for diagnosis of the crater's origin was desired.

The site was photographed with a single frame exposure. The albedo is about average for mare surface; the USGS recommended value was 0.092 (0.071 corrected) as shown as the albedo histogram in Figure 4-27. Exposure was in-

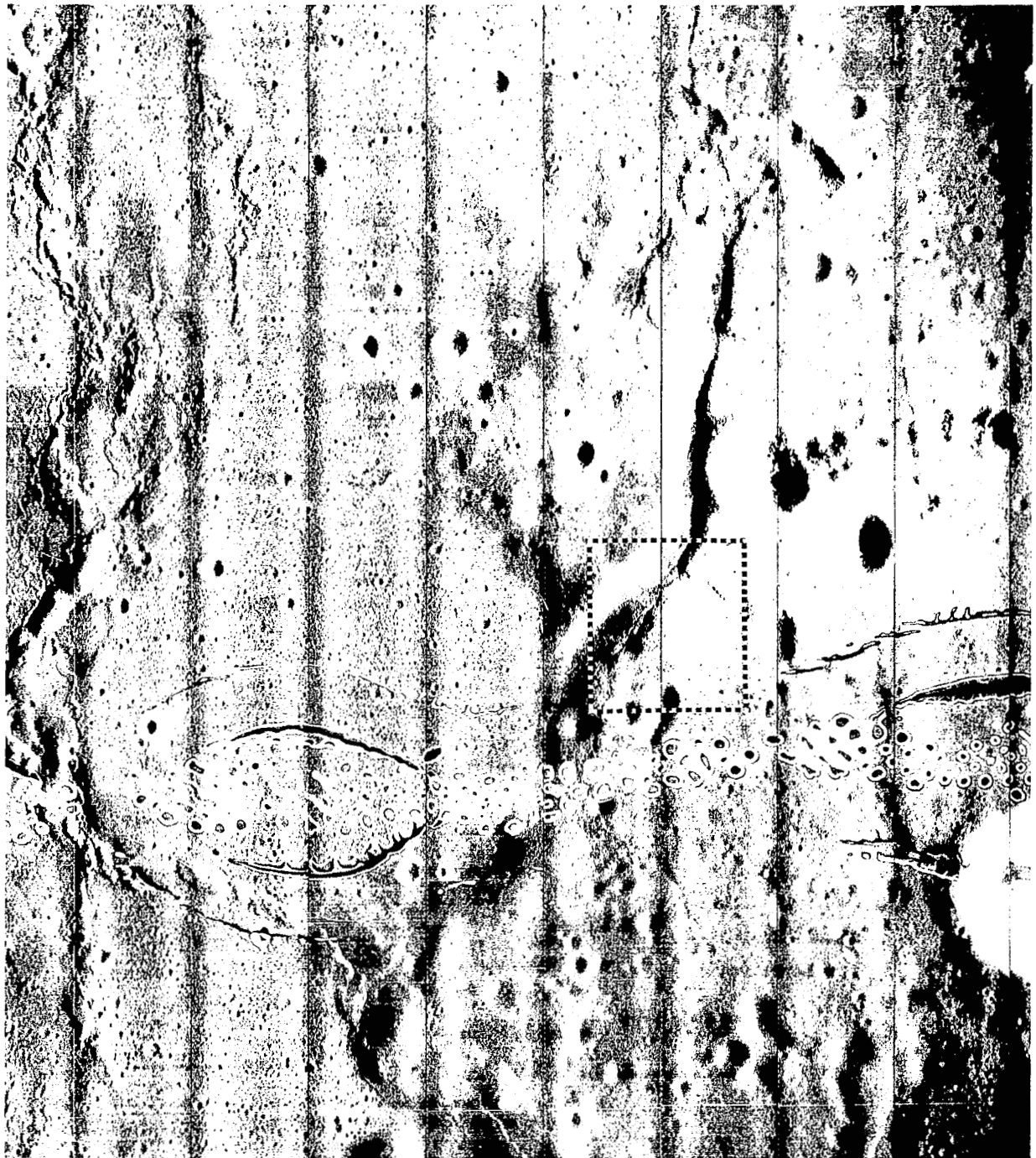


**Figure 4-27: Albedo Distribution for Site V-15.1, Dawes**

advertently biased toward slight underexposure by neglecting to account for reflectance of the telephoto folding mirror in the lens transmission value used. This was corrected for later sites.

At the time of exposure, the camera was well centered on the crater so that the northern half was included within the telephoto frame. This includes the zone of the interior wall that ranges from hard shadow to brightly lighted.





A portion of Wide-Angle Frame 68 reproduced at GRE scale. An example of a lace band processing defect is shown.

**Figure 4-25: Site V-14, Littrow Rilles; Wide Angle**



A portion of Telephoto Frame 67, reproduced at GRE scale, showing detail of surface texture and rille slopes present. Area shown is south of the bright crater at right center in Figure 4-25.

**Figure 4-26: Site V-14, Littrow Rilles; Telephoto**

If the crater had been perfectly centered in the frame, the zones of better illumination on the north and south sides would have been outside the telephoto field of view.

The wide-angle frame, receiving slightly more exposure, shows good detail on the crater floor and over the surrounding mare surface where the ejecta pattern from Dawes is seen. A series of rilles west of Dawes is well shown and the effect of the crater ejecta on them is apparent. The illumination angle was such that the rather unusual structure of the crater is shown to advantage (Figure 4-28).

Although GRE film evaluation indicated a slight underexposure for the outer mare surface in the telephoto, as expected, satisfactory paper prints were prepared with little indication of significant information loss. Very good detail is shown on the crater floor (see Figure 4-29) and a portion of the inner wall, and some detail is shown over all of the lighted slope in the paper print. Much excellent detail on the bright, illuminated inner slope is evident on the GRE film record.

Resolution of both wide-angle and telephoto frames was excellent. Detail down to three scan lines was observed on both frames.

#### 4.4.2.9 Site V-18, Dionysius

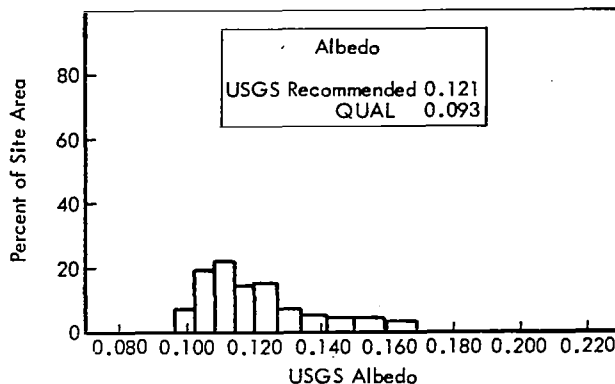
*Location: 17.98°E longitude, 2.57°N latitude*

*Altitude: 96.2 km Frames: 80-83*

*Phase angle: 83.93 degrees Alpha: -14.67 degrees*

*QUAL Albedo: 0.093 Shutter speed: 0.02 second*

Dionysius, about 18 kilometers in diameter, has characteristics of a very young crater. It has a high albedo, as may be seen in its albedo histogram, Figure 4-30. A prominent ray system surrounds the crater, with both light and dark rays present. The feature also is the site of a high thermal anomaly. This site is also included in the AAP group since a landing here could provide opportunity to sample both light and dark rays (which may be from different subsurface layers), mare material, nearby terra, and rim material of Ritter whose origin is doubtful.



**Figure 4-30: Albedo Distribution for Site V-18, Dionysius**

The site location was planned to be centered east of Dionysius on the low, flatter rim material rather than the crater itself.

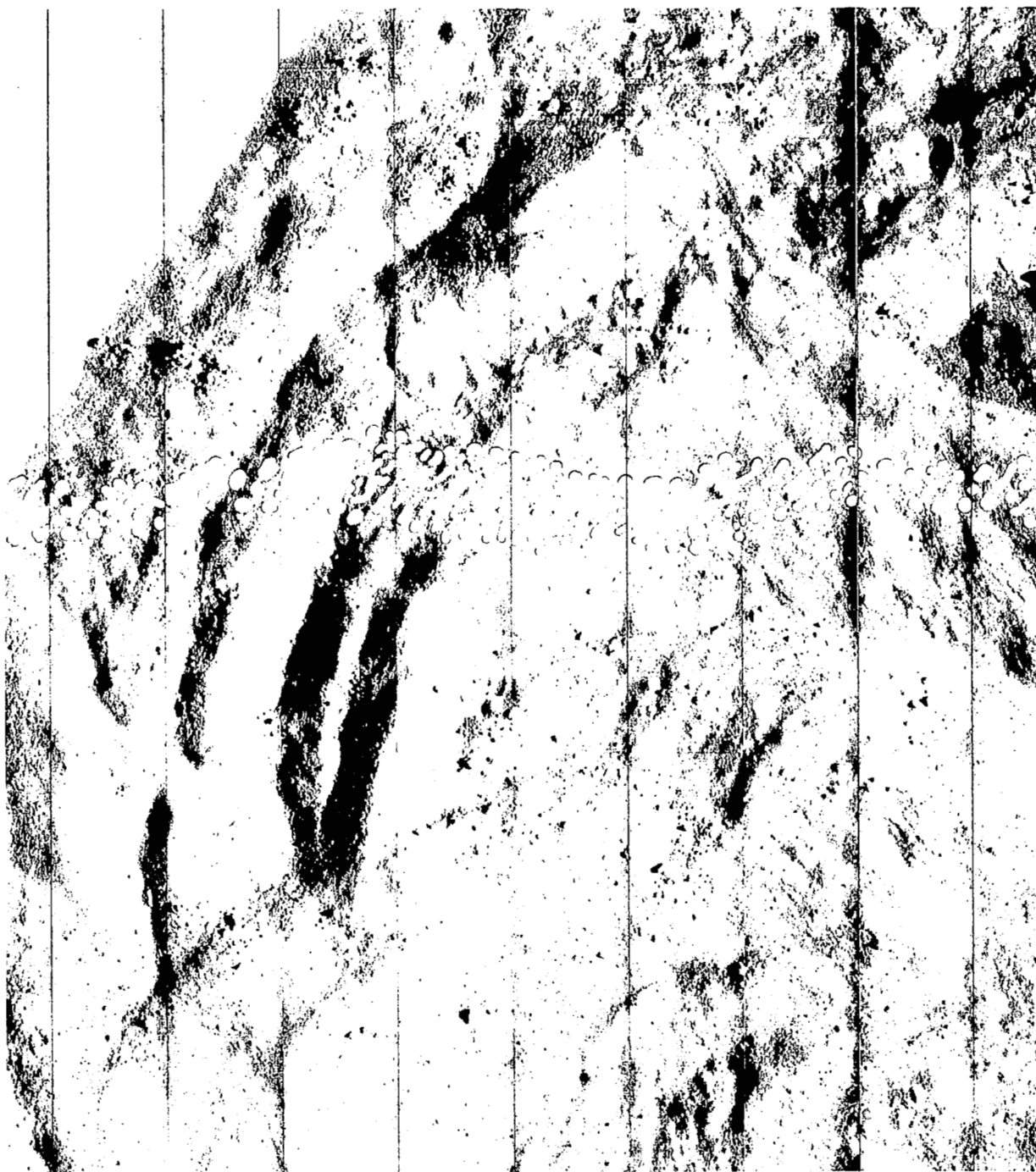
The site was photographed by a sequence of four frames exposed in the fast mode. As planned, the sequence of photographs was centered east of Dionysius. The wide-angle field of view, however, includes that crater and the craters Ritter and Ritter B, C, and D. Although the telephoto frames include a portion of the eastern inner slope of Dionysius, it is in hard shadow and no detail is present. The outer rim and the rilles, Rima Ritter II, III, and IV, are included in telephoto coverage.

Exposure appears to be generally satisfactory for this area of wide albedo range. In the wide-angle frames, the bright interior slopes of Dionysius are overexposed as expected, but most of the outer rim and darker mare are well shown (Figure 4-31). The telephoto frames show good detail in the brighter areas of rayed surface and are only slightly underexposed in darker mare areas. Detail is lost only on the shaded slopes of darker areas and in the hard shadows. Very close to the eastern edge of Dionysius, where the surface is exceptionally bright due to the combination of high albedo and some sunward slope, there are areas in the telephoto frames that are overexposed to the point of loss of detail. Detail of the outer rim area of interest was recorded very well in telephoto frames, as may be seen in Figure 4-32. Since the luminance range of the area was such that both over and under exposure occurred



A portion of Wide-Angle Frame 70 near center of photograph. Some processing “freckles” are present.

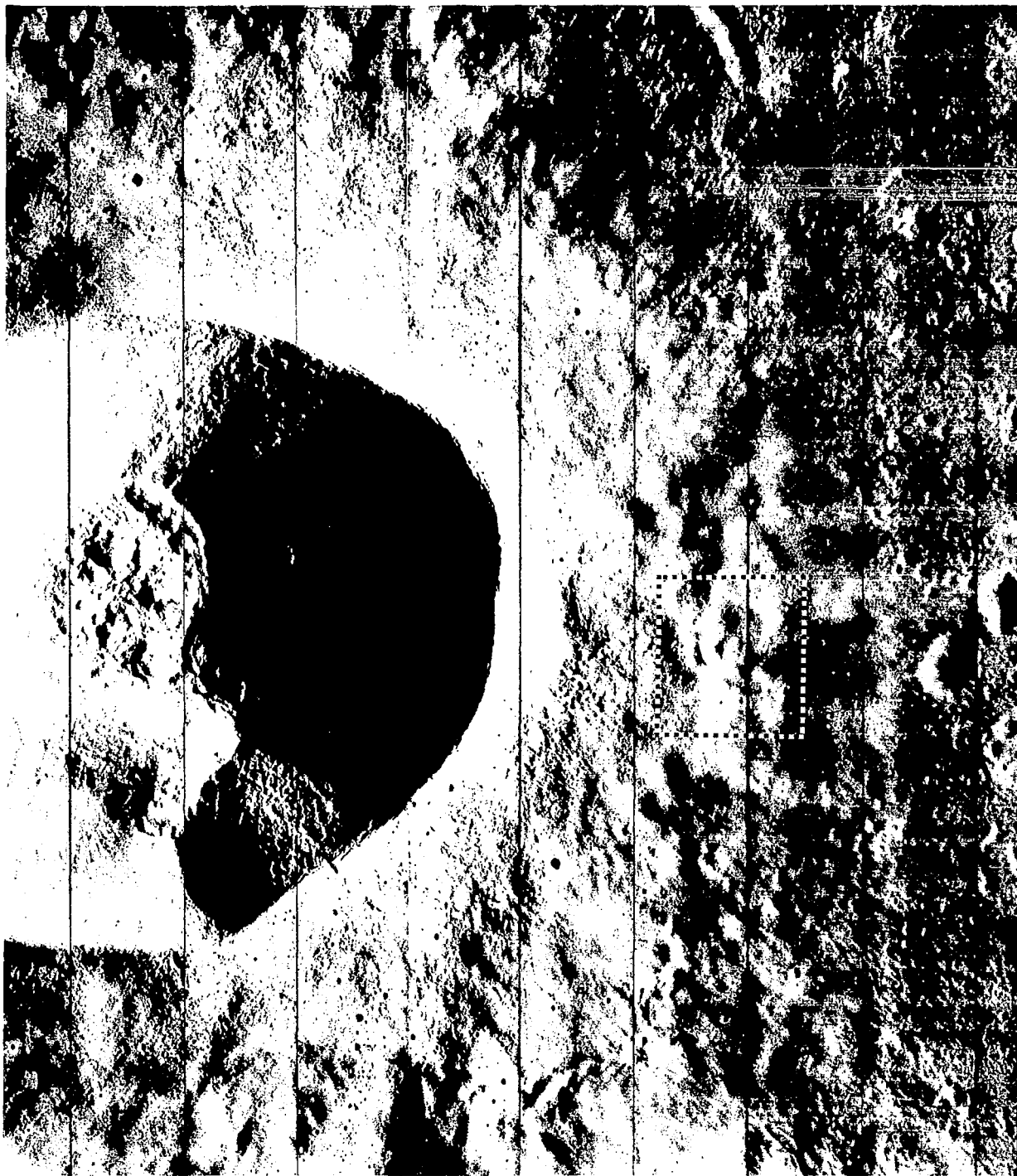
**Figure 4-28: Site V-15.1, Dawes; Wide Angle**



A portion of Telephoto Frame 70 showing detail present on floor of Dawes. Note that some detail is present on sunward wall.

**Figure 4-29: Site V-15.1, Dawes; Telephoto**





A part of Wide-Angle Frame 83 showing crater and part of eastern outer rim. Area outlined shown in Figure 4-32.

**Figure 4-31: Site V-18, Dionysius; Wide Angle**



A part of Telephoto Frame 81 showing detail of smooth outer rim area of special interest. Area shown is east of crater.

**Figure 4-32: Site V-18, Dionysius; Telephoto**

within the frames where slopes were not extreme, the selection of 0.02 second for shutter speed was correct. No preferential exposure bias was requested.

Both telephoto and wide-angle photographs had acceptable resolution. Detail spanning as few as four scan lines was observed in all frames examined using the GRE film.

#### 4.4.2.10 Site V-19, Abulfeda Crater Chain

*Location: 13.94°E longitude, 15.00°S latitude*

*Altitude: 112.9 km Frame: 84*

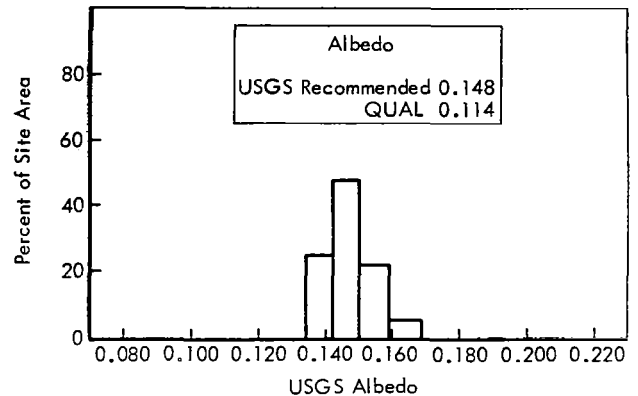
*Phase angle: 71.2 degrees Alpha: +1.64 degrees*

*QUAL Albedo: 0.114 Shutter speed: 0.02 second*

Abulfeda is a large crater, approximately 55 kilometers in diameter, located southeast of Sinus Medii in the southern highlands between Mare Nubium and Mare Nectaris. The main feature of interest at this site was the large crater chain that meets Abulfeda tangentially. A single dual-frame exposure, centered over the point of tangency, was planned for this site to supplement the data obtained in Lunar Orbiter Mission IV. In addition to showing details of the crater chain, it was expected to obtain additional detail of the subdued rim and the crater basin, which appears to be partially filled by mare-type material.

The selected exposure time of 0.02 second produced wide-angle and telephoto frames of very good photographic quality. Topography characteristics of this site resulted in a wide luminance range, which caused some loss of detail in bright highlights and hard shadows when system limits were exceeded. As seen on positive GRE film, the end framelets of the telephoto frame were typically denser than the frame center because of the characteristic off-axis falloff of transmitted light by the 610-mm lens. The decrease in luminance away from the highlighted central crater also contributed to the higher average density of the end framelets. These effects are not always noticeable in opaque positive prints because of controls used in making such prints. Overall densities and contrast were satisfactory for the telephoto and wide-angle photographs. A histogram of the

albedo characteristics for this site is shown in Figure 4-33.



**Figure 4-33: Albedo Distribution for Site V-19, Abulfeda Crater Chain**

The wide-angle photograph was centered on the southern rim of Abulfeda where it intersects the crater chain. Consequently, frame content of this site corresponds closely to that required by mission planning. Terrain characteristics are well delineated, with good contrast and detail (Figure 4-34). Spacecraft altitude for this site photography was approximately 112.9 kilometers.

Surface texture is shown in excellent detail in the telephoto frame because of the low Sun angle at the time of photography. However, because of slope orientation to or away from the Sun, the low Sun angle also resulted in fairly large surface areas of high luminance or dark shadow where surface details were not recorded. Where slope changes were gradual, terrain details were enhanced by the combination of more favorable illumination, surface, and camera geometry. An example of surface texture at this site as seen in the central portion of the telephoto frame is given in Figure 4-35. Resolution was very good in the telephoto and wide-angle photographs. Craters spanning as few as three scan lines can be discerned in the central areas of the frames.

#### 4.4.2.11 Site V-21, South of Alexander

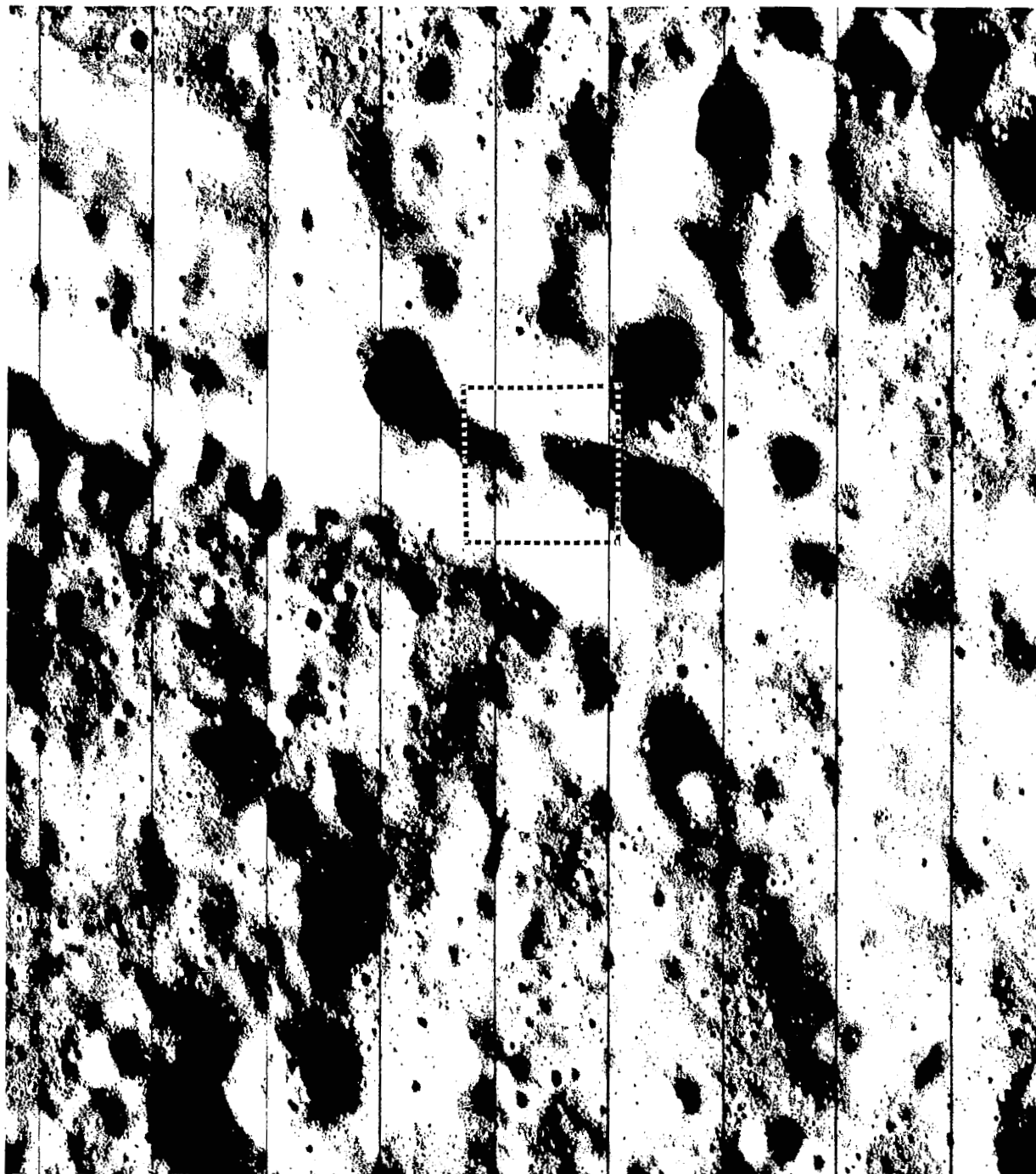
*Location: 13.50°E longitude, 38.65°N latitude*

*Altitude: 178.0 km Frames: 86-89*

*Phase angle: 70.55 degrees Alpha: +0.84 degree*

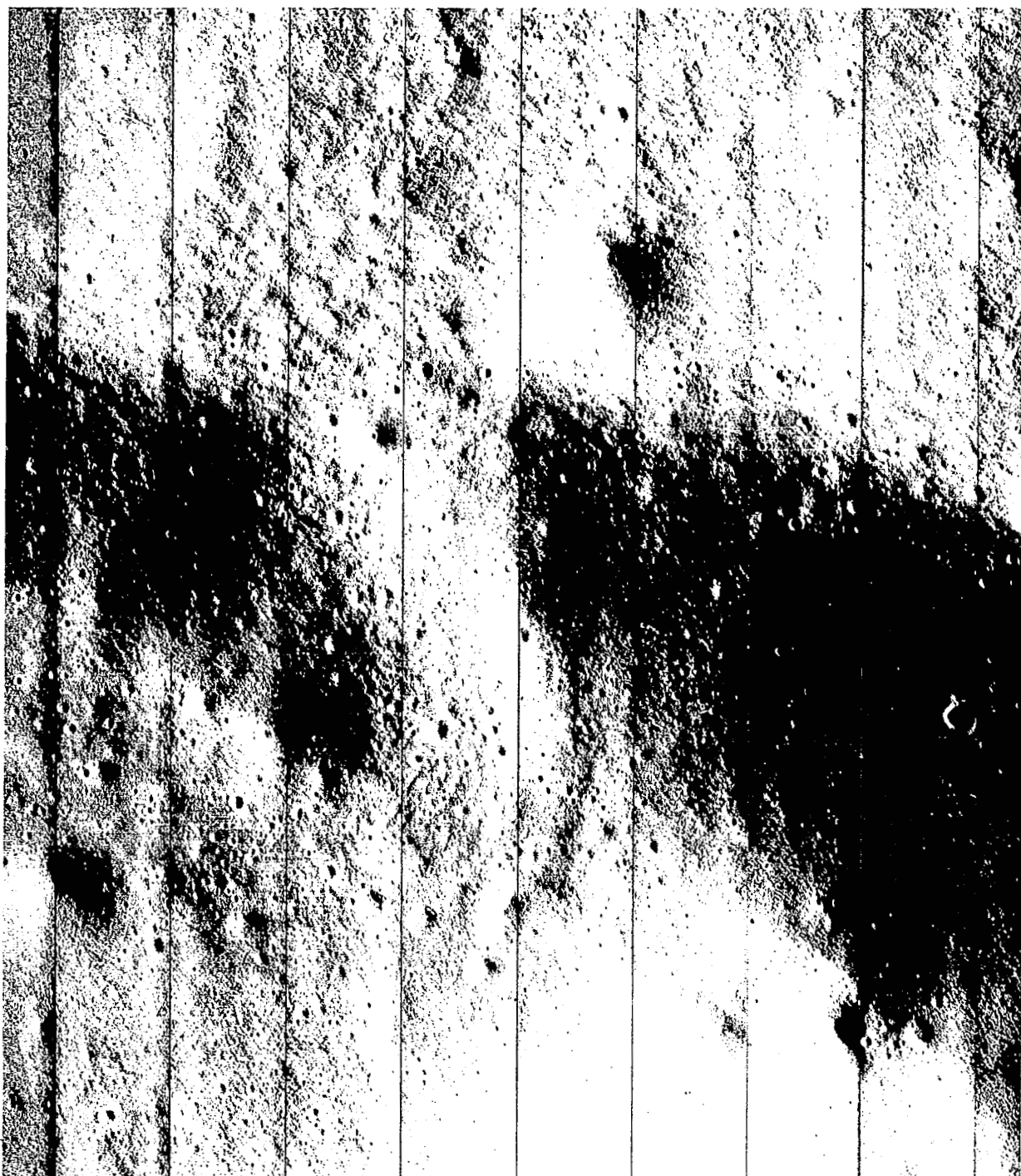
*QUAL Albedo: 0.102 Shutter speed: 0.02 second*





A portion of Wide-Angle Frame 84 showing crater chain and terra near Abulfeda. Area outlined shown in Figure 4-35.

**Figure 4-34: Site V-19, Abulfeda Crater Chain; Wide Angle**



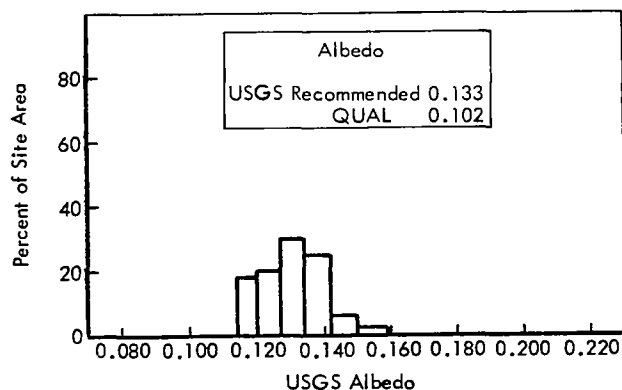
A part of Telephoto Frame 84 showing detail present in a section of the chain. Note surface texture shown on chain slopes and the rounded rim profile.

**Figure 4-35: Site V-19, Abulfeda Crater Chain; Telephoto**

The area of this site presents a variety of terrain for investigation by photography and, because landing may be possible here, by future on-site study. The site is, therefore, included among those designated as AAP. The area includes the upland-type terrain between Alexander and Mare Serenitatis as well as the mare surface and the crater floor, the latter pitted by secondary craters from Eudoxus. The possible relation of particular upland terrain characteristics to modifying effects of the Imbrium ejecta was of interest. The site also included the well-defined Rima Callipus I and a more poorly defined structural band that includes a braided wrinkle ridge with associated elongated craters and noticeably high albedo.

The site was photographed with a sequence of four frames exposed in the fast mode. Wide-angle photography includes all areas of interest mentioned above, with Callipus included at the western side of the coverage. Most of Alexander is within the field of view of the last wide-angle frame. The first two frames of telephoto coverage are entirely within the hummocky upland area; the third includes the higher hills of the south rim of Alexander and the adjacent crater floor. The last telephoto frame is mostly the floor of Alexander, but includes the mountainous rim at the western end.

Because the area to be photographed included both mare and terra, both of interest, exposure was based on the average albedo as shown in the histogram, Figure 4-36. Considering the



**Figure 4-36: Albedo Distribution for Site V-21; South of Alexander**

variety of terrain included in the wide-angle coverage, the exposure is good. The more nearly level areas of both mare and terra are properly exposed and only the highly luminous sunward slopes, particularly in the terra, are overexposed (Figure 4-37). Of the telephoto frames, the first three are entirely or predominantly terra having a "smooth," rolling topography. Because of this, there are appreciable areas of low luminance but which show detail. Few of the bright areas exceed the system luminance limit; thus, fine surface detail is present over most of these frames (Figure 4-38). The mare area, although of lower albedo, shows very good detail that is sharply defined. Detail in the lighted interior slopes of many of the larger craters of rounded contour is present.

Resolution of both telephoto and wide-angle frames is very good, ranging between three and four scan lines in all frames examined as GRE film.

#### 4.4.2.12 Site V-22, Sulpicius Gallus Rilles

*Location: 9.33°E longitude, 21.00°N latitude*

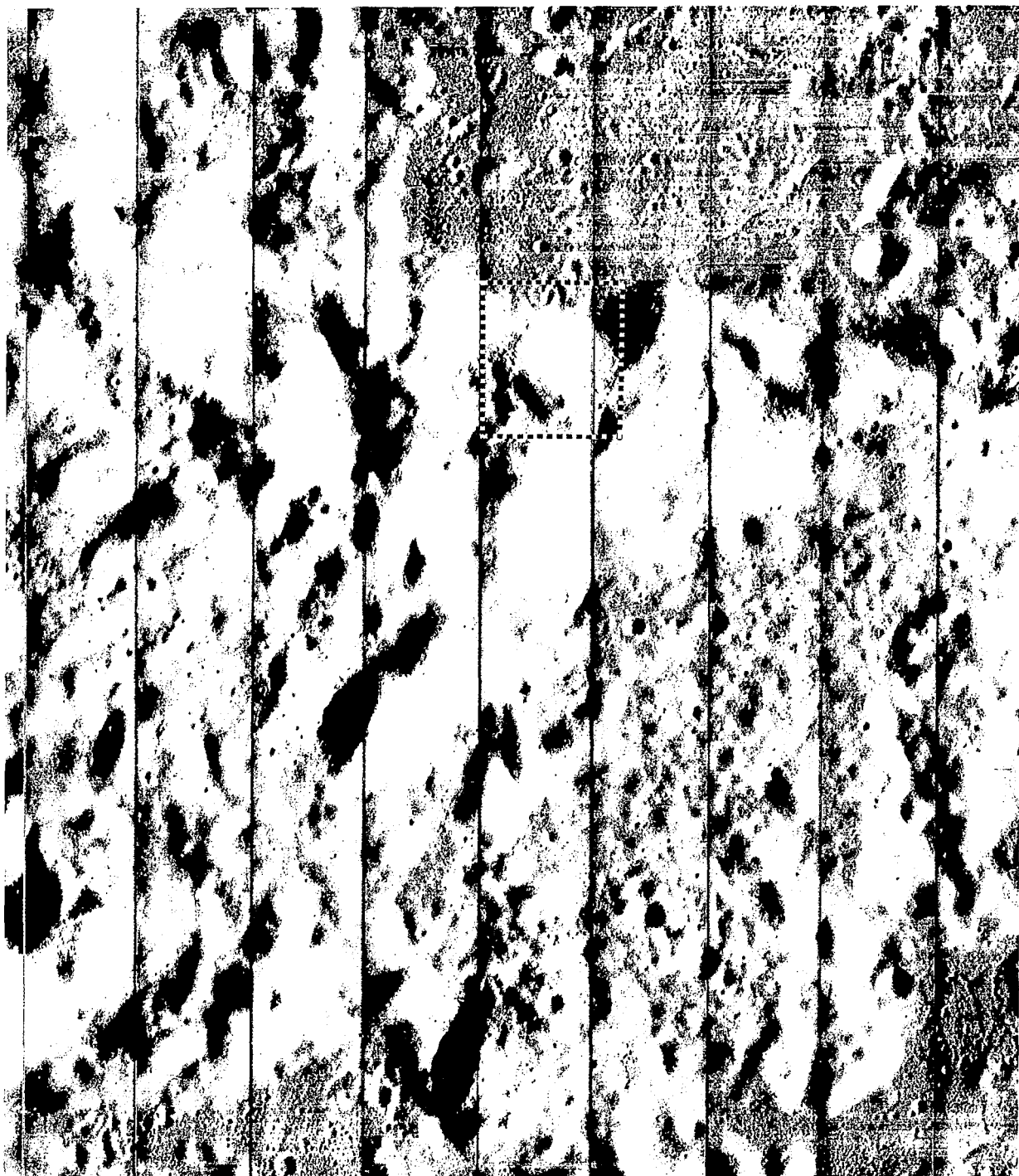
*Altitude 118.3 km Frames: 90-93*

*Phase angle: 61.07 degrees Alpha: +9.62 degrees*

*QUAL Albedo: 0.063 Shutter speed: 0.04 second*

The features of interest at this site comprise the complex of rilles located close to the southwestern edge of Mare Serenitatis by a shoulder of the Haemus Mountains. A dark material that seems to blanket both terra and mare apparently originated from or is associated with the rilles. The texture of this material, details of its extrusion or ejection from the rilles, and relation to other geological units were of interest. Mission IV photography indicated that the rilles and associated units are young. Since these features are related to and are within a mare area and thus may be presumed to offer landing possibilities, this site has been included within the group of AAP sites.

The site was photographed with a sequence of four frames exposed in the fast mode. Since the features of interest were within the mare area, the exposure was selected to optimize on this area, thus biasing the site average albedo (see Figure 4-39) toward a lower value for the QUAL



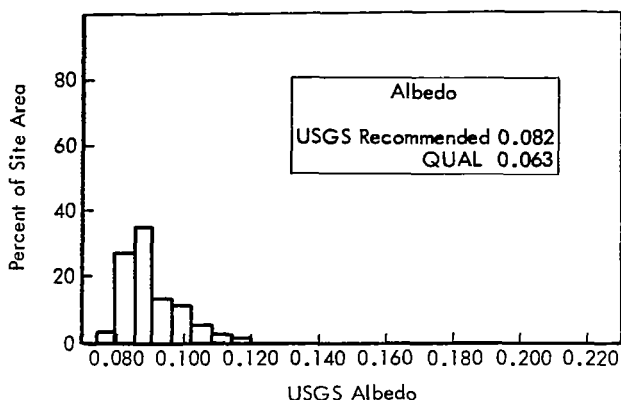
A part of Wide-Angle Frame 86. Detail is lost on sunward terra slopes because of luminance extreme.

**Figure 4-37: Site V-21, South of Alexander; Wide Angle**



This is a portion of Telephoto Frame 88 showing detail present on terra slopes and hill summits. Note that detail is shown on slopes where it is lost in the wide angle photograph.

**Figure 4-38: Site V-21, South of Alexander; Telephoto**



**Figure 4-39: Albedo Distribution for Site V-22, Sulpius Gallus Rilles**

computations. Some overexposure of brighter terra areas was accepted (Figure 4-40).

The rille system is very well covered by the telephoto frames. About half of each frame is within the mare area and half within the terra. This camera orientation provides telephoto coverage of both the principal part of the rille system and a portion of the Haemus Mountain terrain. Areas having the dark blanket material are included in the telephoto coverage.

Exposure was very good for the mare areas. Only terra areas of very high luminance were overexposed to the point of data loss. These occurred in the areas adjacent to bright rayed craters and steeper sunward slopes in the terra area. Telephoto frames were generally properly exposed and contain very good detail, except in limited areas of luminance extremes (Figure 4-41).

The resolution of both wide-angle and telephoto frames is good. Examination of GRE film showed detail to between three and four scan-line widths in all frames examined. Although the resolution of the photographs is very good, no distinguishing texture is evident in the areas of dark blanketing and detail does not appear to be appreciably obscured. Textural detail is excellent in much of the terra area included in the telephoto frames, and small areas that appear to have higher albedo are shown.

The dark blanket material is apparent in a number of locations within the telephoto cov-

erage. In some cases it is difficult to distinguish between darkening due to the photometric effect of surface slope and that due to the darker material. Stereoscopic examination would be of great help in defining the cause of the darkening. In many cases, however, close examination of surface details shows that a lower albedo is indeed present and dark-haloed craters are in the area.

#### *4.4.2.13 Site V-23.2, Hyginus Rilles*

*Location: 6.00°E longitude, 8.25°N latitude*

*Altitude: 98.6 - 99.2 km Frames: 94-97*

*Phase angle: 51.67 degrees*

*Alpha: +19.91 degrees QUAL Albedo: 0.090*

*Shutter speed: 0.02 second*

The Hyginus rilles are features long known from telescopic observation. Interest in this feature was markedly increased by Mission III and IV photography, which revealed the sharpness of the rilles and associated craters, and other characteristics such as the absence of crater rims.

The system includes the rilles and crater chain, and the large crater complex of Hyginus situated along what may be a fault graben. The fresh appearance revealed by Mission IV photography and the observed high thermal anomaly suggested that bedrock or rock strata might be exposed.

The site, included as one of the AAP sites, was photographed with a sequence of four frames taken in the fast mode. Wide-angle coverage obtained by the sequence extends from Hyginus A on the south, and north to include a portion of Schneckenberg and the nearby low hills. The sequence centerline lies approximately 10 kilometers west of Hyginus. Camera axis positioning and timing of photography thus bring Hyginus and adjacent sections of the rilles within telephoto coverage. Although the site is nearly all within mare area, the albedo extends over a moderately wide range (0.065 - 0.103, corrected), excluding small bright-rayed craters, as seen in the albedo histogram of Figure 4-42.

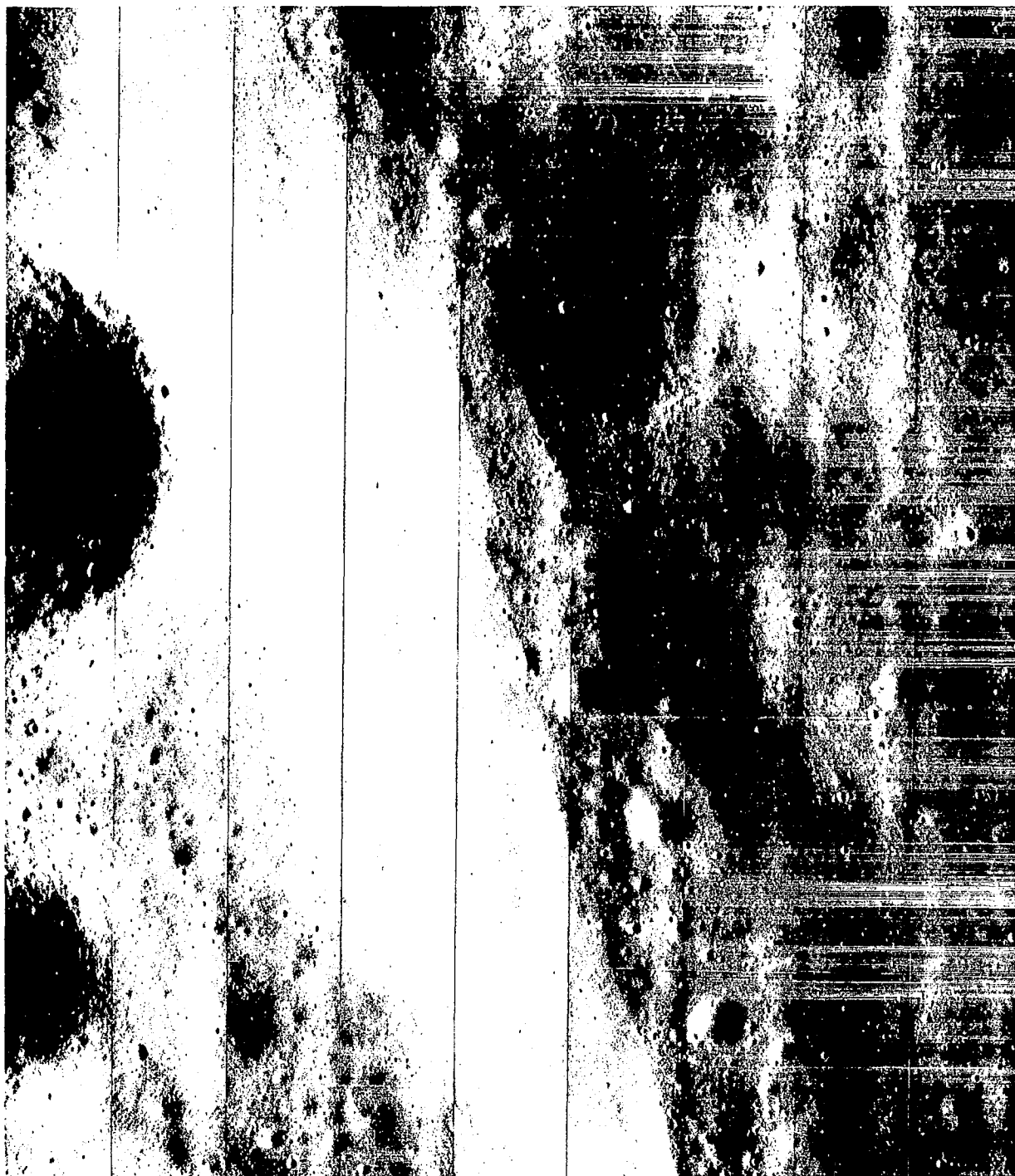
Exposure of both wide-angle and telephoto frames is very good. Only steep sunward slopes



A portion of Wide-Angle Frame 93. Detail is lost in very bright areas, but exposure of mare and terra is very good where surface is more nearly level.

**Figure 4-40; Site V-22, Sulpicius Gallus Rilles; Wide Angle**

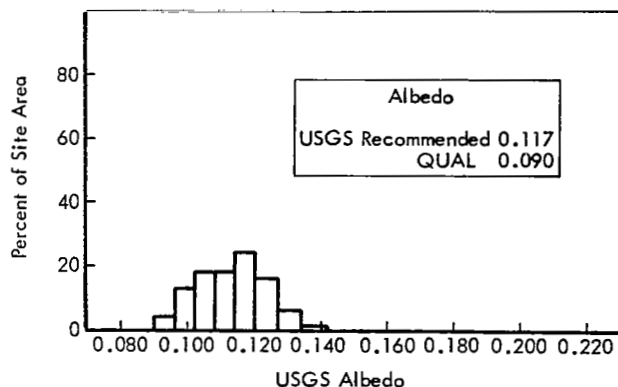




A part of Telephoto Frame 93. A section of a rille adjacent to the very bright crater. Note detail present in rille including sunward slopes.

**Figure 4-41: Site V-22, Sulpicius Gallus Rilles; Telephoto**





**Figure 4-42: Albedo Distribution for Site V-23.2, Hyginus Rilles**

within craters and on sections of the rilles where luminance is very high are overexposed so that detail is obscured. More nearly level areas, such as the surrounding mare, the floor of Hyginus, and the rilles were exposed for near-optimum density. Detail in wide-angle frames is sharp, revealing outcrops or bedded boulders along the edge of the rilles and small fissures along the top rim (Figure 4-43). Small, bright spots are revealed near the floor of the northern extension of Hyginus. Superficially these spots resemble photographic defects but are shown to be, in fact, real by comparison of successive frames. They are also present in the telephoto frames. The brighter area east of Hyginus received somewhat more than optimum exposure in the wide-angle frames but little image was lost.

The telephoto frames provide a very interesting sequence. Exposure is near optimum over nearly all of the area covered except the very bright sunward steep slopes. Excellent detail is shown on those sections of the steep slopes of Hyginus and the rilles where orientation provided more suitable illumination (Figure 4-44). Tracks of rolling boulders are common on the interior slopes of the crater and rilles. This is shown in an enlargement of a short section of Framelet 970 from Telephoto Frame 95 (Figure 4-45). Much detail is shown on the crater floor that is unusual, such as low-profile domes and irregularly shaped depressions. A marked variation in albedo on the crater floor and walls is shown (Figure 4-46).

Resolution is very good, as indicated by the

clarity with which the many boulders are shown. The resolution was further verified by GRE film examination showing detail to three or four scan line dimensions.

#### 4.4.2.14 Site V-24, Hipparchus

*Location: 4.06°E longitude, 4.67°S latitude*

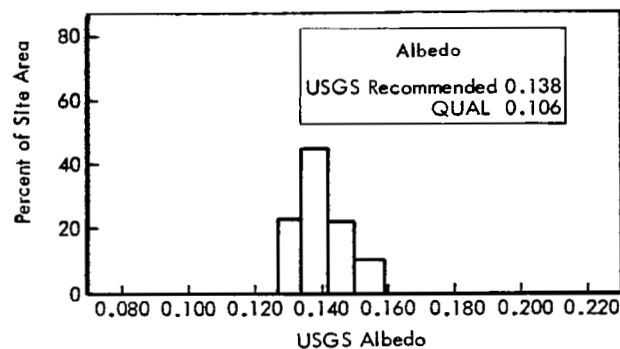
*Altitude: 99.6 km Frames: 98-101*

*Phase angle: 66.8 degrees Alpha: +5.30 degrees*

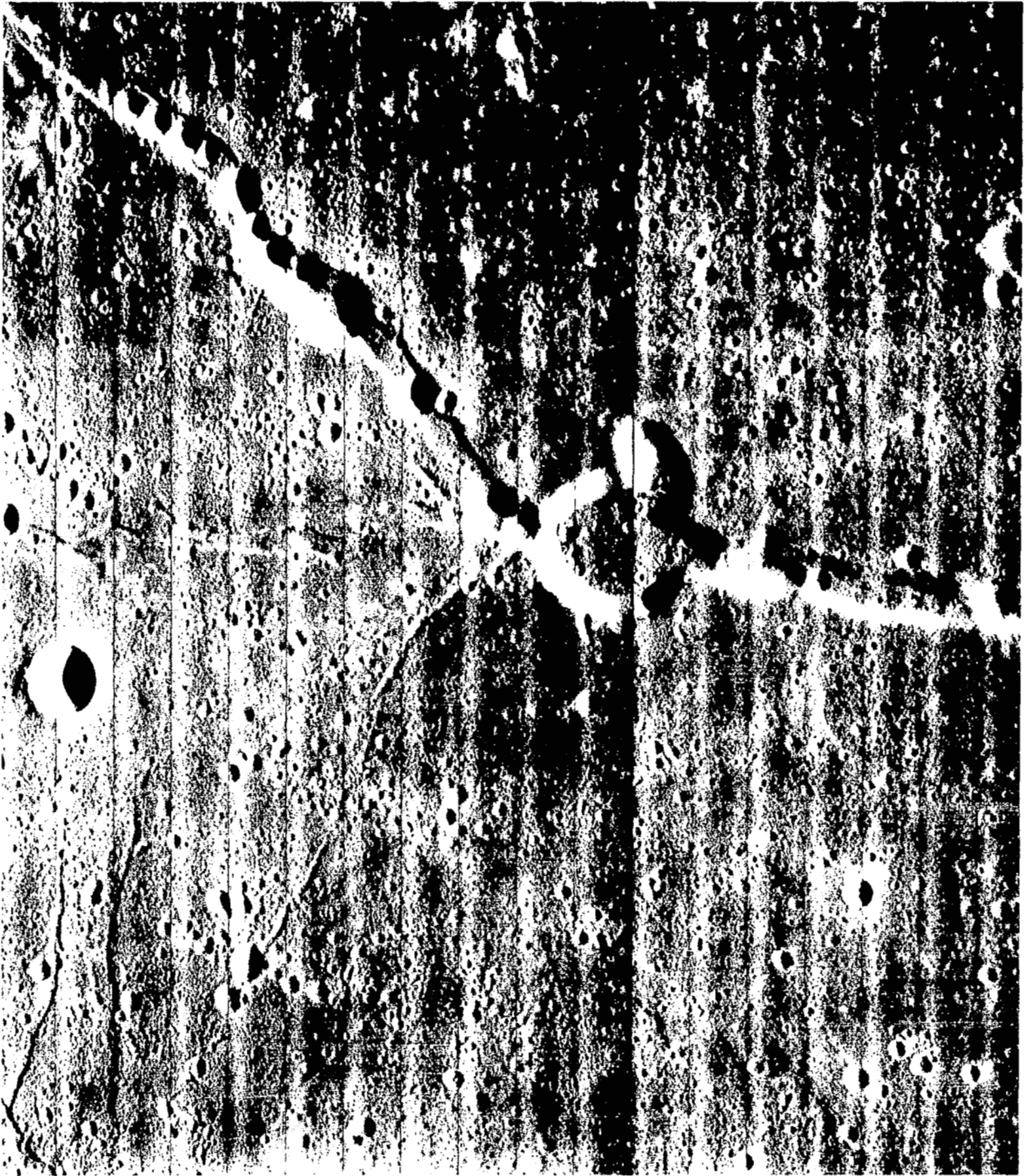
*QUAL Albedo 0.106 Shutter speed: 0.02 second*

Hipparchus is a large, older crater located slightly below the equator in the central highland region southeast of Sinus Medii. It has an irregular cross-section and rim structure, and an approximate diameter of 120 kilometers. Sections of the rim appear to be eroded or destroyed. The floor, or basin, is filled with mare-type material, with some of the earlier structural features such as peaks and smaller craters showing through the fill material in various places. Several relatively large features are located within the boundaries of Hipparchus, including the newer crater Horrocks in the northeast portion, and two smaller craters, Hipparchus N and X. Mission IV photography showed this area to be highly cratered and probably rough at the Surveyor scale. Additional photographs of this site were desired to obtain terrain data of interest to the Surveyor program.

A four-frame sequence in the fast mode was used for this site. An exposure time of 0.02 second produced photographs with satisfactory average densities and good contrast ranges. Albedo distribution for this area is shown in Figure 4-47. Recommended albedo and ex-



**Figure 4-47: Albedo Distribution for Site V-23, Hipparchus**



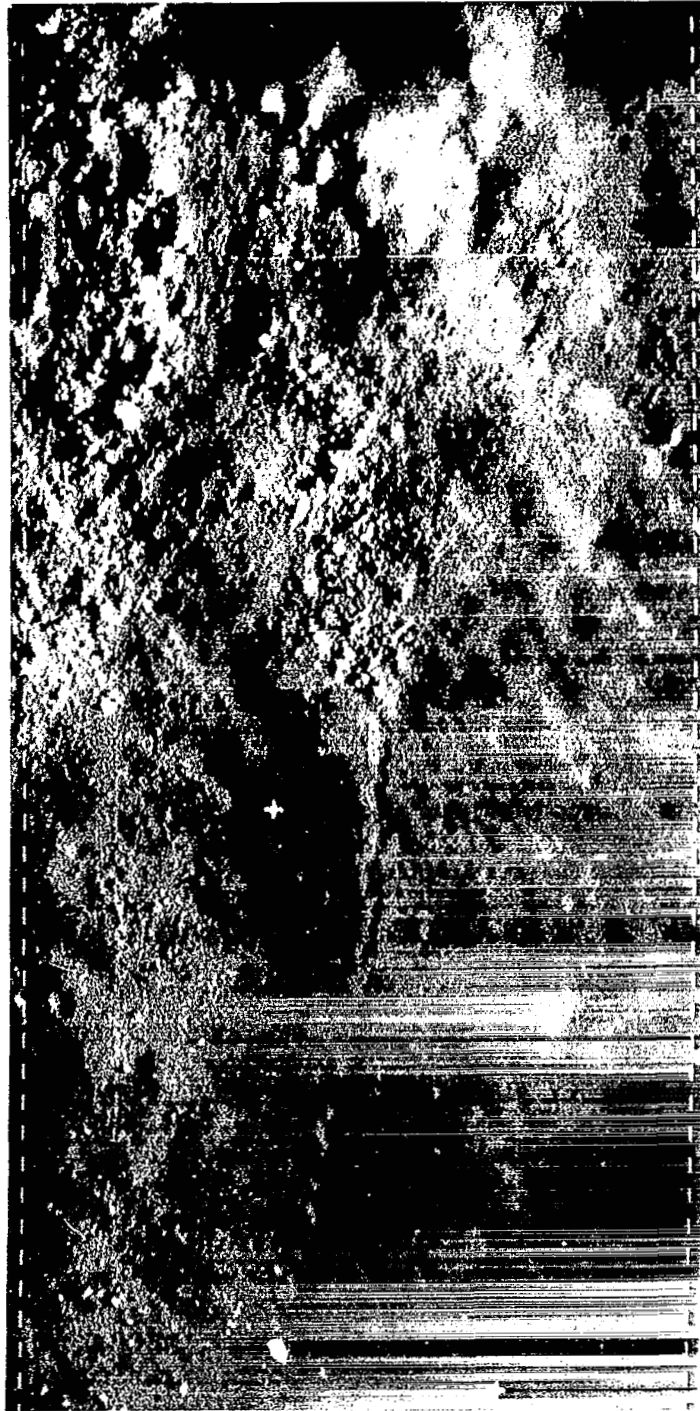
Showing nearly all of Wide-Angle Frame 95, this is the second of a sequence of four frames.

**Figure 4-43: Site V-23.2, Hyginus Rille; Wide Angle**



A part of Telephoto Frame 95, this shows a section of inner wall and floor of crater. Note wall detail in area of illumination transition from hard shadow to sunlit slope.

**Figure 4-44: Site V-23.2, Hyginus Rille; Telephoto**



This photograph is a nearly 5x enlargement of a section of Framelet 970 from Telephoto Frame 95 to illustrate fine detail present.

**Figure 4-45: Site V-23.2, Hyginus Rille; Enlarged Telephoto Image**



This is a part of Telephoto Frame 96 including the northern extension of Hyginus. Note small areas of high albedo.

**Figure 4-46: Site V-23.2, Hyginus Rille; Telephoto**

posure time were satisfactory for photography of the Hipparchus crater floor.

The wide-angle photographs are all of the filled floor area. Rim structure was not included in the camera field of view. The area photographed is predominantly level, with some rolling terrain and occasional rilles. All of the area is heavily cratered with few relatively large topographic features. A profusion of small craters indicates that the floor of Hipparchus is quite rough on a small scale. The terrain is typical of a rough mare area, except for the presence of numerous small domes. Because of the many small craters with their bright slopes and hard shadows, the photographs tend to have a high-contrast appearance.

The telephoto frames are very similar in appearance because of the nature of the terrain. Detail is very good, and small-scale roughness and surface texture of the crater floor is well shown (Figure 4-48). Exposure and contrast are uniformly good in the four-frame sequence. Resolution was very good in all the photographs. Craters as small as three scan lines in diameter may be discerned in the central areas of these frames. Off-axis resolution was also satisfactory. Objects spanned by as few as four scan lines could be identified at the frame ends.

#### *4.4.2.15 Site V-25, Alpine Valley*

*Location: 1.04°E longitude, 48.26°N latitude*

*Altitude: 247.8 km Frame: 102*

*Phase angle: 53.15 degrees*

*Alpha: +22.07 degrees QUAL Albedo: 0.100*

*Shutter speed: 0.02 second*

The Alpine Valley is a very large valley presumed to be a fault feature. Mission IV photography revealed the presence of a narrow, irregular trough near the center of the valley and extending over its entire length. An erosional origin for the trough has been suggested. Numerous geological features of the valley and adjacent area were of interest. In addition to the trough, information concerning the valley scarps, filling material on the valley floor, and the hummocky upland terrain within which the valley is located was desired. The hummocky terrain of the upland area is probably

ejecta from Imbrium. Information concerning the puzzling thick-looking materials on the shoulders of the valley was sought because of its possible volcanic origin.

Because of its size and orientation, photography of the valley so that almost all of it would be within the telephoto frame required special camera orientation. An oblique view with the long axis of the telephoto frame oriented with the valley was necessary. The photograph is thus an oblique toward the southwest, with a tilt of 34 degrees from vertical. Camera orientation was accurately accomplished, and virtually the entire valley was included in the single telephoto frame. Because of the oblique view, wide-angle coverage extends beyond the Alpine Mountains into Mare Imbrium where the peak Pico can be seen (Figure 4-49).

Selection of proper exposure for this photograph presented a difficult problem. The frame included both flat mare and rugged terra. In addition, tilt direction was away from the Sun so that luminance of sunward slopes was enhanced. Consequently, the valley floor, mare, and other more nearly level areas were exposed properly, but the sunward mountain slopes and valley scarp are overexposed so that little detail is shown. Good detail is present on the valley scarp in those sections oriented so that illumination is more nearly grazing. Good surface texture detail of the terra adjacent to the valley is shown in the telephoto frame where illumination does not cause excessive luminance.

Resolution of the wide-angle frame is very good, with detail to three scan lines observed on the GRE film. Detailed examination of the GRE record revealed that resolution of the telephoto frame was not quite as good as that of the wide-angle frame, although detail spanning five to six scan lines was observed. Some indication of slight image smear was noted with microscopic examination of the telephoto GRE record. The V/H sensor could not be used for image motion compensation; misalignment of the spacecraft axis with respect to flight direction was required to position the valley image within the telephoto format.





This is a portion of Telephoto Frame 99 illustrating quality of detail shown on crater floor. Note also detail on sunward slope of hills.

**Figure 4-48: Site V-24, Hipparchus; Telephoto**



This is most of Wide-Angle Frame 102. This photograph, looking southwest down the length of the valley, includes both Alpine Mountains, Mare Imbrium, and Pico.

**Figure 4-49: Site V-25, Alpine Valley; Wide Angle**



#### 4.4.2.16 Site V-26.1, Hadley Rille

*Location:* 3.00°E longitude 25.24°N latitude

*Altitude:* 125.1-137.4 km *Frames:* 104-107

*Phase angle:* 66.04 degrees

*Alpha:* +5.00 degrees *QUAL Albedo:* 0.070

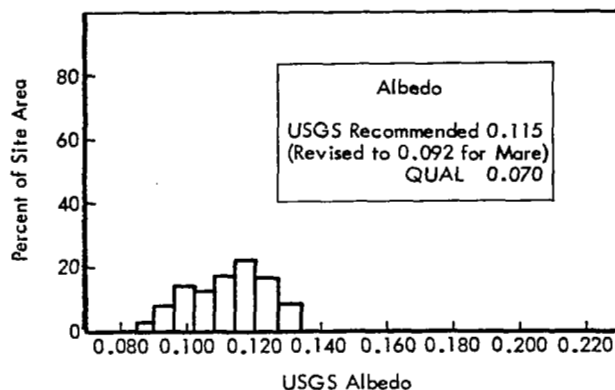
*Shutter speed:* 0.04 second

This site includes not only Hadley rille but a number of other features of geological interest and significance. These include the smooth, sparsely cratered mare; premare light plains-forming material; the high, rugged flank of the Apennine mountains; and a rugged block lying in front of the Apennine scarp. Information leading to understanding the origin of the sinuous Hadley rille, the formation of the mountains, and possible occurrence of structural deformation or deposition of Imbrium ejecta was desired. Data concerning downslope movement of material on the mountainous slopes were sought.

Site photography was accomplished by a four-frame sequence taken in the slow mode providing 50% overlap of the wide-angle frames and noncontiguous telephoto coverage. The coverage includes all features as planned. Use of slow sequencing provided telephoto coverage of a wide range of geological units present in this area; however, because of the noncontiguous telephoto coverage, the entire length of Hadley rille is not shown in these frames.

The varied topography in the area photographed at this site made satisfactory exposure of all areas virtually impossible, particularly in rugged terra. The site includes — in addition to luminance extremes introduced by the topography — areas covering a rather broad range of albedo, as shown in Figure 4-50. Prior to site photography, representatives of user agencies indicated that mare areas were of principal interest and recommended basing exposure on the lower albedos rather than on a site average.

In general, the site photographs are of very good quality. Exposure of the mare area is quite satisfactory, as is that in terra where the surface is not severely sloped. As anticipated, steep sunward slopes are overexposed in both mare and mountainous terra. Inner slopes of much of



**Figure 4-50: Albedo Distribution for Site V-26.1, Hadley Rille**

Hadley rille are steep; thus, detail is lost either by overexposure or by being obscured in hard shadow (Figure 4-51). In those sections of the rille oriented more nearly in an east-west direction, illumination is such that excellent detail is shown. Telephoto coverage includes limited sections of the rille with such orientation that fine detail, including many boulders and rolling-rock tracks, can be seen (Figure 4-52).

Most terra is well shown, and the fine surface texture is very well reproduced in the telephoto frames. Steep slopes in the most rugged sections result in either hard shadows or overexposure sufficient to block detail. Detail is shown only in those limited areas where slope orientation or slope change results in more nearly grazing illumination. Although such areas are limited in extent, they do provide good indication of surface structure that may be representative of much larger areas.

Resolution of both telephoto and wide-angle frames is good, with detail a width of three to four scan lines wide observed.

#### 4.4.2.17 Site V-28, Alphonsus

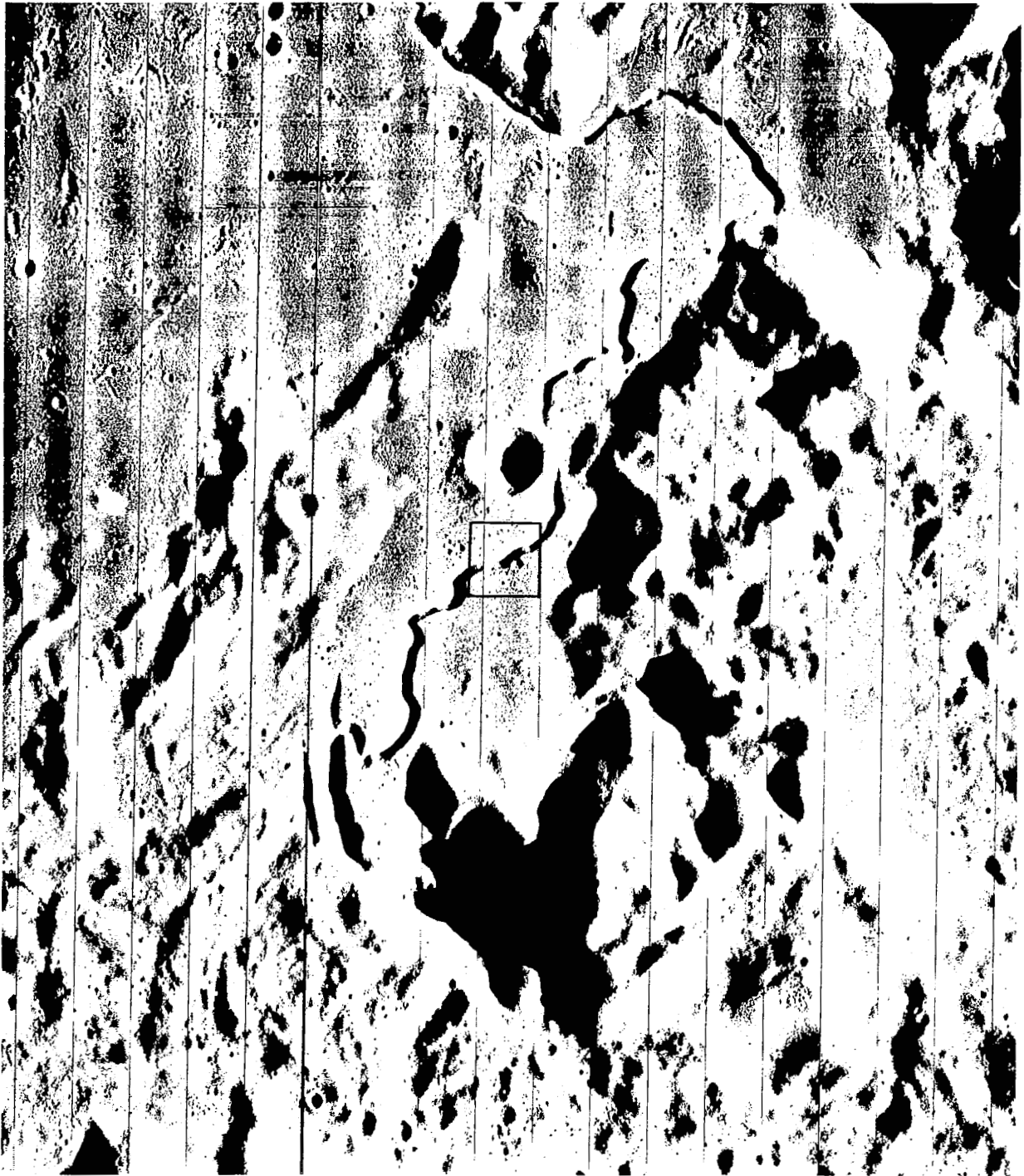
*Location:* 4.14°W longitude, 13.97°S latitude

*Altitude:* 113.8-111.5 km *Frames:* 116-119

*Phase angle:* 87.69 degrees

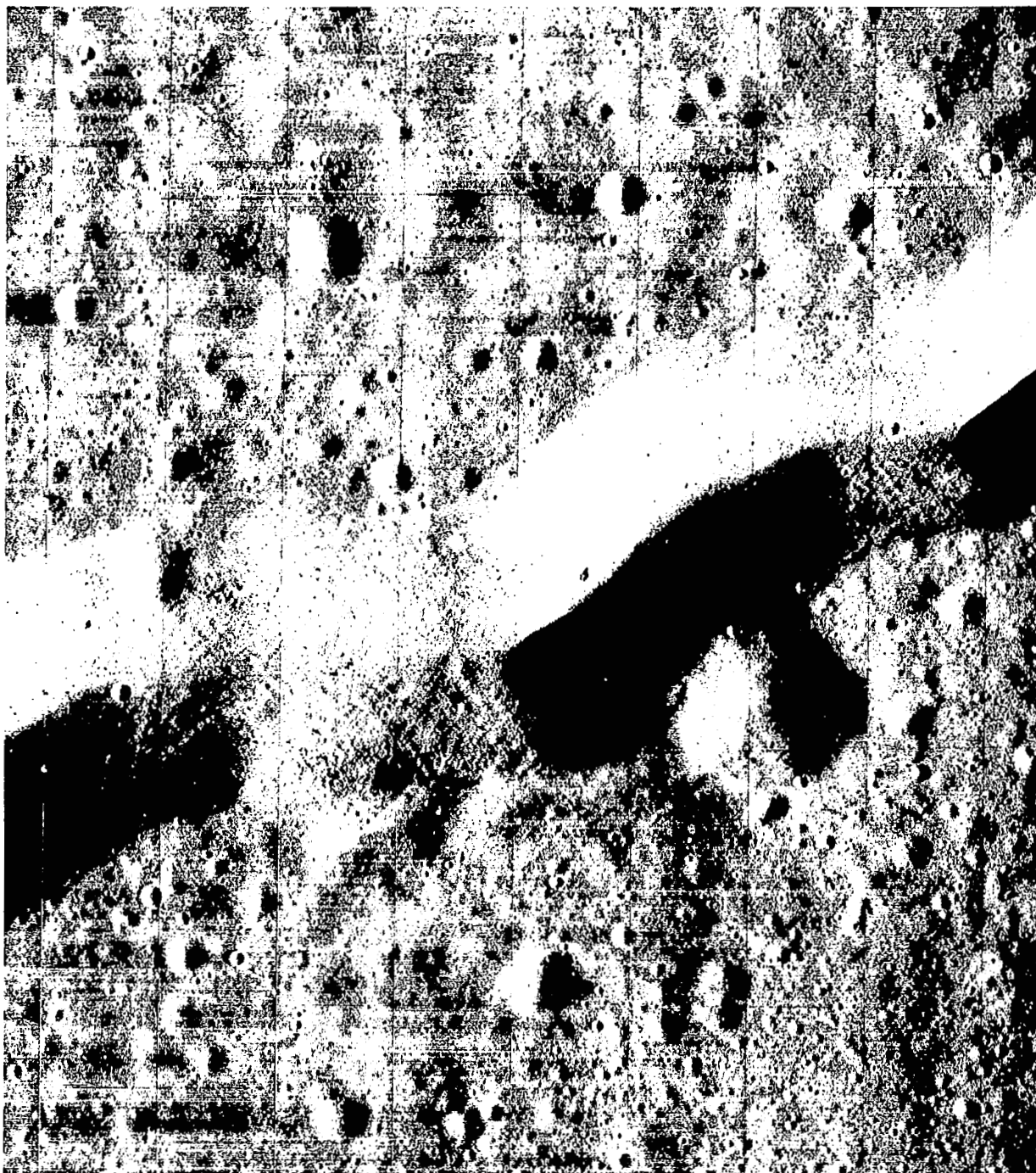
*Alpha:* -14.78 degrees *QUAL Albedo:* 0.088

*Shutter speed:* 0.04 second



Most of Wide-Angle Frame 105 is shown. This is the second of a sequence of four frames with 50% forward overlap. The area outlined is shown as Figure 4-52.

**Figure 4-51: Site V-26.1, Hadley Rille; Wide Angle**



This portion of Telephoto Frame 105 illustrates the slope detail present in the rille where its orientation provides suitable illumination angle.

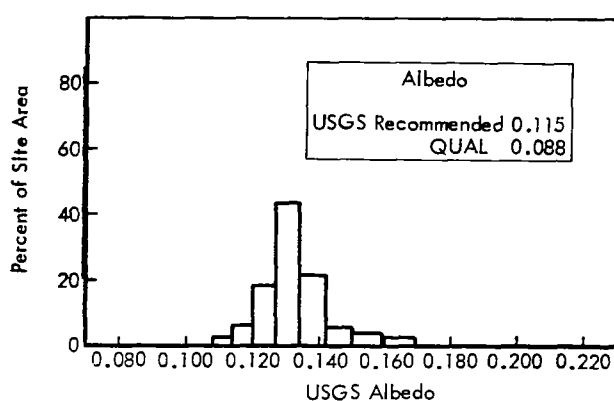
**Figure 4-52: Site V-26.1, Hadley Rille; Telephoto**

Alphonsus has been of particular scientific interest and a subject of telescopic observation for many years because of certain characteristics. Several prominent, dark-haloed craters that have been presumed to be volcanic occur on its floor. Alter and Kozyrev have reported observation of gas clouds in the area, of which the dark craters have been considered a possible source. Ranger IX landed within Alphonsus and produced good photographs of the floor, but as detail and ground resolution improved, area coverage decreased; thus, detailed information was limited to a portion of the floor only. Lunar Orbiter photography, on the other hand, extends detailed information of a major part of the feature.

Because the floor of Alphonsus is considered suitable for a landing, this site is included in the AAP group.

The site was photographed with a sequence of four frames exposed in the fast mode. Wide-angle coverage obtained by the sequence includes the western half of Alphonsus from east of the central peak to the edge of the mare surface on the west. Telephoto coverage includes a portion of the western rim of Alphonsus and the floor including the large, dark-haloed crater complex.

This site includes a rather wide range of albedo, as shown in the histogram (Figure 4-53). The



**Figure 4-53: Albedo Distribution for Site V-28, Alphonsus**

albedo recommended for QUAL exposure prediction computations was 0.088, although the albedo ranges between about 0.083 and 0.130 (corrected). Principal interest in the site was the lower-albedo floor.

Exposure obtained was very near optimum for the crater floor area in both wide-angle and telephoto frames. The western inner slope of Alphonsus is overexposed, as are most sunward slopes of terra-type hills and the central peak. These bright slopes do show some detail in the telephoto frames; thus, additional information may be obtainable by use of the enhancement technique employed at Langley Research Center in preparing additional GRE-reconstructed record from the magnetic-tape video signal recording. The telephoto frames show very good detail. The dark-haloed craters, included in Frame 118 and evident in the wide-angle photographs (Figure 4-54), do not seem, in the telephoto frames, to differ markedly from others in appearance (Figure 4-55). While an albedo difference is present, the lowered luminance is similar to that produced by surface slope. It will be noted, however, that the sunward slopes of the dark craters show more evidence of detail as a result of the reduced exposure.

Resolution of all frames was in the three- to four-scan line range near the camera axis.

#### *4.4.2.18 Site V-29, Rima Bode II*

*Location: 3.99°W longitude, 12.77°N latitude*

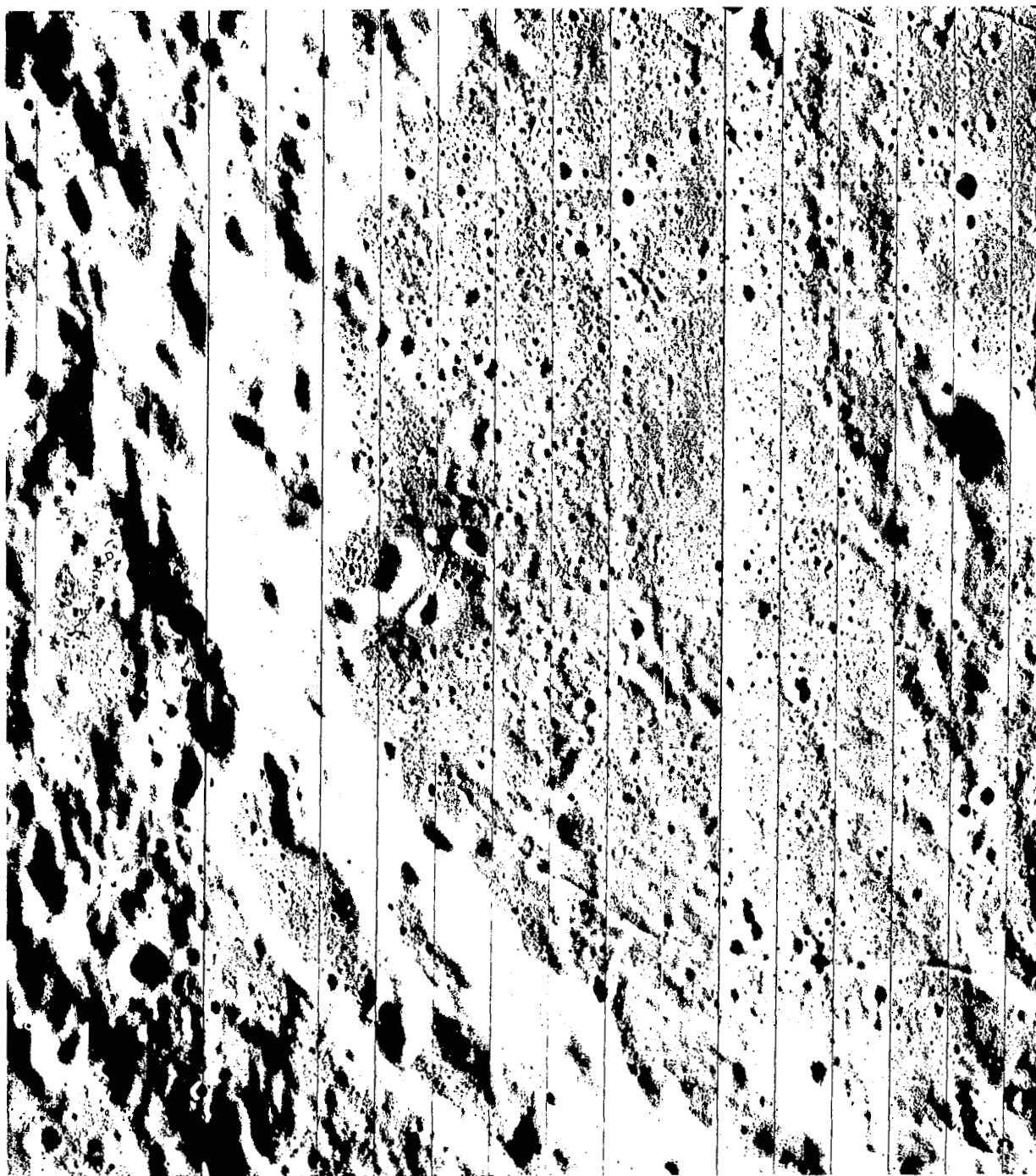
*Altitude: 104.5 km Frames: 120-123*

*Phase angle: 83.1 degrees*

*Alpha: -12.75 degrees QUAL Albedo: 0.070*

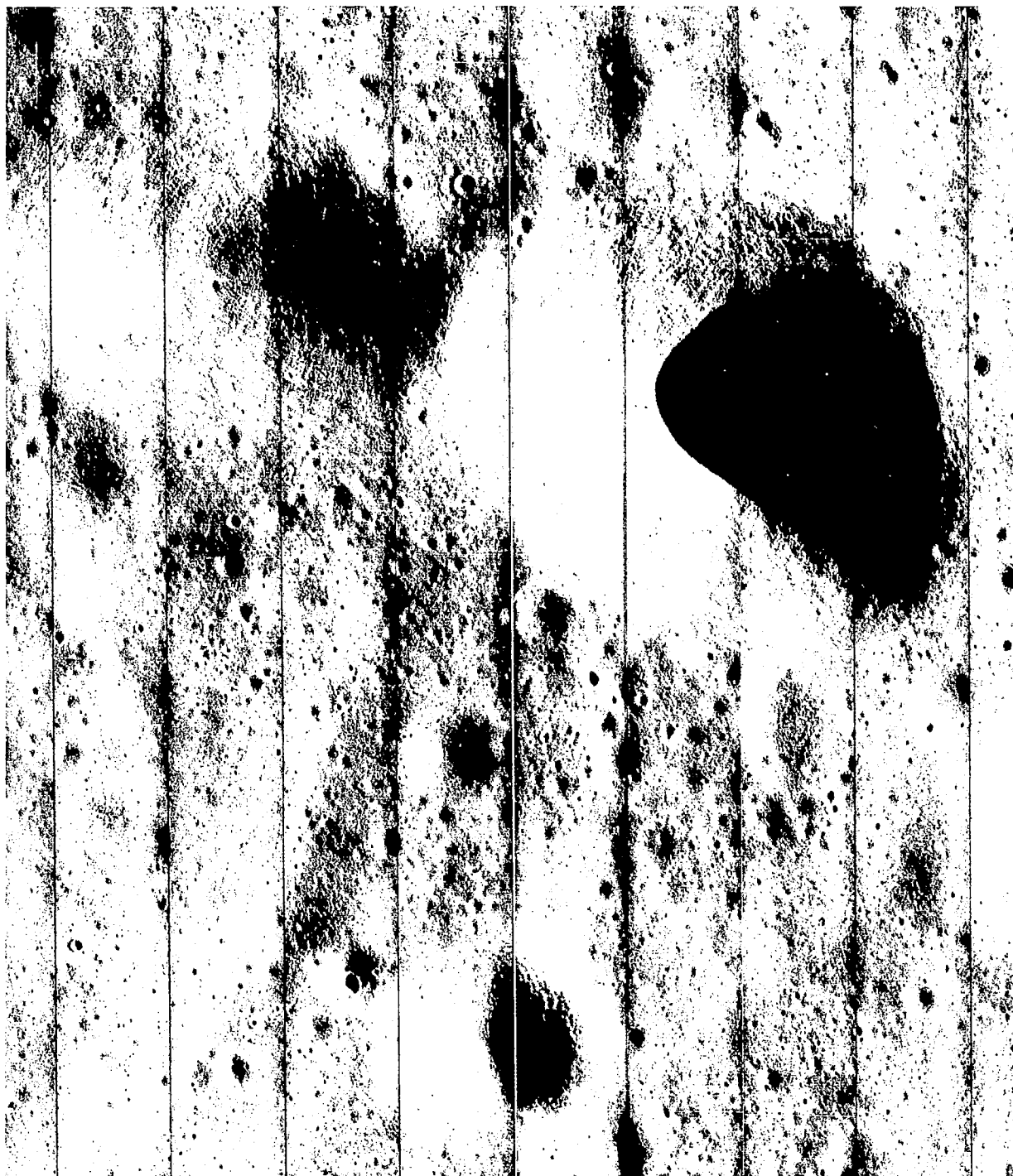
*Shutter speed: 0.04 second*

Rima Bode II is located in a combination of plains area and uplands terrain that extends southward from the Appennine Mountains and lies between Sinus Aestuum and Mare Vaporum. The rille is relatively straight and runs in a general east-west direction through plains areas as well as portions of upland terrain. The rille is tangent to an elongate crater that has displayed a high thermal anomaly during eclipse. Part of the area through which the rille passes has a dark, flat, mare-like appearance. Some of the sloped terrain also appears to be covered by



This photograph, including most of Wide-Angle Frame 118, shows the dark-haloed crater near the western side of crater. Note albedo difference.

**Figure 4-54: Site V-28, Alphonsus; Wide Angle**



This portion of Telephoto Frame 118 includes the prominent dark-haloed crater. Note that the albedo difference of the halo is less evident than in the wide-angle photograph.

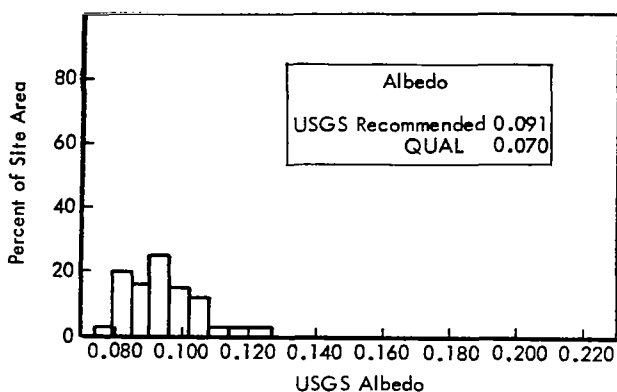
**Figure 4-55: Site V-28, Alphonsus; Telephoto**



a dark mantling material. Two well-defined lesser craters, Bode C and D, are located slightly south of the rille. The Rima Bode II area is of interest because of these diverse geologic features.

The rille and the crater may be the source of some of the mantling materials and the elongate crater is presumably volcanic. Mission IV photography indicated that the crater was relatively new.

An exposure time of 0.04 second was selected for the fast four-frame sequence used for Site V-29. Distribution of albedos for this site is shown in histogram form in Figure 4-56. Ex-



**Figure 4-56: Albedo Distribution for Site V-29, Rima Bode II**

posure for the wide-angle frames was good. Contrast range and tonal values were satisfactory. The selected exposure time, the maximum available, resulted in some tendency to underexpose the telephoto frames because of the generally low albedo. Frame ends were fairly dense in the later case, although frame centers were quite good. Characteristically, off-axis light transmission falloff was also a contributory factor to the slight underexposure noticeable in the end framelets of the 610-mm-lens photographs. The off-axis light transmission falloff is less marked in the 80-mm lens.

The wide-angle photographs are well centered on the rille. Plains and terra areas and some moderately bright craters are included in these frames. The scene has a wide luminance range.

Since the main rille is oriented in a general east-west direction, it was photographed under good illumination conditions with a minimum of detail lost by excessive brightness or deep shadow. The elongated or double crater bordering the rille is shown with a short three-crater chain, which may be a subsidence feature. Craters Bode C and E and Marco Polo C are also encompassed in the four wide-angle frames. Small details are well defined in these photographs, represented by most of Wide-Angle Frame 122 in Figure 4-57.

Image quality of the telephoto frames was satisfactory in spite of the tendency to underexposure. The four telephoto frames include a fairly extensive portion of the rille. Good detail of the elongated crater and its associated crater chain is shown in the middle portion of Telephoto Frame 122. Structural features, including fine details such as rocks and projections, may be seen on the rille and crater slopes where photographic conditions were optimum. Some detail is lost in very bright highlighted slopes and areas in deep shadow. Surface texture and small crater detail are very good. Resolution was good in both telephoto and wide-angle photographs. Craters and rocks spanning between three and four scan lines could be identified. A portion of Telephoto Frame 122 is shown in Figure 4-58.

#### 4.4.2.19 Site V-30, Tycho

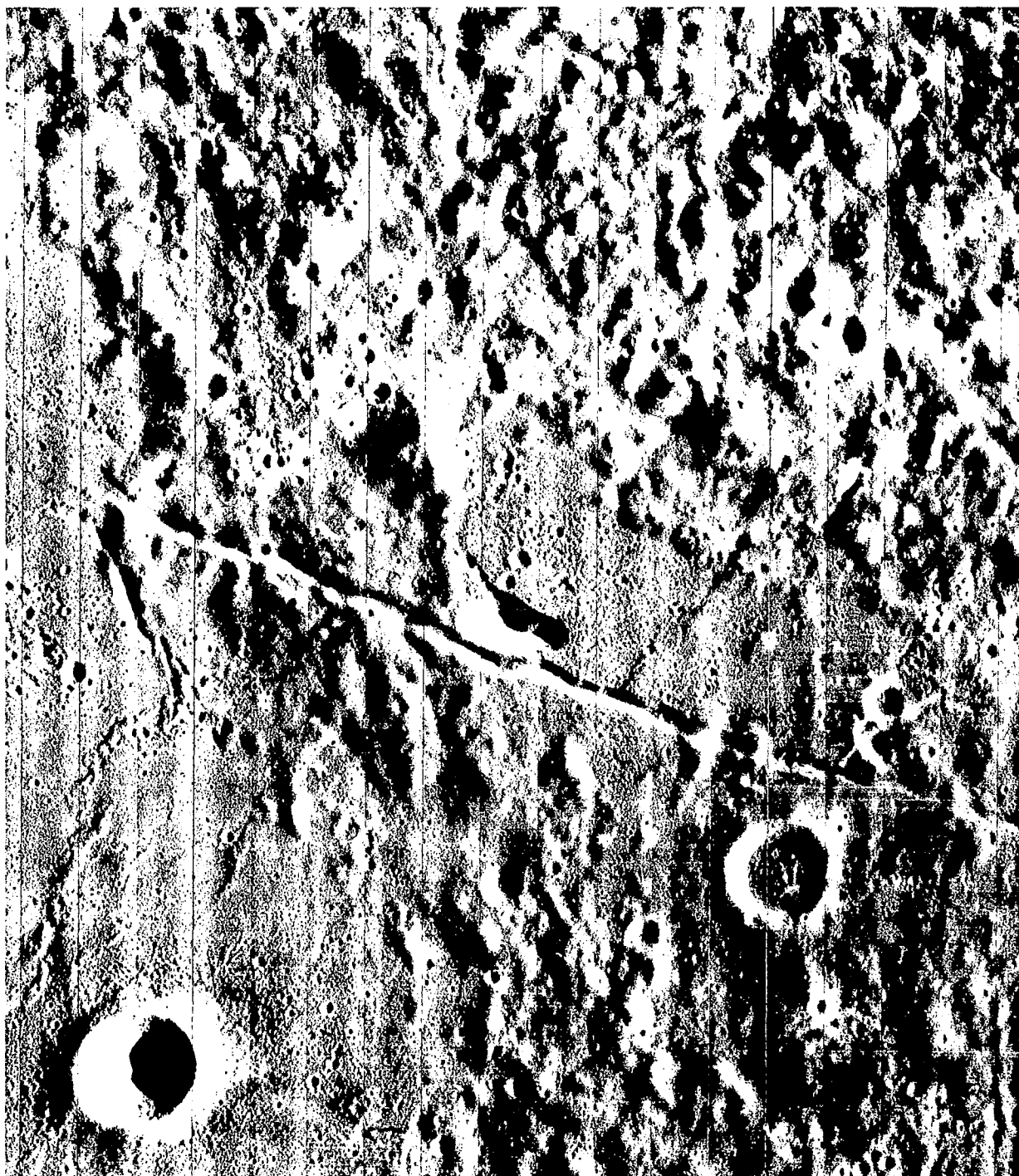
*Location: 11.75°W longitude, 41.98°S latitude*

*Altitude: 218-210 km Frames: 125-128*

*Phase angle: 79.80 degrees Alpha: +1.06 degrees*

*QUAL Albedo: 0.119 Shutter speed: 0.04 second*

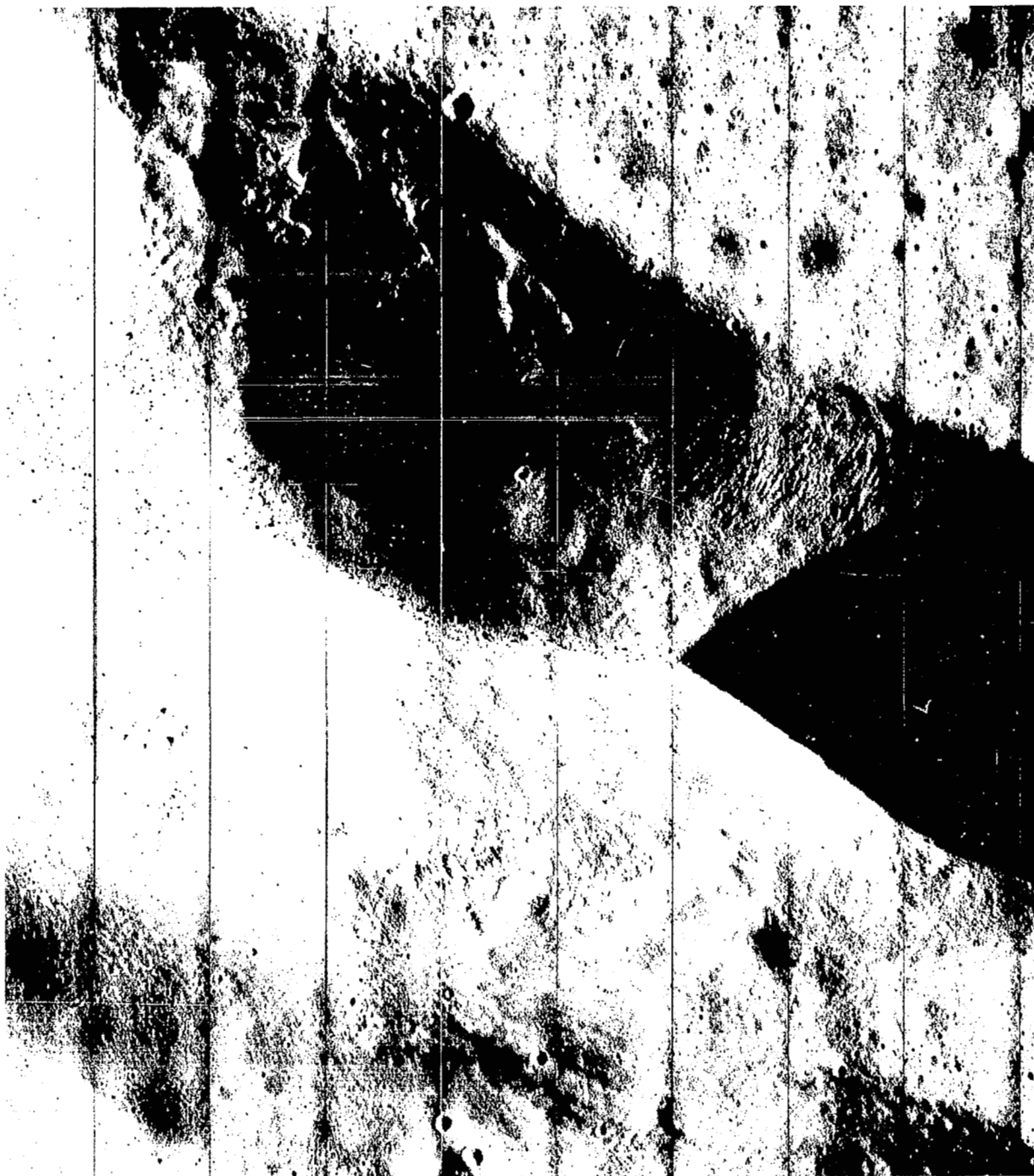
Tycho, about 80 kilometers in diameter, is one of the most prominent lunar features because of its high luminance and very extensive bright ray system. It is the location of a major thermal anomaly and has a high radar reflectivity. These characteristics generally are associated with very young craters. Since the crater is located entirely within the southern highland, it was expected that this site would provide significant geological information concerning highland structure and material properties. Characteristics relating to the high radar and thermal anomalies also were of interest.



Most of Wide-Angle Frame 122, the third of a sequence of four.

**Figure 4-57: Site V-29, Rima Bode II; Wide Angle**



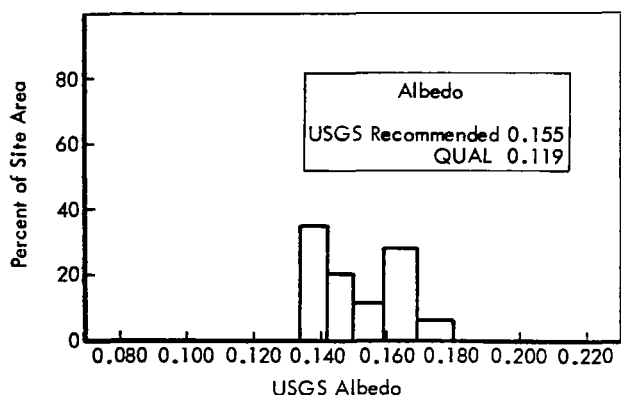


A part of Telephoto Frame 122, illustrating detail shown on interior of elongated crater near Rima Bode II and on the rille slopes.

**Figure 4-58: Site V-29, Rima Bode II; Telephoto**

The site was photographed with a four-frame sequence taken in the fast mode. The crater is nearly centered in Wide-Angle Frame 125. Coverage includes the outer rim area from about 15 kilometers south of the southern rim to about 100 kilometers beyond the northern rim and thus a part of the dark halo. The telephoto coverage includes a portion of the crater floor and extends north across the northern rim.

Selection of the proper shutter speed for exposure control was complicated by the high albedo of the site, as shown in Figure 4-59, and



**Figure 4-59: Albedo Distribution for Site V-30, Tycho**

the very rough and rugged terrain containing a high percentage of quite steep slopes. It was apparent that sunward slopes undoubtedly would be overexposed even at the fastest shutter speed and, on the other hand, there would be many areas of hard shadow. Selection, then, was based on the recommended albedo of 0.119 (corrected) and a level surface.

The first immediate impression of the photographs is that of extremely high contrast caused by the profusion of hard shadows and overexposed slopes as seen in Figure 4-60 from Wide-angle Frame 126. However, upon closer examination it is found that more nearly level areas and particularly the small smooth "lake-like" areas show excellent detail and exposure. This effect is present in both wide-angle and telephoto frames. Considering the above factors, it becomes apparent that the shutter speed selected was the correct one.

In the telephoto frames, appreciable areas exceed the luminance limits of the system. However, the high contrast sharply delineates the extremely complex structure of the crater floor in fine detail (see Figure 4-61). Outer rim detail, where blast effects of the cratering event have apparently resulted in a less blocky or rugged topography, is shown with excellent quality (see Figure 4-62).

Resolution is very good in both wide-angle and telephoto frames where detail has not been lost due to the luminance extremes. Features spanning three to four scan lines were observed on the examined GRE record. The sequence provides an excellent record of the character of a recent upland crater and effects of the violent event on the surrounding area.

#### *4.4.2.20 Site V-31, Sinuous Rille Complex East of Plato*

*Location: 2.52°W longitude, 44.60°N latitude*

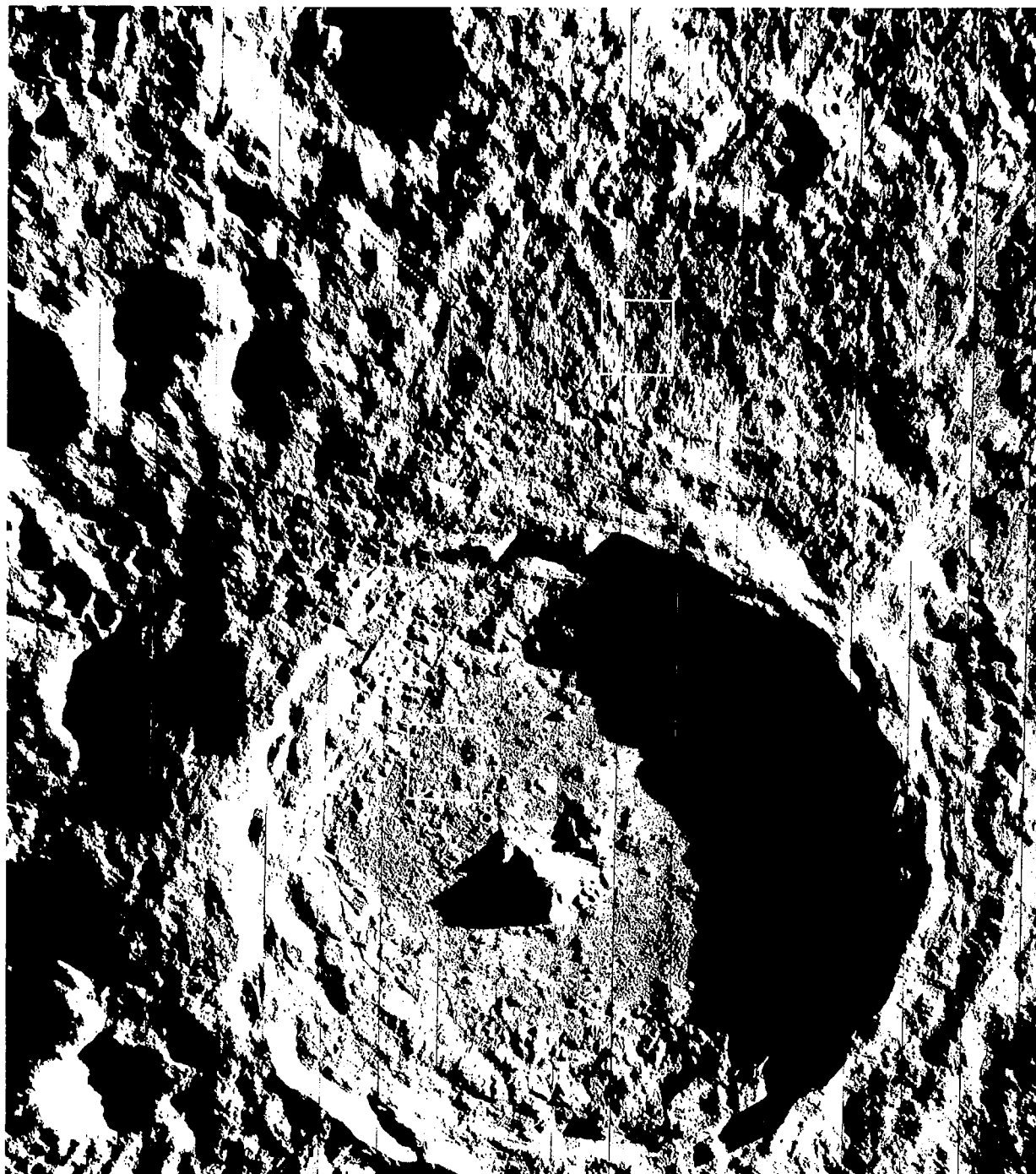
*Altitude: 230-240 km Frames: 129-132*

*Phase angle: 78.87 degrees Alpha: -5.88 degrees*

*QUAL Albedo: 0.098 Shutter speed: 0.04 second*

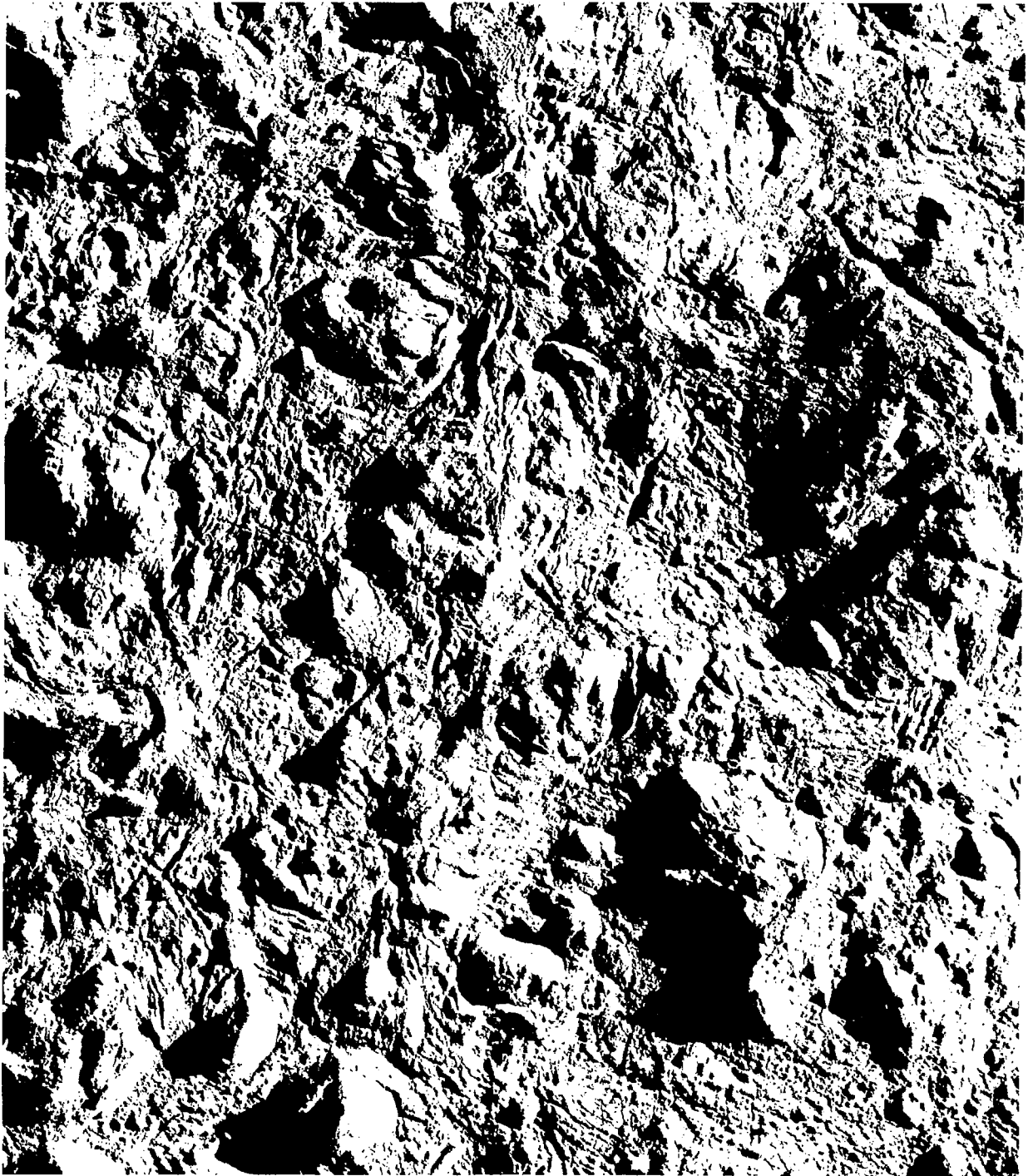
This site includes a complex system of meandering rilles located in both smooth and rugged terra, and thus provides one of the best areas for study of this class of feature. In other areas such as the vicinity of Aristarchus and the Harbinger Mountains (Site V-46), similar meandering rilles occur in mare surface. A comparison of characteristics of these features in two different geological units may be made. The significance of this very interesting class of rilles became more apparent as a result of Mission IV photography, which showed these rilles to be quite numerous. Indications that their origin may be related to flow rather than tensions were derived from study of Mission IV photographs.

The site was photographed with a four-frame sequence taken in the fast mode. Wide-angle coverage extends from the northern edge of Mare Imbrium, across the terra to near Mare Frigoris, and between the western end of the Alpine Valley and Plato. Only a small segment of the eastern side of Plato is included. Telephoto coverage includes the rugged terra west



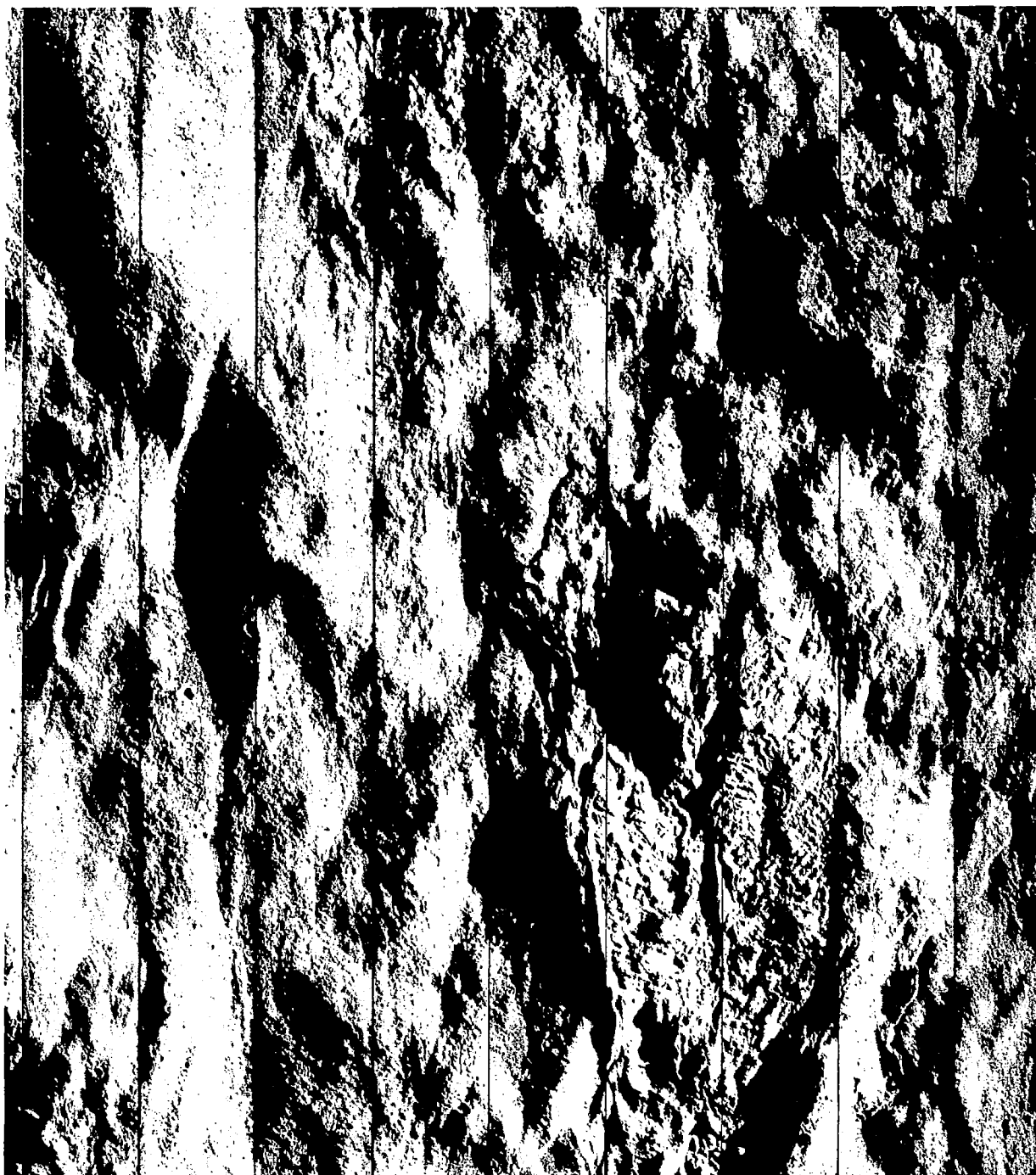
Most of Wide-Angle Frame 126. Note extreme contrast. Areas shown in Figures 4-61 and 4-62 are outlined. Arrow shows approximate Surveyor VII landing site.

**Figure 4-60: Site V-30, Tycho; Wide Angle**



A portion of Telephoto Frame 125 showing detail of crater floor. Extreme contrast.

**Figure 4-61: Site V-30, Tycho Floor; Telephoto**

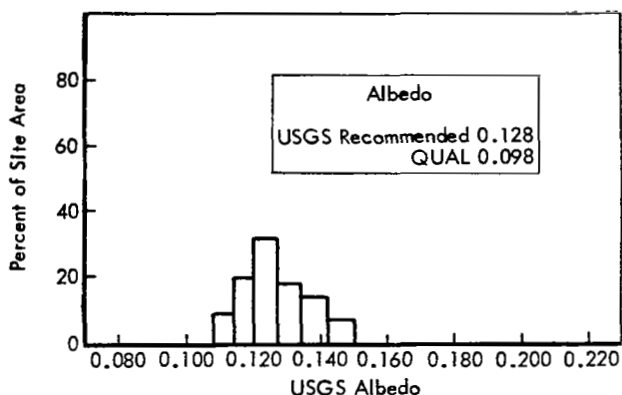


A part of Telephoto Frame 128 illustrating detail shown in outer rim. Area shown is of the northern rim as outlined in Figure 4-60.

**Figure 4-62: Site V-30, Tycho Rim; Telephoto**

of the Alpine Valley and the smoother terra, including the principal sinuous rille.

The area including the sinuous rille is predominantly of light plains-forming material, but the site includes both light mare and terra, resulting in an albedo range between 0.083 and 0.115 (corrected) (see Figures 4-63 and -64). Exposure



**Figure 4-63: Albedo Distribution for Site V-31, Sinuous Rille East of Plato**

for the site was computed using a near-average albedo value of 0.098. The shutter speed of 0.04 second resulted in near-optimum exposure of the principal area in both wide-angle and telephoto frames. Because of the meandering character of the rille, and its widely varying orientation with respect to the direction of illumination, good lighting of rille inner slopes occurs in many sections and surface detail is very well shown, as seen in Figure 4-65.

In addition to providing very good telephoto coverage showing detailed characteristics of the smooth terra, fine surface texture on steep slopes of the mountains west of the Alpine Valley was recorded. Although slopes facing the Sun directly are overexposed, there are numerous places where slope orientation provided near-grazing illumination and the texture and fine detail existing on these slopes are very well shown. This sequence provides good quality photographs of a variety of terrain and terrain features, rather than being limited to the sinuous rille.

Photographic resolution was determined to be adequate for detection and identification of

features to between three and four scan lines.

#### **4.4.2.21 Site V-32, Eratosthenes**

*Location: 10.62°W longitude, 13.21°N latitude*

*Altitude: 103-108 km Frames: 133-136*

*Phase angle: 60.41 degrees*

*Alpha: +11.71 degrees*

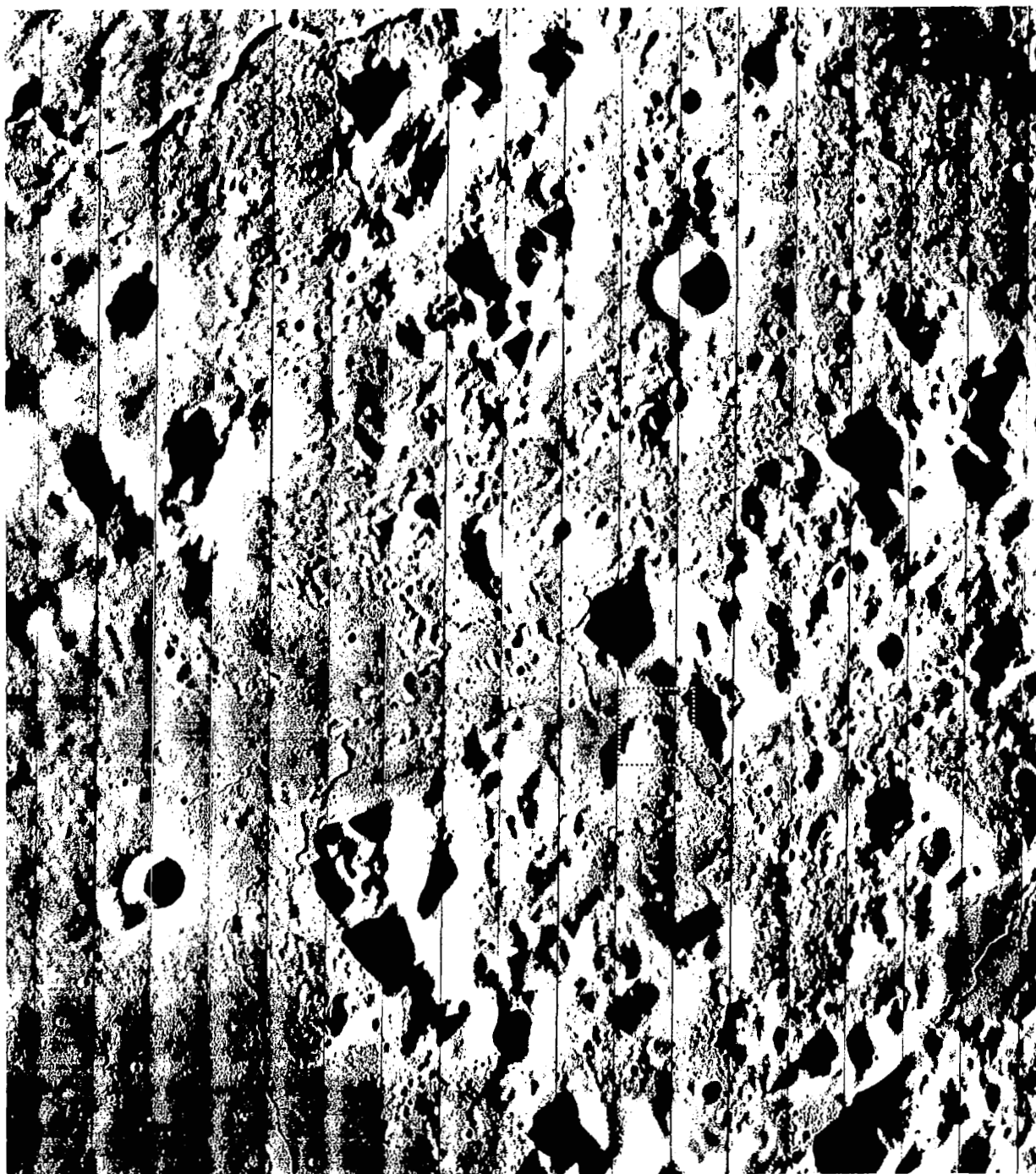
*QUAL Albedo: 0.093 Shutter speed: 0.02 second*

Mission V sites include several major young rayed craters such as Tycho (Site V-30), Copernicus (Site V-37), and Aristarchus (Site V-48) that have been grouped in the Copernican stratigraphic system, the youngest geological system. Site V-32 was intended to provide comparison of the characteristics of the Copernican system and the next older — the Eratosthenian. The principal distinguishing characteristic of the latter is the absence of bright rays. Additional detailed information regarding the differences in amount of erosion, subsequent cratering, characteristics of secondary craters, type of filling, etc., was desired. Eratosthenes also exhibits structural characteristics of interest.

The site was photographed using a four-frame sequence, which was exposed in the slow mode to provide broader wide-angle coverage and telephoto sampling over a greater area at the expense of losing contiguous telephoto coverage. Wide-angle coverage of the area extends from about 100 kilometers south of Eratosthenes to about 30 kilometers north of its rim. The centerline of the sequence passes across the eastern side of Eratosthenes; all of the crater except a very small section of the western rim crest is within the field of view. Telephoto coverage of the first frame of the sequence includes only the ejecta area of the outer rim. Following frames carry coverage across the crater rim and onto the floor.

The albedo distribution within the site area (see Figure 4-66) ranges between 0.074 and 0.093 (corrected), with the higher range more predominant as the area lies in and near the southwestern end of the Apennine Mountains. Exposure computations were based on the higher value to provide better detail in the brighter areas.





Most of Wide-Angle Frame 131 is shown.

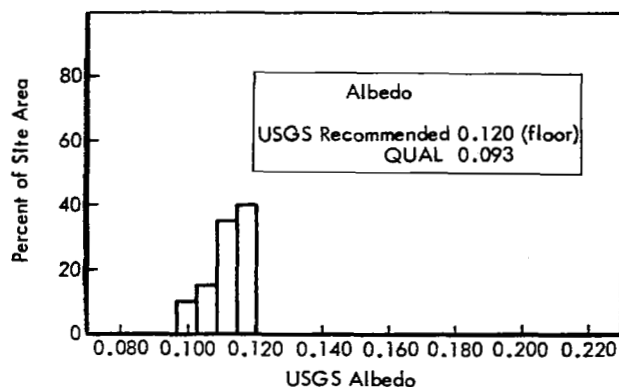
**Figure 4-64: Site V-31, Sinuous Rille East of Plato; Wide Angle**



Part of Telephoto Frame 130 showing a portion of rille and some of the terra hills. Note detail on slopes where rille is oriented east-west.

**Figure 4-65: Site V-31, Sinuous Rille East of Plato; Telephoto**





**Figure 4-66: Albedo Distribution for Site V-32, Eratosthenes**

Exposure of the wide-angle photographs was generally satisfactory. The lighter areas surrounding the crater and the crater floor are well exposed. Darker areas outside the crater tended to be slightly underexposed but not enough to cause loss of data. On the other hand, some areas within the crater and on the western inner crater walls facing the Sun were overexposed. Figure 4-67 is representative of the wide-angle photographs.

General exposure of the telephoto frames is such that little data on sunward gentle slopes are lost but are adequate to show good detail on more level areas and slight slopes away from the Sun. In some cases, underexposure appeared to cause loss of data although some image showed that hard shadow was not present. Because only the eastern inner slope of Eratosthenes is included within the telephoto coverage, appreciable hard shadow is present but very good detail is present in the illuminated areas (see Figure 4-68). Two dark-haloed craters located about 10 kilometers south of the crater rim are included in the telephoto coverage (Frame 134).

#### 4.4.2.22 Site V-33, Area of Copernicus CD

*Location: 14.75°W longitude, 6.51°N latitude*

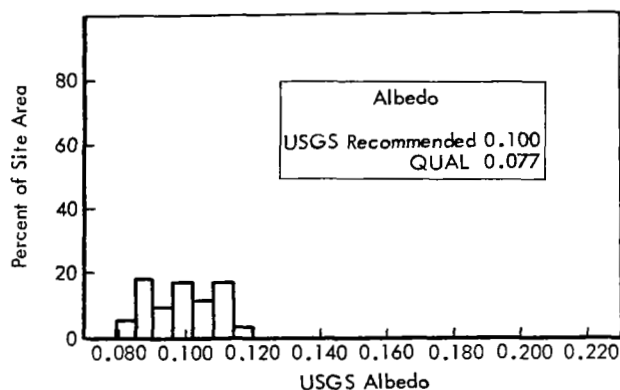
*Altitude: 99.4 km Frame: 137*

*Phase angle: 59.0 degrees Alpha: +13.86 degrees QUAL Albedo: 0.077 Shutter speed: 0.04 second*

This site is southeast of Copernicus near the minor crater Copernicus CD. The area is fairly

flat and appears to be a complex field of dark volcanic matter that includes domes, craters, and layered materials. Secondary craters of Copernicus are also present in this region. Relative ages of the volcanic materials and the secondary craters are of geologic interest. Mission IV photographs indicate the presence of young materials in this area. Additional photographs of this site were desired to obtain data concerning surface characteristics and age relationships of the predominant features.

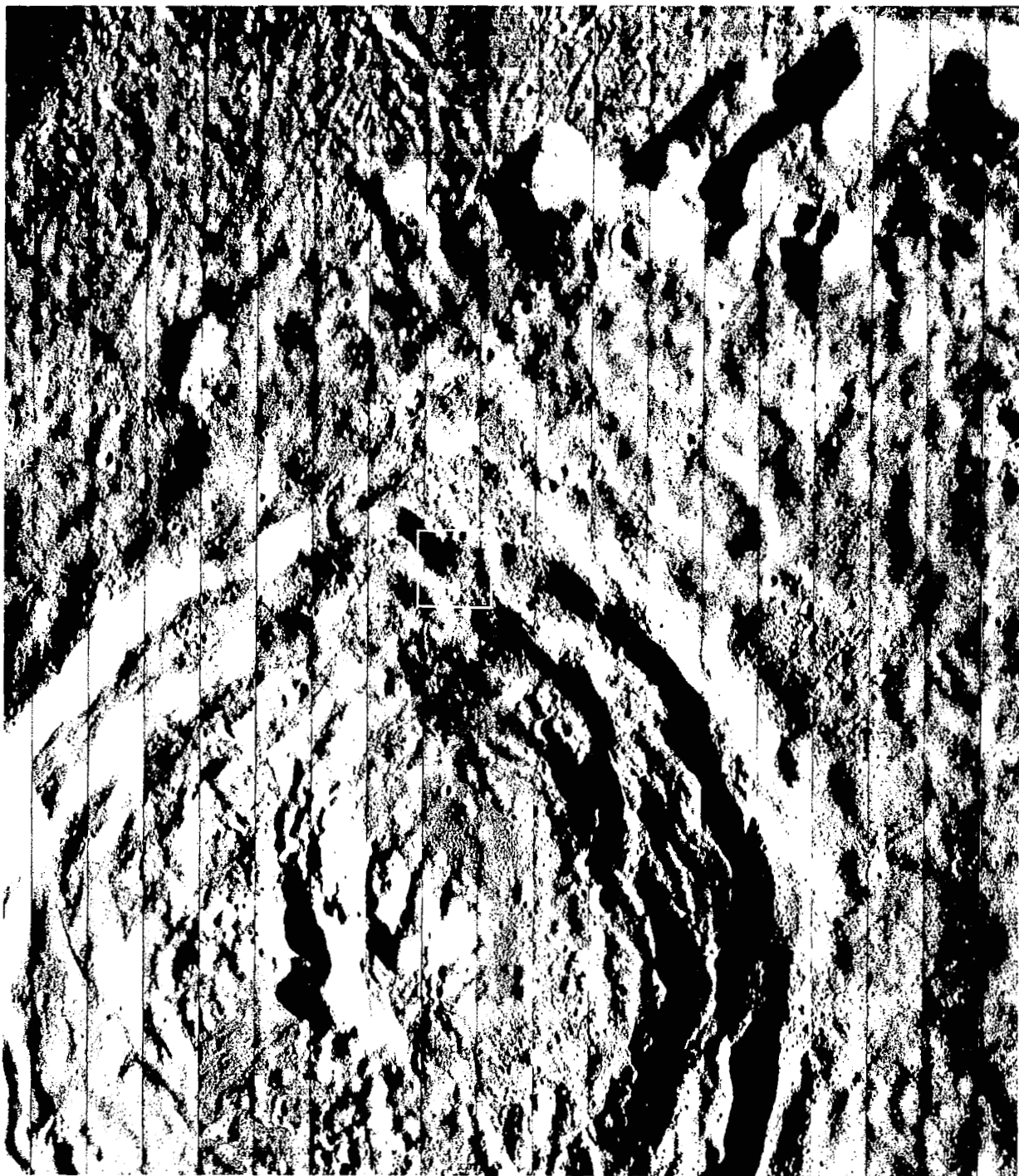
The shutter speed of 0.04 second was selected to produce optimum image quality of the flat portion of the terrain. It was anticipated that detail would be lost in sunlit slopes where luminance exceeded system limits. Albedo distribution for this site is given in Figure 4-69.



**Figure 4-69: Albedo Distribution for Site V-33, Area of Copernicus CD**

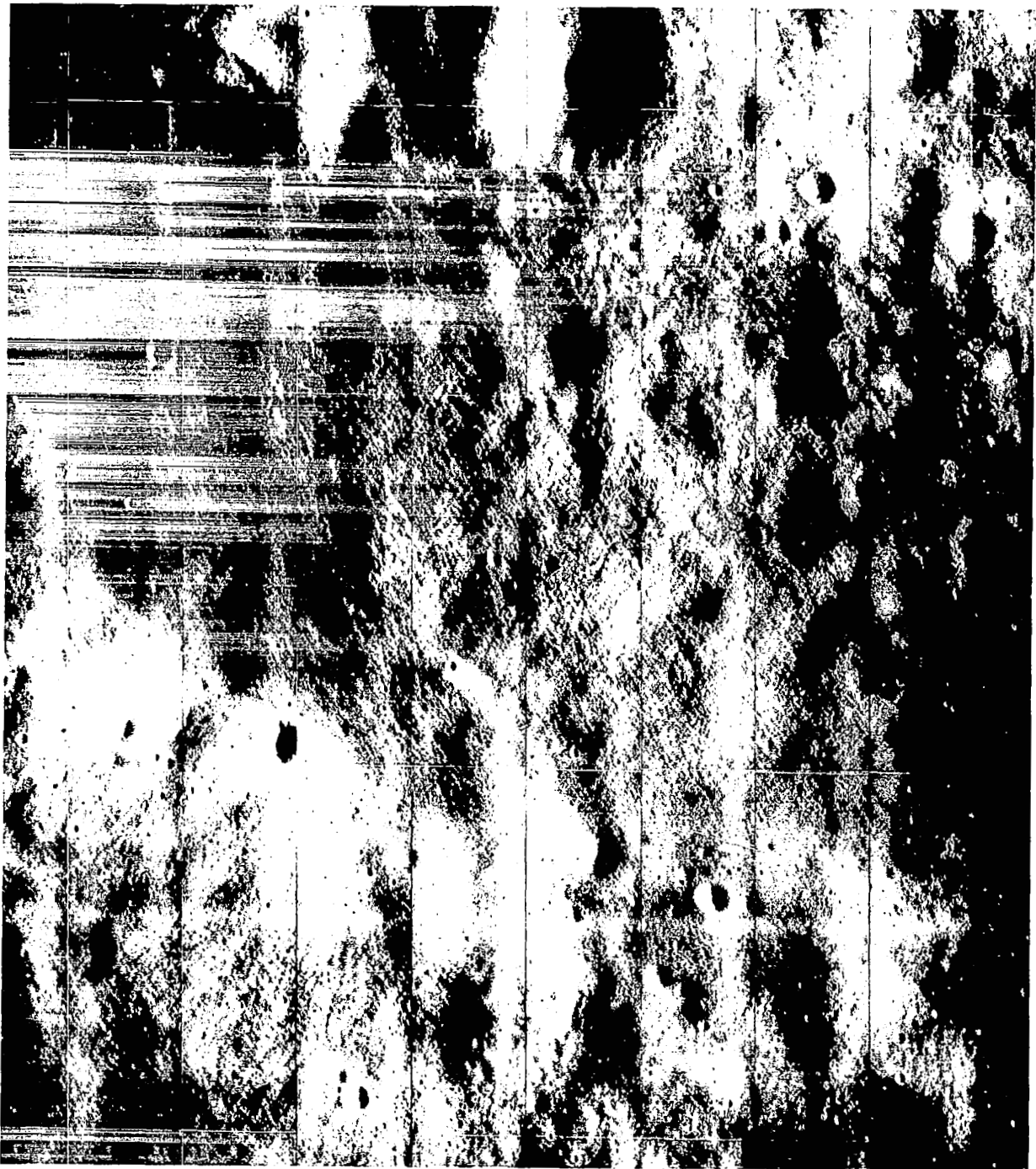
The selected exposure time produced wide-angle and telephoto frames of good photographic quality with very good detail of the level areas in the terrain. Satisfactory image densities and contrast ranges were obtained in both photographs. Examination of the second-generation positive GRE 35-mm film indicated that very satisfactory positive prints could be made from the reconstructed record.

Surface texture was very good in both wide-angle and telephoto frames. As anticipated, some loss of detail occurred in bright slopes and deep shadow areas. However, the proportion of such areas in the scene to frame coverage was small. Consequently, the loss of such informa-



Wide-Angle Frame 136, the last of a four-frame slow sequence.

**Figure 4-67: Site V-32, Eratosthenes; Wide Angle**



A part of Telephoto Frame 136. The area shown is outlined in Figure 4-67. Illustrates the detail shown on the inner crater slopes.

**Figure 4-68: Site V-32, Eratosthenes; Telephoto**

tion was minimal. The wide-angle photograph includes a large group of Copernican secondaries and dark-haloed craters of special interest (see Figure 4-70). A considerable number of these secondary craters is included in the telephoto frame, thus providing a means for a detailed evaluation of their character. Note that in Figure 4-71, the lower albedo of the dark-haloed craters is not as evident as in the wide-angle photograph. Resolution of detail appeared to be slightly better in the telephoto frame than in the wide-angle photograph. Observed resolution limits for small craters were approximately three and four scan lines, respectively.

#### 4.4.2.23 Site V-34, Fra Mauro

*Location: 16.66°W longitude, 7.18°S latitude*

*Altitude: 104.0-103.1 km Frames: 138-141*

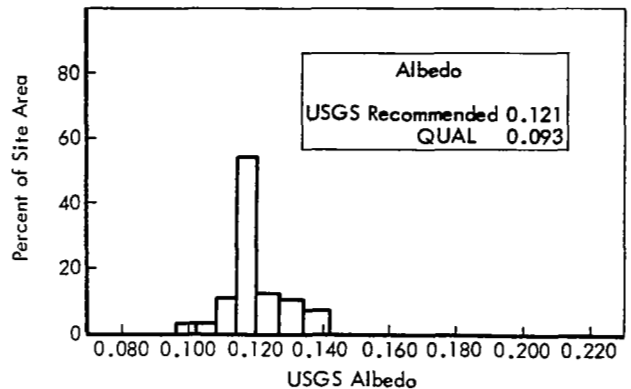
*Phase angle: 74.20 degrees Alpha: -0.56 degree*

*QUAL Albedo: 0.093 Shutter speed: 0.04 second*

The site includes the southern part of Fra Mauro and the ring hills separating Fra Mauro, Parry, and Bonpland. These three features appear to be very old filled craters. This site was selected entirely on the basis of Mission IV photography. Of principal interest is a line of small, dark domes near the south-central edge of Fra Mauro first discovered on the Lunar Orbiter photographs. In addition to the domes, other features of interest included: the hummocky Imbrium ejecta, the smooth ring hills or old crater rims, and linear rilles. Two linear rilles appear to intersect the hills. Where a rille passes by the line of small domes, it appears to be filled. This site has been included in the AAP site group.

The site is predominantly of a mare-like terrain, except for the ring hills, but is brighter than average for mare. The albedo distribution, Figure 4-72, reflects the proportionately large area of near-uniform albedo, smaller area of the brighter rim hills, and limited amount of darker surface. Exposure was computed on the basis of the greater area having a corrected albedo near 0.093.

Exposure of both wide-angle and telephoto frames appears to be near optimum for the principal areas of interest. Only the bright sun-



**Figure 4-72: Albedo Distribution for Site V-34, Fra Mauro**

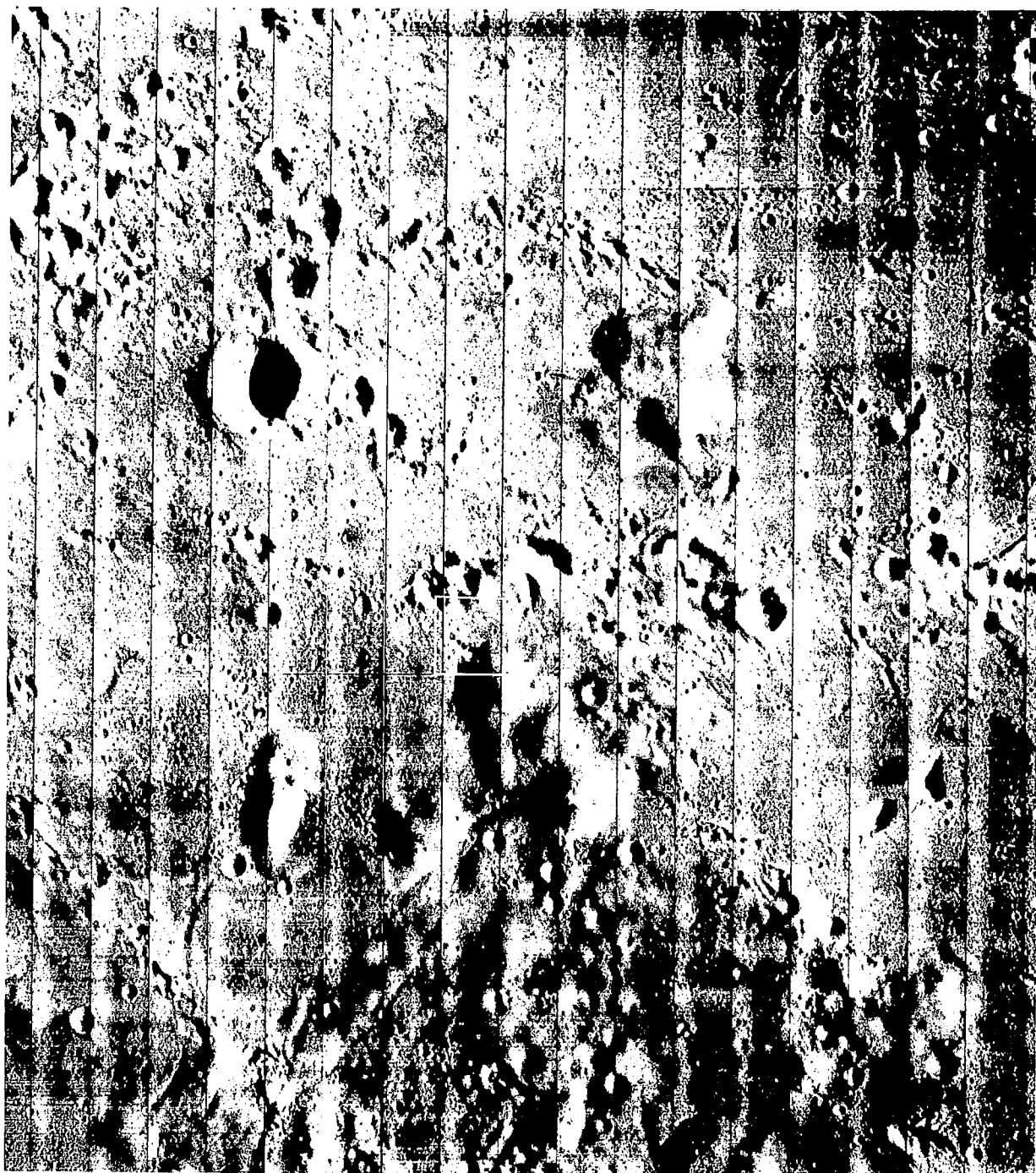
ward slopes of the ring hills are severely overexposed, but good detail is present in many places on these formations. The line of domes is well centered within the site coverage. Figure 4-73 is representative of the wide-angle photography.

The telephoto frames are of very good quality. Dome detail is very well shown, although the lower albedo near these features is not marked in the telephoto coverage. Dark craters in the northern part of Bonpland are shown. The line of domes is included in Telephoto Frames 139 and 140. A portion of Telephoto Frame 139 is shown in Figure 4-74.

The western end of Telephoto Frame 138 includes the crest of the ring hills between Fra Mauro and Bonpland. Slopes are not excessive in this area and the surface texture of this formation is shown to great advantage, as seen in Figure 4-75. Of particular interest to geologists may be what appears to be exposed bedding of boulders on a northerly facing slope. Within this area are several very clearly defined tracks produced by boulders rolling down the slope, with the boulder resting at the lower end. One or two others were noted that are fainter, possibly partly obliterated by erosion or material transport. The resolution of the photographs is exemplified by the clarity with which such detail may be seen.

#### 4.4.2.24 Site V-35, Copernicus Secondaries

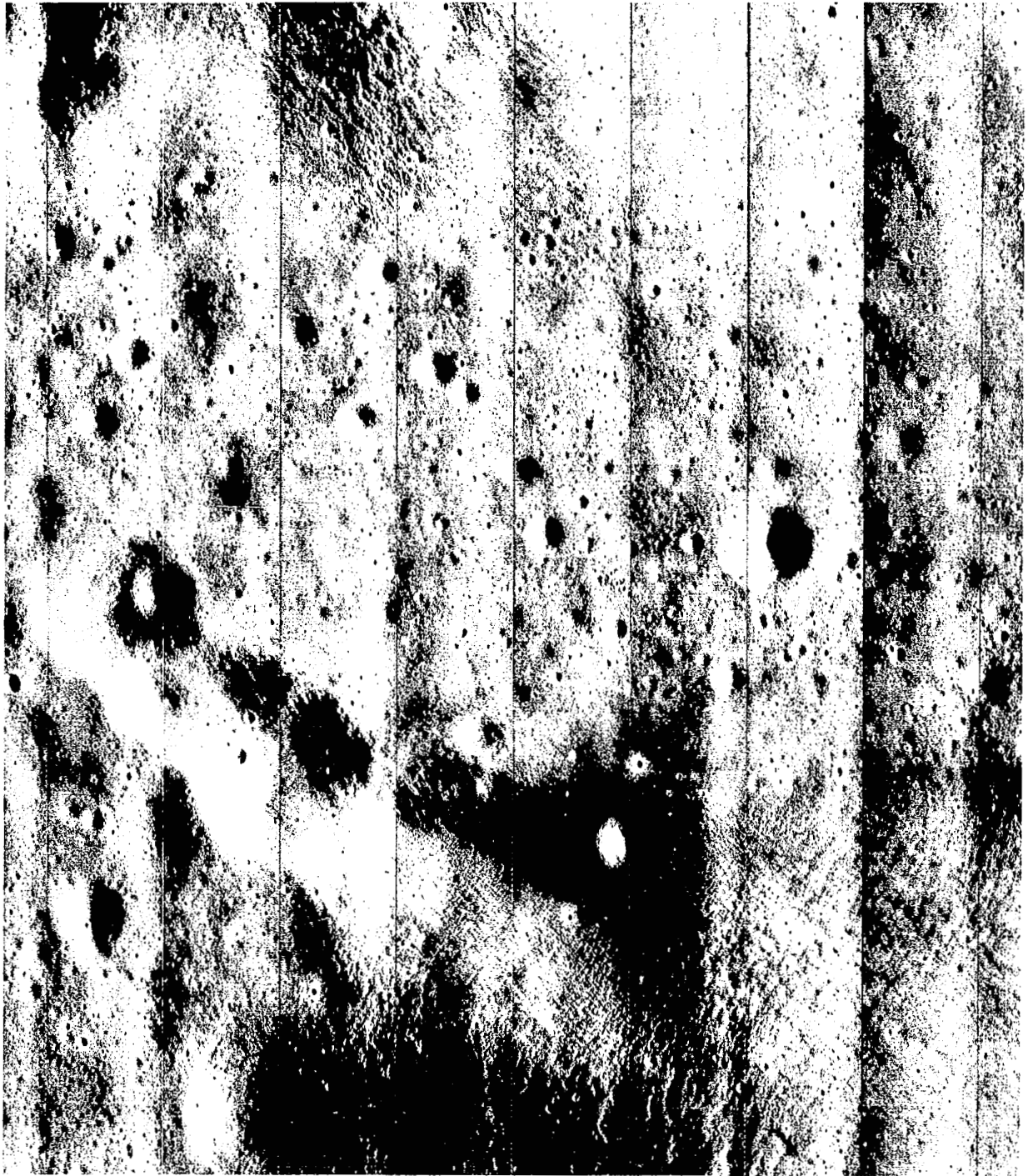
*Location: 16.25°W longitude, 14.38°N latitude*



Wide-Angle Frame 137. Note dark-haloed crater.

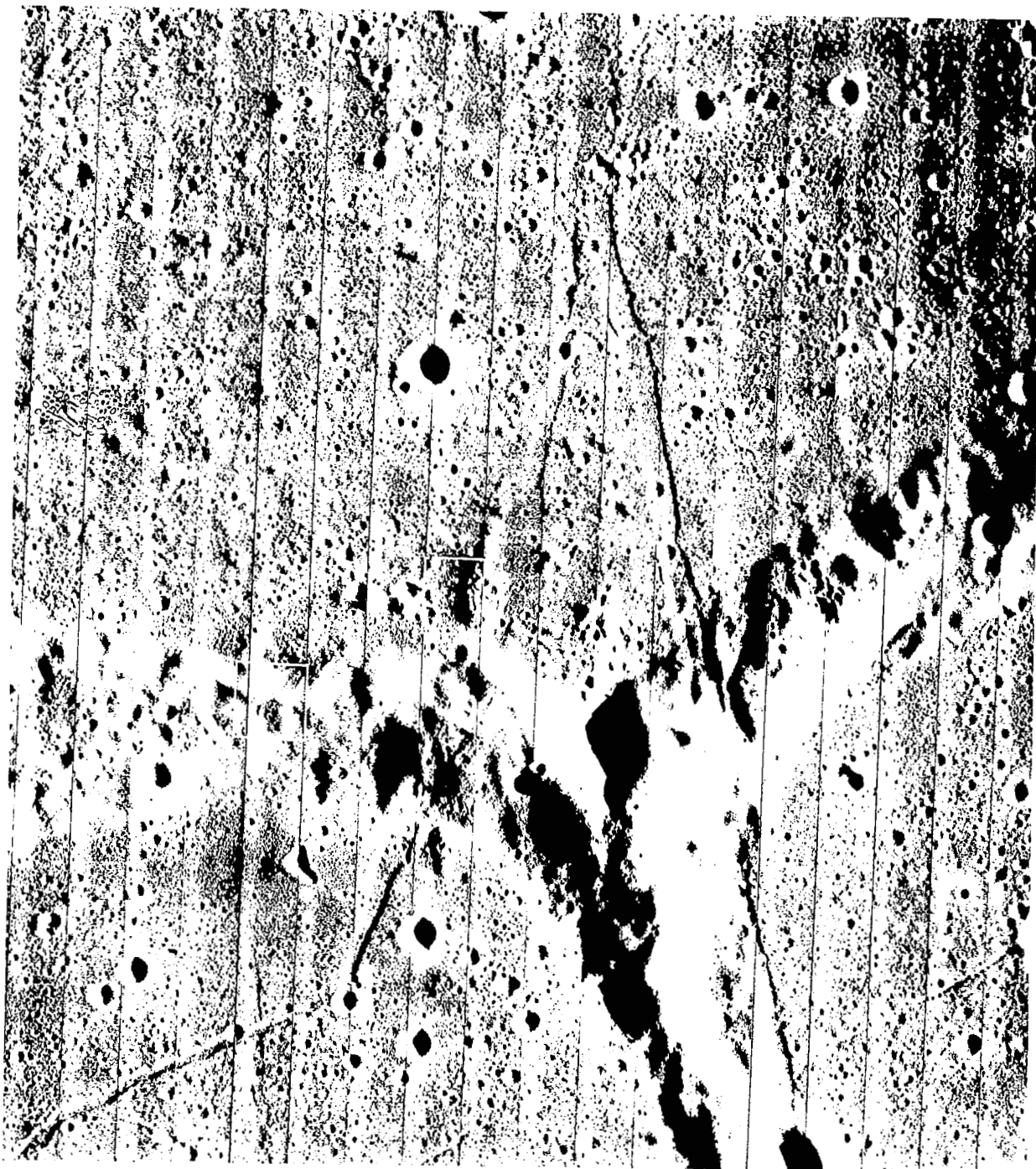
**Figure 4-70: Site V-33, Area of Copernicus CD; Wide Angle**





A portion of the telephoto frame. Area shown is outlined in Figure 4-70. Note that the darker albedo of the dark-haloed crater is not as evident as in the wide-angle frame.

**Figure 4-71: Site V-33, Area of Copernicus CD; Telephoto**



The sunward slopes of the ring hills and the dark mare presents a luminance range exceeding system limitations. Frame 139.

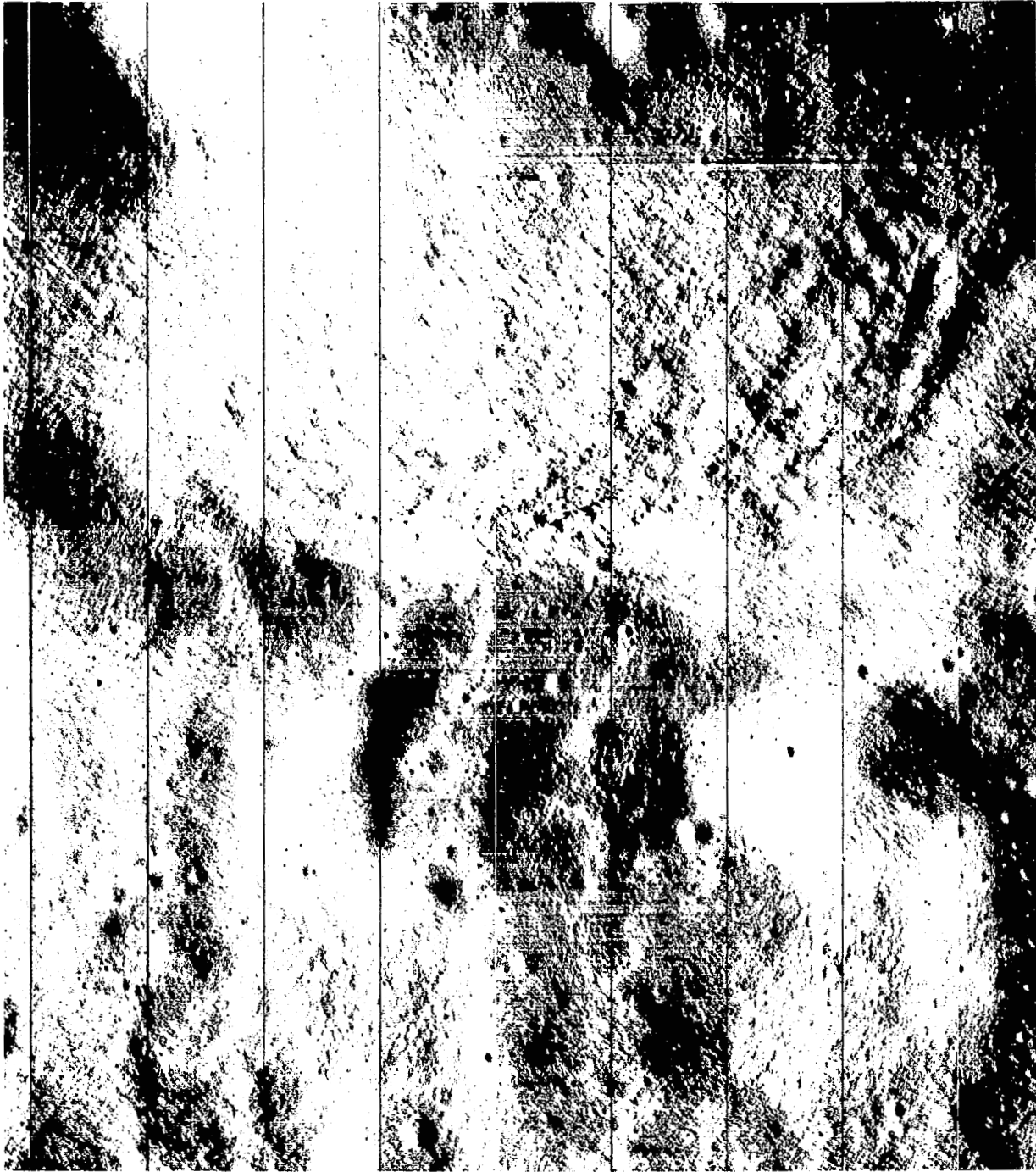
**Figure 4-73: Site V-34, Fra Mauro; Wide Angle**



A portion of Frame 139 showing detail of linear dome outlined in Figure 4-73. Indication of albedo difference is shown.

**Figure 4-74: Site V-34, Fra Mauro; Telephoto**





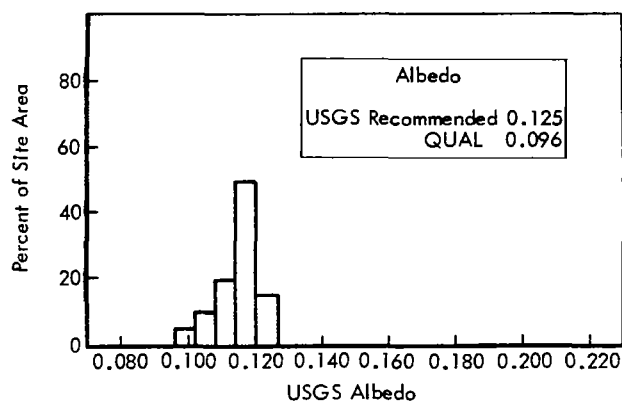
A portion of Frame 138. Area shown is also outlined in Figure 4-73. Note that areas appearing overexposed in the wide-angle frame are shown here with very good detail.

**Figure 4-75: Site V-34, Fra Mauro; Telephoto**

*Altitude: 105.6-110.7 km Frames: 142-145*  
*Phase angle: 80.48 degrees Alpha: -9.11 degrees*  
*QUAL Albedo: 0.096*  
*Shutter speed: 0.04 second*

The site, located in an area northeast of Copernicus that has a high density of secondary craters produced by Copernican ejecta, was centered near Rima Stadius. This feature, thought to be a crater chain, was shown by Mission IV to be almost certainly a line of secondary impact craters, rather than a pre-Copernican volcanic chain. More detailed information was desired on this feature and on the other secondary impact craters than could be obtained from the Mission IV high-altitude photographs.

Although the site includes both highland area and mare surface, it is within the rays surrounding Copernicus where the albedo is generally high. The albedo distribution is shown in Figure 4-76. Considering the type of feature of greater



**Figure 4-76: Albedo Distribution for Site V-35, Copernicus Secondary Craters**

interest within the site, exposure optimized for the brighter areas was desired. QUAL program computations to determine proper shutter speed were based on a corrected albedo of 0.096.

The site was photographed with a sequence of four frames exposed in the slow sequencing rate. Although not providing contiguous telephoto coverage, this mode of sequencing permits sampling a broader area. Forward overlap of the wide-angle photographs is suitable for stereo examination. Wide-angle coverage of this

site extends from about 11.30°N to 17.5°N latitude and from about 14.5 to 17.6°W longitude. Coverage includes the target feature, Rima Stadius, adequately centered to be included in telephoto frames.

Exposure of both telephoto and wide-angle frames is generally satisfactory. A rather wide range of albedo occurs within the area and the topography, while not mountainous, is cratered and hummocky as a result of the high density of secondary craters. A broad luminance range was present, resulting in a varied exposure level. Brighter areas are generally well shown, however, except on steep sunward slopes. The telephoto frames show considerable variation due to the surface characteristics and in some areas exposure is less than optimum, but image detail is not lost. The trend to underexposure occurs mainly in the northern part of the coverage where the albedo is lowest. It should be noted that the maximum exposure (0.04 second) was used.

Resolution of the photographs was satisfactory. Detail spanning four scan lines was observed on the GRE film.

#### *4.4.2.25 Site V-36, Copernicus H*

*Location: 18.22°W longitude, 6.80°N latitude*  
*Altitude: 100.2-100.7 km Frames: 146-149*  
*Phase angle: 87.91 Alpha: -16.45 degrees*  
*QUAL Albedo: 0.077 Shutter speed: 0.04 second*

Copernicus H is one of the largest (4 kilometers) and apparently youngest dark-haloed craters. This crater was shown in profile in the Mission II oblique photograph of Copernicus (Site IIS-12, Frame 162). The dark halo and its conical shape shown in the Mission II photograph have suggested that this crater may be of volcanic origin. However, that it was produced by impact in dark material cannot be discounted. More detailed information suitable for diagnostic purposes was desired, to establish the origin of the crater as well as to contribute to understanding of the origin of the many other much smaller dark-haloed craters that have been observed.

This sequence also was expected to include details of the Copernicus rim that would not be

included in the main Copernicus sequence, Site V-37. The site, located southeast of Copernicus, lies within the area blanketed by bright rays and the albedo is mostly typical of this type of surface, as seen in the distribution plot, Figure 4-77. Because the dark crater was the

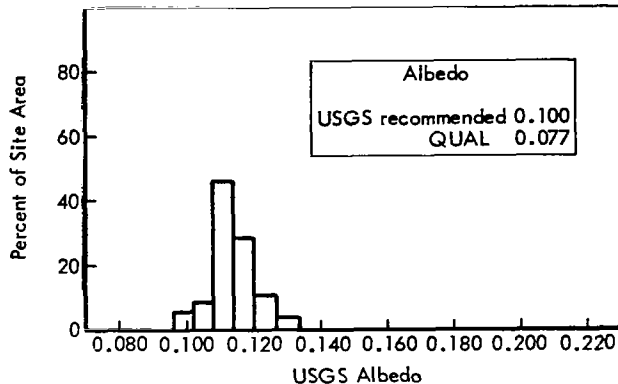


Figure 4-77: Albedo Distribution for Site V-36, Copernicus H

main feature of concern, the lower albedo range was used in the QUAL computations for shutter speed selection.

Coverage by the sequence was closely centered on Copernicus H, thus included coverage of the outer Copernicus rim both north and south of the target feature. Copernicus H is shown almost entirely on Frame 147, with a portion of the northern side and its outer rim included in Frame 148.

Exposure of the site was very satisfactory. The area surrounding Copernicus H is well shown in the wide-angle coverage although, as expected, the brighter rays surrounding the crater were exposed somewhat more than optimum. Quality of wide-angle photography is shown in Figure 4-78, which reproduces a portion of Frame 149 at GRE film scale. The hummocky surface of the ejecta blanket, coupled with the higher albedo, resulted in some overexposure on the sunward slopes. Where these outer areas are the subject of principal study, rather than the dark crater, appreciably increased information may be derived by use of the enhancement technique in use at Langley Research Center in preparing GRE reconstructions from the magnetic-tape video signal recording.

The telephoto frames, receiving slightly less exposure than the wide-angle frames because of system optical characteristics, show very good detail of the Copernicus ejecta blanket and its terrain characteristics. The area surrounding Copernicus H is well shown although slopes resulted in a broad luminance range. Within the crater itself, the western sunward slope is overexposed and the eastern slope and floor are hidden in hard shadow. Inner slope detail is very well shown in limited areas on the north and south slopes. Ejecta boulders and rubble from the crater littering its outer rim are shown. The dark halo surrounding the crater is not plainly evident in the telephoto frames because of its indistinct limits and the difficult distinction from the photometric effects of the rolling terrain. A portion of Telephoto Frame 147 is reproduced at GRE film scale in Figure 4-79 to illustrate the detail shown.

#### 4.4.2.26 Site V-37, Copernicus

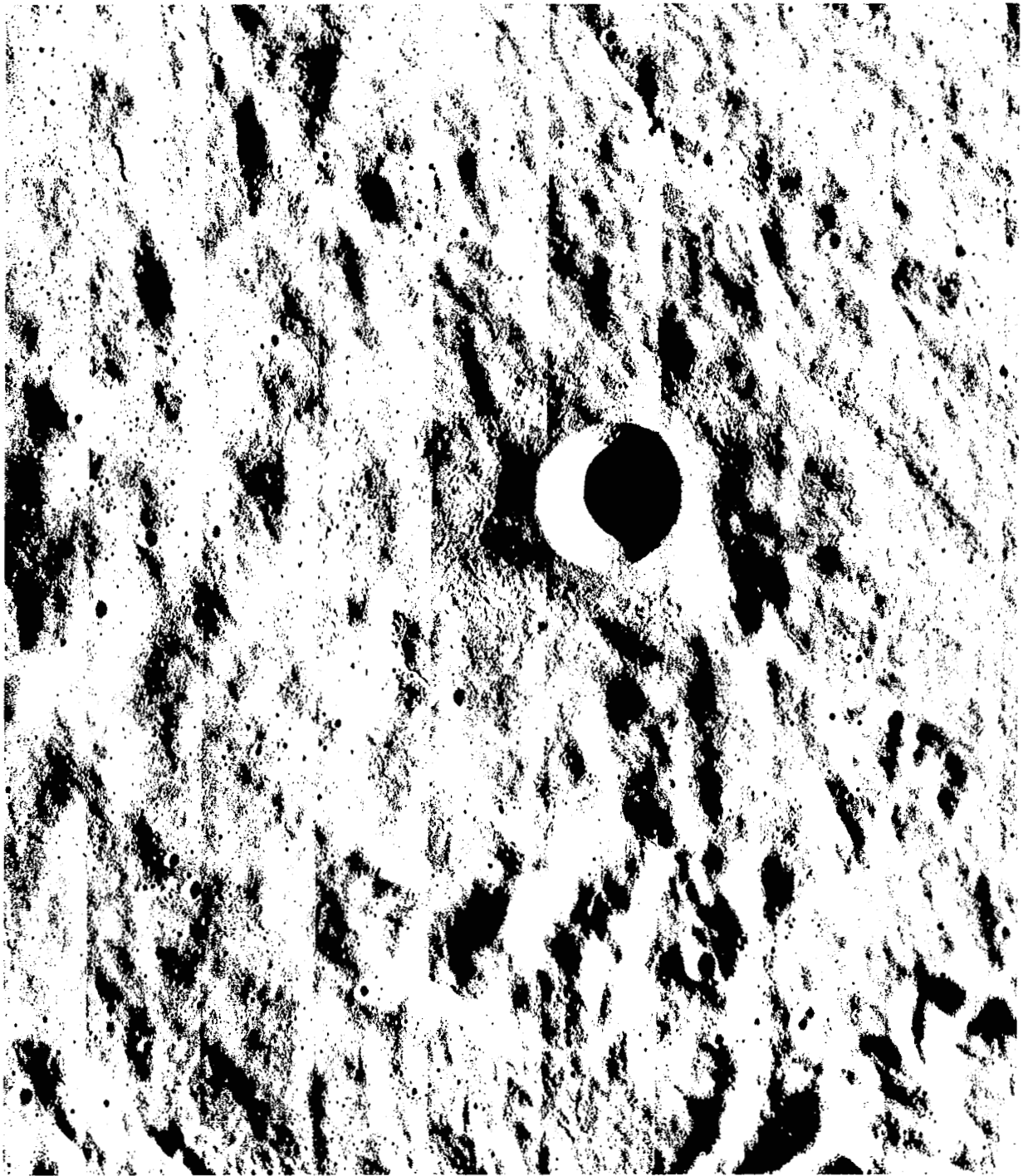
*Location: 20.27°W longitude, 10.15°N latitude*

*Altitude: 102.4-104.3 km Frames: 150-157*

*Phase angle: 77.8 degrees Alpha: -5.85 degrees*

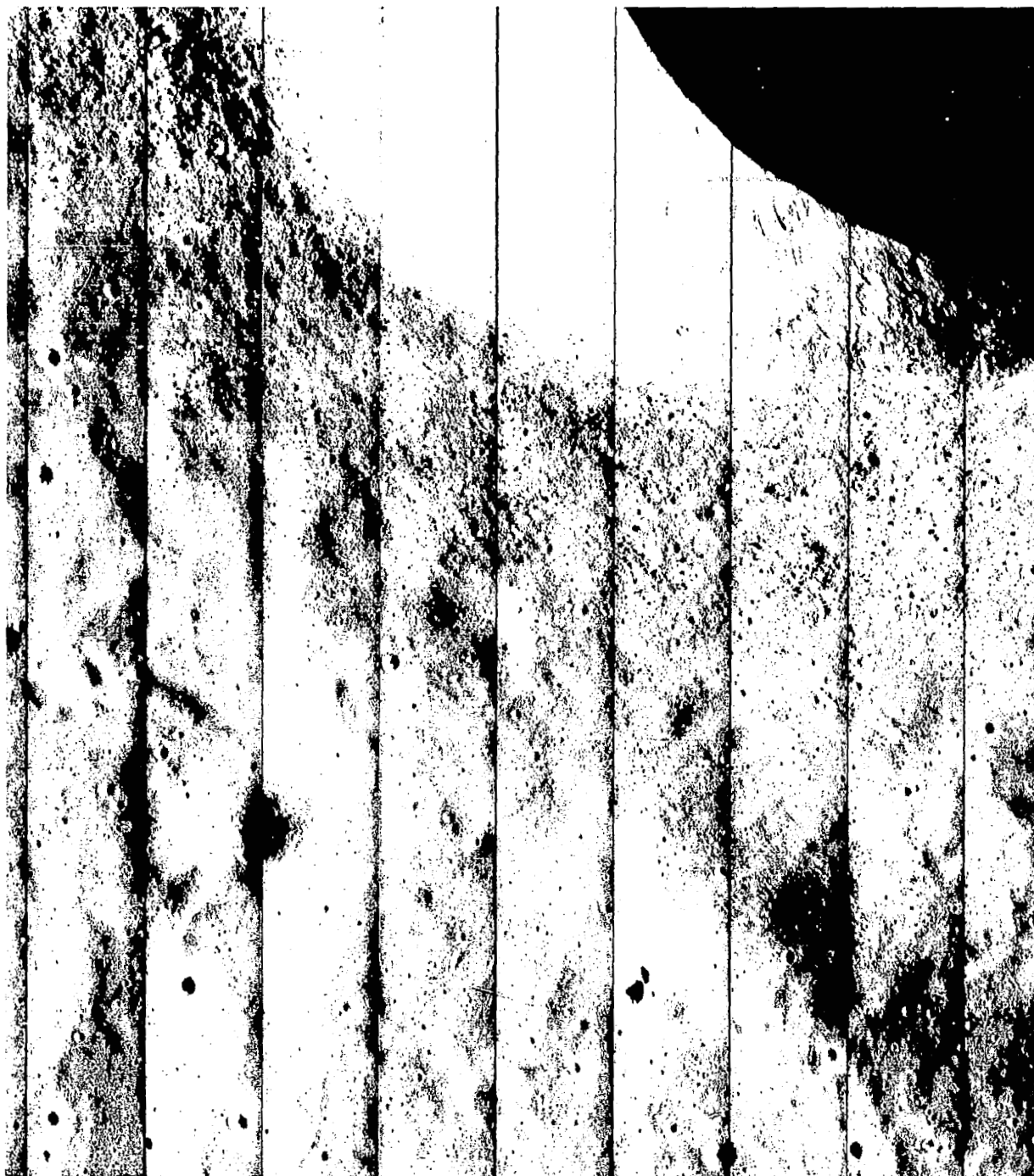
*QUAL Albedo: 0.109 Shutter speed: 0.02 second*

Copernicus is a very prominent and interesting crater located near the equator in the northwest quadrant of the Moon. The crater, which is approximately 100 kilometers in diameter, is made even more prominent by its associated ejecta, secondary crater, and bright-ray system that create a radial pattern nearly 600 kilometers across around the crater. The rim structure of Copernicus rises as much as 3,850 meters above the crater floor. Many types of terrain are present in the basin, walls, and rim. Relatively smooth level areas exist in portions of the crater floor, although much of the basin is very rough. Mission IV photographs suggested possible areas suitable for future landing sites in the northwest section of the floor; the site is therefore included in the group of AAP sites. Additional photographs of Copernicus were desired to obtain more data concerning its many geologic features as well as to locate suitable areas for future landing sites on the very large crater floor. Exposure time for the eight-frame sequence in the fast mode used for this site was selected to produce optimum images of the crater walls



A portion of Wide-Angle Frame 149 showing area around Copernicus H at the same scale as the GRE film. The dark halo is evident.

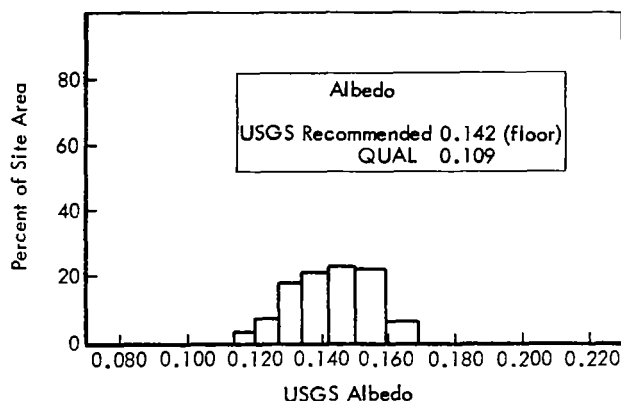
**Figure 4-78: Site V-36, Copernicus H; Wide Angle**



A portion of Telephoto Frame 147. A corner of Copernicus H including interior slope detail and outer rim is shown. The halo is less evident than in wide-angle photography.

**Figure 4-79: Site V-36, Copernicus H; Telephoto**

and floor. The shutter speed of 0.02 second resulted in wide-angle and telephoto frames of very good photographic quality. Average densities and contrast range were very satisfactory. A histogram illustrating the distribution of albedos for this site is given in Figure 4-80.



**Figure 4-80: Albedo Distribution for Site V-37; Copernicus**

Because of the illumination geometry existent at the time of photography, the steep western scarps of the crater and the sunward slopes of the central peaks had a high luminance that exceeded system limits. Consequently, these areas were overexposed with resulting loss of detail. Characteristically, some loss of detail also occurred in hard-shadow areas.

Under the orbital conditions of this mission, and because of the size of Copernicus, a fast eight-frame sequence was required to photograph the entire crater. At the beginning of the sequence (Frame 150), the south rim is at the edge of the wide-angle photograph. The last wide-angle frame of the sequence includes the north rim and some 40 to 50 kilometers of the adjoining terrain extending northward. Except for a very small portion of the east rim, the entire crater and a representative part of the outer rim are included in the sequence. Detail of the floor and the rim structure is excellent in the wide-angle photographs (see Figures 4-81 and -82). Figure 4-81 is shown at GRE film scale.

Telephoto frames provide contiguous high-resolution coverage of the crater floor over an area extending approximately from the central

peaks across to the northern rim terraces and onto the adjoining outer rim. The telephoto sequence provides an excellent representative sample of the principal geological features of Copernicus. It should be noted here that this sequence also provides vertical coverage of the crater details shown in the well-known oblique photograph of Copernicus obtained in Lunar Orbiter Mission II. Detail is very good. Small craters and rocks, which surmount nearly every hill on the crater floor, are sharply defined. Figures 4-83 and -84, reproduced at GRE film scale, represent detail shown on the crater floor. Features spanning as few as three scan lines can be identified on the GRE film. System luminance limits were exceeded only on the steep sunward slopes of the central peaks and the inner crater wall scarps. Where detail is lost in such bright slopes, varied orientation of similar features provides more grazing illumination to reveal characteristics that may be representative of the high-luminance areas.

#### 4.4.2.27 Site V-38, Imbrium Flows

*Location: 22.08°W longitude, 32.41°N latitude*

*Altitude: 153-157 km Frames: 159-162*

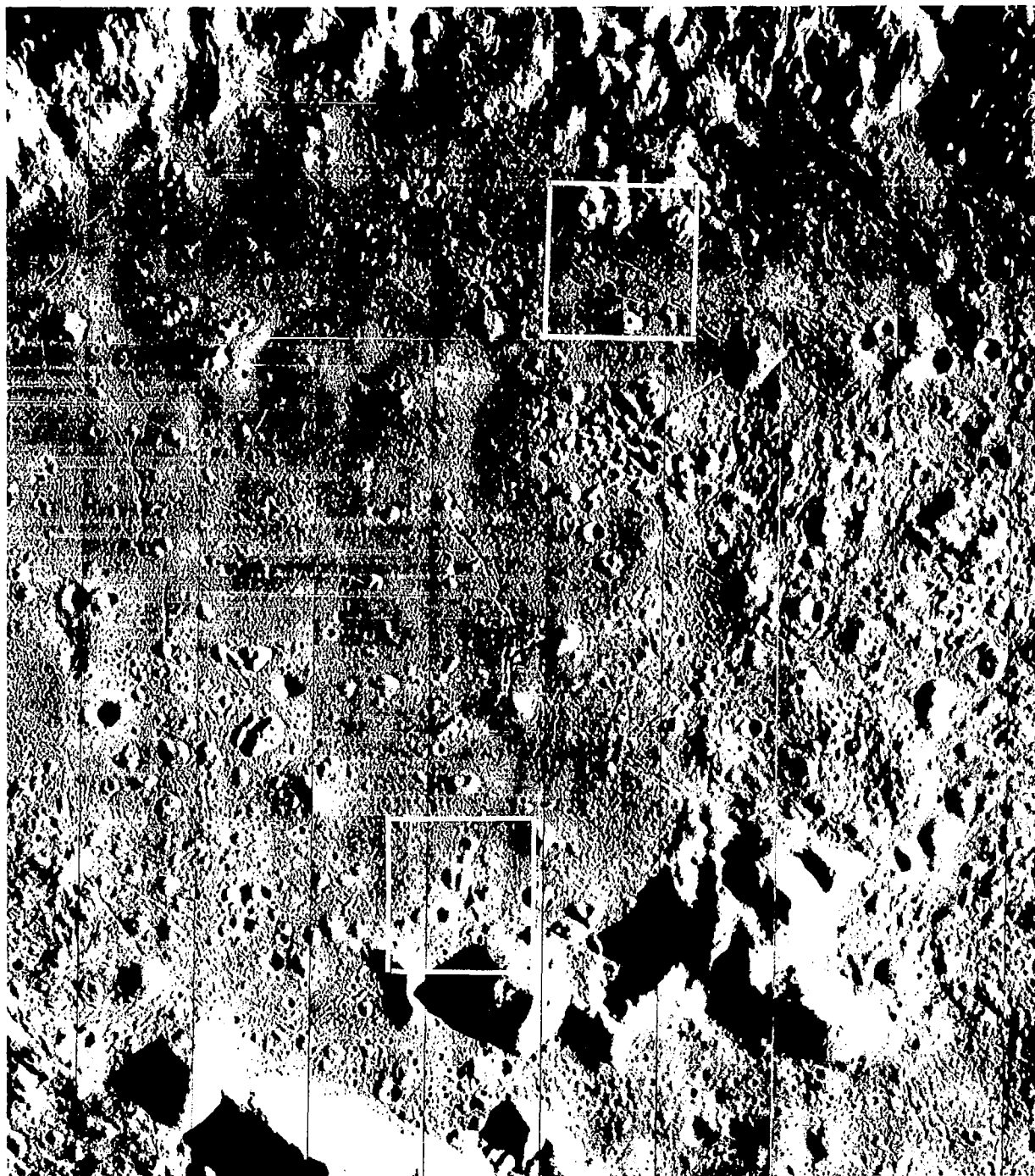
*Phase angle: 72.60 degrees Alpha: +0.17 degree*

*QUAL Albedo: 0.063 Shutter speed: 0.04 second*

For many years it has been postulated, using Earth-based observation as the basis, that the maria were the result of superposed basaltic-type flows of volcanic origin. Mission IV photography presented strong evidence in support of this theory. Additional photography of flow fronts shown in Mission IV photography was desired from Mission V to furnish detail of beds, if any, and the slope of the front which, if not excessively eroded, would be indicative of material viscosity. An indication of age differential can be obtained from the relative crater density of the two units. This site is included among those selected for AAP.

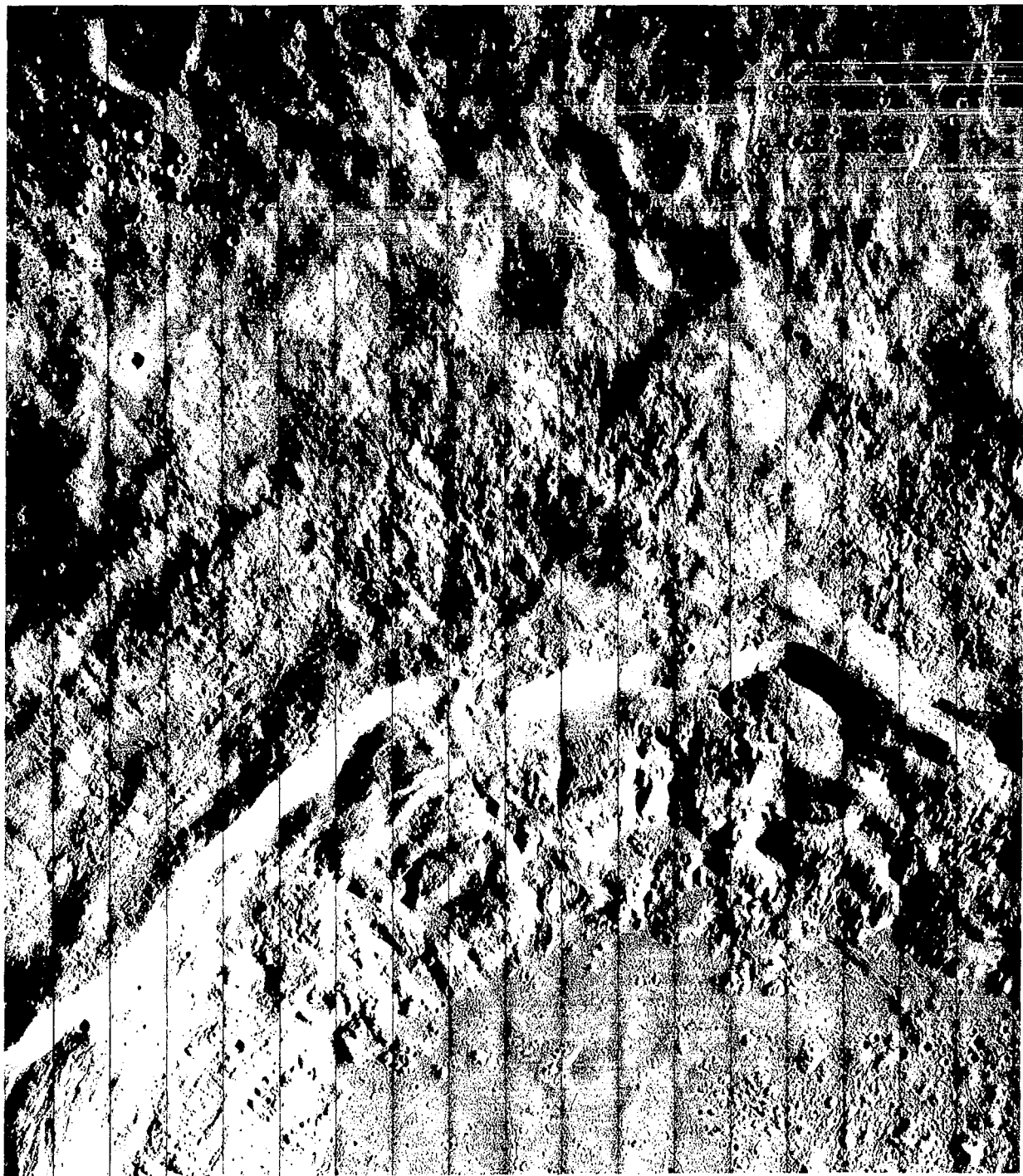
The site is located in the central part of Mare Imbrium remote from major rayed craters. As a result, the area is generally quite flat. The albedo is rather uniformly low, as shown in the albedo distribution plot, Figure 4-85. Because of the flat terrain and narrow albedo range, selection of the shutter speed for exposure control was simplified.





A portion of Frame 151 reproduced at GRE film scale. The area extends from the central peak to the north edge of floor. Outlined areas are shown in Figures 4-83 and -84.

**Figure 4-81: Site V-37, Copernicus; Wide Angle**



This figure includes most of Frame 157 showing the northern extension of the outer rim photographed.

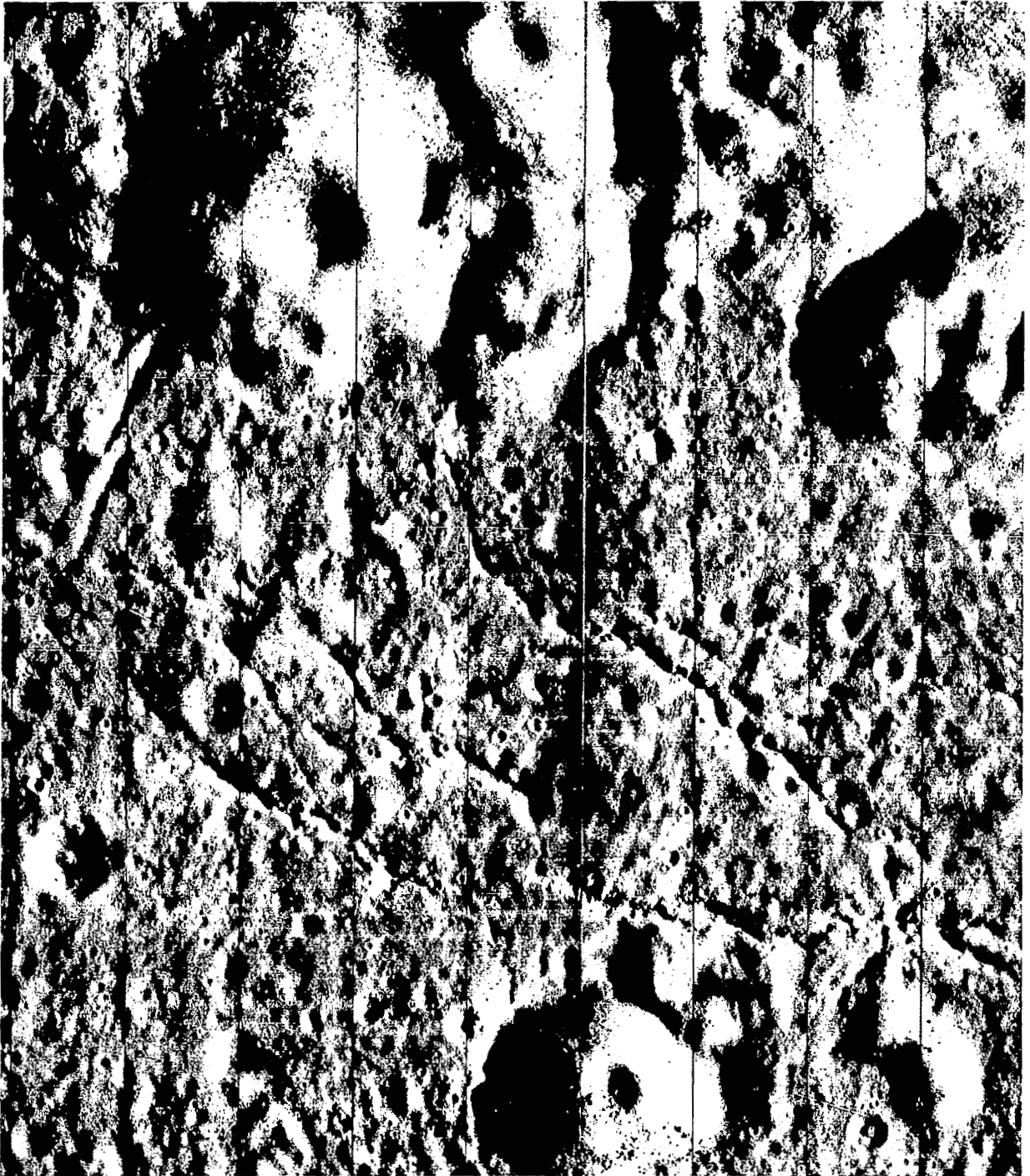
**Figure 4-82: Site V-37, Copernicus; Wide Angle**





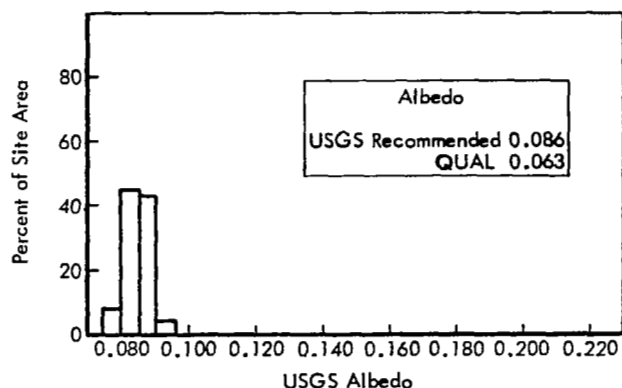
A portion of Telephoto Frame 152, reproduced at GRE film scale showing detail of a central peak slope and central floor.

**Figure 4-83: Site V-37, Copernicus; Telephoto**



This is a portion of Telephoto Frame 154 showing detail of northern floor area that appeared "smooth." This is the upper area outlined in Figure 4-81.

**Figure 4-84: Site V-37, Copernicus; Telephoto**



**Figure 4-85: Albedo Distribution for Site V-38, Imbrium Flows**

The site was photographed using a four-frame sequence taken in the fast mode. Coverage by the sequence was centered slightly north of the northern tip of the prominent flow front southeast of the crater Carlini. The telephoto frames provide very good coverage of the flow front in the vicinity of the well-defined northern tip.

Exposure of both wide-angle and telephoto frames is good, with the exposure differential between the cameras presenting no significant problem. The telephoto frames received near-optimum exposure as desired. Although incident angle of illumination was near 73 degrees (17-degree Sun elevation), little of the flow-front slope is lost in hard shadow because of its slope and irregular shape (Figure 4-86).

Detail throughout the photographs is excellent, with resolution of craters spanning three to four scan lines observed on the GRE films of all four frames.

These photographs provide an excellent example representative of central Mare Imbrium characteristics.

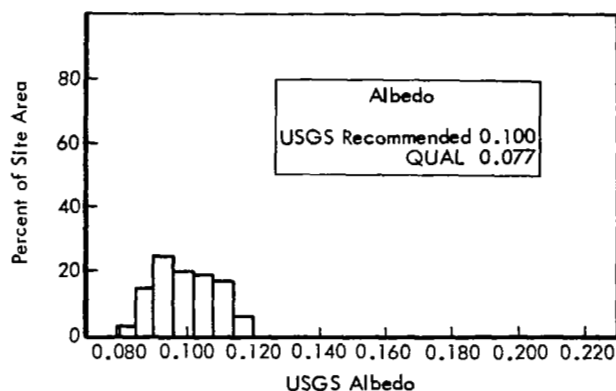
**4.4.2.28 Site V-40, Dome Near Tobias Mayer**  
*Location: 30.94°W longitude, 12.93°N latitude*  
*Altitude: 107.0 – 108.1 km*  
*Frames: 164 – 167 Phase Angle: 72.76 degrees*  
*Alpha: +0.25 degree QUAL Albedo: 0.077*  
*Shutter speed: 0.04 second*

This site was selected to obtain information

regarding the low broad mare domes. The ACIC Lunar Chart, LAC 57 Kepler, shows a number of domes southwest of Tobias Mayer. The target, a dome lying against an island of rugged terra material, was selected so that contact with the island could be investigated to determine how the dome was emplaced – whether by intrusion or extrusion. Although these dome formations are relatively common, their origin is uncertain.

The area photographed includes, besides the dome, a variety of other features such as a sinuous rille, an elongated crater near the summit of the dome, and a broad, flat-floored rille. The variety of features in the area, not well known before Mission IV photography, makes the area a potentially good landing site; thus, the site is included in the AAP group.

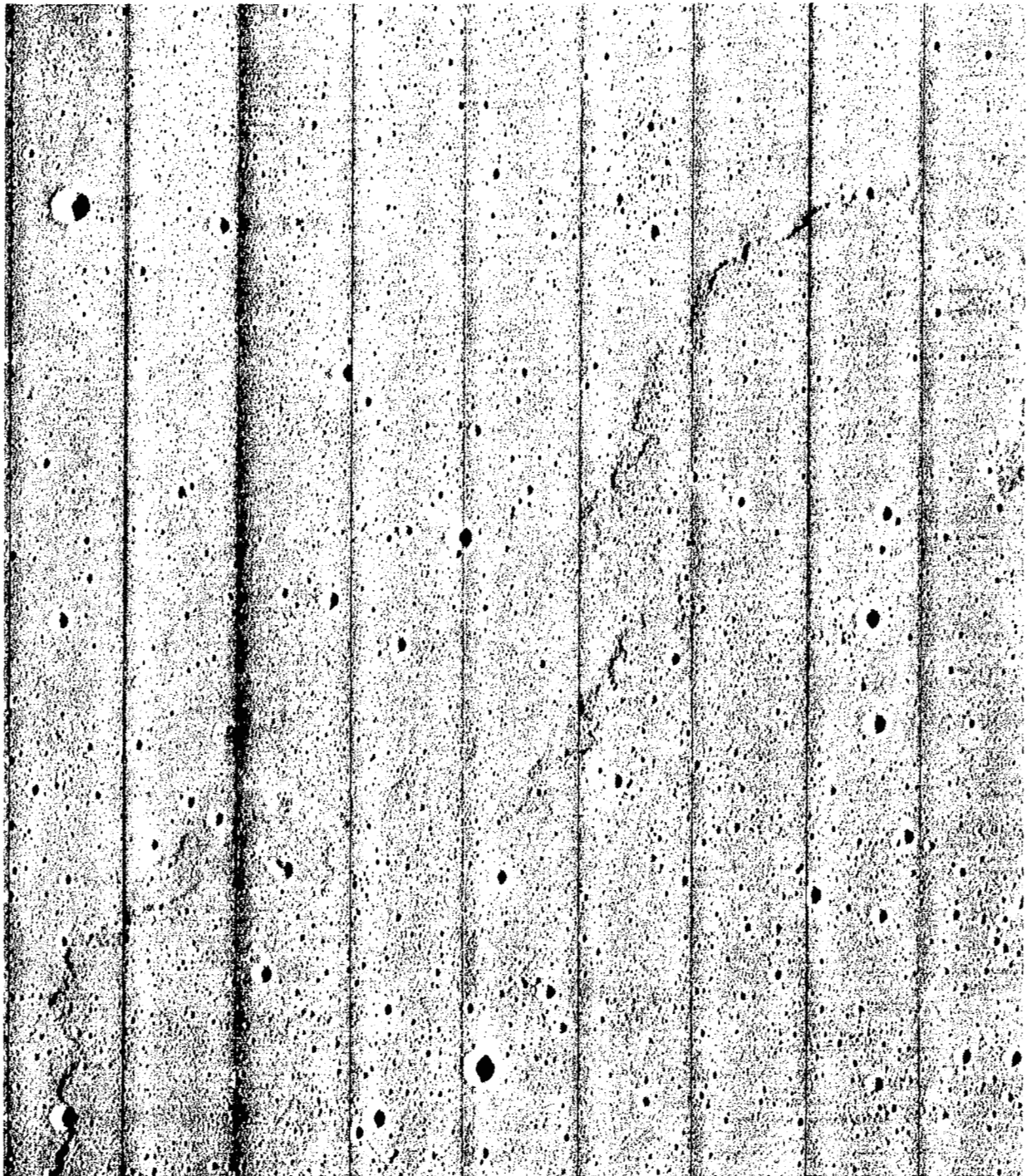
The site was photographed with a sequence of four frames taken in the fast mode. The area is principally mare-type surface, although it includes some terra; thus, the albedo is mostly rather low, but has a range extending from corrected values of 0.061 to 0.093 (USGS :0.079 to 0.120), as shown in Figure 4-87. An albedo of



**Figure 4-87: Albedo Distribution for Site V-40, Tobias Mayer Dome**

0.077 was used in the QUAL program to compute densities for selection of shutter speed since the dome is more characteristic of mare surface.

Exposure of both wide-angle and telephoto frames is very good for the mare surface. The combination of albedo range and steep slopes



This is a portion of Wide-Angle Frame 161, reproduced at GRE film scale, showing both sunward and shaded flow faces. A small albedo difference between the flow areas is evident.

**Figure 4-86: Site V-38, Imbrium Flows; Wide Angle**

of mountainous terra resulted in a wide range of luminance that exceeded the system limit in some locations. Because of the Sun angle and the small slope change of the dome, its boundaries are not prominent in the wide-angle frames but may be established (Figure 4-88). Detail is well shown in the telephoto frames. At the scale provided by the telephoto lens, the edge of the dome is not as prominent as in the wide-angle frames. There is no marked variation in surface characteristics to differentiate the dome other than a slight slope change and associated subtle change in luminance. Detail is present on much of the area of the hills where the luminance range does not exceed or fall below system limits.

Resolution of the photography is good, with features spanning between three and four scan lines recognized.

#### 4.4.2.29 Site V-41, Vitello

*Location:* 37.57°W longitude, 30.61°S latitude

*Altitude:* 167.4 km *Frame:* 168

*Phase angle:* 69.94 degrees *Alpha:* +10.5 degrees

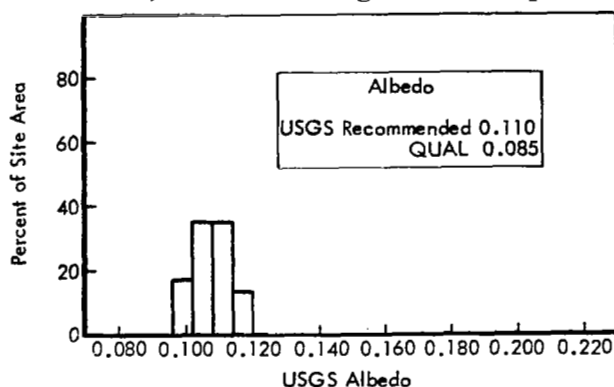
*QUAL Albedo:* 0.085 *Shutter speed:* 0.04 second

This site was selected for Mission V photography because of a combination of unusual characteristics. Vitello appears to be a rather old crater since there is no evidence of rays or other ejecta pattern associated with it, and the interior seems eroded. However, the crater is the site of a high thermal anomaly usually associated with younger bright craters. In addition, the floor has an extensive system of cracks that Mission IV photography suggested as being relatively fresh and deep. It was hoped that Mission V photography, particularly the telephoto coverage, would provide information that would help resolve the problems presented by the seemingly conflicting observations.

The crater is about 40 kilometers in diameter, and because of the altitude of photography a single-frame exposure was adequate to provide the necessary coverage.

Although wide-angle coverage is about equally divided between mare and terra surface, the floor of the crater was of principal interest. Ex-

posure was selected for near the average albedo of this area, as shown in Figure 4-89. Exposure



**Figure 4-89: Albedo Distribution for Site V-41; Vitello**

of the photographs is very good to show detail on the crater floor. Because of the hummocky character of the floor, the prominent central peak complex and the deep cracks, luminance is broadly variable even within quite limited areas (Figure 4-90). Exposure in general, however, indicated that the selected shutter speed of 0.04 second was most suitable. Telephoto exposure appears to be excellent for showing surface characteristics over the crater floor where illumination was within normal range (Figure 4-91). A portion of the eastern outer rim is included in the telephoto frame. Surface texture in this area is shown to great advantage. The portion of western outer rim within the telephoto frame is lost in deep shadow.

Detail in the telephoto frame is excellent. Resolution was found to be three scan lines, which shows many areas littered with exposed boulders, and surface details indicating structural characteristics of the floors. Interior slope detail of the large cracks on the floor is well shown where the orientation of the crack with respect to the Sun results in suitable illumination.

#### 4.4.2.30 Site V-43.2, Gassendi

*Location:* 40.0°W longitude, 17.0°S latitude

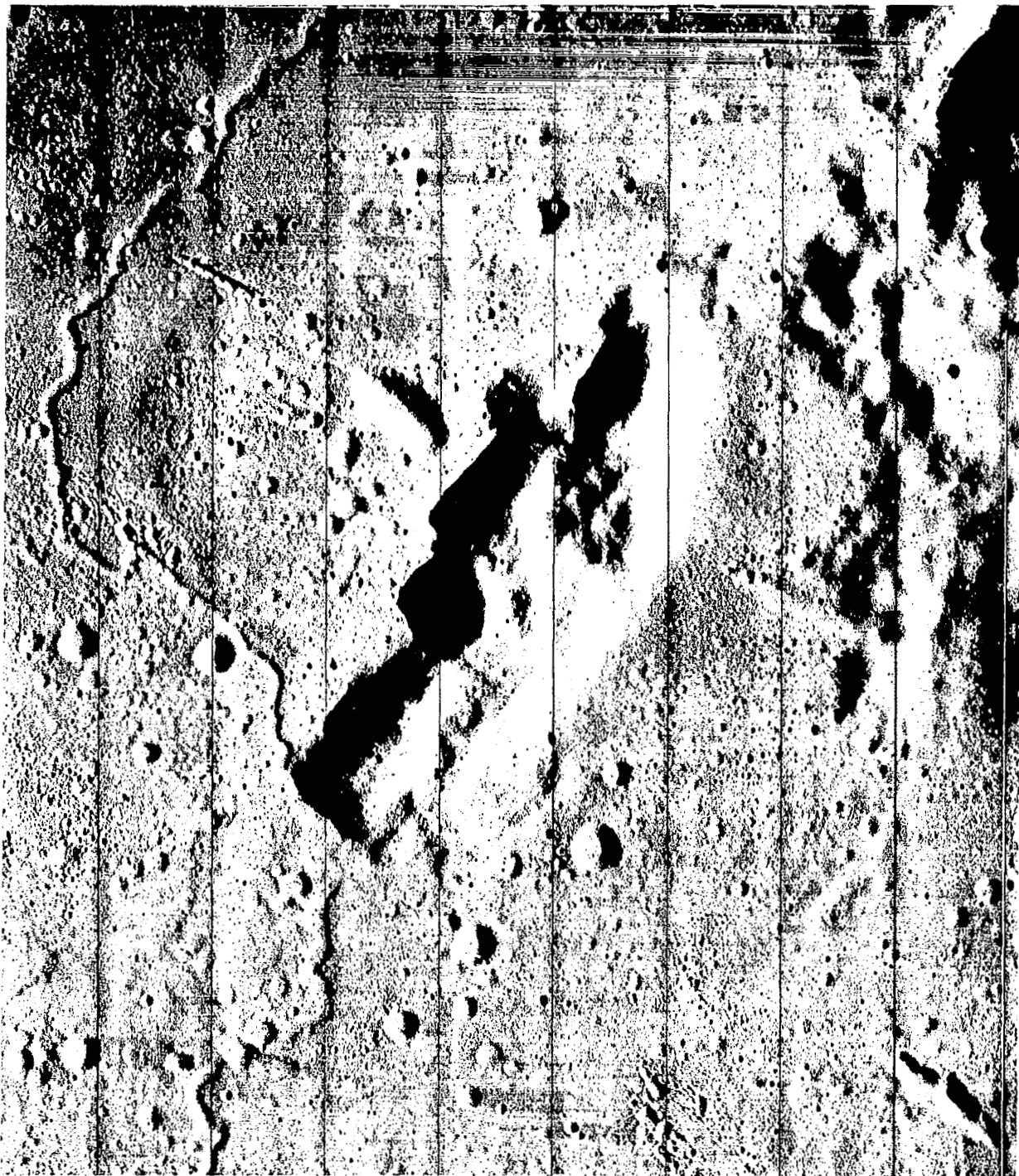
*Altitude:* 119.7 - 128.9 km *Frames:* 177 - 180

*Phase angle:* 82.2 degrees

*Alpha:* -5.60 degrees *QUAL Albedo:* 0.090

*Shutter speed:* 0.04 second





Portion of Wide-Angle Frame 164, showing area of dome at GRE film scale. Note slight luminance change defining dome slopes.

**Figure 4-88: Site V-40, Dome Near Tobias Mayer; Wide Angle**



A portion of Wide-Angle Frame 168 centered on crater. Lace defect is present.

**Figure 4-90: Site V-41, Vitello; Wide Angle**



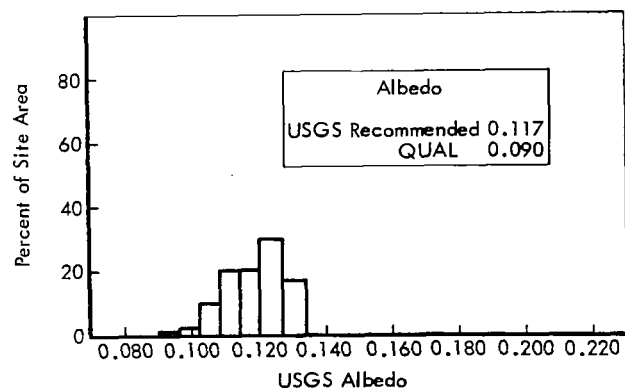
A portion of Telephoto Frame 168 showing detail on crater floor. Floor is very well exposed. Note resolution of rocks on floor.

**Figure 4-91: Site V-41, Vitello; Telephoto**



Cassendi is a large crater approximately 105 kilometers in diameter located astride the northern rim of Mare Humorum. The northern rim of the crater borders on rough upland terrain; the southern rim projects into the relatively smooth surface of Mare Humorum. Cassendi is considered older than the mare material in the Humorum basin, but younger than the basin. The floor of Cassendi is split by a system of rilles in which, it was hoped, exposed beds of floor material might be visible. Some of the rilles are bordered by ridges, which may be uplifted parts of the floor or volcanic constructional features. The southern portion of the crater and sections of the rim appear to be filled by mare material, which also extends onto the crater floor from the Mare Humorum basin. Additional photography of this site was planned to obtain more information on the varied geological features observed in this area.

A shutter speed of 0.04 second was used for the four-frame sequence in the slow mode. Overall image densities and contrast ranges were satisfactory, although some tendency towards overexposure or underexposure occurred occasionally because of variations in surface characteristics and illumination geometry. The selected shutter speed produced photographs that revealed good detail and fine surface texture of the crater floor. Albedo distribution for this site is given in Figure 4-92.



**Figure 4-92: Albedo Distribution for Site V-43.2; Cassendi**

Site coverage by the wide-angle photographs extends from the part of Mare Humorum south

of the target to the upland area north of craters Cassendi A and B. The coverage permits comparison of characteristics of the mare area adjacent to Cassendi with those of similar mare areas engulfing parts of the crater rim and extending into the crater basin. Surface details and texture are very good. Some lace occurs over the photographs, but little information is lost because of the overlap in the four-frame sequence. Spacecraft altitude decreased from approximately 129 to 120 kilometers in the course of the four-frame sequence. Scale factors for the wide-angle and telephoto frames must, therefore, be properly identified for each photograph. Identification of small craters three or four scan lines in cross section was possible in all wide-angle photographs. Figure 4-93 from Frame 178 represents the wide-angle photography of this feature.

The irregular luminosity and rilled character of the Cassendi crater floor enhanced the detail recorded in the telephoto frames. Surface texture and small features are particularly good. Detail is present in most sunward slopes, except where such slopes are unusually steep. Some detail is lost on the central peak because of bright sunlit slopes and hard shadow areas (Figure 4-94).

As in Vitello, clusters of rocks surmount many hummocks. Interesting trails left by rolling rocks may be seen in some areas as in Framelets 977 to 978 of Telephoto Frame 179. In Framelet 972 of the same frame, rock trails have been partly covered by small craters. Evidence of tracks almost obliterated by erosion or surface movement is also present. Small craters, projections, and rocks spanning as few as three scan lines can be identified in the telephoto sequence.

#### 4.4.2.31 Site V-45.1, Domes Near

*Gruithuisen, and Gruithuisen K*

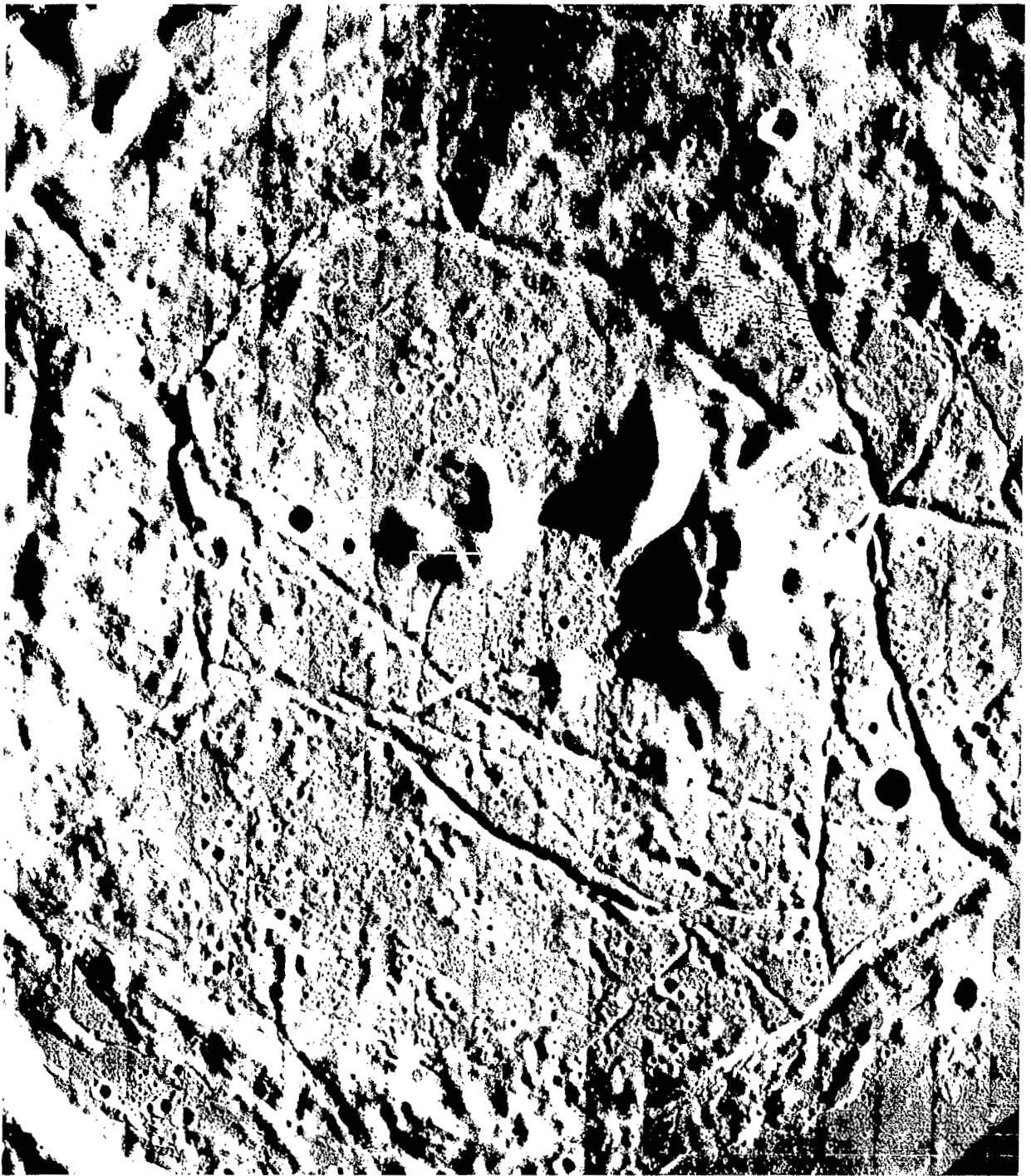
*Location: 41.47°W longitude, 35.56°N latitude*

*Altitude: 165 – 170 km Frames: 182 – 185*

*Phase angle: 68.72 degrees*

*Alpha: +5.88 degrees QUAL Albedo: 0.080*

*Shutter speed: 0.04 second*



Wide-Angle Frame 178, the second of a sequence of four. Exposure of floor is satisfactory, but bright central peaks are overexposed on sunward side.

**Figure 4-93: Site V-43.2, Cassendi; Wide Angle**



This portion of Telephoto Frame 178 shows a part of a central peak as shown outlined in Figure 4-93. Note excellent detail of surface texture.

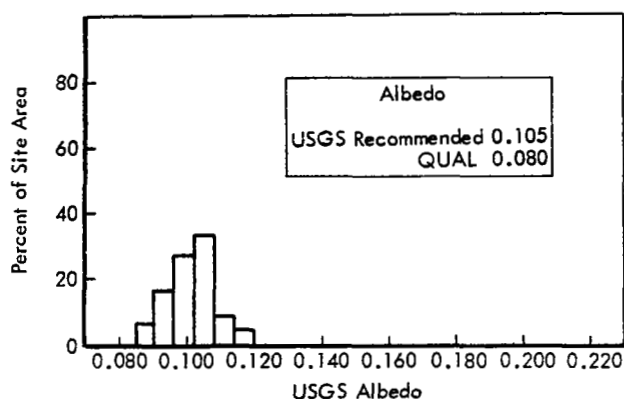
**Figure 4-94: Site V-43.2, Cassendi, Telephoto**

Site V-45.1 includes two types of feature of special interest: the domes near Gruithuisen, specifically Gruithuisen  $\gamma$  (gamma); and the crater Gruithuisen K. There are three major domes in the group that are high relative to their width of 15 to 25 kilometers and may have the largest total volume of known domical structures. These structures are believed to be of volcanic origin. Mission IV photography showed a prominent summit crater on dome  $\gamma$  and considerable surface texture on all three. The domes were selected as a site so that telephoto photographs of Mission V might provide information concerning the type of material forming the domes.

Gruithuisen K is one of a class of peculiar craters having multiple internal concentric rings. Double-ringed craters were known prior to Mission IV photography, but not multiple-ringed ones. Furthermore, no details of these craters were known nor was it realized that they are relatively common. The target crater has an inner ring that appears to be upturned edges of a saucer-shaped object lying in the center of the crater. The next outer zone appears to be broken into segments. The outer rim appears to be eroded to a rounded contour.

The site was photographed with a four-frame sequence taken in the fast mode. Because of the relative positions of the domes and Gruithuisen K, the camera axis had to be directed between the two to obtain telephoto coverage of both. Thus, to include Gruithuisen K, only one dome,  $\gamma$ , is included in the telephoto coverage. All are shown in the wide-angle photographs. An average albedo for the site, as shown in Figure 4-95, was used in computing densities for shutter speed selection.

On the average, exposure of both wide-angle and telephoto frames is near optimum for the near-level or gently sloped areas. As a result, surface detail is shown very well over most of the photographs. The domes, being more hummocky, have a wider luminance range over most of the surface, but detail is obscured only in limited areas and the surface is generally well represented. The crater Gruithuisen K appears at the western edge of the telephoto coverage



**Figure 4-95: Albedo Distribution for Site V-45.1, Domes Near Gruithuisen and Gruithuisen K**

and the western slope is outside the field of view. Very good detail is shown on the north and south inner slopes, the floor, and the outer rim.

Exposure was such that good detail is shown on both the mare and upland surfaces; thus, the sequence provides much information regarding the very sharply defined contact between these two geological units that occurs between the two target features. An unusual crater chain that is included in the southwestern part of the wide-angle coverage is also seen.

Site photography is represented by Figures 4-96, -97, and -98. The first, including most of Wide-Angle Frame 184, shows the general area of the domes. Figure 4-97, a portion of Telephoto Frame 185, shows the dome surface and its contact with the mare. The third, a part of Telephoto Frame 183, illustrates the detail shown in both mare and terra areas.

Resolution of both telephoto and wide-angle frames was consistently between three and four scan lines.

#### *4.4.2.32 Site V-46, Harbinger Mountains*

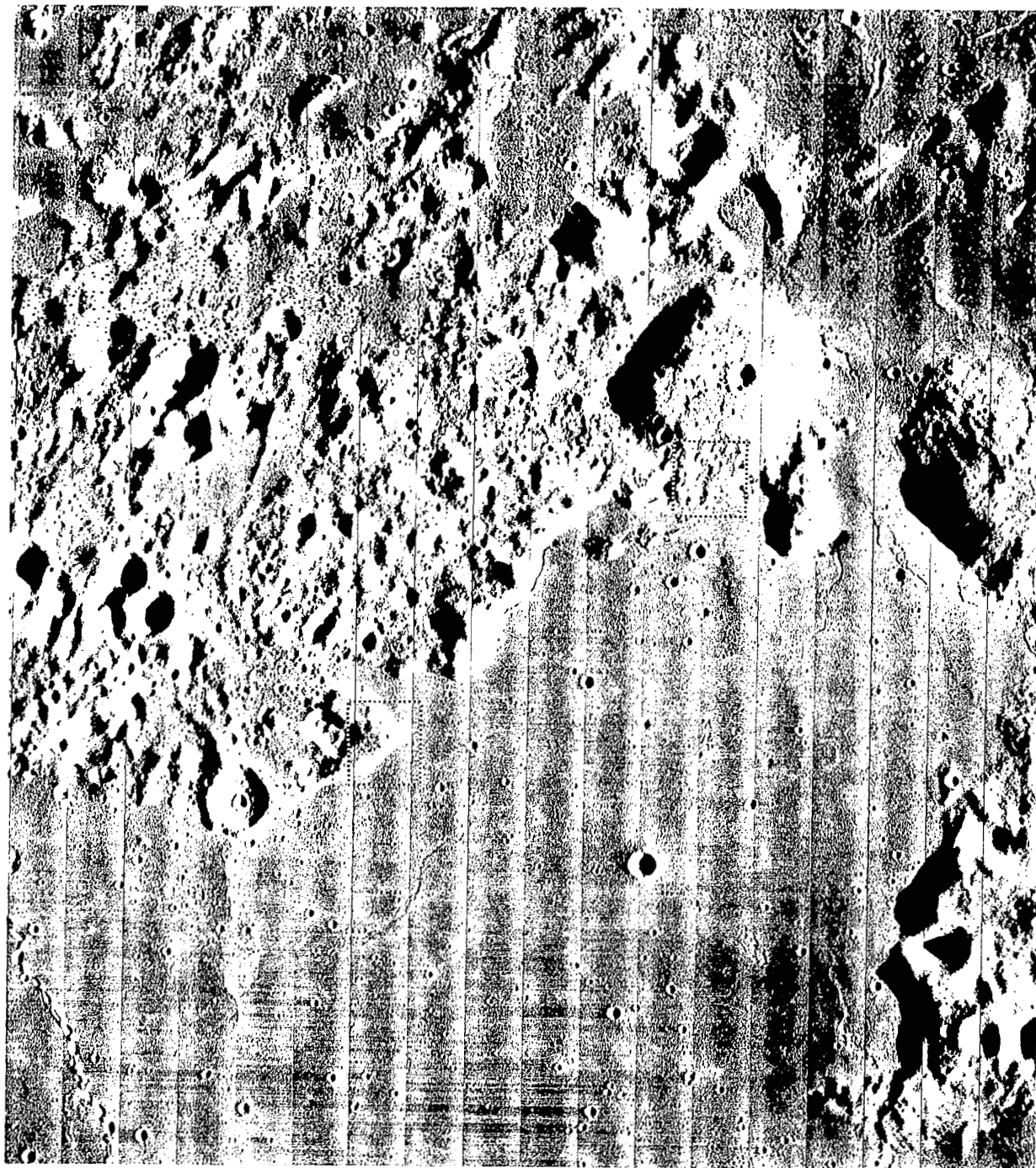
*Location: 43.64°W longitude, 27.05°N latitude*

*Altitude: 134 – 142 km Frames: 186 – 193*

*Phase angle: 73.53 degrees*

*Alpha: +0.34 degree QUAL Albedo: 0.075*

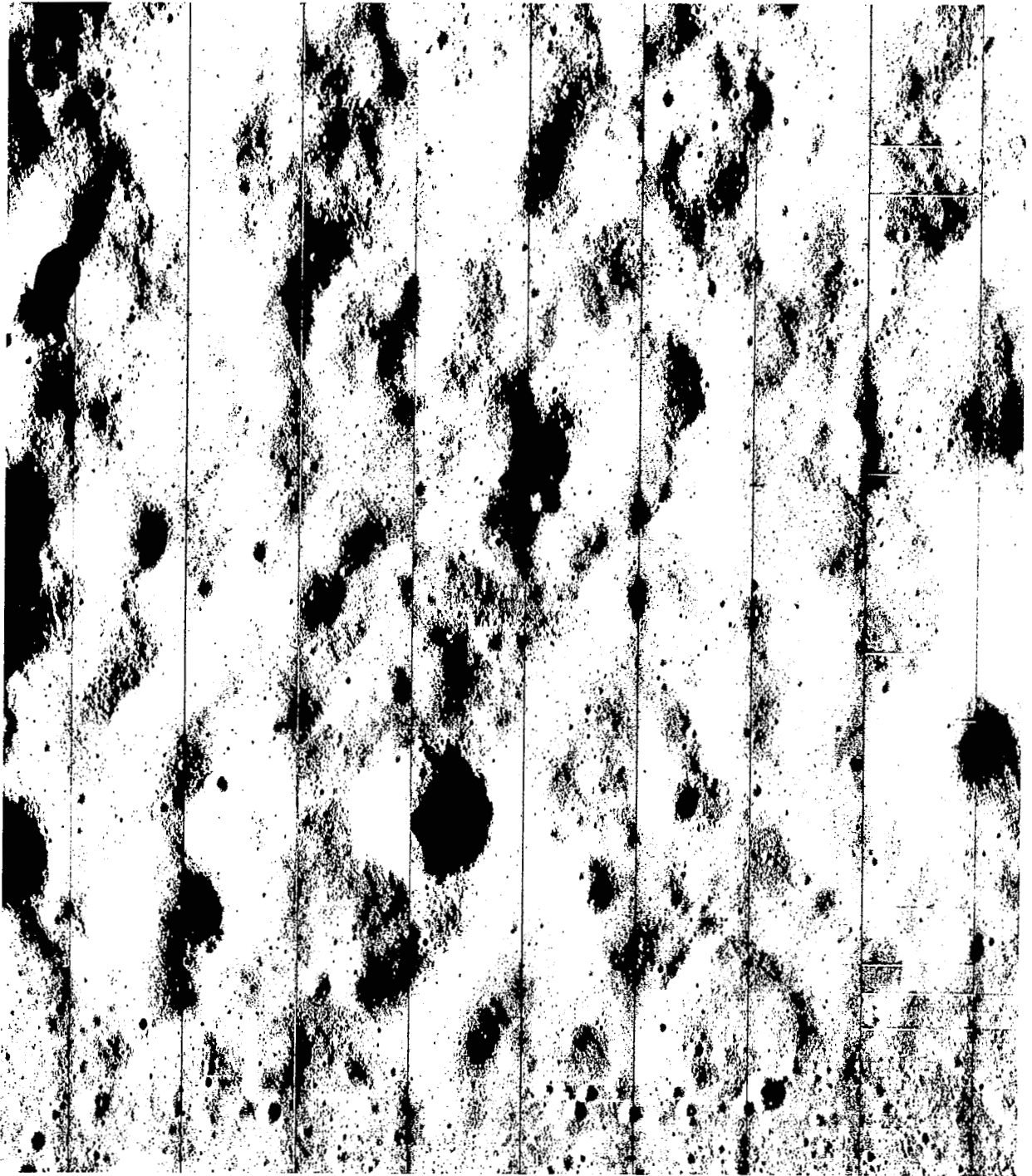
*Shutter speed: 0.04 second*



Most of Wide-Angle Frame 184. Area of domes includes both mare and terra surface of different albedo.

**Figure 4-96: Site V-45.1, Domes Near Gruithuisen and Gruithuisen K; Wide Angle**





A portion of Telephoto Frame 185 showing detail of dome surface and contrast with mare. Video dropouts are seen.

**Figure 4-97: Site V-45.1, Domes Near Gruithuisen and Gruithuisen K; Telephoto**



A portion of Telephoto Frame 183. Although of different albedo, both mare and terra are satisfactorily exposed. Note representation of surface detail of both types.

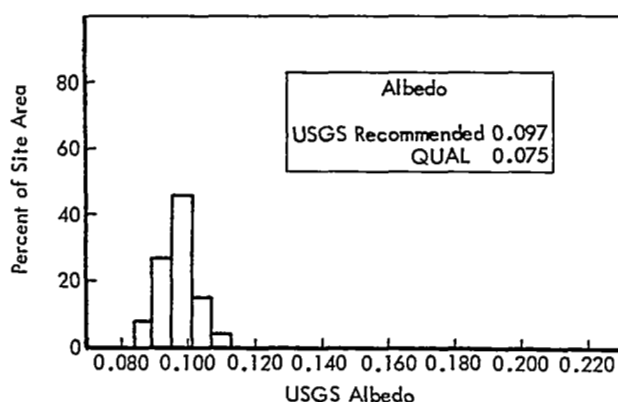
**Figure 4-98: Site V-45.1, Domes Near Gruithuisen and Gruithuisen K; Telephoto**



On the basis of Mission IV photography this site, northwest of Aristarchus, was selected instead of one chosen earlier farther west in the Krieger area. The site was selected because of the many sinuous rilles and the occurrence of two types of material presumed to be volcanic in origin. Many of the sinuous rilles have craters at the broader end. Because of the possible erosive origin of the rilles, the occurrence of outflow deposits was a question to be answered. The greater resolution of Mission V telephoto photography was expected to furnish much more information concerning the possible origin of these interesting features.

The material presumed to be volcanic occurs in two forms, smooth and flat, like mare material, and undulating. Additional detailed information to further characterize these geological units was desired.

Because of the extent of the sinuous rilles, an eight-frame sequence taken in the fast mode to provide contiguous telephoto coverage extends from south to the old crater Prinz, north to the crater Angstrom, thus including the complex of sinuous rilles and a major portion of the Harbinger Mountains. The area is principally mare surface except for isolated mountain peaks and the ring hills of Prinz. Although the area lies within the Aristarchus rays, the albedo distribution of the area of interest is typically that of mare, as shown in Figure 4-99. The albedo



**Figure 4-99: Albedo Distribution for Site V-46, Harbinger Mountains**

used in determining shutter speed was very close to the average for the site, to obtain the best detail of the rilles and of the more terra-like terrain.

The general quality of the photographs in the sequence was very good. Exposure of both telephoto and wide-angle frames is near optimum for showing detail in the rilles and on the mare surface that has a very high density of small craters. Most of Wide-Angle Frame 188 is shown in Figure 4-100 to illustrate the character of these site photographs. Very good detail is shown on most of the terra-like surfaces included in the telephoto frames, although steeper sunward slopes are overexposed. The varying orientation of the sinuous rilles results in excellent detail on both sides, except for those sections facing more directly toward or away from the Sun (Figure 4-101).

The sequence contains a great deal of information concerning the effects of Aristarchus ejecta, both in production of secondary craters and deposition of ray material. Blanketing of the surface by ray material is evident in telephoto frames; the albedo effect is more apparent in the wide-angle frames.

Resolution of all frames was found consistently to be near three scan lines.

#### 4.4.2.33 Site V-48, Aristarchus

*Location: 47.43°W longitude, 23.14°N latitude*

*Altitude: 125 - 131 km Frames: 194 - 201*

*Phase Angle: 74.65 degrees Alpha: -0.65 degree*

*QUAL Albedo: 0.154 Shutter speed: 0.02 second*

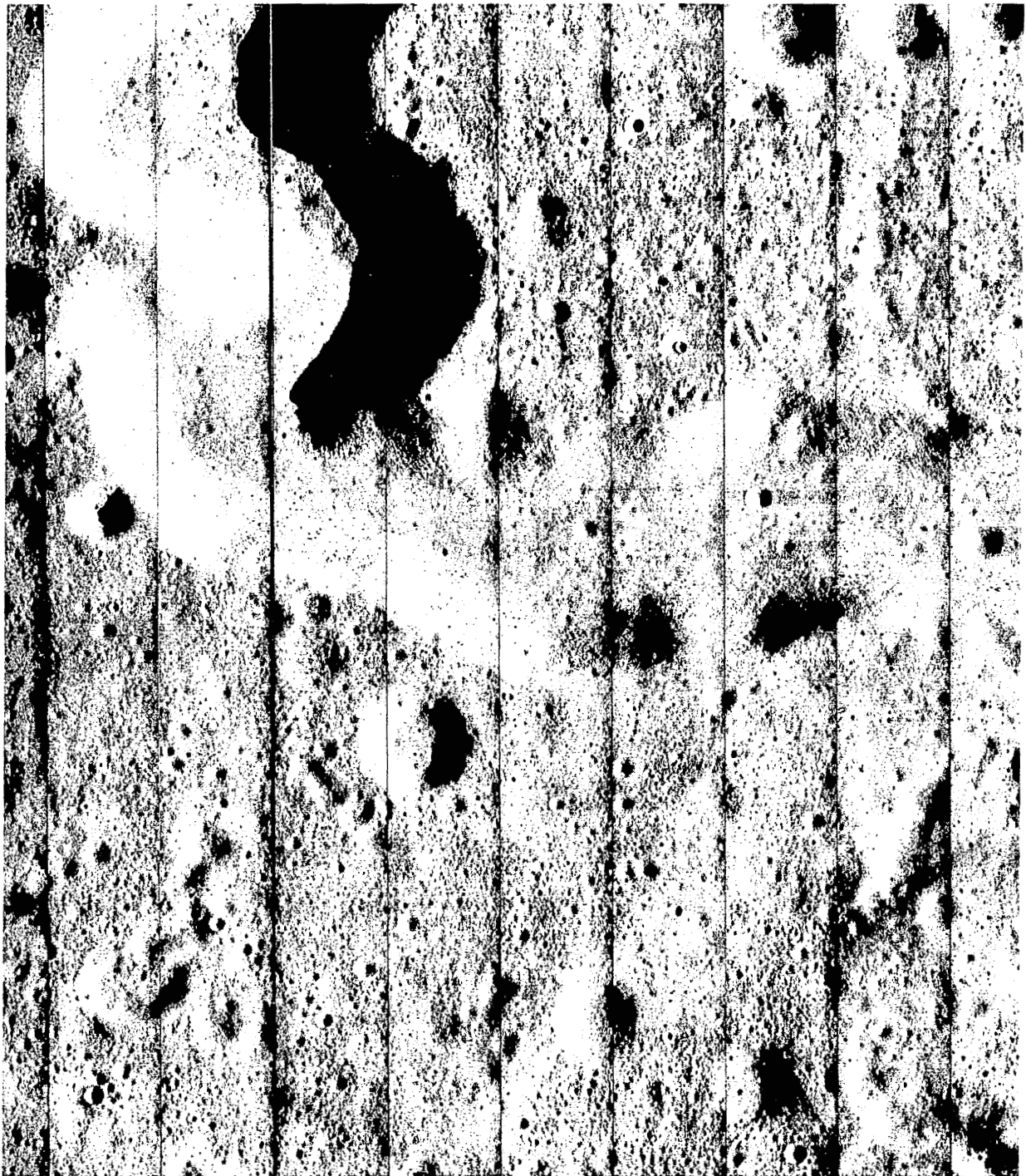
Aristarchus is presumably among the youngest of the medium-sized craters. Its walls are the brightest on the Moon and the crater has a prominent thermal anomaly. Aristarchus is also the site of more reported transient events than any other site on the Moon. Of these, the red glows reported in 1963 by observers in Flagstaff are among the best documented.

Prior to Mission IV the planned target was the crater walls but, because Mission IV photography revealed much detail in the rim materials and secondary craters, planned coverage was increased from four to eight frames.



Wide-Angle Frame 188. This is the third frame of an eight-frame sequence, representative of area photographed.

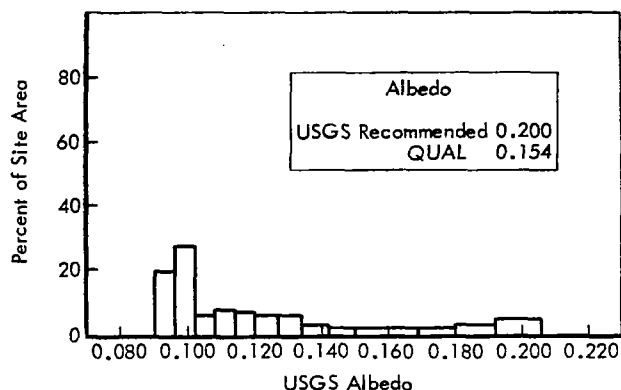
**Figure 4-100: Site V-46, Harbinger Mountains; Wide Angle**



This portion of Telephoto Frame 188 shows a portion of a rille (outlined in Figure 4-100) where orientation changes. Note difference in detail of slopes where orientation differs.

**Figure 4-101: Site V-46, Harbinger Mountains; Telephoto**

The site was photographed using the fast-sequencing mode to provide telephoto coverage of the entire crater and a portion of the outer rim. The site has the highest albedo of the sites photographed on Mission V as well as the broadest range (0.069 to 0.158 corrected), as shown in the distribution plot, Figure 4-102.



**Figure 4-102: Albedo Distribution for Site V-48, Aristarchus**

Because detail of the bright crater interior was highly desirable, exposure was based on the upper end of the albedo range.

The wide-angle frames begin coverage about two crater diameters (80 kilometers) south of the crater rim to about 40 kilometers north of the northern rim edge. The crater is almost perfectly centered in the east-west direction and spans about a third of the frame width. The wide-angle frames represented by Figure 4-103 thus provide excellent coverage of the outer rim and surrounding area that is intensely affected by the cratering ejecta. Secondary craters, hummocky ejecta blanket, and terrain features apparently modified by blast effect and melting are shown very well. Exposure, optimized for the high albedo, is good in the crater, with the detail very well shown. The outer rim area, beyond the very bright zone close to the rim, is underexposed as expected, but quite good image detail is present. Simple density control in preparing paper prints can bring out the detail in these areas at the expense of apparent overexposure of the bright areas.

Telephoto coverage of the crater is excellent. Targeting of the camera was very accurate, as

required to avoid missing rim detail. The crater diameter was almost exactly that of the telephoto field of view long axis. Coverage by the telephoto lens begins in the dune-like area of the ejecta blanket south of the crater rim, and provides contiguous coverage of the entire crater and on to the northern outer rim slope. The outer rim appears slightly dark because exposure was optimized for the brighter interior. However, detail is not lost even on the western side.

Telephoto photography of the entire crater is of outstanding quality. Examples showing portions of frames covering the inner wall and floor, part of the central peak and nearby floor, and the southeastern outer rim are presented in Figures 4-104, -105, and -106. The areas included in these figures have been outlined in Figure 4-103.

#### 4.4.2.34 Site V-49, Cobra Head

*Location: 49.50°W longitude, 25.33°N latitude*

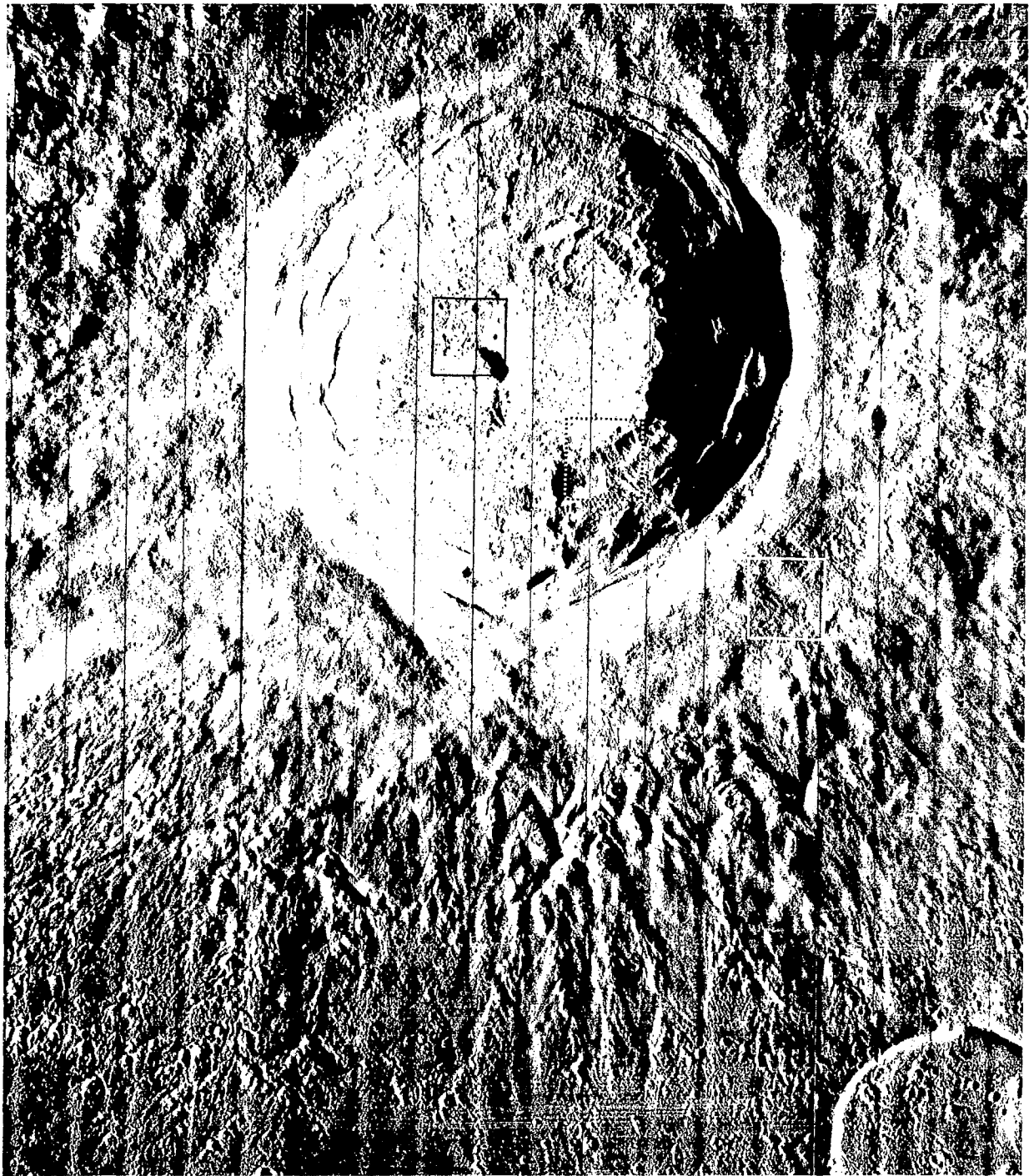
*Altitude: 132 – 135 km Frames: 202 – 205*

*Phase angle: 68.48 degrees Alpha: +6.13 degrees*

*QUAL Albedo: 0.079 Shutter speed: 0.04 second*

The Cobra Head is a depression in a large, steep mound located at the eastern end of Schröter's Valley, the largest sinuous rille known on the Moon. The site is of interest because of the uncertainty of the origin of Schröter's Valley and other sinuous rilles. It is believed by some that the rille may be a channel eroded by material erupted from the Cobra Head mound. The subsidiary sinuous rille on the floor of Schröter's Valley, first seen clearly by Mission IV photography, may represent a repeat of the event forming the larger rille. Some indication of slumping of the valley walls has been reported from Earth-based observation. In addition, two patches of smooth, dark material – one of which appears redder than the other – are included in the site, and the possibility of textural difference that might be revealed by the greater resolution of Mission V photography was of interest.

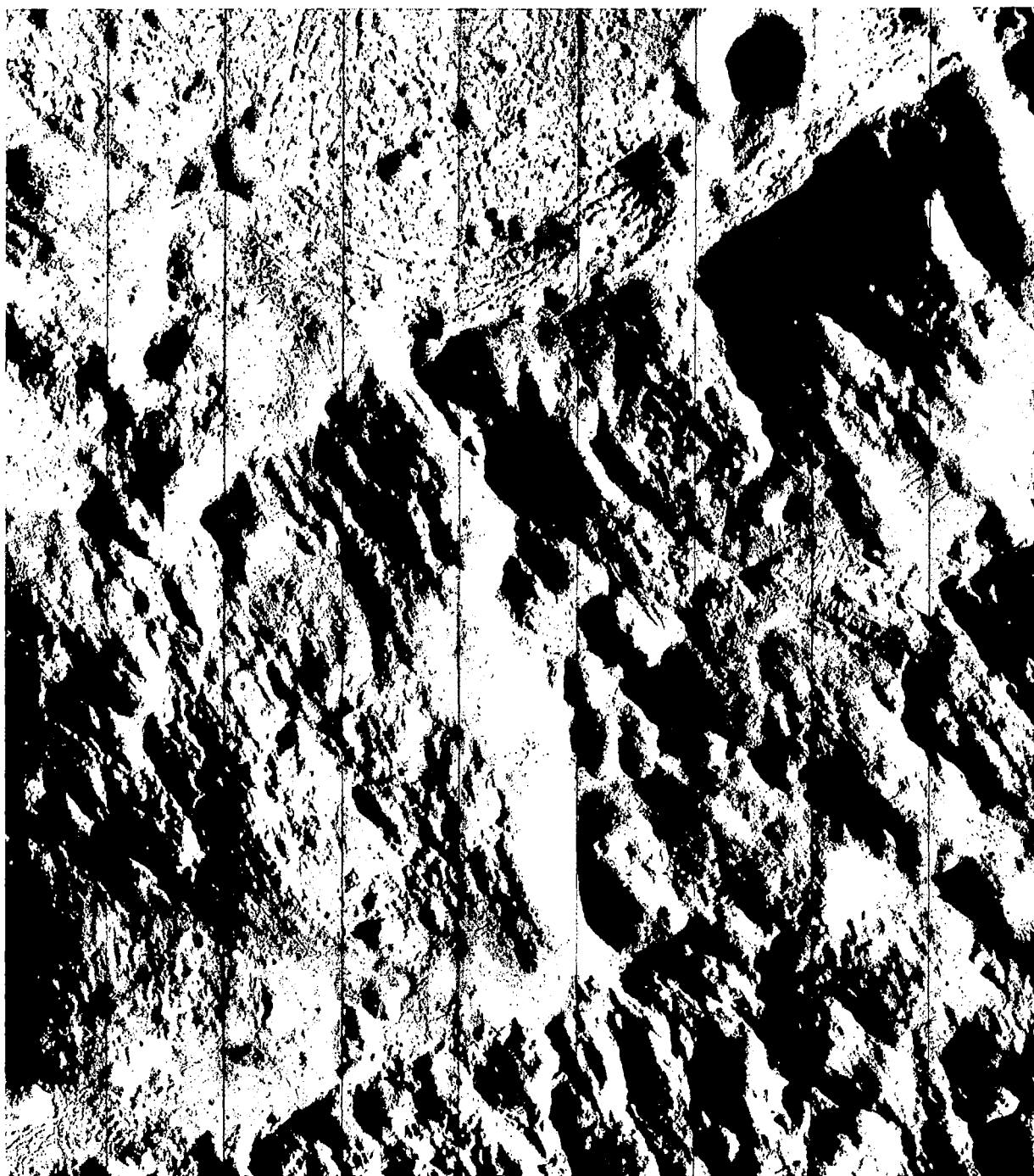
The site was photographed with a four-frame sequence taken in the fast mode. Although the site is principally mare material, its proximity to Aristarchus accounts for areas of high albedo,



Wide-Angle Frame 197, the fourth of a sequence of eight.

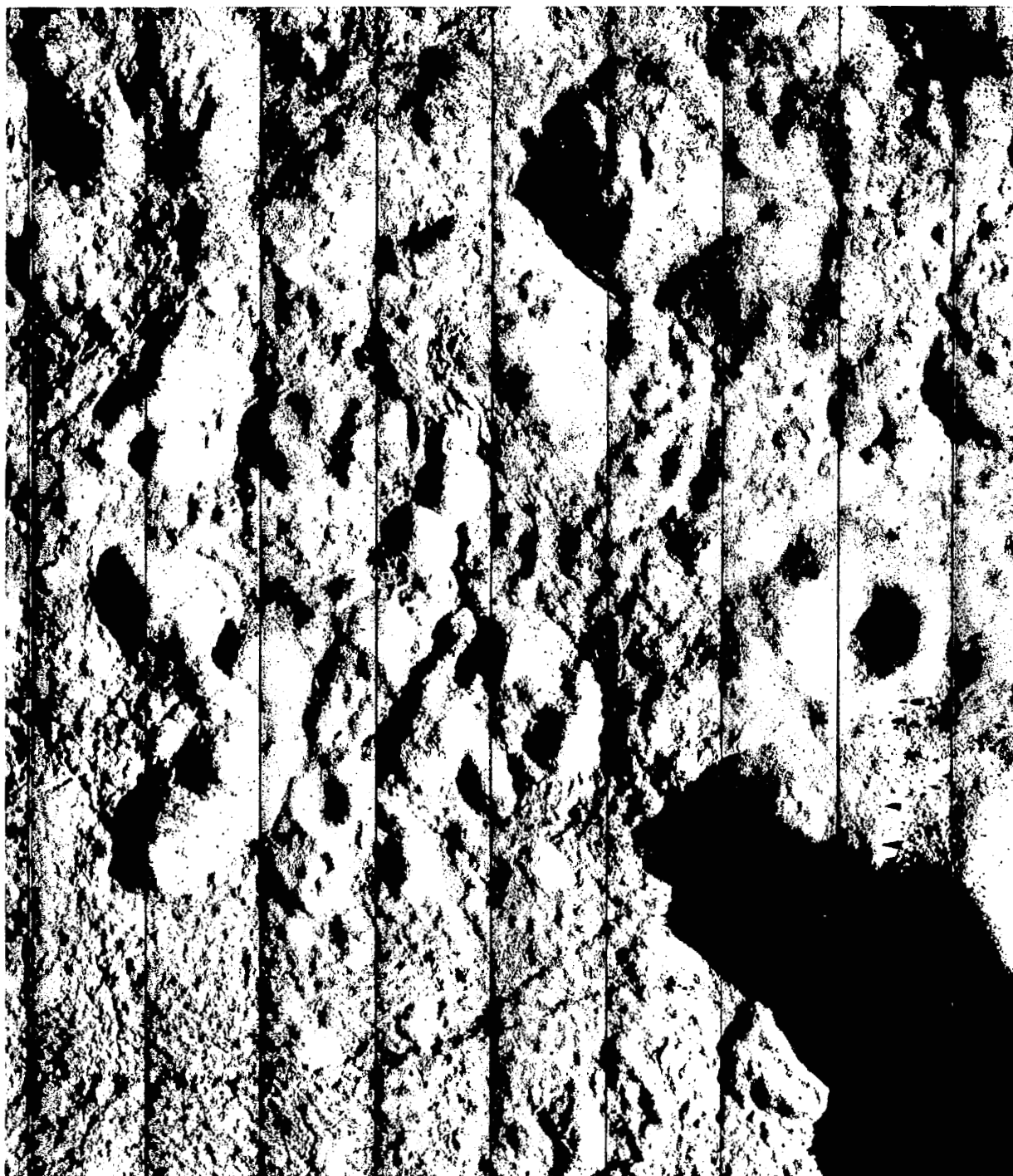
**Figure 4-103: Site V-48, Aristarchus; Wide Angle**





A portion of Telephoto Frame 198 showing detail of inner wall and part of floor. Area shown is outlined by broken line in Figure 4-103.

**Figure 4-104: Site V-48, Aristarchus; Telephoto**



A portion of Telephoto Frame 199 showing detail of part of central peak and floor. Note detail of rock-strewn areas. Area shown is outlined by solid black line in Figure 4-103.

**Figure 4-105: Site V-48 Aristarchus; Telephoto**

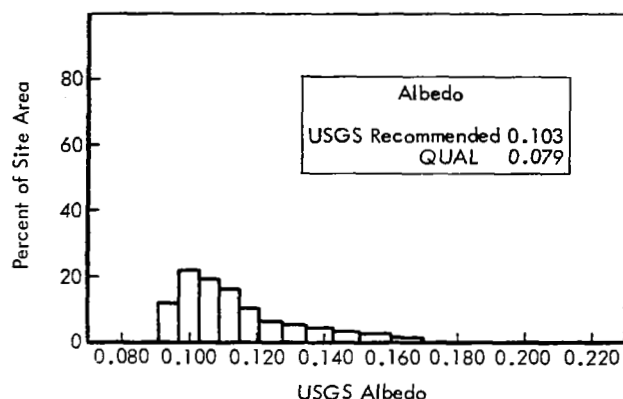




A portion of Telephoto Frame 197 showing detail of outer rim photography. This portion of the southeast rim is shown outlined by a solid white line in Figure 4-103.

**Figure 4-106: Site V-48, Aristarchus; Telephoto**

as shown in Figure 4-107. Because the darker areas were most important in this site, computa-



**Figure 4-107: Albedo Distribution for Site V-49, Cobra Head**

tions at predicted film densities for shutter speed selection were based on the lower albedo.

At the beginning of the sequence of photographs, the camera axis was slightly north of the Cobra Head depression; hence, this feature is not completely within the telephoto coverage. However, the wide-angle coverage includes all of it as well as the surrounding area. It is apparent from the wide-angle coverage that, although the telephoto coverage misses part of the depression, little information is lost because most of the interior is obscured by hard shadow. The head of Schröter's Valley is within telephoto coverage where it joins the depression and its width is great enough for the floor to be illuminated (See Figure 4-108). An appreciable length of the valley is also included in the telephoto frames.

General exposure of both wide-angle and telephoto frames is very good, with detail obscured only on the steep sunward slopes and in hard shadow. Detail on the valley floor and surrounding area is very well shown. Excellent detail of the interior boulder-littered slopes of the valley exists where orientation with respect to the Sun provides lower angle illumination. Several examples of rolling-rock tracks can be found in these areas. Because of its meandering character, characteristics of the inner sinuous

rille, including sections that appear to be filled by downward movement of material on the valley wall, may be seen (Figure 4-109).

#### 4.4.2.35 Site V-50, Aristarchus Plateau

*Location: 52.73°W longitude, 27.86°N latitude*

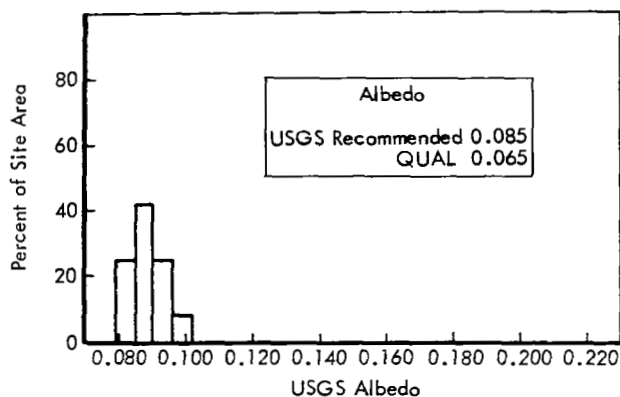
*Altitude: 139.5-142.9 km Frames: 206-209*

*Phase angle: 68.9 degrees Alpha: +5.98 degrees*

*QUAL Albedo: 0.065 Shutter speed: 0.04 second*

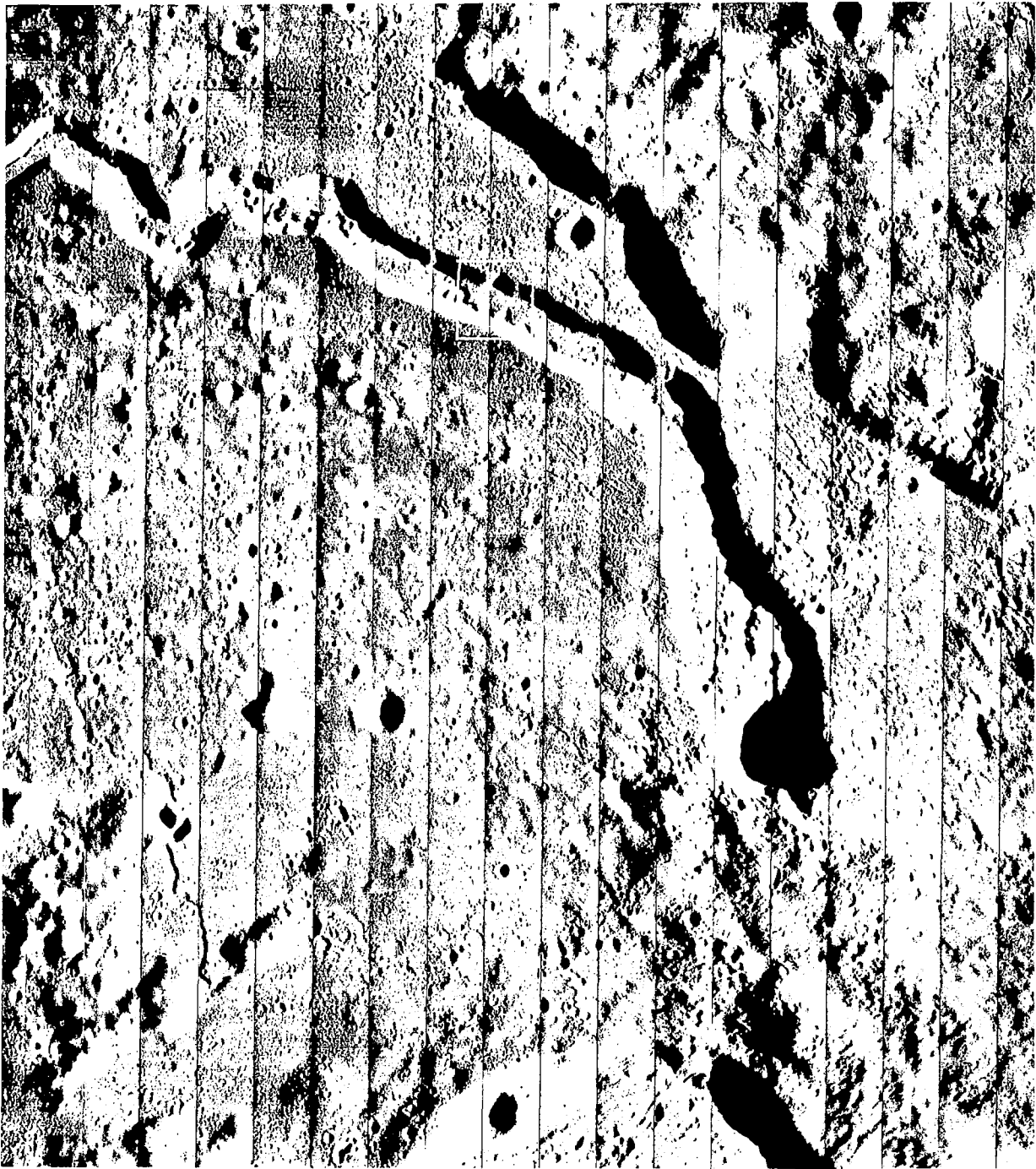
This plateau lies northwest of the crater Aristarchus. The area of interest is centered over a bright hill, Herodotus X, which is situated northwesterly from Schröter's Valley and the older crater Herodotus. A wide variety of terrain features is included in this site. Units of this complex are hilly material that may represent a thin covering over older terrain; a smoother, newer material that forms pools within the first; and assorted domes, cones, chain craters, and rilles. Lunar Orbiter Mission IV photographs provided an excellent view of the regional relationships of the geological units in the complex. Additional photographs, particularly high-resolution frames, were desired to obtain detailed views of the major features.

The selected exposure time of 0.04 second produced wide-angle photographs with good image densities and contrasts. Exposure time was based on a corrected albedo of 0.065. Albedo characteristics for this site are shown in Figure 4-110. Some underexposure, particularly at



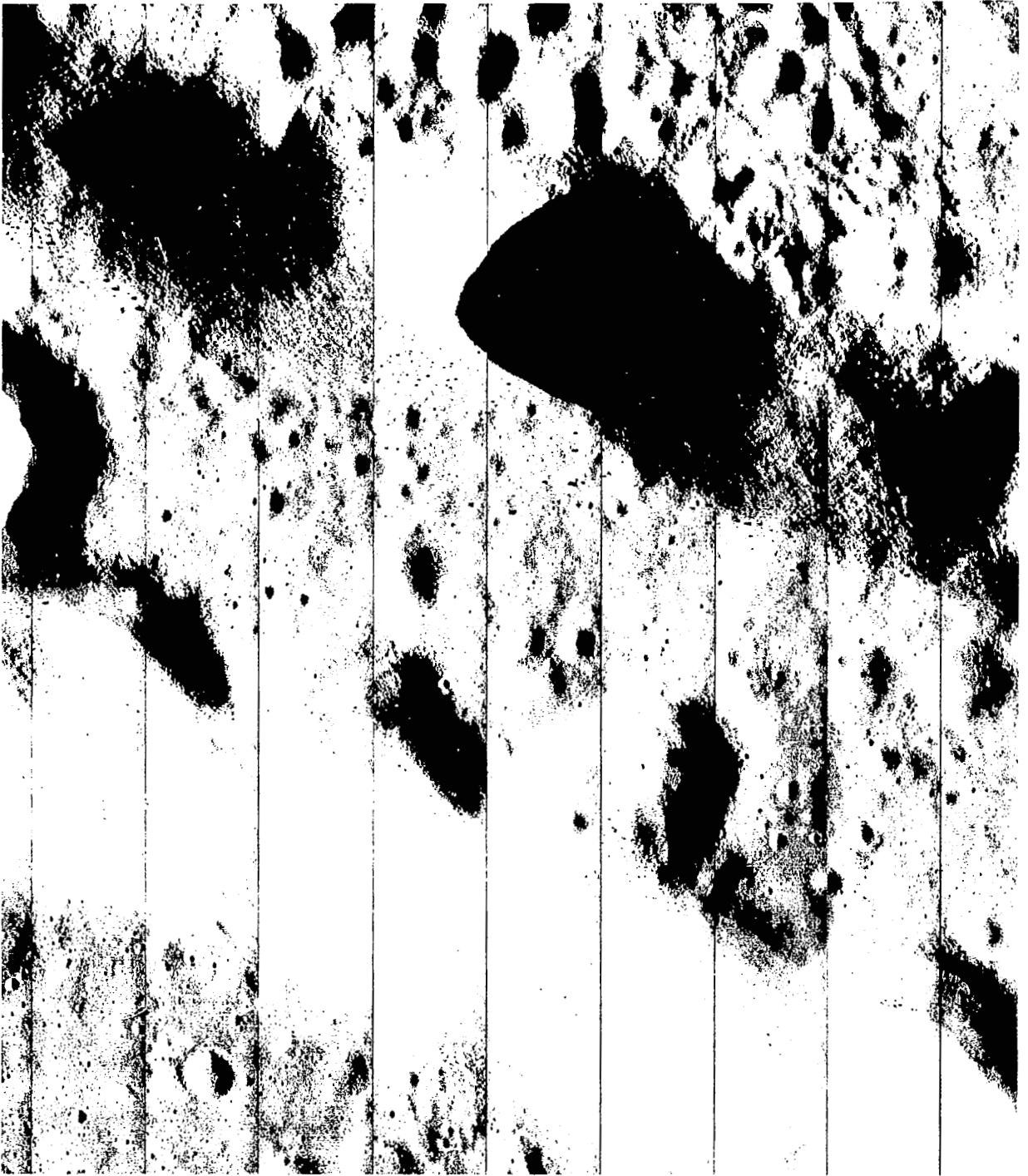
**Figure 4-110: Albedo Distribution for Site V-50, Aristarchus Plateau**

frame ends, was observed in the telephoto frames. As seen on positive GRE film, the end



Most of Wide-Angle Frame 202. Good exposure was obtained in this area of high surface contrasts.

**Figure 4-108: Site V-49, Cobra Head; Wide Angle**



This is a section of Telephoto Frame 204 showing representation of detail in Schröter's Valley. Area shown is outlined in Figure 4-108.

**Figure 4-109: Site V-49, Cobra Head; Telephoto**

framelets were often quite dense, whereas the central framelets were satisfactory, although slightly denser than normal. Off-axis light transmission fall-off of the 610-mm lens, illumination geometry, and scene characteristics were contributing factors toward unexposure of some of the telephoto end framelets. Except for occasional very dense frame ends, detail and contrast in the 610-mm photographs were good.

Site coverage in the wide-angle frame sequence extends northeast from the northern bend of Schröter's Valley, through the adjoining portion of the Aristarchus Plateau, and includes some of the mare area north of the plateau. Although the area is relatively rough, it does not include many of the large topographic features that produce extensive hard-shadow areas. The plateau and mare areas were generally within system luminance limits except for steep slopes. Consequently, the many types of surface features have been recorded with very good detail as seen in Figure 4-111. Spacecraft altitude for this four-frame sequence in the fast mode was fairly consistent, ranging from 139.5 to 142.9 kilometers from Frames 206 to 209.

Overall detail in the telephoto frames was good, although some portions had dense low-contrast images with some accompanying loss in definition. Surface texture and small features are very good for most of the area photographed, as illustrated by Figure 4-112. The area shown is outlined in Figure 4-111. Some information was lost in very bright areas such as the sunward slopes of the hill Herodotus X. However, good detail was recorded on other portions of the hill where conditions of illumination resulted in a favorable luminance range. In both the telephoto and wide-angle photographs, small craters spanned by as few as four scan lines could be identified.

#### 4.4.2.36 Site V-51, Marius Hills

*Location: 56.02°W longitude, 13.66°N latitude*

*Altitude: 108 - 111 km Frames: 210 - 217*

*Phase angle: 65.30 degrees*

*Alpha: +10.12 degrees QUAL Albedo: 0.060*

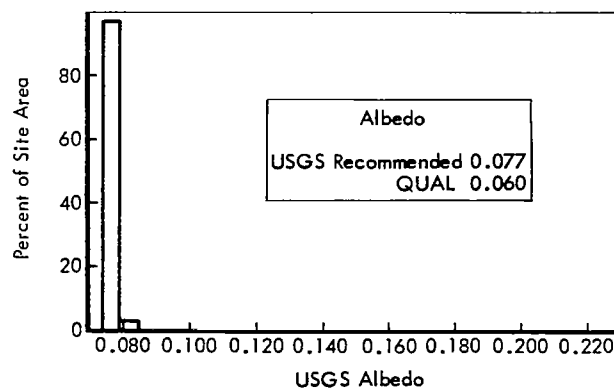
*Shutter speed: 0.04 second*

The unique characteristics of this area were not known prior to Lunar Orbiter photography. By

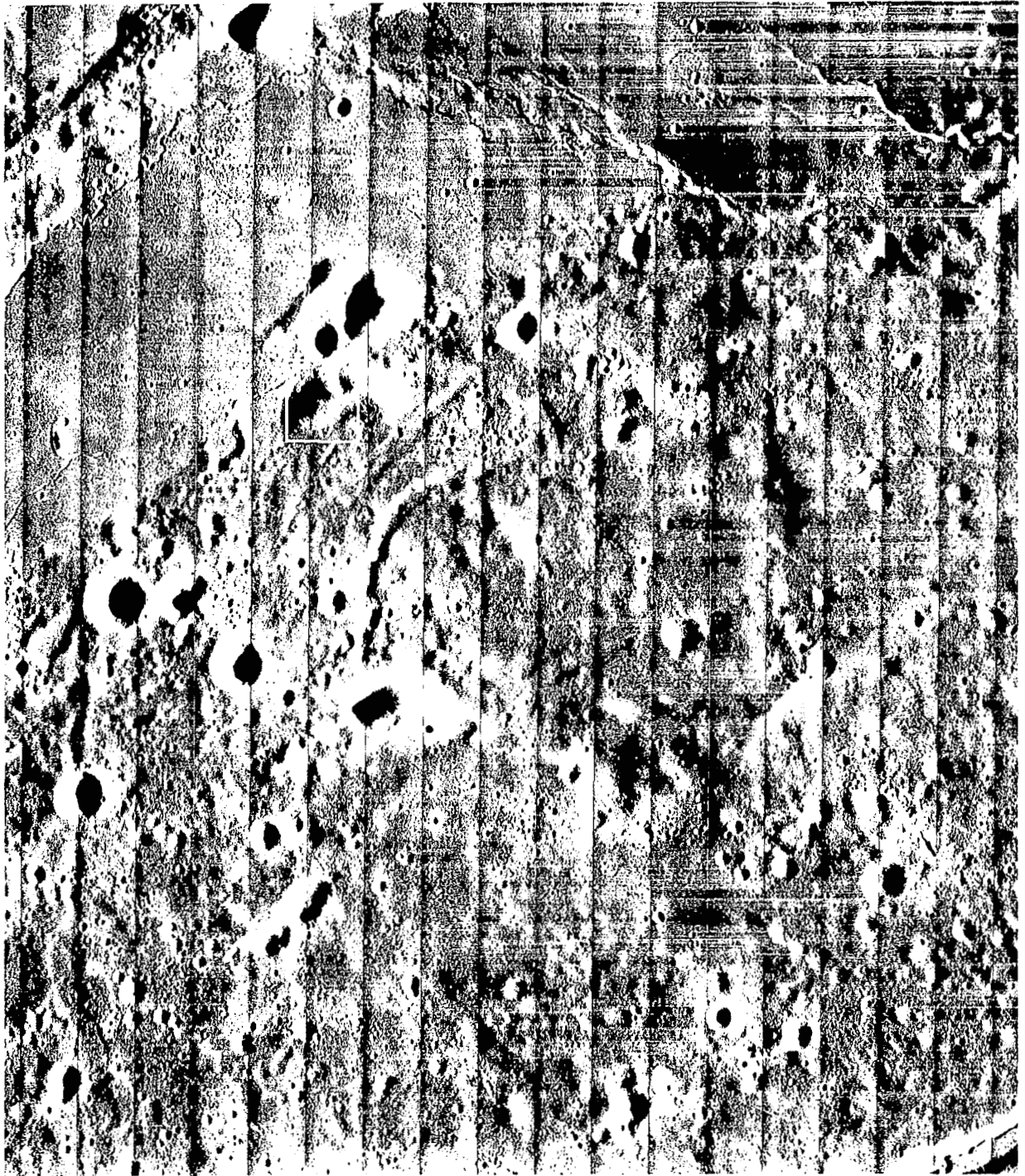
Earth-based observation, the area north of Marius appeared to be slightly uplifted and of lower albedo than the surrounding mare. Numerous domes scattered over the area could be seen. The area was selected as a secondary site for Mission II (Site IIS-15) and photographed as a northerly oblique. The geological complexity of this area was revealed by the above photograph and further demonstrated by Mission IV photography. Mission IV photographs were responsible for the particular choice of target position within the area as one displaying as great a variety of features as possible.

Mission IV photographs showed that the area has many types of constructional features presumably of volcanic origin, such as rough-surfaced domes, cones, flows, and craters of all descriptions. Sinuous rilles with craters at one end, crater chains associated with linear rilles, groups of secondary craters produced by clusters of ejecta fragments, and prominent wrinkle ridges are present. Because of its extreme complexity and occurrence of areas that may be suitable for landing, the area has been included as a potential AAP site.

The area including the many interesting formations is extensive and, therefore, was photographed by a sequence of eight frames taken in the fast mode. The site is entirely dark mare, as shown by the albedo distribution histogram, Figure 4-113, and has the lowest albedo of any Mission V site.



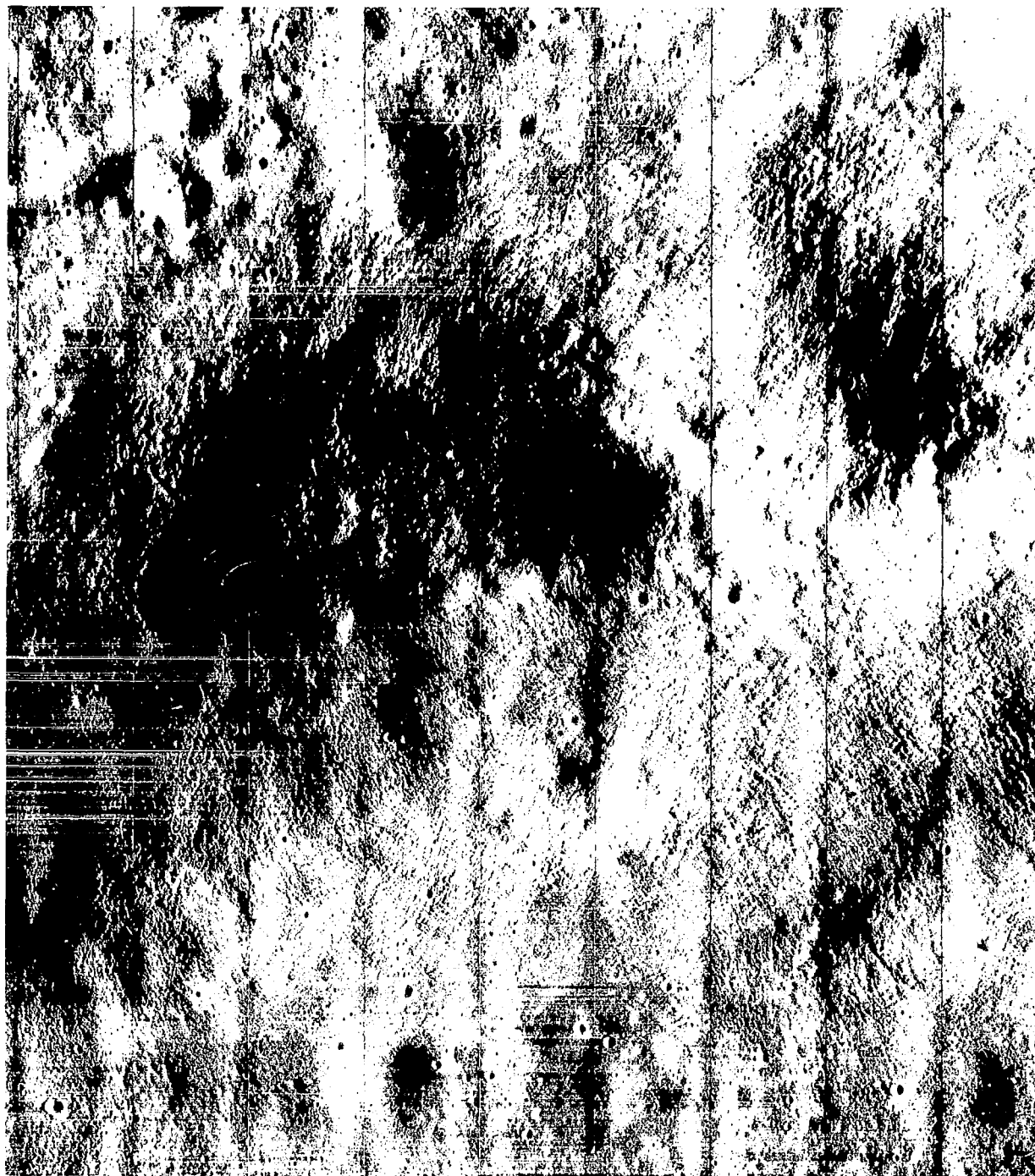
**Figure 4-113: Albedo Distribution for Site V-51, Marius Hills**



Wide-Angle Frame 207. Luminance was too high on the very bright hills. Note apparent low albedo of terra-like plateau surface.

**Figure 4-111: Site V-50, Aristarchus Plateau; Wide Angle**





A portion of Telephoto Frame 208 including both terra and mare surface indicating detail of photography. Area shown is outlined in Figure 4-111.

**Figure 4-112: Site V-50, Aristarchus Plateau; Telephoto**



Exposure of both wide-angle and telephoto frames is satisfactory and good-quality photographs were obtained. Although the photographs received the maximum exposure possible (0.04 second), the GRE film densities were a little higher than optimum for the telephoto frames (1.4), indicating a slight underexposure. Image quality of the paper prints is good.

The entire area is relatively flat (Figure 4-114). Domes and ridges are of low profile and thus do not present serious luminance extremes. Very little area within the site is obscured by hard shadow or over-exposed highlights. Excellent surface detail characterizing the dome and ridge material is present. The largest sinuous rille with a crater at its head is oriented in a generally east-west direction, and the near optimum illumination of its interior brings out excellent detail of both sides and floor for a distance of 12 to 15 kilometers, a portion of which, shown in Figure 4-115, is outlined in Figure 4-114. The character of the many domes shown in telephoto frames is illustrated in Figure 4-116. This area also is outlined in Figure 4-114. Although exposed, Telephoto Frame 217 was not read out, and Wide-Angle Frame 216 was degraded by the alteration of the Bimat caused by the knurl on the core of the Bimat supply reel. This occurred as the supply of Bimat was exhausted.

This site was the last of the mission and terminated photography by the Lunar Orbiters.

## 4.5 FARSIDE SITES

Mission V farside photography was planned to provide coverage of areas not photographed on previous missions or for which previous photography had been degraded by operational problems. All planned photography was accomplished. The combination of photography acquired on Missions I through V thus provides photographic coverage of essentially the entire Moon at a resolution equivalent to, or better than, that possible from Earth.

Mission V farside coverage, provided by 23 sites, is shown diagrammed in Figure 4-117. All photography was accomplished from near apolune and thus at a relatively high altitude. Principal parameters for the farside sites are listed in Table 4-6

## 4.5.1 General Group Characteristics

### 4.5.1.1 Exposure

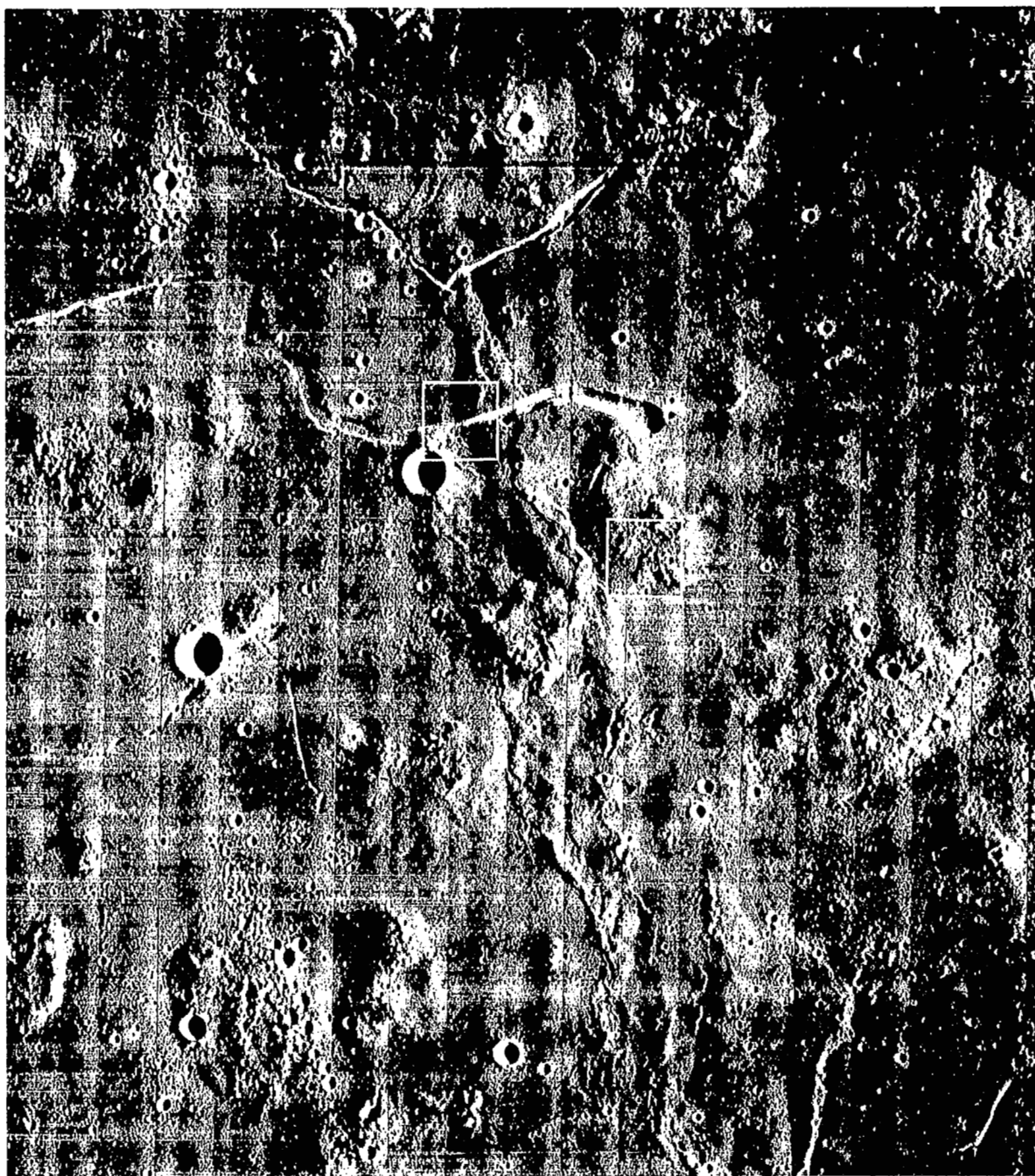
All sites on the farside were exposed with a shutter speed of 0.04 second. The camera axis was pointed more toward the terminator than at the nadir to center the telephoto frame within the band of most suitable illumination. It had been shown previously by earlier mission photography that the farside was predominantly of terra characteristics, with only relatively small, isolated, mare-type areas. Since illumination at all sites at the time of photography was similar, the same shutter speed was appropriate for all. This procedure was successful in all cases (except where spacecraft maneuvers placed the principal point too close to or beyond the terminator in the dark). Of the 23 sites, the camera was pointed in such a direction that telephoto coverage was not obtained for only two.

The high altitude resulted in wide-angle coverage extending from the terminator to the bright limb, thus spanning a wide luminance range. However, because of this, each wide-angle frame includes optimum illumination even though the corresponding telephoto frame may not, because of its narrower field of view and the illumination variation introduced by only a very small change in camera pointing direction.

Prediction of the shutter speed for exposure control is based on illumination and observation geometry and albedo of the surface. Geometrical parameters existing at the time of exposure can be predicted with an accuracy adequate for exposure control. However, although albedos for most of the nearside have been measured from Earth, considerable uncertainty about farside characteristics still exists. Therefore, accurate prediction of farside exposure for limited areal coverage required use of stochastic techniques based on experience gained during previous missions. The generally high quality of Mission V farside photography has demonstrated the validity of this technique.

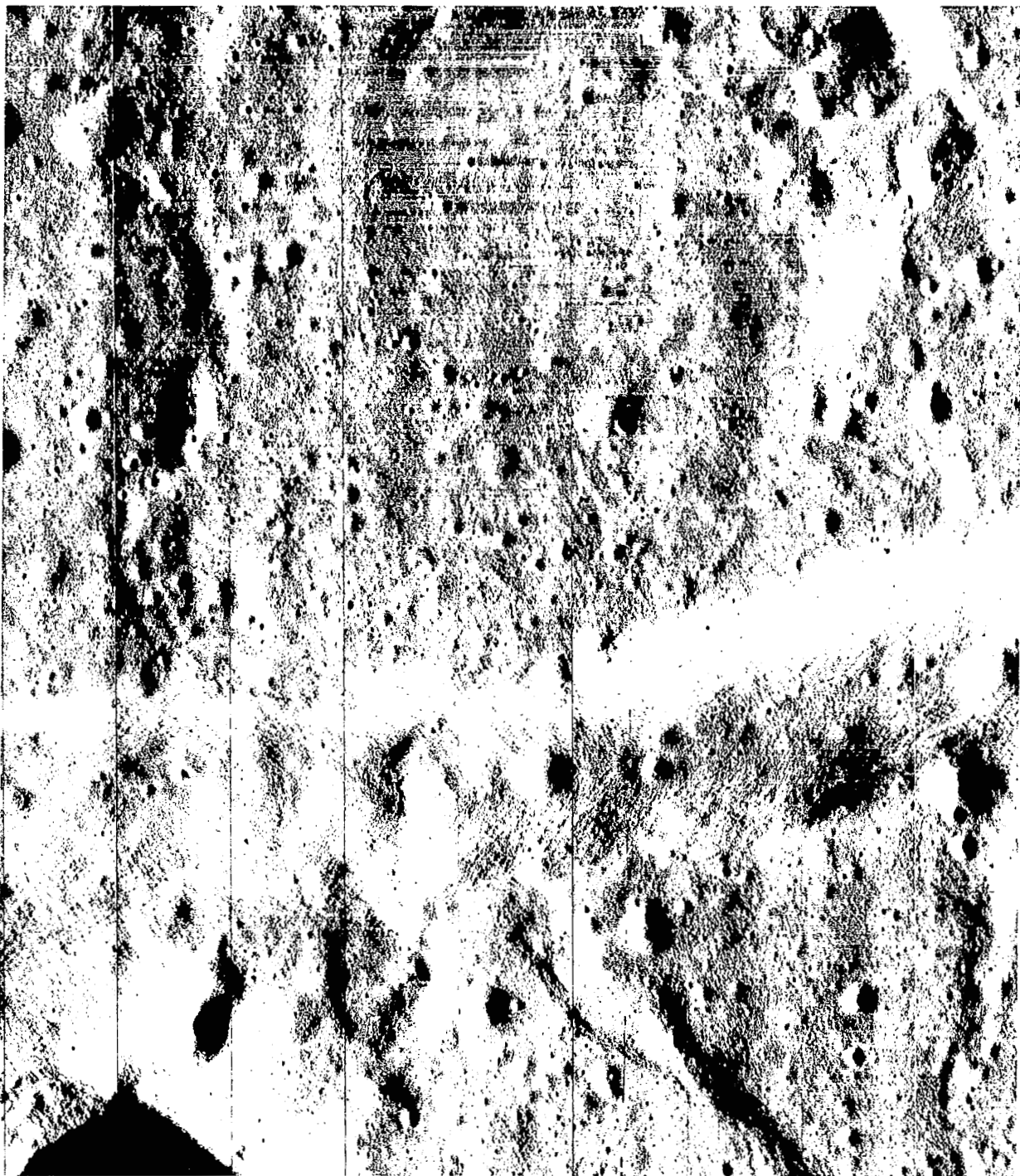
## 4.5.2 Photographs

Figures 4-118 and -119 are shown here as representative of the many farside photographs taken. They are from Site VA-21, Frame 103 taken near apolune of the final ellipse over the central



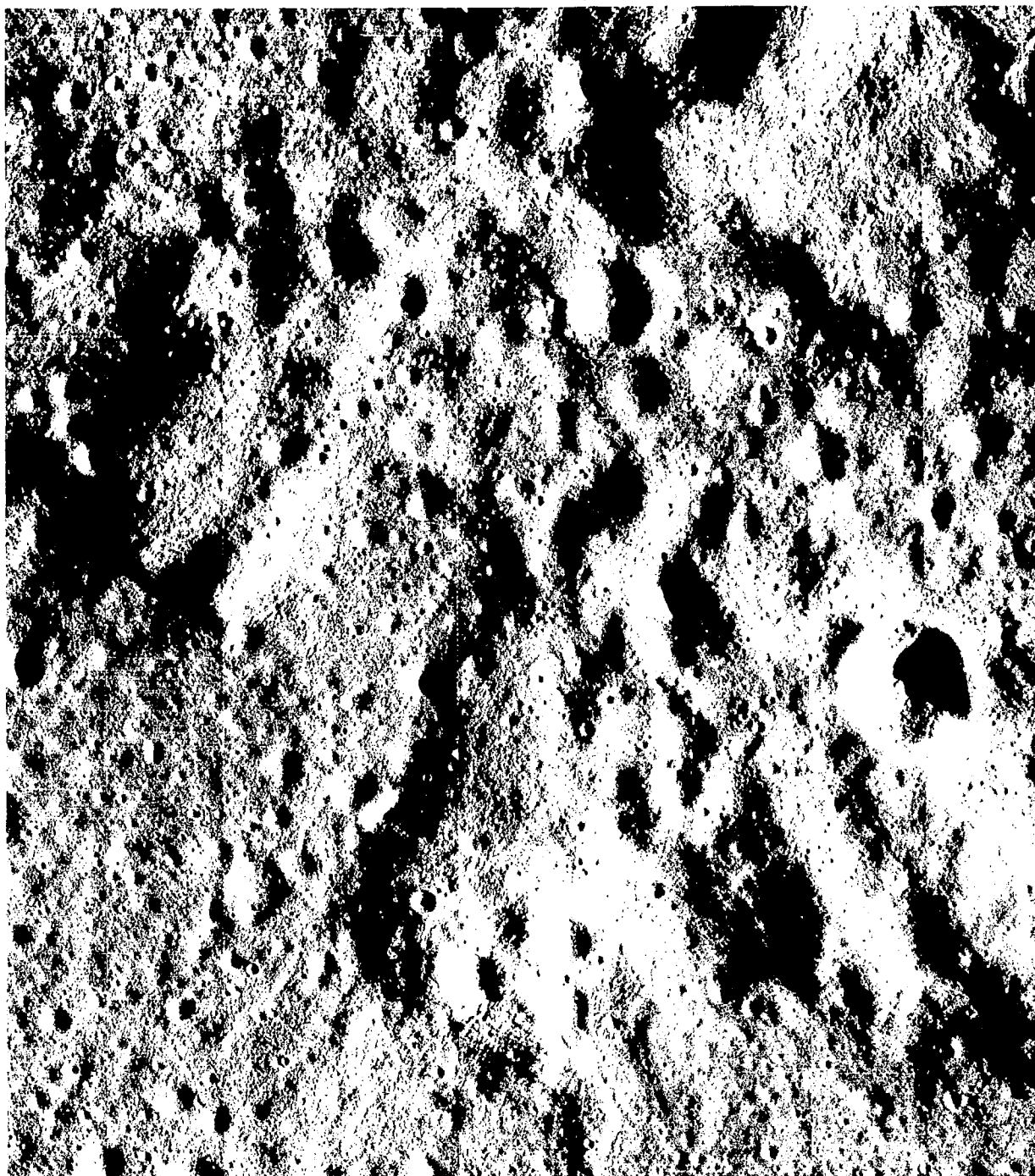
Wide-Angle Frame 212. This is representative of the area photographed.

**Figure 4-114: Site V-51, Marius Hills; Wide Angle**



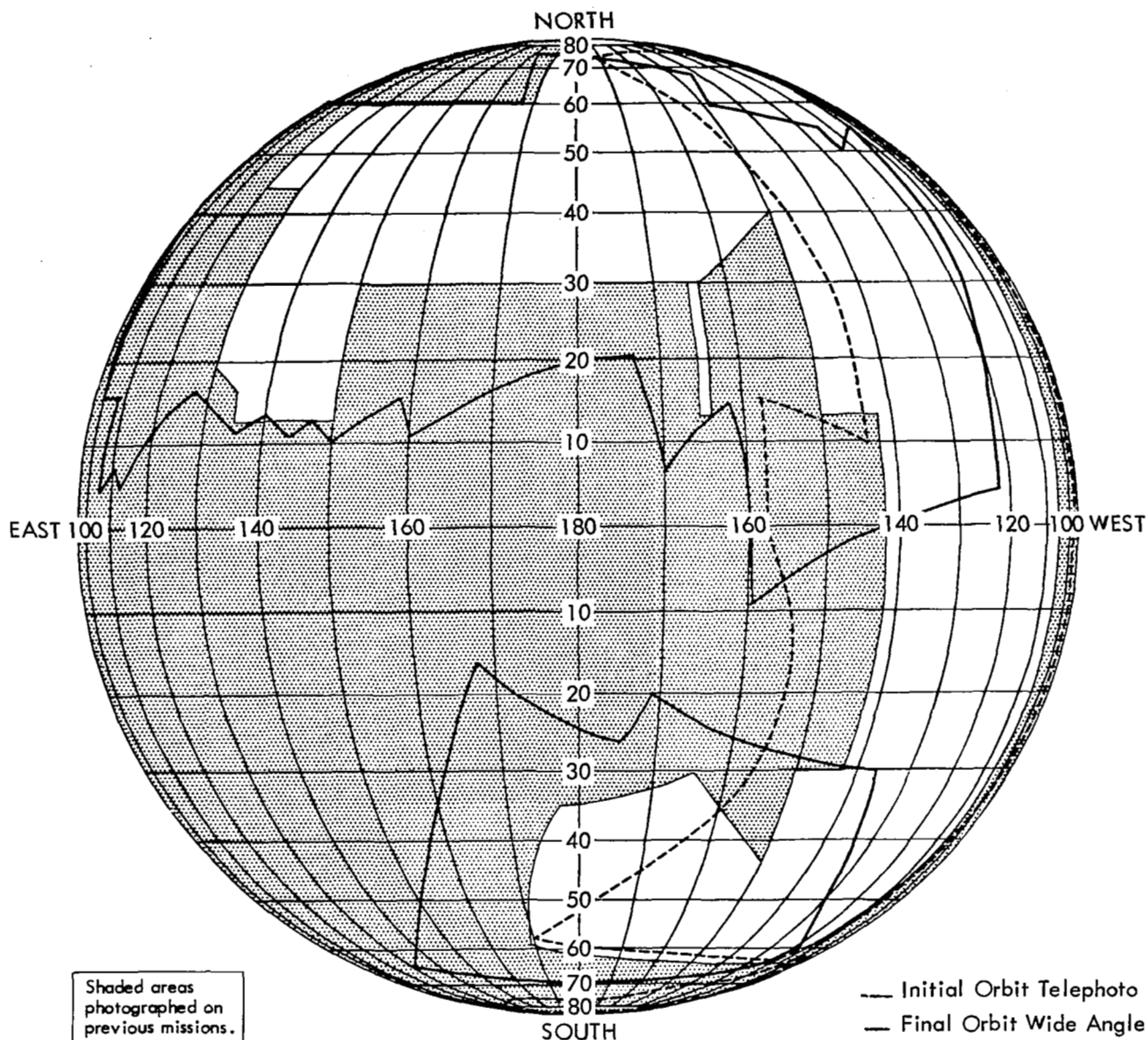
This is a portion of Telephoto Frame 213 showing detail present in interior of large east-west trending rille. Area shown is outlined in Figure 4-114.

**Figure 4-115: Site V-51, Marius Hills; Telephoto**



A portion of Telephoto Frame 212 showing one of the hills. Little difference in albedo exists between hills and mare surface. Area shown is outlined in Figure 4-114.

**Figure 4-116: Site V-51, Marius Hills; Telephoto**



**Figure 4-117: Envelope of Photographs Comprising Mission V Farside Coverage**

eastern area. The first, Figure 4-118, is most of the wide-angle frame and the second is a portion of the telephoto frame reproduced at GRE film scale to illustrate the detail obtained from near-apolune altitude (1,234 kilometers).

The principal problem in farside photography is related to the general topographic character of that part of the Moon. Except for a very limited number of large filled craters, the farside is of rugged, heavily cratered terra. As a

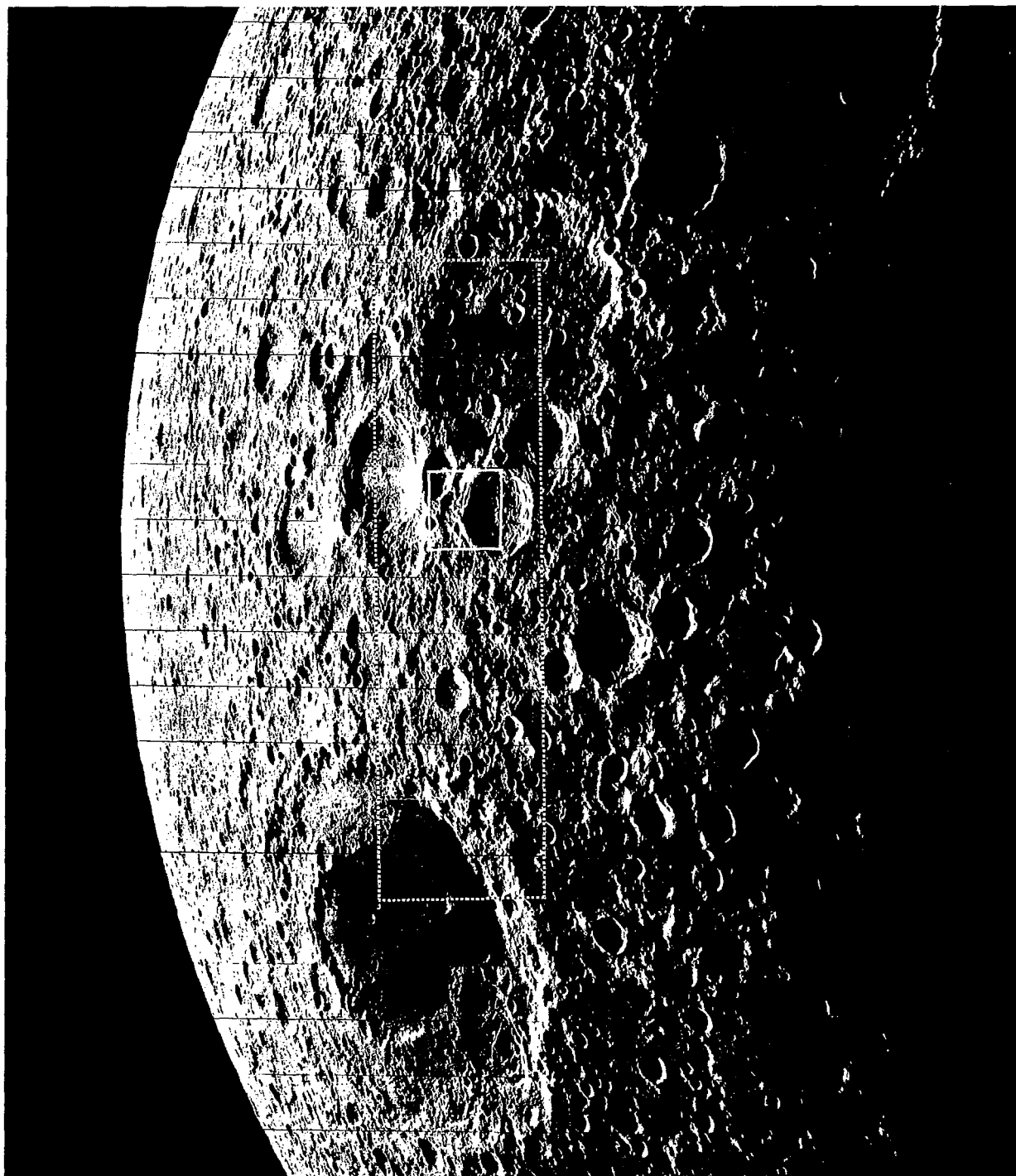
consequence, much rather steeply sloped terrain is present, leading to an extreme luminance range including much hard shadow in the band illuminated by the normally optimum Sun angle. Where the wide range of luminance exceeded system limits, some detail in highlighted slopes and deep shadow areas was lost by clipping in the photo-video-chain. In more nearly level areas, such as large crater floors, the limited mare-type surfaces and intercrater areas were well exposed. In areas where clipping and the



**Table 4-6: Farside Site Principal Photographic Parameters**

Sites	Frames	Principal Point		Altitude (km)	Phase Angle (deg)	Alpha (deg)	QUAL.Albedo (corrected)	Shutter Speed (sec)	Photo Orbit
		Longitude	Latitude						
VA-1	5 - 12	110°W	60°N	2648	106.8	-23.7	0.099	0.04	2
VA-2	13 - 20	103°W	13°N	5755	122.0	-35.4	0.110	0.04	2
VA-3	21	179°W	84°S	3343	119.8	-36.8	0.109	0.04	3
VA-4	22	115°W	27°S	5107	126.1	-43.6	0.108	0.04	4
VA-5	23	— BLANK	—	—	—	—	—	—	4
VA-6	24	119°W	26°N	5006	118.7	-35.0	0.109	0.04	5
VA-7.1	25	128°W	59°N	2549	106.3	-23.4	0.100	0.04	6
VA-8	26	127°W	27°S	5067	125.2	-42.2	0.099	0.04	7
VA-9	27	— EARTH	—	—	—	—	—	0.01	8
VA-10	28	132°W	26°N	5010	117.7	-34.8	0.099	0.04	8
VA-11.2	29	145°W	59°N	2546	106.8	-26.4	0.108	0.04	9
VA-12	30	140°W	27°S	5067	124.2	-41.6	0.108	0.04	10
VA-13	31	135°W	28°N	1361	129.7	-41.0	0.108	0.04	11
VA-14	32	138°W	25°N	1395	129.8	-40.1	0.120	0.04	13
VA-15	39	158°W	38°N	1250	130.1	-49.5	0.108	0.04	19
VA-16	43*	151°W	48°S	1189	129.9	-35.6	0.108	0.04	25
VA-17	53	175°W	49°N	1188	125.3	-44.0	0.108	0.04	29
VA-18	65	170°W	47°S	1190	129.6	-37.0	0.108	0.04	35
VA-19	79	168°E	39°N	1242	127.2	-47.4	0.108	0.04	39
VA-20	85	160°E	39°N	1237	126.6	-46.9	0.108	0.04	44
VA-21	103	152°E	39°N	1234	125.7	-45.9	0.108	0.04	49
VA-22	124	144°E	39°N	1234	124.8	-45.0	0.108	0.04	54
VA-23	158	128°E	38°N	1230	123.1	-43.2	0.108	0.04	64
VA-24	163	122°E	38°N	1228	122.8	-43.3	0.108	0.04	67
VA-25	181	110°E	42°N	1179	120.1	-40.9	0.108	0.04	74

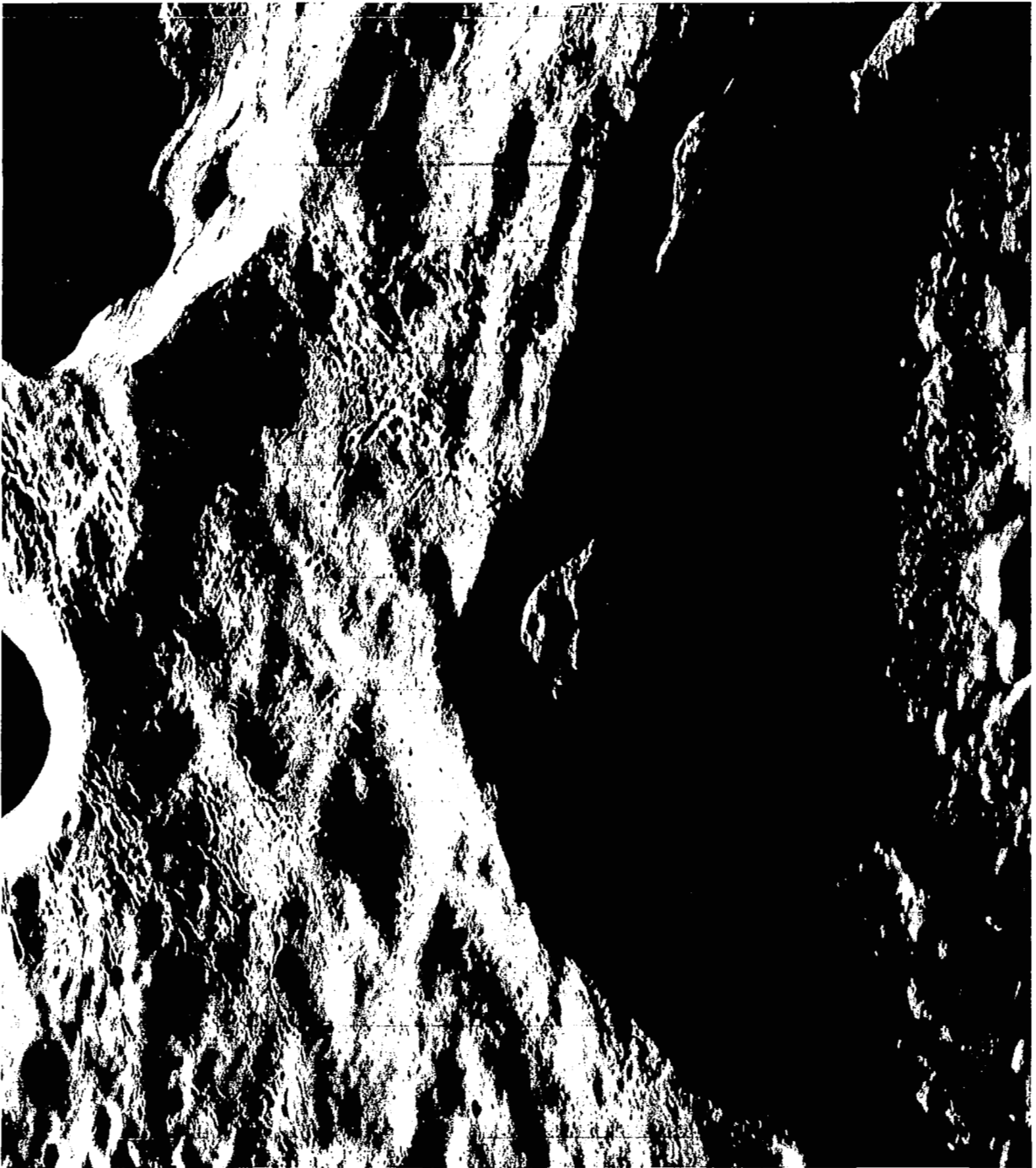
\*Frame 43 telephoto blank. Field of view beyond terminator in dark.



Telephoto coverage is outlined.

**Figure 4-118: Site VA-21; Representative Wide-Angle Photograph of Farside**





A small portion of the frame is shown reproduced at GRE film scale to demonstrate quality.

**Figure 4-119: Site VA-21; Representative Telephoto Photograph of Farside**

accompanying loss of detail did occur, the resulting high contrast sharply delineates the gross topographic features.

As expected, the combination of spacecraft orbital progression and changes in altitude and latitude resulted in variations in the width of the illuminated lunar limb viewed by the photo subsystem. The wide-angle photographs taken from altitudes of approximately 5,000 to 6,000 kilometers encompassed the entire lunar sphere and recorded good surface detail in the illuminated limb. Wide-angle photographs taken at the lower altitudes, from 1,200 to 2,700 kilometers, resulted in better use of the frame format because of larger, more detailed images. Both wide-angle and telephoto frames were of good photographic quality despite relatively high phase angles, which ranged from 106 to 130 degrees. Resolution was particularly good in the bands where photographic geometry and illumination resulted in good density ranges. Where conditions were favorable, craters spanning as few as three scan lines could be discerned in both the telephoto and wide-angle photographs.

Considerable detail was also recorded in the bright-limb areas toward the lunar horizon, where surface characteristics and illumination and camera geometry resulted in very bright, low-contrast areas.

## 4.6 EARTH PHOTOGRAPH

### 4.6.1 Acquisition

An Earth photograph was not originally planned for Mission V. There was, however, a blank film-set frame scheduled near the apolune between Orbits 7 and 8. At that time, the Earth, as seen from the Moon, would be almost fully illuminated. It was decided, therefore, to use this otherwise blank frame for an Earth photograph. Mission and operations directives were issued on Day 218 (August 6, 1967) implementing this plan. The directives called for a two-axis maneuver to point the camera axis at the center of the Earth, with time of photography no later than 8 hours after the previous photograph since film movement requirements still had to be met. The Earth photograph was identified as Site VA-9. Although not specifically

stated, it was implicit that this photograph would not include any of the Moon as in Mission I. First, due to orbit geometry, the Earth never "set" (occulted), making it difficult to include both the Earth and Moon in the same photograph. Second, it was designed to expose the film for the Earth alone to obtain the best resolution.

The Earth photograph design resulted in the following commands.

Photo time	Day 220, 09:05:00 GMT
Roll	-166.62 degrees
Pitch	-38.49 degrees

This time was 7 hours, 23 minutes after the previous photograph (VA-8), satisfying the film movement constraint. The relative positions of the Earth, Sun, Moon, and spacecraft at time of photography are indicated in Figure 4-120. At the time the photograph was taken, the spacecraft was 5,871 kilometers above the Moon and 361,730 kilometers from Earth. From this position, Earth subtended 1.985 degrees.

### 4.6.2 Photographic Results

The photograph was exposed using a shutter speed of 0.01 second. Because of the very high albedo of Earth (about 0.36), some overexposure was expected, even when using the fastest shutter speed. The GRE record of the telephoto frame appears overexposed and of low contrast. Detail is present but generally faint. The image enhancement technique using the magnetic-tape video record used at Langley Research Center was used to advantage on this photograph. This technique made possible the production of a good-quality print, as shown in Figure 4-121.

Resolution of photographs throughout the mission was excellent; therefore, it is reasonable to assume that the slight fuzziness of the Earth image is due to effects of its atmosphere.

Although there is much cloud cover, continental outlines can be seen. As an aid in identification, a computer-drawn sketch showing location of land masses is shown in Figure 4-122. The approximate apparent terminator is shown. Al-

S/C Longitude =  $76.4^{\circ}$  E  
S/C Latitude =  $8.5^{\circ}$  N

Sun Longitude =  $44.9^{\circ}$  E  
Sun Latitude =  $16.4^{\circ}$  N

Orbit 8  
Camera-On Time 8 Aug 1967, 09:05:00

Roll = -  $166.62^{\circ}$  Deg  
Pitch = -  $38.49^{\circ}$  Deg

Off-Sun Angle  $38.5^{\circ}$  Deg

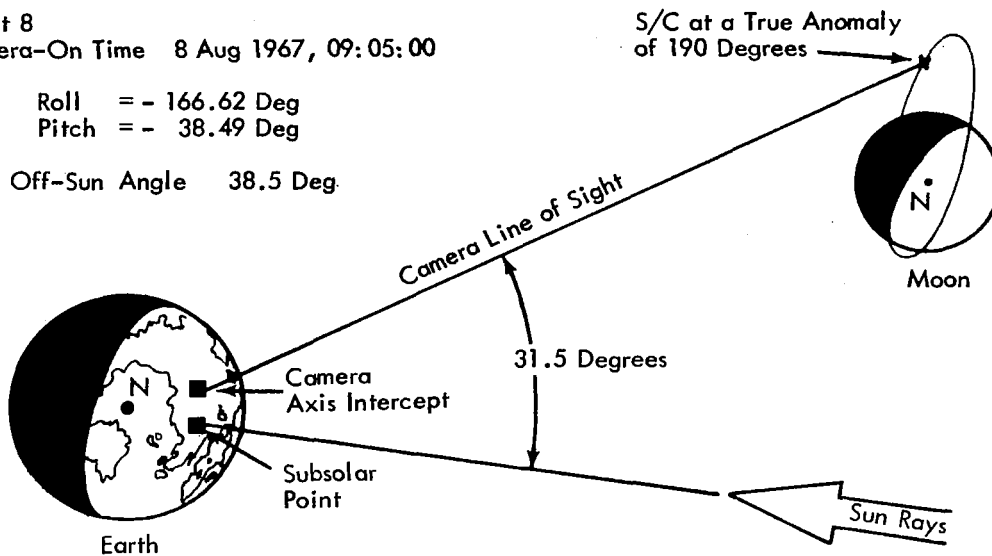
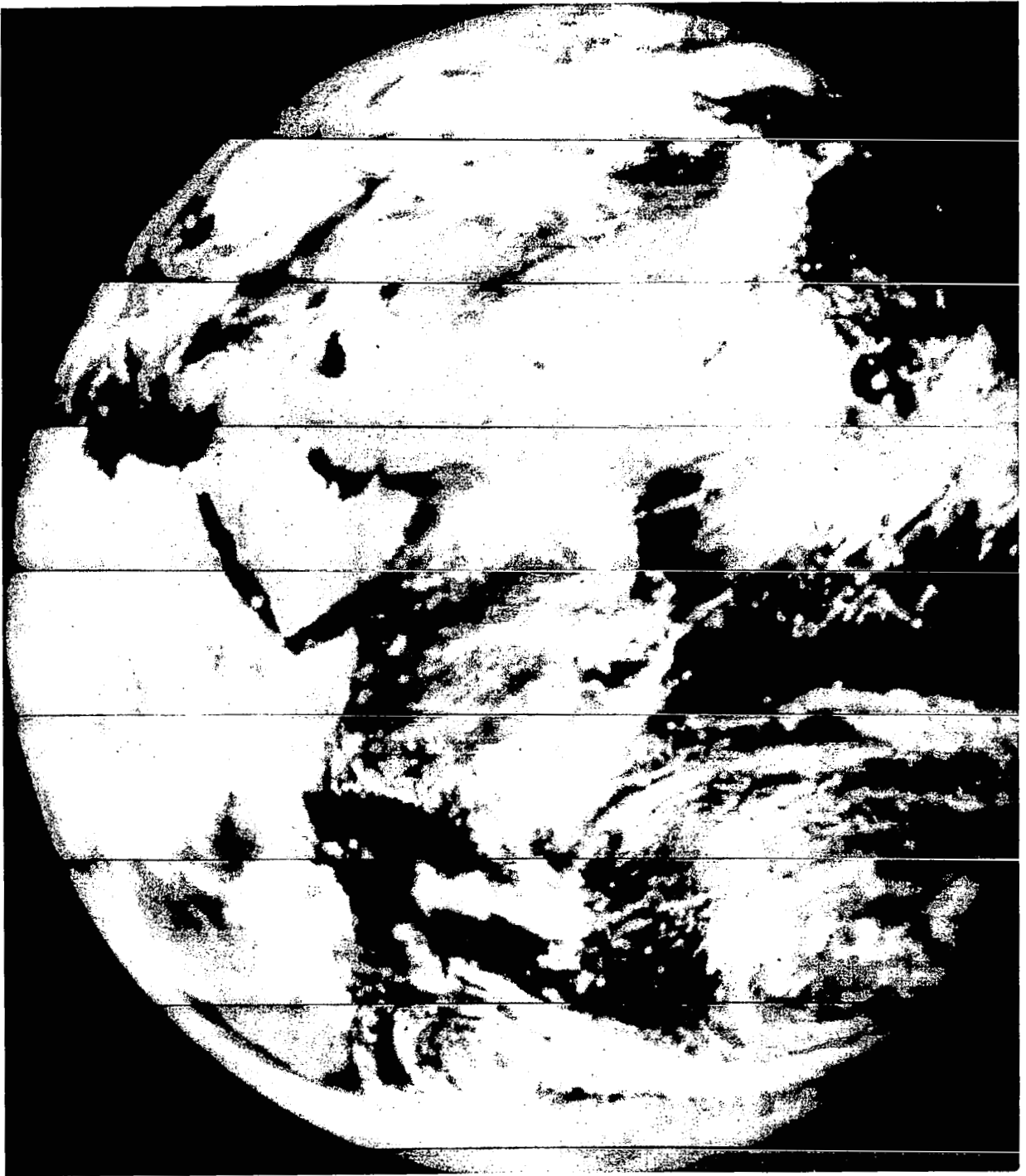


Figure 4-120: Site VA-9, Earth Photo Geometry

though the true terminator lies at about  $135^{\circ}$ E longitude, exposure limitations cause it to appear further west.

The photograph provides a graphic illustration of possibilities for worldwide synoptic weather observation from the Moon or cislunar space.



**Figure 4-121: Site VA-9, Earth**



**Figure 4-122: Location Diagram for Earth Photograph**



## 5.0 Photographic Supporting Data

Interpretation and use of the photographs from Mission V for scientific and engineering purposes of either qualitative or quantitative nature require specific information regarding the photographic parameters, including spacecraft location, orientation, altitude, and velocity at the time of exposure. Computer programs have been developed that combine prediction requirements for mission control with postmission data requirements to provide the necessary information.

The basic information concerning each photograph is summarized in tabular form. A discussion of data accuracies is presented to assist the user in his studies, interpretations, and applications of the photographs. More complete and detailed data will be found in *Postmission Photo Supporting Data* for Mission V (to be published), which contains reproductions of the pertinent computer program data printouts, and appropriate explanatory information.

### 5.1 INPUT DATA SUMMARY

Data used in computing the tables of photographic supporting data were obtained primarily from the times of exposure as recorded on the photographic film, postflight analysis of doppler tracking, and postmission evaluation of spacecraft attitude.

#### 5.1.1 Spacecraft Position and Velocity

Spacecraft position and velocity are defined by the state vector at the time of the photographic exposure. The state vector, in selenocentric coordinates, for each photographic sequence was obtained by processing tracking-data arcs that encompass the actual time of exposure. This state vector was computed at the epoch time stated in the orbit determination report. Integration of the vector to within 8 minutes before the exposure time was based on the Langley Research Center lunar harmonics dated July 28, 1967, as modified by the harmonics solved for in the orbit determination computations. The Langley Research Center lunar harmonics, dated November 11, 1966, were used to integrate the state vector in the EVAL computer

program. This method provided accurate spacecraft position and velocity input data for computation of the photo supporting data.

#### 5.1.2 Spacecraft Attitude

Spacecraft attitude, and thus location of the principal point and corners of the photographs, their orientation, and photographic geometry are derived from the attitude maneuvers executed from a known attitude reference. The relative position of photo site coordinates with respect to the lunar orbit, and orientation of spacecraft axes with respect to the celestial references are the basis for the designed photo maneuvers. Spacecraft maneuver control was based on the concept of a Sun-Canopus-spacecraft attitude update during each orbit. The roll axis was accurately established by open-loop tracking of Canopus and noting the error signal for attitude computation. Known spacecraft attitude drift rates and biases were added to the design maneuver during computation of the maneuver commands to point the camera axis at the desired target position at the commanded time for the photographs. During the photographic sequences, the flight control limit cycle was selected to maintain the spacecraft attitude within  $\pm 0.2$  degree of the commanded value. Since there were no indications of significant deviation of actual from commanded maneuvers, use of the commanded values for the supporting data computations is considered valid.

#### 5.1.3 Camera-On Time

Time of exposure of each photographic frame was obtained from the binary time code exposed on the film simultaneously with the actuation of the 80-mm (wide-angle) shutter. The focal-plane shutter for the telephoto lens was actuated a nominal 40 milliseconds before the 80-mm shutter. In one case, Frame 217 (where processing ended), the time code was not obtained; thus, the actual time of exposure was not available. For that frame, the exposure time was derived by biasing from the commanded time an amount determined from a comparison of actual and commanded times for other frames in the sequence.



Actual time of exposure as used in computations is listed in the tabulation of data.

#### 5.1.4 Planetary Constants

Planetary data influencing the spacecraft orbit were taken from a magnetic tape ephemeris provided by the Jet Propulsion Laboratory. The ephemeris contained the most recently established positions and velocities of the Sun, planets, and the Moon. These include refined estimates of the planetary gravitational relationships and Eckert's corrections to the lunar ephemeris. To satisfy the Earth-Moon constraint equation that relates the gravitational constants of each body, the radius of the Earth, and sine parallax, new values were used by EVAL to scale the ephemeris properly.

The lunar gravitational field is represented by an expansion of spherical harmonics. Two sets of harmonic coefficients were obtained from the NASA Langley Research Center by correspondence dated November 11, 1966, and July 28, 1967. The sets of coefficients are designated as LRC 11/11 and LRC 7/28 harmonics, respectively.

### 5.2 COMPUTATIONAL PROCEDURE

Computational procedures used in preparing the photo supporting data resemble, in some respects, operational procedures during the mission. There are significant differences, however, and the two should not be confused.

Procedures used in computing the photo supporting data were based on determining the state vector to within 8 minutes prior to camera-on time. The state vector was integrated ahead from this initial condition to the actual time of exposure, with the spacecraft oriented to the celestial reference. Using the state vectors computed for the actual camera-on time, spacecraft axes were rotated by the design maneuver magnitudes corrected for spacecraft characteristics, and the supporting data computations made. Each successive frame in a multiframe sequence was computed in a similar manner.

### 5.3 ACCURACY OF CALCULATIONS

The accuracy of data presented in the tabulation of photographic supporting data, Table 5-4, has been estimated by performing a simplified error analysis using typical photographic and orbital parameters, and the best estimates of errors in the flight hardware. For simplification, the study was confined to an investigation of uncertainties in photo location and spacecraft altitude for locations typical for sites photographed from the three orbital ellipses. A near-nadir camera pointing direction has been assumed, and oblique photography has not been included in the analysis.

The analysis considered the following four cases to represent the wide range of site locations and photographic parameters.

- Case I – initial and intermediate ellipses; true anomaly = 135 degrees.
- Case II – final ellipse; true anomaly = 0 degrees.
- Case III – final ellipse; true anomaly = 45 degrees.
- Case IV – final ellipse; true anomaly = 135 degrees.

#### 5.3.1 Error Sources

There is some uncertainty in the exact value of each primary input to the photo evaluation (EVAL) program. These include attitude maneuvers, time of photography, and state vector; each contributes to the total uncertainty or error in the photograph parameters. The following discussion identifies the various factors and their relationship to the uncertainty in longitude and latitude of the photo centers (principal points) and corners, and in spacecraft altitude.

##### 5.3.1.1 Timing Errors

After the time-code data is corrected for spacecraft clock errors and converted to GMT, an uncertainty of 0.1 second, corresponding to the time resolution of the coding, still exists. An additional 0.04-second error exists for the telephoto frame, since the time code lights are

activated by operation of the wide-angle shutter, and the focal-plane shutter is 40 milliseconds earlier. In some cases, frame times were further manually rounded off to the nearest 0.1 second, introducing an additional  $\pm 0.5$  second of error, giving an RSS total of 0.119 second for the telephoto frames and 0.112 second for the wide-angle frame. The probability density of the timing error tends to be uniform, so that the standard deviation is 0.577 times the maximum value, giving the 1-sigma values:

$$\sigma_t(\text{telephoto}) = 0.0687 \text{ second}$$

$$\sigma_t(\text{wide angle}) = 0.0645 \text{ second}$$

Due to the second-order nature of the difference in timing error, the telephoto value will be used and denoted by  $\sigma_{t^\circ}$ .

Values for the horizontal velocity ( $v_h$ ) for each of the four cases considered are:

Case I	$v_h = 0.750 \text{ km/sec}$
Case II	$v_h = 1.85 \text{ km/sec}$
Case III	$v_h = 1.74 \text{ km/sec}$
Case IV	$v_h = 1.17 \text{ km/sec}$

The downrange distance error is obtained by:

$$\text{error} = (v_h) (\sigma_{t^\circ})$$

and for the four cases amounts to:

Case I	0.0515 km
Case II	0.127 km
Case III	0.120 km
Case IV	0.0804 km

The downrange distance error can be converted into degrees of latitude and longitude on the lunar surface by considering the orbital inclination of 85 degrees and the altitude of each case.

$$\sigma_{\text{long}} = \frac{(\text{downrange distance error})}{[R_m / (R_m + h)] (\cos i)} (\text{deg}/30.3 \text{ km})$$

$$\sigma_{\text{lat}} = \frac{(\text{downrange distance error})}{[R_m / (R_m + h)] (\sin i)} (\text{deg}/30.3 \text{ km})$$

where  $R_m$  is the lunar radius,  $h$  is the spacecraft altitude, and  $i$  is the orbit inclination. The factor (deg/30.3 km) relates surface distance in kilometers to angular distance (deg/km).

The errors so obtained are tabulated below.

Case	Altitude (km)	$\sigma_{\text{long}}$ (deg)	$\sigma_{\text{lat}}$ (deg)
I	3,662	0.0000476	0.000545
II	100	0.000346	0.00396
III	202	0.000310	0.00354
IV	1,172	0.000138	0.00158

Uncertainty of the exact photo time contributes to uncertainty in the altitude of photography. Altitude rates ( $\dot{h}$ ) and corresponding altitude uncertainties for each case are:

Case	$\dot{h}$ (km/sec)	$\sigma_h$ (km)
I	0.555	0.0382
II	0.0	0.00687 (using 0.1 km/sec)
III	0.282	0.0194
IV	0.282	0.0194

where  $\sigma_h = (\dot{h}) (\sigma_{t^\circ})$ .

### 5.3.1.2 Attitude Maneuver Errors

Experience has shown that the limit cycle and camera-to-spacecraft misalignment errors are by far the largest contributors to attitude error in each axis. For this reason, it is possible to use a single roll, pitch, and yaw maneuver in computing the contributions of celestial sensors and gyros to the maneuver error. The approximate maneuvers are:

Case Roll (deg) Pitch (deg) Yaw (deg)

I	60	180	0
II	0	0	-85
III	-45	0	-85
IV	50	160	0

For analytical purposes, the composite maneuver applicable to all cases was considered to be, in all cases: roll = 45 degrees, pitch = 100 degrees, and yaw = 60 degrees. Noting that celestial updating is performed for each target site, the initial condition errors may be listed as shown in Table 5-1. The photo maneuver errors are listed in Table 5-2.

**Table 5-1: Initial Condition Errors**

Item	3 $\sigma$ Error (deg)		
	Roll	Pitch	Yaw
Alignment of Canopus tracker null	0.075	0	0
Alignment of Sun sensor null	0	0.017	0.017
Alignment of Sun sensor mirror	0	0.017	0.017
Alignment of IRU	0.02	0.02	0.02
Sun sensor null shift	0	0.006	0.006
Limit cycle error	<u>0.220</u>	<u>0.220</u>	<u>0.220</u>
RSS subtotal	0.234	0.224	0.224

**Table 5-2: Photo Maneuver Errors**

Item	Roll	Pitch	Yaw
Initial condition error	0.234	0.224	0.224
Gyro drift (rate integrating mode)	0.080	0.080	0.080
Gyro error (rate mode)	0.045	0.100	0.070
Gyro resolution error	0.025	0.025	0.025
Voltage/frequency converter error (%)	0.120	0.300	0.180
Voltage/frequency converter error (resoltuion)	0.011	0.011	0.011
Cross-axis drift	0.081	0.050	0.077
Gyro nonorthogonality	0.150	0.310	0.190
Limit cycle error for maneuver	0.220	0.220	0.220
Camera-to-spacecraft misalignment	<u>0.300</u>	<u>0.300</u>	<u>0.300</u>
RSS totals      3 $\sigma$	0.500	0.630	0.530
1 $\sigma$ *	0.222	0.256	0.232
* 1 $\sigma$ =[(0.577) (limit cycle and resolution errors)] due to uniform distribution.			

A value of 0.24 degree can be used as the 1-sigma error for each axis within the accuracy of the analysis. Since these errors are statistically independent, the same value applies to errors described in camera roll, pitch, and crab coordinates, or

$$\sigma_r = 0.24 \text{ deg}, \sigma_p = 0.24 \text{ deg}, \text{ and } \sigma_c = 0.24 \text{ deg}$$

The  $\sigma_r$  error results in a cross-frame positioning error and the  $\sigma_p$  in an along-frame positioning error. These cross- and along-frame errors are rotated through the 85-degree inclination angle into latitude-longitude errors. Since again the roll and pitch errors are statistically independent, the errors in the latitude and longitude directions are also 0.24 degree, giving the following errors.

$$\begin{aligned} \text{Case I} \quad \sigma_{\text{long}} &= \sigma_{\text{lat}} = 0.506 \text{ deg} \\ &= [0.24 \text{ deg}/57.3 \times h \times 1/(30.3 \text{ deg/km})] \end{aligned}$$

$$\text{Case II} \quad \sigma_{\text{long}} = \sigma_{\text{lat}} = 0.0138 \text{ deg}$$

$$\text{Case III} \quad \sigma_{\text{long}} = \sigma_{\text{lat}} = 0.0280 \text{ deg}$$

$$\text{Case IV} \quad \sigma_{\text{long}} = \sigma_{\text{lat}} = 0.162 \text{ deg}$$

### 5.3.1.3 Uncertainty in State Vectors

Accuracy of the state vectors must be considered with the uncertainties in camera attitude. Based on postflight analysis of the tracking data over a data arc encompassing the camera-on time, typical uncertainties in the state vector are theoretically within 500 meters (1 sigma) for Cases II, III, and IV. This figure is only slightly pessimistic for Case I, where higher spacecraft altitude results for representative targets. Taking this error on each axis in selenographic coordinates (of lunar arrival date), assuming statistical independence, and rotating this Cartesian matrix through the Eulerian angles of: angle of the line of ascending node, inclination, and true anomaly (plus argument of perilune), the same uncertainty (500 meters) results in roll, pitch, and crab coordinates. The resulting uncertainties in the latitude and longitude directions are:

$$\begin{aligned} \text{Case I} \quad \sigma_{\text{long}} &= \sigma_{\text{lat}} = 0.500 \text{ km} \\ &[R_m / (R_m + h)] (1/30.3 \text{ deg/km}) \\ &= 0.0053 \text{ deg} \end{aligned}$$

$$\text{Case II} \quad \sigma_{\text{long}} = \sigma_{\text{lat}} = 0.0156 \text{ deg}$$

$$\text{Case III} \quad \sigma_{\text{long}} = \sigma_{\text{lat}} = 0.0148 \text{ deg}$$

$$\text{Case IV} \quad \sigma_{\text{long}} = \sigma_{\text{lat}} = 0.00985 \text{ deg}$$

The spacecraft altitude uncertainty,  $\sigma_h$  = 0.500 km.

### 5.3.1.4 Uncertainty in Site Elevation

For the near-nadir camera axis intersects considered in this study, site-elevation uncertainty has no noticeable effect on location of the photo centers. However, location of the photo corners is directly dependent on site elevation; this relationship was investigated for both the telephoto and wide-angle fields of view. The uncertainty in mean Moon radius, giving rise to the error in photo corners, is known to within about 1 kilometer (1 sigma).

**Telephoto lens** — The telephoto field of view is 20.36 degrees in the cross-range direction and 5.17 degrees in the downrange direction. Standard deviations of the photo corners in longitude and latitude, in terms of inclination angle  $i$  and downrange and cross-range standard deviations  $\sigma_d = (\sigma R_m \tan 5.17 \text{ deg}/2)$  and  $\sigma_c$

$= (\sigma R_m \tan 20.36 \text{ deg}/2)$ , respectively, resulting

from  $\sigma R_m$  are:

$$\sigma_{\text{long}} = \left( \sqrt{\sigma_d^2 \cos^2 i + \sigma_c^2 \sin^2 i + 2\sigma_{dc}^2 \sin i \cos i} \right) (1 \text{ deg}/30.3 \text{ km})$$

$$\sigma_{\text{lat}} = \left( \sqrt{\sigma_d^2 \sin^2 i + \sigma_c^2 \cos^2 i - 2\sigma_{dc}^2 \sin i \cos i} \right) (1 \text{ deg}/30.3 \text{ km})$$

where:

$$\begin{aligned} \sigma_{dc}^2 &= E(dc) = E(\Delta R_m \tan 5.17 \text{ deg}/2) \\ &\quad (\Delta R_m \tan 20.36 \text{ deg}/2) \\ &= \sigma R_m^2 (0.0454)(0.177) \\ &= \sigma R_m^2 (0.00803). \end{aligned}$$

The results for the telephoto lens are:

Case I  $\sigma_{\text{long}} = 0.00595 \text{ deg}$ ,  $\sigma_{\text{lat}} = 0.000984 \text{ deg}$

Case II  $\sigma_{\text{long}} = 0.00595 \text{ deg}$ ,  $\sigma_{\text{lat}} = 0.000984 \text{ deg}$

Case III  $\sigma_{\text{long}} = 0.00595 \text{ deg}$ ,  $\sigma_{\text{lat}} = 0.000984 \text{ deg}$

Case IV  $\sigma_{\text{long}} = 0.00595 \text{ deg}$ ,  $\sigma_{\text{lat}} = 0.000984 \text{ deg}$

*Wide-angle lens* -- The wide-angle-lens field of view is 37.93 degrees downrange by 44.24 degrees crossrange. Proceeding in the same manner, but changing

$$\sigma_d = (\sigma_{R_m} \tan 37.92 \text{ deg}/2)$$

$$\sigma_c = (\sigma_{R_m} \tan 44.24 \text{ deg}/2)$$

$$\begin{aligned} \sigma_{dc}^2 &= (\sigma_{R_m}^2 \tan 37.92 \text{ deg} \tan 44.24 \text{ deg})/2 \\ &= \sigma_{R_m}^2 (0.304)(0.406) \\ &= \sigma_{R_m}^2 (0.140) \end{aligned}$$

the results are:

Case I  $\sigma_{\text{long}} = 0.0144 \text{ deg}$ ,  $\sigma_{\text{lat}} = 0.0102 \text{ deg}$

Case II  $\sigma_{\text{long}} = 0.0144 \text{ deg}$ ,  $\sigma_{\text{lat}} = 0.0102 \text{ deg}$

Case III  $\sigma_{\text{long}} = 0.0144 \text{ deg}$ ,  $\sigma_{\text{lat}} = 0.0102 \text{ deg}$

Case IV  $\sigma_{\text{long}} = 0.0144 \text{ deg}$ ,  $\sigma_{\text{lat}} = 0.0102 \text{ deg}$

### 5.3.2 Summation of Errors

Sources considered in this study contributing to uncertainty in photo locations and altitude are statistically independent, so that their effects may be RSS'd to obtain the total error; the only constraint is that site elevation uncertainty is assumed to contribute to error only in photo corners, not photo centers. The total error is given in Table 5-3.

It may be seen, from the preceding discussion, that the accuracy of locations of Lunar Orbiter photographs -- as a class -- cannot be stated

Table 5-3: Summation of Errors

	Errors					
	Photo Center		Photo Corners			
			Telephoto		Wide Angle	
	deg	km	deg	km	deg	km
Case I	0					
Longitude (deg)	0.506	15.4	0.506	15.4	0.506	15.4
Latitude (deg)	0.506	15.4	0.506	15.4	0.506	15.4
Altitude (km)	—	0.503	—	—	—	—
Case II						
Longitude (deg)	0.0205	0.633	0.0218	0.67	0.0254	0.77
Latitude (deg)	0.0213	0.645	0.0213	0.645	0.0236	0.715
Altitude (km)	—	0.500	—	—	—	—
Case III						
Longitude (deg)	0.0317	0.96	0.0323	0.98	0.0348	1.05
Latitude (deg)	0.0320	0.97	0.0320	0.97	0.0336	1.02
Altitude (km)	—	0.500	—	—	—	—
Case IV						
Longitude (deg)	0.162	4.9	0.162	4.9	0.163	4.95
Latitude (deg)	0.162	4.9	0.162	4.9	0.162	4.9
Altitude (km)	—	0.500	—	—	—	—

simply. Errors are dependent on a set of variable parameters specific to individual photographs or, in some cases, to a small group such as those comprising a multiple-frame sequence where changes in critical parameters during the sequence may be small.

As stated in the introduction to this section, the foregoing discussion has been limited to photography with a near-vertical camera axis. Appreciable tilt has been used in many photographs -- for oblique views, convergent telephoto stereo, and for special photography of specific targets. In these cases, critical parameters such as line-of-sight distance may vary appreciably within a single photograph. Consequently the accuracy of position of points within the photograph, relative to selenographic coordinates, also will vary. In addition, the uncertainties in selenographic coordinates relative to ground control points as established from Earth-based observation must be considered. Therefore, where positional accuracy is critical to use of the photographs, errors must be evaluated in terms of parameters specific to those photographs.

It is pertinent to include, also, a discussion of the correctness of the spacecraft position uncertainties used. The uncertainties are computed as covariance within the operation of the orbit determination program (ODPL). The covariance is derived from the manner in which the set of observed doppler frequencies fit calculated data (observed - calculated = residual). Only the noise, or scatter, in the residuals contribute to the covariance, so systematic trends in the fit do not affect the values calculated. Thus, the existence of unknowns (e.g. lunar gravitational model error) is not represented as enlarged uncertainty. As a result, the calculated covariances are unrealistically small (typically in the tenths of kilometers) and do not agree with observed discrepancies in photograph location (kilometers).

During Mission V, an empirical correction of -3 seconds was applied to commanded camera-on time in response to observed downrange photo location errors of about 6 kilometers in the early photographs. These were due to a fairly consistent bias in position prediction.

Postflight analysis has reduced most of these discrepancies to a few kilometers; however, the larger discrepancies still exist in certain cases.

The solution to these difficulties lies in a state-of-the-art improvement in the method of tracking-data processing. This effort is being made at present under a NASA contract.

## 5.4 PHOTOGRAPHIC DISTORTION

Photographic representation of the lunar surface is subject to certain distortions such that within any one photograph there is not a constant spatial or photometric relation between the image and the actual lunar surface photographed. There are three basic sources of such distortions:

- Characteristics of the camera and subsidiary systems necessary to production of the photograph in the form in which it is used on Earth;
- Camera attitude with reference to the object plane;
- Physical characteristics of the subject being photographed.

### 5.4.1 Photo System Distortions

Included in this group of possible distortions are those related to lens characteristics, the photo-video chain, GRE, and -- in the case of photographic prints -- reassembly technique and photographic printing control. With the exception of the reassembly process and print making, these distortions are inherent in the photo system and are independent of the type of mission or orbital parameters. They affect not only the relative spatial, but also the photometric, representation. Some of the distortions may be corrected on the basis of premission calibrations, and the pre-exposed reseau marks and edge data on the spacecraft film. These distortions have been discussed in *Lunar Orbiter I Final Report, NASA CR847*. The principal sources of distortion related to the photosub-system are:

- Camera lens radial and tangential distortion;
- Camera lens transmissivity variation off-axis;
- Image motion compensation (V/H sensor) error;
- Optical-mechanical scanner nonlinearity;
- Scanner image-density limitation;

- Film characteristics;
- Film instabilities;
- Line-scan tube focus;
- White-level variation;
- GRE;
- Reassembly.

While the above list may appear rather long, most of the above factors are of significance only to precise quantitative metric and photometric measurements to which at least some degree of correction can be made. The pre-exposed reseau marks permit the determination and correction of metrical distortions introduced subsequent to formation of the latent image on the spacecraft film. Thus all distortions — except camera lens distortions, image motion during exposure, and those related to photometric representation in the above list — are correctable on the basis of preflight calibrations.

#### 5.4.2 Geometric Distortions

The linear scale relationship between the photographic image and the lunar surface will be affected when the focal plane and the surface are not parallel. In such a case, the scale ratio will be variable within the frame, and the rectilinear coverage defined by the camera format will be distorted. This effect is most pronounced in highly oblique photographs. Where camera tilt is not extreme (less than 30 degrees off-vertical), these distortions ordinarily can be corrected by rectification techniques commonly employed in aerial photogrammetry when the camera attitude is known.

#### 5.4.3 Lunar Characteristics

Three principal factors related to Moon characteristics — spherical surface, unique photometric characteristic, and lack of atmosphere — affect the photographs.

The spherical surface introduces the problem of representing a curved surface on a plane. Curvature becomes a serious problem when photography is conducted from a high altitude and coverage extends over a wide range of latitude and longitude. This factor, then, is most serious for farside apolune photography. Further, it results in greater distortion in wide-angle photographs than in those of the telephoto lens,

which has a narrow field of view and thus less broad coverage. This problem can be complicated even more where the camera axis is not directed to the nadir and tilt is not along an axis of the format. Since this is a purely geometric distortion, it can be corrected by appropriate computations.

The photometric characteristic of the Moon results in a marked variation in surface luminance as a function of the illumination and observation geometry. While average luminance of an area can be predicted on the basis of the geometry designed for photography of a site, because of terrain roughness some areas within the field of view have a luminance either above or below system capability for recording (i.e., both over and under exposure can occur within a photograph).

Lack of an atmosphere makes high resolution in the photographs possible from high altitudes. No distortion due to atmospheric turbulence nor obscuration by haze occurs as they do in terrestrial photography. However, because of the lack of atmosphere and its associated light scattering, shadows are completely black and devoid of any detail. Low solar elevation, desirable for showing low surface relief, produces more extensive shadow and thus increased loss of data.

### 5.5 PHOTOGRAPHIC SUPPORTING DATA TABLES

The information presented in the table of supporting data included in this section has been extracted from the computer program EVAL-tabulated output. The complete tabulation is included as a part of a NASA publication, *Photo Supporting Data* (in preparation) in the form of computer printout reproductions. Data provided by the printout but not included in this volume are the selenographic coordinates of 44 points, defining the coverage of both telephoto and wide-angle photographs of each frame more completely than the location of the four corners given below. Additional photographic parameters and spacecraft flight parameters are also included.



The data in Table 5-4 are organized according to the site groups as presented in Section 4.0:

- Apollo sites;
- Science and AAP sites;
- Farside sites;
- Earth photograph.

Within each group, the data are listed by site number and frame number in the sequence

taken. Thus, the Mission V site numbers are not all in numerical sequence for the complete mission. A cross-index of Mission V photographs and photographic data is included in the final report, *Appendices*, NASA CR (to be published).

The terms of each line in the table are defined below. Those terms pertaining to geometric relationships are also illustrated in Figure 5-1.

## Definition of Terms

*Site number* -- Identification of the photographic site according to NASA designation. Mission (V), followed by number. Decimal indicates revision of location from original planned position. Letter "A" designates farside apolune photograph. Lower case letter following site number indicates multiple pass over site. An asterisk identifies the AAP sites. For example:

- V-18 Original planned coverage of Littrow
- V-5.1 Revised coverage of Messier
- V-16a First-pass coverage of Apollo Site IIP-6
- VA-5 Apolune farside photograph
- V-14\* AAP site

*Frame number* -- Sequential order of exposure. Actual photography began with Frame 5. Includes both simultaneous telephoto and wide-angle photographs.

*Altitude* -- Distance, in kilometers, of the spacecraft above the mean lunar radius (1,738.09 km).

*Latitude (longitude)* -- Latitude (longitude) of the spacecraft nadir point, in selenographic coordinates at time of exposure.

*Tilt angle* -- Angle between camera axis and spacecraft nadir line.

*Tilt azimuth* -- Angle, measured clockwise at the nadir point, from north to the line between nadir and principal point.

*Swing angle* -- Angle between the cross-axis of film frame (long, or Y' axis) and a line from nadir point to principal point. Measured clockwise from Y' axis.

*North deviation* -- Angle, measured clockwise at nadir, between north and Y' axis.

*Time of exposure* -- Actual GMT of exposure as derived from the time code exposed on the film.

*Sun azimuth* -- Horizontal angle (azimuth) of the Sun's rays measured clockwise from north at principal point.

*Incident angle* -- Angle between the Sun's rays and surface normal at principal point. Assumes level surface.

*Emission angle* -- Angle between camera axis and surface normal at principal point. Assumes level surface.

*Phase angle* -- Angle between camera axis and the Sun's rays.

*Alpha* -- Angle between projection of the surface normal into the phase angle plane, and camera axis. Alpha is positive in value when camera axis is between surface normal and the Sun's rays, and negative when surface normal is between camera axis and the Sun's rays.

*Albedo* -- Reflectance of lunar surface when both line-of-sight and illumination are precisely normal to the surface. The albedo listed is the corrected value as used in QUAL computations for selecting shutter speed (see Section 6.3.1).

*Shutter speed* -- Nominal duration of time the shutters are open for exposing the film. Expressed as a decimal fraction of a second.

*Scale factor* -- Ratio of lens focal length to slant distance to ground principal point. Ratio of a unit measure on the spacecraft film image to the same unit measure on the ground at principal point.

*Tilt distance* -- Distance, in millimeters, measured on the spacecraft film image or focal plane, between principal point and position of nadir. Distance is given whether or not the nadir point image is included within the format.

*Principal point* -- Location of camera axis intersection with the surface of the mean lunar sphere of 1,738.09-kilometer radius. Location given in selenographic coordinates. (Referenced to photographs: intersection of camera axis and focal plane).

*Slant distance* -- Distance, in kilometers, from spacecraft camera to ground principal point.  
*Corner coordinates* -- Selenographic coordinates of the corners of ground coverage by each photograph. (Because of surface curvature and

camera tilt, the corners may not exactly define coverage. More precise definition of coverage is provided by additional edge-point coordinates listed in the EVAL computation printout included in Volume VII of the final report.)

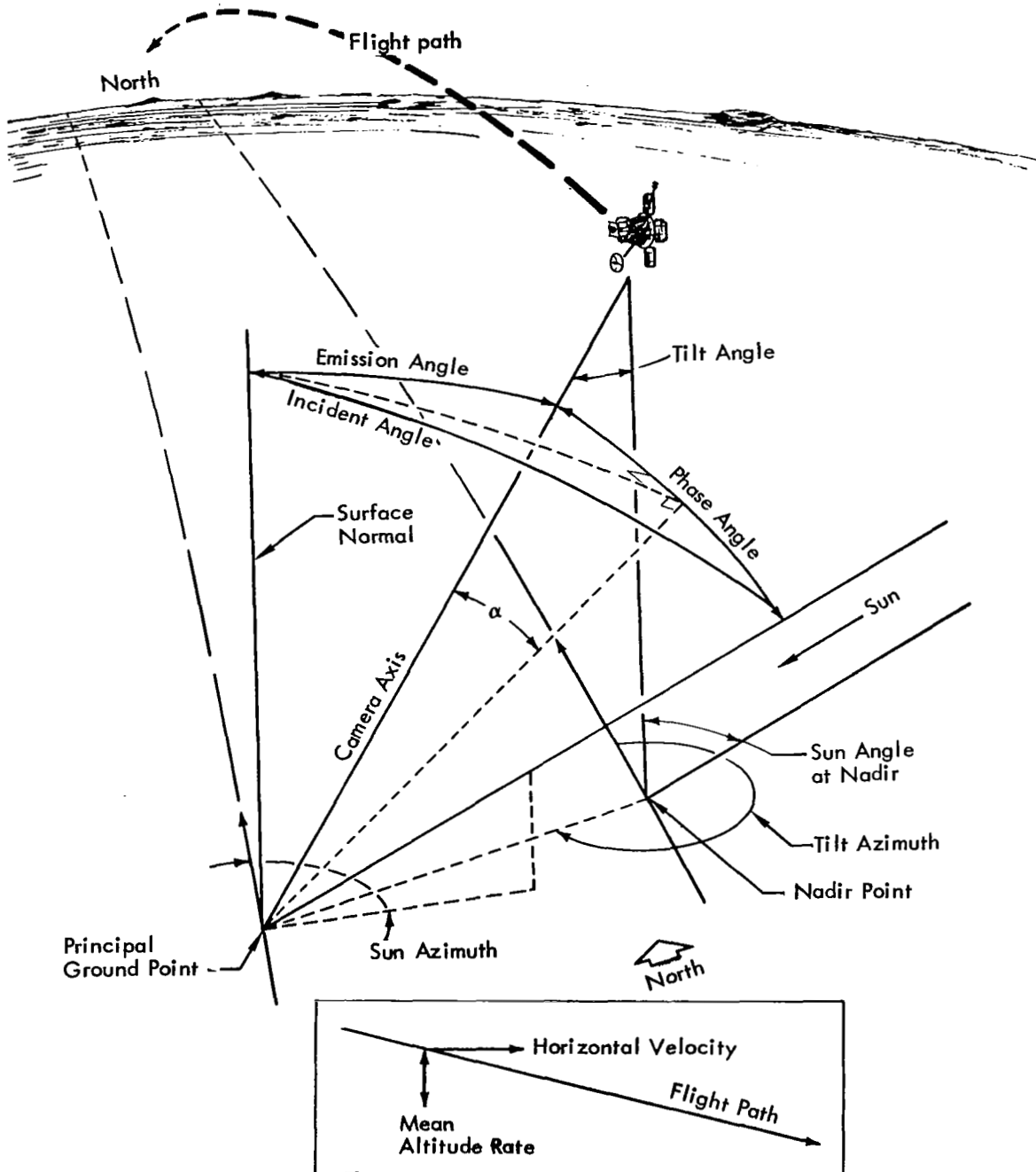


Figure 5-1: Geometry of Photographic Parameters



**Table 5-4**

**Photographic**

**Supporting Data**

LINE	SITE NUMBER	V-3.1	V-6	V-8a			
	FRAME NUMBER	38	42	44	45	46	47
	EXPOSURE TIME (GMT)						
1	Day: Hour	222:09	222:22	223:08	223:08	223:08	223:08
2	Minute: Second	49:36.3	34:08.6	07:25.5	07:28.8	07:33.2	07:37.4
	S/C POSITION						
3	Altitude (km)	98	97	97	97	97	97
4	Altitude Rate (m/sec)	-16	-16	-18	-16	-14	-13
5	Latitude (deg)	-0.99	-0.96	-1.39	-1.20	-0.94	-0.70
6	Longitude (deg)	55.51	48.47	43.17	43.19	43.21	43.23
	S/C ORIENTATION						
7	Tilt Angle (deg)	59.23	50.74	4.47	4.45	4.44	4.43
8	Tilt Azimuth (deg)	270.20	269.71	267.44	269.86	273.12	276.24
9	Swing Angle (deg)	177.35	176.23	172.40	174.83	178.10	181.23
10	North Deviation (deg)	87.22	86.36	84.94	84.96	84.98	85.00
	PHOTOGRAPHY						
	ILLUMINATION						
11	Sun Azimuth (deg)	88.19	88.16	87.90	87.98	88.08	88.18
12	Incident Angle (deg)	73.47	72.17	68.76	68.73	68.70	68.67
13	Emission Angle (deg)	65.18	54.85	4.72	4.70	4.68	4.68
14	Phase Angle (deg)	8.52	17.38	64.04	64.04	64.04	64.04
15	Alpha (deg)	64.54	54.74	4.72	4.70	4.66	4.63
16	QUAL Albedo	0.075	0.075	0.075	0.075	0.075	0.075
17	Shutter Speed (sec)	0.01	0.01	0.02	0.02	0.02	0.02
	PHOTOGRAPHS						
	TELEPHOTO						
	CORNER COORD. (deg)						
18	A: Latitude	-0.27	-0.58	-1.20	-1.00	-0.73	-0.48
19	A: Longitude	43.62	42.10	42.35	42.36	42.39	42.41
20	B: Latitude	-0.79	-0.83	-1.31	-1.11	-0.84	-0.58
21	B: Longitude	51.65	45.68	43.50	43.52	43.54	43.56
22	C: Latitude	-1.25	-1.21	-1.59	-1.39	-1.12	-0.87
23	C: Longitude	51.61	45.65	43.48	43.49	43.51	43.54
24	D: Latitude	-1.40	-1.23	-1.49	-1.29	-1.03	-0.77
25	D: Longitude	43.28	41.99	42.32	42.34	42.36	42.38
26	Scale Factor ( $\times 10^6$ )	2.90	3.79	6.26	6.27	6.27	6.27
27	Tilt Distance (mm)	1024.37	746.39	47.71	47.49	47.32	47.30
	WIDE ANGLE						
	CORNER COORD. (deg)						
28	A: Latitude	4.85	4.61	-0.14	0.06	0.33	0.59
29	A: Longitude	39.71	33.02	41.66	41.68	41.70	41.72
30	B: Latitude	0.24	0.10	-0.44	-0.24	0.03	0.28
31	B: Longitude	53.09	46.77	44.28	44.30	44.32	44.34
32	C: Latitude	-2.40	-2.26	-2.59	-2.38	-2.11	-1.86
33	C: Longitude	52.92	46.61	44.10	44.12	44.14	44.16
34	D: Latitude	-6.80	-6.08	-2.43	-2.23	-1.96	-1.70
35	D: Longitude	38.23	32.43	41.45	41.47	41.49	41.52
36	Scale Factor ( $\times 10^6$ )	0.38	0.50	0.82	0.82	0.82	0.82
37	Tilt Distance (mm)	134.34	97.89	6.26	6.23	6.21	6.20
	PRINCIPAL POINT						
38	Latitude (deg)	-0.97	-0.98	-1.40	-1.20	-0.93	-0.68
39	Longitude (deg)	49.55	44.36	42.92	42.94	42.96	42.98
40	Slant Distance (km)	210	161	97	97	97	97

LINE	V-8b				V-9.1	V-11a			
	48	49	50	51	52	55	56	57	58
1	223:11	223:11	223:11	223:11	223:14	224:00	224:00	224:00	224:00
2	18:35.2	18:40.0	18:45.0	18:49.8	30:52.2	04:00.2	04:04.7	04:09.1	04:13.6
3	97	97	97	97	97	96	96	96	96
4	-17	-15	-13	-11	12	7	9	11	12
5	-1.27	-0.99	-0.70	-0.43	2.88	2.12	2.38	2.64	2.90
6	41.42	41.44	41.47	41.49	40.00	34.66	34.68	34.70	34.73
7	24.94	24.93	24.93	24.93	51.40	8.05	8.05	8.05	8.06
8	96.37	95.76	95.14	94.55	270.40	272.70	274.54	276.34	278.18
9	1.59	0.93	0.25	359.59	177.61	177.81	179.67	181.48	183.34
10	85.92	85.79	85.66	85.53	87.50	85.16	85.19	85.23	85.27
11	87.82	87.94	88.07	88.19	89.39	89.27	89.37	89.47	89.58
12	67.15	67.12	67.08	67.05	72.51	69.26	69.23	69.20	69.18
13	26.43	26.43	26.42	26.42	55.58	8.50	8.49	8.50	8.51
14	93.33	93.33	93.33	93.33	16.94	60.77	60.77	60.77	60.77
15	-26.22	-26.25	-26.28	-26.31	55.56	8.48	8.45	8.43	8.40
16	0.075	0.075	0.075	0.075	0.079	0.079	0.079	0.079	0.079
17	0.04	0.04	0.04	0.04	0.01	0.02	0.02	0.02	0.02
18	-1.23	-0.94	-0.63	-0.34	3.29	2.34	2.62	2.88	3.16
19	42.27	42.29	42.32	42.34	33.43	33.63	33.65	33.67	33.69
20	-1.32	-1.03	-0.73	-0.44	3.06	2.24	2.51	2.78	3.05
21	43.70	43.72	43.75	43.77	37.15	34.79	34.81	34.83	34.86
22	-1.67	-1.38	-1.08	-0.79	2.67	1.96	2.23	2.50	2.77
23	43.67	43.70	43.72	43.74	37.13	34.77	34.79	34.81	34.83
24	-1.52	-1.23	-0.93	-0.64	2.63	2.05	2.32	2.59	2.86
25	42.24	42.27	42.29	42.32	33.35	33.61	33.63	33.65	33.67
26	5.67	5.68	5.68	5.68	3.76	6.28	6.28	6.28	6.28
27	283.67	283.59	283.56	283.57	764.19	86.28	86.22	86.25	86.37
28	-0.30	-0.01	0.29	0.59	8.53	3.44	3.72	3.99	4.26
29	41.66	41.68	41.71	41.73	24.00	32.90	32.92	32.94	32.96
30	-0.07	0.23	0.53	0.83	3.99	3.08	3.35	3.62	3.90
31	45.09	45.12	45.16	45.19	38.24	35.54	35.57	35.59	35.62
32	-3.17	-2.87	-2.56	-2.27	1.64	1.00	1.27	1.54	1.81
33	44.87	44.89	44.90	44.91	38.12	35.37	35.39	35.41	35.43
34	-2.34	-2.04	-1.74	-1.45	-2.42	1.09	1.36	1.63	1.90
35	41.48	41.51	41.54	41.56	23.73	32.70	32.72	32.75	32.77
36	0.74	0.74	0.74	0.75	0.49	0.82	0.82	0.82	0.82
37	37.20	37.19	37.19	37.19	100.22	11.32	11.31	11.31	11.33
38	-1.43	-1.14	-0.84	-0.54	2.90	2.15	2.42	2.69	2.96
39	42.91	42.93	42.95	42.98	35.81	34.21	34.24	34.26	34.28
40	108	107	107	107	162	97	97	97	97



LINE	SITE NUMBER	V-11b				V-13	V-16a
	FRAME NUMBER	59	60	61	62	64	71
	EXPOSURE TIME (GMT)						
1	Day: Hour	224:03	224:03	224:03	224:03	224:09	224:19
2	Minute: Second	15:08.8	15:13.6	15:18.4	15:23.3	36:53.4	10:02.3
	S/C POSITION						
3	Altitude (km)	96	96	96	96	96	96
4	Altitude Rate (m/sec)	8	10	12	14	-3	-7
5	Latitude (deg)	2.26	2.53	2.81	3.09	0.70	0.32
6	Longitude (deg)	32.93	32.95	32.97	32.99	29.29	24.01
	S/C ORIENTATION						
7	Tilt Angle (deg)	22.56	22.56	22.56	22.57	50.98	3.32
8	Tilt Azimuth (deg)	95.65	94.98	94.32	93.64	269.99	266.59
9	Swing Angle (deg)	0.77	0.05	359.32	358.59	176.95	171.92
10	North Deviation (deg)	85.56	85.44	85.32	85.20	86.98	85.33
	PHOTOGRAPHY						
	ILLUMINATION						
11	Sun Azimuth (deg)	89.31	89.43	89.55	89.68	88.70	88.58
12	Incident Angle (deg)	67.61	67.58	67.55	67.52	73.41	69.95
13	Emission Angle (deg)	23.89	23.88	23.89	23.89	55.05	3.50
14	Phase Angle (deg)	91.36	91.36	91.36	91.36	18.39	66.45
15	Alpha (deg)	-23.77	-23.80	-23.82	-23.85	54.99	3.50
16	QUAL Albedo	0.079	0.079	0.079	0.079	0.075	0.075
17	Shutter Speed (sec)	0.04	0.04	0.04	0.04	0.01	0.02
	PHOTOGRAPHS						
	TELEPHOTO						
	CORNER COORD. (deg)						
18	A: Latitude	2.33	2.62	2.91	3.21	1.08	0.50
19	A: Longitude	33.63	33.65	33.68	33.70	22.95	23.27
20	B: Latitude	2.23	2.52	2.81	3.11	0.85	0.40
21	B: Longitude	34.99	35.02	35.04	35.07	26.52	24.40
22	C: Latitude	1.90	2.19	2.48	2.77	0.47	0.12
23	C: Longitude	34.96	34.99	35.01	35.04	26.50	24.38
24	D: Latitude	2.04	2.33	2.62	2.92	0.44	0.21
25	D: Longitude	33.61	33.63	33.65	33.68	22.87	23.24
26	Scale Factor ( $\times 10^6$ )	5.84	5.83	5.84	5.83	3.84	6.36
27	Tilt Distance (mm)	253.48	253.44	253.45	253.51	752.68	35.37
	WIDE ANGLE						
	CORNER COORD. (deg)						
28	A: Latitude	3.24	3.54	3.83	4.13	6.03	1.53
29	A: Longitude	33.04	33.06	33.08	33.11	13.55	22.60
30	B: Latitude	3.42	3.71	4.01	4.31	1.77	1.27
31	B: Longitude	36.28	36.31	36.35	36.38	27.60	25.17
32	C: Latitude	0.49	0.79	1.08	1.39	-0.55	-0.86
33	C: Longitude	36.03	36.05	36.07	36.09	27.46	25.01
34	D: Latitude	1.23	1.53	1.82	2.12	-4.85	-0.70
35	D: Longitude	32.86	32.89	32.91	32.93	12.03	22.41
36	Scale Factor ( $\times 10^6$ )	0.77	0.77	0.77	0.76	0.50	0.83
37	Tilt Distance (mm)	33.24	33.24	33.24	33.25	98.71	4.64
	PRINCIPAL POINT						
38	Latitude (deg)	2.13	2.42	2.71	3.01	0.70	0.31
39	Longitude (deg)	34.24	34.27	34.29	34.32	25.22	23.83
40	Slant Distance (km)	104	104	105	105	159	96

LINE	V-16a			V-16b				V-27a	
	72	73	74	75	76	77	78	108	109
1	224:19	224:19	224:19	224:22	224:22	224:22	224:22	226:15	226:15
2	10:06.7	10:11.1	10:15.5	21:09.1	21:13.9	21:18.8	21:23.8	44:46.0	44:50.5
3	96	96	96	96	96	96	96	97	97
4	-5	-3	-1	-6	-4	-2	0	-15	-13
5	0.57	0.83	1.08	0.46	0.73	1.01	1.30	-0.13	0.13
6	24.03	24.05	24.07	22.28	22.30	22.32	22.34	-0.53	-0.51
7	3.29	3.29	3.30	26.08	26.08	26.08	26.08	10.14	10.13
8	270.97	275.39	279.80	95.54	94.98	94.40	93.81	270.91	272.36
9	176.31	180.73	185.15	1.04	0.41	359.77	359.11	176.16	177.63
10	85.34	85.36	85.38	86.12	85.98	85.84	85.70	85.26	85.31
11	88.67	88.77	88.87	88.57	88.69	88.80	88.93	88.45	88.54
12	69.92	69.89	69.87	68.33	68.30	68.27	68.24	72.22	72.19
13	3.47	3.47	3.48	27.64	27.63	27.63	27.64	10.72	10.70
14	66.45	66.45	66.45	95.79	95.79	95.79	95.79	61.51	61.51
15	3.47	3.44	3.41	-27.49	-27.51	-27.54	-27.56	10.70	10.67
16	0.075	0.075	0.075	0.075	0.075	0.075	0.075	0.080	0.080
17	0.02	0.02	0.02	0.04	0.04	0.04	0.04	0.02	0.02
18	0.77	1.03	1.30	0.50	0.80	1.09	1.40	0.08	0.36
19	23.29	23.31	23.33	23.18	23.21	23.23	23.25	-1.71	-1.69
20	0.67	0.94	1.21	0.42	0.71	1.01	1.31	-0.03	0.25
21	24.42	24.44	24.47	24.63	24.65	24.68	24.70	-0.52	-0.50
22	0.39	0.66	0.92	0.07	0.36	0.65	0.96	-0.31	-0.04
23	24.40	24.42	24.44	24.60	24.63	24.65	24.67	-0.54	-0.52
24	0.48	0.75	1.01	0.21	0.50	0.80	1.11	-0.22	0.05
25	23.27	23.29	23.31	23.16	23.18	23.21	23.23	-1.74	-1.71
26	6.37	6.37	6.37	5.68	5.69	5.69	5.69	6.16	6.17
27	35.09	35.02	35.16	298.61	298.57	298.57	298.60	109.11	108.96
28	1.80	2.07	2.34	1.42	1.71	2.01	2.31	1.22	1.49
29	22.62	22.64	22.65	22.57	22.60	22.62	22.64	-2.47	-2.46
30	1.54	1.80	2.07	1.70	1.99	2.29	2.60	0.82	1.09
31	25.20	25.22	25.24	26.06	26.10	26.13	26.17	0.23	0.25
32	-0.59	-0.32	-0.05	-1.44	-1.15	-0.84	-0.54	-1.27	-1.00
33	25.03	25.04	25.06	25.84	25.85	25.87	25.88	0.07	0.09
34	-0.44	-0.17	0.10	-0.60	-0.30	-0.00	0.30	-1.23	-0.95
35	22.43	22.45	22.48	22.41	22.43	22.46	22.48	-2.70	-2.67
36	0.83	0.83	0.83	0.75	0.75	0.74	0.75	0.81	0.81
37	4.60	4.59	4.61	39.16	39.16	39.16	39.16	14.31	14.29
38	0.58	0.84	1.11	0.31	0.60	0.89	1.20	-0.12	0.15
39	23.85	23.87	23.89	23.82	23.85	23.87	23.89	-1.11	-1.08
40	96	96	96	107	107	107	107	99	99

LINE	SITE NUMBER	V-27a		V-27b			
	FRAME NUMBER	110	111	112	113	114	115
	EXPOSURE TIME (GMT)						
1	Day: Hour	226:15	226:15	226:18	226:18	226:18	226:18
2	Minute: Second	44:55.0	44:59.5	55:49.1	55:53.8	55:58.6	56:03.3
	S/C POSITION						
3	Altitude (km)	97	97	97	97	97	97
4	Altitude Rate (m/sec)	-11	-9	-14	-13	-11	-9
5	Latitude (deg)	0.39	0.65	-0.09	0.18	0.46	0.73
6	Longitude (deg)	-0.49	-0.47	-2.27	-2.25	-2.23	-2.21
	S/C ORIENTATION						
7	Tilt Angle (deg)	10.12	10.12	19.83	19.83	19.82	19.82
8	Tilt Azimuth (deg)	273.82	275.27	96.73	95.98	95.21	94.46
9	Swing Angle (deg)	179.10	180.58	2.28	1.49	0.67	359.87
10	North Deviation (deg)	85.36	85.41	86.00	85.90	85.80	85.69
	PHOTOGRAPHY						
	ILLUMINATION						
11	Sun Azimuth (deg)	88.63	88.72	88.40	88.50	88.60	88.70
12	Incident Angle (deg)	72.16	72.13	70.61	70.58	70.55	70.52
13	Emission Angle (deg)	10.69	10.69	21.00	20.99	20.98	20.98
14	Phase Angle (deg)	61.51	61.51	91.41	91.41	91.41	91.41
15	Alpha (deg)	10.64	10.61	-20.82	-20.84	-20.87	-20.90
16	QUAL Albedo	0.080	0.080	0.080	0.080	0.080	0.080
17	Shutter Speed (sec)	0.02	0.02	0.04	0.04	0.04	0.04
	PHOTOGRAPHS						
	TELEPHOTO						
	CORNER COORD. (deg)						
18	A: Latitude	0.63	0.90	-0.03	0.26	0.55	0.83
19	A: Longitude	-1.67	-1.64	-1.72	-1.70	-1.68	-1.65
20	B: Latitude	0.52	0.79	-0.11	0.17	0.46	0.75
21	B: Longitude	-0.48	-0.46	-0.40	-0.37	-0.35	-0.33
22	C: Latitude	0.24	0.51	-0.45	-0.16	0.13	0.42
23	C: Longitude	-0.50	-0.48	-0.42	-0.40	-0.38	-0.36
24	D: Latitude	0.32	0.60	-0.32	-0.03	0.26	0.54
25	D: Longitude	-1.69	-1.67	-1.74	-1.72	-1.70	-1.68
26	Scale Factor ( $\times 10^6$ )	6.17	6.17	5.86	5.87	5.87	5.87
27	Tilt Distance (mm)	108.88	108.88	220.03	219.93	219.88	219.87
	WIDE ANGLE						
	CORNER COORD. (deg)						
28	A: Latitude	1.77	2.04	0.90	1.19	1.48	1.76
29	A: Longitude	-2.44	-2.42	-2.32	-2.30	-2.28	-2.26
30	B: Latitude	1.37	1.64	1.04	1.32	1.62	1.90
31	B: Longitude	0.28	0.30	0.78	0.81	0.84	0.87
32	C: Latitude	-0.72	-0.45	-1.79	-1.50	-1.20	-0.91
33	C: Longitude	0.11	0.13	0.60	0.61	0.62	0.64
34	D: Latitude	-0.68	-0.40	-1.15	-0.86	-0.57	-0.28
35	D: Longitude	-2.64	-2.62	-2.49	-2.47	-2.44	-2.42
36	Scale Factor ( $\times 10^6$ )	0.81	0.81	0.77	0.77	0.77	0.77
37	Tilt Distance (mm)	14.28	14.28	28.86	28.84	28.84	28.83
	PRINCIPAL POINT						
38	Latitude (deg)	0.43	0.70	-0.22	0.06	0.35	0.64
39	Longitude (deg)	-1.06	-1.04	-1.12	-1.10	-1.07	-1.05
40	Slant Distance (km)	99	99	104	104	104	104

LINE	V-42a				V-42b				
	169	170	171	172	173	174	175	176	
1	229:07	229:07	229:07	229:07	229:10	229:10	229:10	229:10	
2	23:33.4	23:38.3	23:43.1	23:47.9	34:35.2	34:40.2	34:45.2	34:50.1	
3	104	104	103	103	104	103	103	103	
4	-45	-43	-41	-40	-44	-42	-40	-38	
5	-4.04	-3.76	-3.48	-3.21	-3.79	-3.50	-3.22	-2.94	
6	-35.83	-35.80	-35.78	-35.76	-37.57	-37.54	-37.52	-37.50	
7	7.65	7.62	7.59	7.57	18.00	17.99	17.98	17.98	
8	266.25	268.32	270.37	272.43	97.77	96.88	96.00	95.13	
9	171.47	173.57	175.63	177.71	3.49	2.56	1.63	0.72	
10	85.15	85.19	85.24	85.28	86.22	86.12	86.02	85.92	
11	87.45	87.52	87.60	87.67	87.36	87.45	87.54	87.62	
12	75.19	75.15	75.12	75.08	73.75	73.71	73.68	73.64	
13	8.11	8.07	8.04	8.03	19.11	19.10	19.09	19.08	
14	67.08	67.08	67.08	67.08	92.57	92.57	92.57	92.57	
15	8.11	8.07	8.03	8.00	-18.85	-18.88	-18.91	-18.94	
16	0.064	0.064	0.064	0.064	0.064	0.064	0.064	0.064	
17	0.04	0.04	0.04	0.04	0.04	0.04	0.04	0.04	
18	-3.85	-3.56	-3.27	-2.98	-3.74	-3.43	-3.13	-2.84	
19	-36.92	-36.89	-36.86	-36.84	-37.09	-37.07	-37.05	-37.02	
20	-3.96	-3.67	-3.38	-3.09	-3.82	-3.52	-3.22	-2.92	
21	-35.66	-35.64	-35.62	-35.59	-35.72	-35.70	-35.68	-35.65	
22	-4.27	-3.97	-3.68	-3.39	-4.17	-3.86	-3.56	-3.26	
23	-35.69	-35.67	-35.64	-35.62	-35.74	-35.72	-35.70	-35.68	
24	-4.17	-3.88	-3.59	-3.29	-4.04	-3.74	-3.44	-3.14	
25	-36.94	-36.92	-36.89	-36.86	-37.12	-37.09	-37.07	-37.04	
26	5.83	5.84	5.85	5.86	5.58	5.59	5.60	5.62	
27	81.97	81.57	81.28	81.11	198.20	198.05	197.96	197.92	
28	-2.68	-2.39	-2.10	-1.81	-2.75	-2.45	-2.15	-1.85	
29	-37.69	-37.66	-37.64	-37.61	-37.73	-37.71	-37.68	-37.66	
30	-3.06	-2.76	-2.47	-2.18	-2.63	-2.33	-2.03	-1.73	
31	-34.86	-34.83	-34.81	-34.79	-34.53	-34.51	-34.48	-34.46	
32	-5.31	-5.01	-4.72	-4.42	-5.55	-5.24	-4.93	-4.63	
33	-35.03	-35.01	-34.99	-34.97	-34.70	-34.69	-34.68	-34.67	
34	-5.21	-4.91	-4.62	-4.32	-4.93	-4.62	-4.32	-4.02	
35	-37.93	-37.90	-37.87	-37.83	-37.91	-37.88	-37.86	-37.83	
36	0.76	0.77	0.77	0.77	0.73	0.73	0.73	0.74	
37	10.75	10.70	10.66	10.64	25.99	25.97	25.96	25.96	
38	-4.07	-3.77	-3.48	-3.19	-3.94	-3.64	-3.33	-3.04	
39	-36.29	-36.26	-36.24	-36.21	-36.46	-36.44	-36.42	-36.39	
40	105	104	104	104	109	109	109	109	

## SCIENCE AND AAP

LINE	SITE NUMBER	V-1				V-2.1	V-4
	FRAME NUMBER	33	34	35	36	37	40
	EXPOSURE TIME (GMT)						
1	Day: Hour	221:20	221:20	221:20	221:20	222:03	222:12
2	Minute: Second	57:43.3	57:50.0	57:56.5	58:03.0	22:03.6	51:48.1
	S/C POSITION						
3	Altitude (km)	144	142	141	140	123	162
4	Altitude Rate (m/sec)	-183	-181	-179	-176	-139	-215
5	Latitude (deg)	-25.77	-25.41	-25.05	-24.69	-18.95	-30.96
6	Longitude (deg)	60.17	60.21	60.24	60.28	57.38	50.88
	S/C ORIENTATION						
7	Tilt Angle (deg)	5.60	5.38	5.18	5.00	3.47	10.71
8	Tilt Azimuth (deg)	134.34	131.27	128.04	124.57	245.99	110.52
9	Swing Angle (deg)	38.97	35.90	32.68	29.20	150.28	15.30
10	North Deviation (deg)	84.95	84.94	84.92	84.91	84.16	85.74
	PHOTOGRAPHY						
	ILLUMINATION						
11	Sun Azimuth (deg)	79.06	79.17	79.28	79.38	81.46	77.70
12	Incident Angle (deg)	71.92	71.81	71.70	71.60	70.84	73.35
13	Emission Angle (deg)	6.07	5.82	5.60	5.40	3.72	11.72
14	Phase Angle (deg)	75.45	75.45	75.45	75.45	67.26	83.34
15	Alpha (deg)	-3.60	-3.70	-3.80	-3.90	3.58	-10.09
16	QUAL Albedo	0.114	0.114	0.114	0.114	0.105	0.158
17	Shutter Speed (sec)	0.02	0.02	0.02	0.02	0.02	0.02
	PHOTOGRAPHS						
	TELEPHOTO						
	CORNER COORD. (deg)						
18	A: Latitude	-25.80	-25.41	-25.02	-24.64	-18.79	-30.99
19	A: Longitude	59.62	59.67	59.72	59.77	56.39	50.89
20	B: Latitude	-25.96	-25.56	-25.17	-24.79	-18.94	-31.14
21	B: Longitude	61.52	61.55	61.57	61.60	57.92	53.22
22	C: Latitude	-26.39	-25.99	-25.60	-25.21	-19.30	-31.65
23	C: Longitude	61.49	61.51	61.54	61.57	57.88	53.18
24	D: Latitude	-26.23	-25.83	-25.44	-25.05	-19.16	-31.46
25	D: Longitude	59.57	59.62	59.67	59.72	56.34	50.84
26	Scale Factor ( $\times 10^6$ )	4.23	4.26	4.30	4.34	4.96	3.69
27	Tilt Distance (mm)	59.83	57.45	55.31	53.36	37.03	115.40
	WIDE ANGLE						
	CORNER COORD. (deg)						
28	A: Latitude	-24.35	-23.97	-23.59	-23.22	-17.46	-29.40
29	A: Longitude	58.66	58.72	58.78	58.83	55.53	49.78
30	B: Latitude	-24.60	-24.21	-23.83	-23.45	-17.85	-29.47
31	B: Longitude	62.88	62.89	62.91	62.93	58.97	54.99
32	C: Latitude	-28.03	-27.61	-27.20	-26.79	-20.60	-33.62
33	C: Longitude	62.72	62.72	62.73	62.73	58.74	54.88
34	D: Latitude	-27.53	-27.12	-26.72	-26.31	-20.32	-32.88
35	D: Longitude	58.20	58.27	58.35	58.41	55.14	49.29
36	Scale Factor ( $\times 10^6$ )	0.55	0.56	0.56	0.57	0.65	0.48
37	Tilt Distance (mm)	7.85	7.53	7.25	7.00	4.86	15.13
	PRINCIPAL POINT						
38	Latitude (deg)	-26.10	-25.70	-25.31	-24.92	-19.05	-31.31
39	Longitude (deg)	60.54	60.21	60.61	60.65	57.14	51.99
40	Slant Distance (km)	144	143	142	141	123	165

LINE	V-5.1	V-6	V-10	V-12	V-14 *				V-15.1*
	41	42 **	54	63	66	67	68	69	70
1	222:16		223:20	224:06	224:12	224:12	224:12	224:12	224:16
2	11:26.5		45:36.9	25:30.7	54:00.9	54:06.6	54:12.5	54:18.2	03:49.2
3	98		131	96	121	121	122	123	111
4	-27		-162	-10	139	141	143	145	110
5	-2.44		-22.69	-0.28	21.33	21.65	21.98	22.30	17.02
6	51.86		34.26	30.97	29.29	29.32	29.35	29.38	27.14
7	53.49		57.62	29.32	1.44	1.75	2.08	2.40	11.76
8	274.99		227.61	94.93	352.82	355.05	356.65	357.79	282.75
9	179.37		110.96	0.41	257.86	260.08	261.67	262.80	188.36
10	86.63		40.11	86.19	85.05	85.04	85.03	85.01	86.13
11	87.84		82.72	88.26	97.10	97.24	97.40	97.54	95.01
12	72.58		79.45	67.54	68.75	68.77	68.78	68.79	69.53
13	58.13		65.25	31.11	1.54	1.88	2.23	2.57	12.52
14	15.90		33.85	98.46	68.38	68.38	68.38	68.38	57.13
15	55.24		35.22	-30.96	0.36	0.37	0.38	0.39	12.40
16	0.077		0.110	0.152	0.066	0.066	0.066	0.066	0.071
17	0.01		0.01	0.02	0.02	0.02	0.02	0.02	0.02
18	-1.37		-26.70	-0.23	21.67	22.02	22.37	22.72	17.41
19	44.35		26.16	32.08	28.52	28.55	28.57	28.60	25.62
20	-1.97		-27.40	-0.32	21.55	21.89	22.25	22.59	17.30
21	48.75		30.26	33.63	30.06	30.10	30.14	30.18	27.06
22	-2.37		-28.66	-0.69	21.19	21.53	21.88	22.22	16.97
23	48.71		29.42	33.60	30.02	30.06	30.10	30.14	27.04
24	-2.12		-28.36	-0.53	21.31	21.66	22.01	22.35	17.06
25	44.25		23.64	32.05	28.49	28.52	28.54	28.57	25.60
26	3.49		2.23	5.50	5.06	5.02	4.99	4.95	5.38
27	824.14		962.10	342.55	15.33	18.67	22.16	25.53	127.02
28	4.30		-23.47	0.69	22.96	23.32	23.69	24.04	18.76
29	37.09		27.63	31.45	27.62	27.63	27.64	27.66	24.61
30	-1.06		-25.48	1.07	22.67	23.02	23.38	23.74	18.27
31	49.98		32.86	35.27	31.18	31.23	31.29	31.35	27.97
32	-3.50		-40.33	-2.33	19.93	20.26	20.61	20.94	15.90
33	49.73		26.04	35.02	30.86	30.90	30.95	30.99	27.75
34	-6.58		( OFF )	-1.34	20.20	20.53	20.88	21.22	15.90
35	34.63		( LIMB )	31.29	27.43	27.45	27.47	27.48	24.48
36	0.46		0.29	0.72	0.66	0.66	0.65	0.65	0.70
37	108.08		126.18	44.93	2.01	2.45	2.91	3.35	16.66
38	-2.03		-27.70	-0.44	21.43	21.78	22.13	22.47	17.19
39	47.24		27.90	32.75	29.28	29.31	29.34	29.37	26.36
40	175		273	111	121	121	122	123	113

\* AAP \*\*Not applicable to this group; see "Apollo Site" group.

LINE	SITE NUMBER	V-18 *				V-19	V-21*
	FRAME NUMBER	80	81	82	83	84	86
	EXPOSURE TIME (GMT)						
1	Day: Hour	225:07	225:07	225:07	225:07	225:11	225:20
2	Minute: Second	54:55.6	55:00.1	55:04.6	55:09.1	00:57.6	49:42.4
	S/C POSITION						
3	Altitude (km)	96	96	96	96	113	176
4	Altitude Rate (m/sec)	6	8	10	11	-114	235
5	Latitude (deg)	2.37	2.63	2.89	3.15	-14.89	37.63
6	Longitude (deg)	17.17	17.19	17.21	17.23	14.04	13.42
	S/C ORIENTATION						
7	Tilt Angle (deg)	13.93	13.93	13.93	13.94	2.20	3.02
8	Tilt Azimuth (deg)	95.57	94.52	93.48	92.43	218.74	358.54
9	Swing Angle (deg)	0.99	359.91	358.83	357.75	123.94	262.86
10	North Deviation (deg)	85.57	85.50	85.43	85.36	85.15	84.32
	PHOTOGRAPHY						
	ILLUMINATION						
11	Sun Azimuth (deg)	89.33	89.43	89.54	89.64	83.68	103.25
12	Incident Angle (deg)	69.30	69.27	69.25	69.22	72.81	71.36
13	Emission Angle (deg)	14.72	14.72	14.72	14.73	2.34	3.33
14	Phase Angle (deg)	83.93	83.93	83.93	83.93	71.16	70.55
15	Alpha (deg)	-14.64	-14.67	-14.69	-14.71	1.64	0.78
16	QUAL Albedo	0.093	0.093	0.093	0.093	0.114	0.102
17	Shutter Speed (sec)	0.02	0.02	0.02	0.02	0.02	0.02
	PHOTOGRAPHS						
	TELEPHOTO						
	CORNER COORD. (deg)						
18	A: Latitude	2.48	2.76	3.03	3.30	-14.78	38.29
19	A: Longitude	17.39	17.41	17.43	17.46	13.27	12.12
20	B: Latitude	2.40	2.67	2.95	3.22	-14.89	38.08
21	B: Longitude	18.61	18.63	18.65	18.68	14.65	14.77
22	C: Latitude	2.09	2.36	2.64	2.91	-15.23	37.56
23	C: Longitude	18.58	18.60	18.63	18.65	14.62	14.68
24	D: Latitude	2.20	2.48	2.75	3.02	-15.12	37.77
25	D: Longitude	17.37	17.39	17.41	17.43	13.24	12.07
26	Scale Factor ( $\times 10^6$ )	6.15	6.14	6.14	6.14	5.40	3.47
27	Tilt Distance (mm)	151.29	151.27	151.31	151.40	23.40	32.22
	WIDE ANGLE						
	CORNER COORD. (deg)						
28	A: Latitude	3.41	3.69	3.96	4.24	-13.59	40.21
29	A: Longitude	16.80	16.82	16.84	16.86	12.49	10.49
30	B: Latitude	3.43	3.71	3.99	4.26	-13.86	39.70
31	B: Longitude	19.62	19.65	19.68	19.71	15.59	16.83
32	C: Latitude	0.90	1.17	1.45	1.72	-16.42	35.70
33	C: Longitude	19.42	19.44	19.46	19.48	15.42	16.04
34	D: Latitude	1.38	1.65	1.92	2.20	-16.18	36.15
35	D: Longitude	16.63	16.65	16.68	16.70	12.21	10.27
36	Scale Factor ( $\times 10^6$ )	0.81	0.81	0.81	0.80	0.71	0.45
37	Tilt Distance (mm)	19.84	19.84	19.84	19.86	3.07	4.23
	PRINCIPAL POINT						
38	Latitude (deg)	2.30	2.57	2.84	3.12	-15.00	37.93
39	Longitude (deg)	17.96	17.98	18.00	18.02	13.95	13.41
40	Slant Distance (km)	99	99	99	99	113	176

\* AAP



LINE	V-21 *			V-22 *				V-23.2*	
	87	88	89	90	91	92	93	94	95
1	225:20	225:20	225:20	225:23	225:23	225:23	225:23	226:03	226:03
2	49:50.8	49:59.3	50:07.9	55:25.5	55:31.0	55:36.6	55:42.3	02:41.7	02:46.5
3	178	180	182	117	118	119	119	99	99
4	237	240	243	126	128	130	132	37	39
5	38.07	38.52	38.97	20.11	20.42	20.73	21.05	7.18	7.46
6	13.48	13.54	13.59	9.87	9.90	9.93	9.95	7.04	7.06
7	3.47	3.91	4.36	9.07	9.12	9.18	9.25	18.86	18.86
8	359.51	0.27	0.88	282.77	284.69	286.63	288.57	274.50	275.32
9	263.79	264.51	265.09	188.17	190.11	192.06	194.01	179.93	180.79
10	84.28	84.24	84.20	85.80	85.84	85.89	85.94	85.83	85.93
11	103.46	103.66	103.87	95.79	95.92	96.04	96.17	90.90	91.00
12	71.43	71.50	71.56	70.69	70.70	70.71	70.72	71.61	71.59
13	3.82	4.32	4.82	9.69	9.74	9.81	9.89	19.98	19.98
14	70.55	70.55	70.55	61.07	61.07	61.07	61.07	51.67	51.67
15	0.84	0.90	0.95	9.61	9.62	9.63	9.64	19.93	19.91
16	0.102	0.102	0.102	0.063	0.063	0.063	0.063	0.090	0.090
17	0.02	0.02	0.02	0.04	0.04	0.04	0.04	0.02	0.02
18	38.79	39.29	39.80	20.48	20.82	21.15	21.50	7.49	7.78
19	12.15	12.19	12.23	8.46	8.47	8.49	8.51	5.22	5.24
20	38.58	39.07	39.58	20.36	20.69	21.03	21.37	7.37	7.66
21	14.85	14.94	15.04	9.98	10.01	10.04	10.07	6.55	6.57
22	38.05	38.54	39.04	20.02	20.35	20.68	21.02	7.08	7.37
23	14.77	14.86	14.95	9.95	9.98	10.01	10.04	6.53	6.55
24	38.26	38.75	39.25	20.12	20.45	20.79	21.13	7.16	7.45
25	12.10	12.14	12.18	8.43	8.45	8.47	8.49	5.20	5.21
26	3.43	3.38	3.34	5.13	5.10	5.07	5.04	5.83	5.82
27	36.94	41.72	46.55	97.39	97.90	98.55	99.32	208.41	208.42
28	40.74	41.28	41.82	21.85	22.19	22.55	22.90	8.81	9.11
29	10.48	10.48	10.47	7.43	7.44	7.44	7.44	4.22	4.23
30	40.22	40.74	41.27	21.39	21.74	22.08	22.43	8.20	8.50
31	16.97	17.12	17.27	10.97	11.01	11.05	11.10	7.31	7.33
32	36.17	36.65	37.13	18.86	19.19	19.52	19.85	6.13	6.42
33	16.14	16.24	16.35	10.72	10.75	10.79	10.82	7.14	7.17
34	36.62	37.10	37.59	18.93	19.25	19.58	19.92	6.00	6.29
35	10.28	10.29	10.31	7.27	7.29	7.30	7.31	4.01	4.04
36	0.45	0.44	0.44	0.67	0.67	0.66	0.66	0.77	0.76
37	4.84	5.47	6.10	12.77	12.84	12.92	13.02	27.33	27.33
38	38.42	38.92	39.42	20.25	20.58	20.91	21.26	7.27	7.56
39	13.47	13.54	13.60	9.23	9.25	9.28	9.30	5.92	5.94
40	178	180	182	119	120	120	121	105	105

\* AAP

LINE	SITE NUMBER	V-23.2 *		V-24			
	FRAME NUMBER	96	97	98	99	100	101
	EXPOSURE TIME (GMT)						
1	Day: Hour	226:03	226:03	226:06	226:06	226:06	226:06
2	Minute: Second	02:51.2	02:56.0	10:11.8	10:16.4	10:20.9	10:25.4
	S/C POSITION						
3	Altitude (km)	99	99	100	100	100	99
4	Altitude Rate (m/sec)	41	43	-49	-47	-45	-43
5	Latitude (deg)	7.73	8.00	-5.05	-4.79	-4.53	-4.27
6	Longitude (deg)	7.08	7.10	4.32	4.34	4.36	4.38
	S/C ORIENTATION						
7	Tilt Angle (deg)	18.87	18.88	5.08	5.03	5.00	4.98
8	Tilt Azimuth (deg)	276.11	276.92	263.23	266.18	269.10	272.05
9	Swing Angle (deg)	181.62	182.48	168.51	171.46	174.40	177.37
10	North Deviation (deg)	86.02	86.12	85.22	85.25	85.27	85.30
	PHOTOGRAPHY						
	ILLUMINATION						
11	Sun Azimuth (deg)	91.10	91.20	86.84	86.93	87.01	87.10
12	Incident Angle (deg)	71.58	71.56	72.16	72.12	72.08	72.05
13	Emission Angle (deg)	19.99	20.00	5.37	5.32	5.29	5.27
14	Phase Angle (deg)	51.67	51.67	66.80	66.80	66.80	66.80
15	Alpha (deg)	19.89	19.87	5.36	5.32	5.29	5.25
16	QUAL Albedo	0.090	0.090	0.106	0.106	0.106	0.106
17	Shutter Speed (sec)	0.02	0.02	0.02	0.02	0.02	0.02
	PHOTOGRAPHS						
	TELEPHOTO						
	CORNER COORD. (deg)						
18	A: Latitude	8.07	8.36	-4.89	-4.61	-4.34	-4.06
19	A: Longitude	5.26	5.27	3.43	3.45	3.48	3.50
20	B: Latitude	7.95	8.24	-4.99	-4.71	-4.44	-4.17
21	B: Longitude	6.59	6.62	4.62	4.65	4.67	4.69
22	C: Latitude	7.65	7.94	-5.28	-5.00	-4.73	-4.46
23	C: Longitude	6.57	6.59	4.60	4.62	4.64	4.66
24	D: Latitude	7.73	8.03	-5.19	-4.91	-4.64	-4.36
25	D: Longitude	5.23	5.25	3.40	3.43	3.45	3.48
26	Scale Factor ( $\times 10^6$ )	5.81	5.80	6.08	6.09	6.10	6.12
27	Tilt Distance (mm)	208.48	208.59	54.22	53.73	53.39	53.19
	WIDE ANGLE						
	CORNER COORD. (deg)						
28	A: Latitude	9.40	9.70	-3.79	-3.51	-3.24	-2.97
29	A: Longitude	4.24	4.25	2.72	2.74	2.76	2.79
30	B: Latitude	8.79	9.08	-4.10	-3.82	-3.55	-3.28
31	B: Longitude	7.36	7.38	5.42	5.44	5.46	5.48
32	C: Latitude	6.71	7.00	-6.30	-6.02	-5.74	-5.46
33	C: Longitude	7.19	7.21	5.25	5.27	5.29	5.31
34	D: Latitude	6.58	6.87	-6.16	-5.88	-5.60	-5.33
35	D: Longitude	4.06	4.08	2.49	2.52	2.55	2.58
36	Scale Factor ( $\times 10^6$ )	0.76	0.76	0.80	0.80	0.80	0.80
37	Tilt Distance (mm)	27.34	27.36	7.11	7.05	7.00	6.98
	PRINCIPAL POINT						
38	Latitude (deg)	7.85	8.14	-5.09	-4.81	-4.54	-4.26
39	Longitude (deg)	5.96	5.98	4.02	4.05	4.07	4.09
40	Slant Distance (km)	105	105	100	100	100	100

\* AAP

LINE	V-25	V-26.1				V-28 *			
	102	104	105	106	107	116	117	118	119
1	226:09	226:12	226:12	226:12	226:12	226:22	226:22	226:22	226:22
2	38:23.2	40:36.4	41:02.8	41:27.6	41:53.1	02:43.4	02:48.8	02:54.2	02:55.5
3	248	125	129	133	137	113	113	112	112
4	304	146	156	165	174	-112	-110	-108	-106
5	51.22	23.38	24.85	26.22	27.63	-14.23	-13.92	-13.62	-13.32
6	8.65	3.18	3.32	3.45	3.59	-5.15	-5.12	-5.10	-5.07
7	34.09	4.60	4.86	5.46	6.33	14.53	14.48	14.44	14.41
8	241.89	276.31	293.98	307.82	318.66	103.75	102.58	101.39	100.23
9	179.26	181.44	199.12	212.95	223.78	9.69	8.48	7.27	6.06
10	116.57	85.30	85.37	85.44	85.50	86.65	86.57	86.49	86.41
11	101.77	96.92	97.52	98.09	98.67	83.93	84.03	84.12	84.21
12	77.79	70.97	71.04	71.13	71.23	73.04	72.98	72.93	72.88
13	39.83	4.93	5.22	5.88	6.84	15.50	15.44	15.40	15.36
14	53.15	66.04	66.04	66.04	66.04	87.69	87.69	87.69	87.69
15	22.07	4.93	5.00	5.06	5.13	-14.71	-14.76	-14.81	-14.85
16	0.100	0.070	0.070	0.070	0.070	0.088	0.088	0.088	0.088
17	0.02	0.04	0.04	0.04	0.04	0.04	0.04	0.04	0.04
18	47.06	23.67	25.25	26.75	28.28	-14.24	-13.92	-13.59	-13.27
19	-2.95	2.01	2.11	2.19	2.28	-4.87	-4.84	-4.82	-4.79
20	49.71	23.54	25.12	26.61	28.13	-14.33	-14.00	-13.68	-13.36
21	3.36	3.63	3.81	3.97	4.15	-3.38	-3.37	-3.35	-3.34
22	49.02	23.17	24.74	26.21	27.73	-14.70	-14.37	-14.04	-13.72
23	3.99	3.60	3.77	3.93	4.10	-3.40	-3.39	-3.37	-3.36
24	46.16	23.29	24.86	26.34	27.86	-14.57	-14.25	-13.92	-13.60
25	-2.03	1.98	2.08	2.17	2.26	-4.89	-4.87	-4.84	-4.82
26	1.97	4.86	4.71	4.56	4.41	5.20	5.23	5.26	5.29
27	412.88	49.05	51.84	58.32	67.71	158.06	157.55	157.12	156.75
28	46.17	25.04	26.69	28.25	29.86	-13.16	-12.84	-12.52	-12.20
29	-16.86	1.00	1.03	1.04	1.05	-5.58	-5.55	-5.53	-5.50
30	52.65	24.65	26.28	27.82	29.40	-13.10	-12.78	-12.46	-12.14
31	4.09	4.75	4.99	5.23	5.49	-2.20	-2.19	-2.17	-2.16
32	47.96	21.89	23.43	24.88	26.36	-16.13	-15.79	-15.45	-15.12
33	8.22	4.46	4.65	4.84	5.04	-2.29	-2.29	-2.29	-2.29
34	36.67	22.07	23.61	25.07	26.56	-15.57	-15.23	-14.90	-14.57
35	-6.01	0.78	0.85	0.90	0.96	-5.79	-5.76	-5.73	-5.70
36	0.26	0.64	0.62	0.60	0.58	0.68	0.69	0.69	0.69
37	54.15	6.43	6.80	7.65	8.88	20.73	20.66	20.61	20.56
38	48.26	23.42	25.00	26.48	28.00	-14.46	-14.13	-13.80	-13.48
39	1.04	2.82	2.95	3.08	3.21	-4.17	-4.15	-4.13	-4.11
40	310	126	130	134	138	117	117	116	115

\* AAP

LINE	SITE NUMBER	V-29				V-30	
	FRAME NUMBER	120	121	122	123	125	126
	EXPOSURE TIME (GMT)						
1	Day: Hour	227:01	227:01	227:01	227:01	227:04	227:04
2	Minute: Second	21:29.6	21:34.5	21:39.4	21:44.4	16:05.0	16:15.2
	S/C POSITION						
3	Altitude (km)	104	104	105	105	218	215
4	Altitude Rate (m/sec)	72	74	76	78	-280	-277
5	Latitude (deg)	12.35	12.63	12.90	13.19	-42.22	-41.71
6	Longitude (deg)	-4.78	-4.75	-4.73	-4.71	-11.81	-11.73
	S/C ORIENTATION						
7	Tilt Angle (deg)	12.00	12.02	12.04	12.08	5.03	4.51
8	Tilt Azimuth (deg)	91.65	90.34	89.04	87.72	184.71	184.45
9	Swing Angle (deg)	356.60	355.25	353.92	352.56	88.36	88.15
10	North Deviation (deg)	84.83	84.76	84.69	84.61	83.58	83.65
	PHOTOGRAPHY						
	ILLUMINATION						
11	Sun Azimuth (deg)	92.90	93.01	93.13	93.24	79.76	79.79
12	Incident Angle (deg)	70.40	70.39	70.38	70.36	81.22	81.05
13	Emission Angle (deg)	12.73	12.75	12.78	12.82	5.66	5.07
14	Phase Angle (deg)	83.13	83.13	83.13	83.13	79.80	79.80
15	Alpha (deg)	-12.73	-12.74	-12.76	-12.77	1.38	1.22
16	QUAL Albedo	0.070	0.070	0.070	0.070	0.119	0.119
17	Shutter Speed (sec)	0.04	0.04	0.04	0.04	0.04	0.04
	PHOTOGRAPHS						
	TELEPHOTO						
	CORNER COORD. (deg)						
18	A: Latitude	12.53	12.83	13.12	13.43	-42.37	-41.79
19	A: Longitude	-4.65	-4.62	-4.60	-4.57	-13.58	-13.45
20	B: Latitude	12.43	12.72	13.02	13.32	-42.66	-42.07
21	B: Longitude	-3.33	-3.29	-3.26	-3.23	-10.08	-10.03
22	C: Latitude	12.10	12.39	12.69	12.99	-43.32	-42.72
23	C: Longitude	-3.36	-3.33	-3.30	-3.26	-10.15	-10.10
24	D: Latitude	12.23	12.52	12.82	13.12	-43.02	-42.43
25	D: Longitude	-4.68	-4.65	-4.63	-4.60	-13.71	-13.58
26	Scale Factor ( $\times 10^6$ )	5.73	5.71	5.69	5.67	2.78	2.82
27	Tilt Distance (mm)	129.67	129.87	130.15	130.50	53.67	48.12
	WIDE ANGLE						
	CORNER COORD. (deg)						
28	A: Latitude	13.56	13.86	14.16	14.47	-40.05	-39.50
29	A: Longitude	-5.31	-5.29	-5.26	-5.24	-15.28	-15.13
30	B: Latitude	13.52	13.82	14.12	14.43	-40.67	-40.10
31	B: Longitude	-2.22	-2.17	-2.13	-2.09	-7.73	-7.72
32	C: Latitude	10.84	11.14	11.43	11.73	-45.77	-45.13
33	C: Longitude	-2.50	-2.47	-2.44	-2.41	-7.88	-7.90
34	D: Latitude	11.34	11.63	11.92	12.23	-45.04	-44.42
35	D: Longitude	-5.49	-5.47	-5.45	-5.43	-16.66	-16.43
36	Scale Factor ( $\times 10^6$ )	0.75	0.75	0.75	0.74	0.36	0.37
37	Tilt Distance (mm)	17.01	17.03	17.07	17.12	7.04	6.31
	PRINCIPAL POINT						
38	Latitude (deg)	12.32	12.62	12.92	13.22	-42.85	-42.27
39	Longitude (deg)	-4.03	-4.00	-3.97	-3.95	-11.88	-11.79
40	Slant Distance (km)	106	107	107	108	219	216

LINE	V-30		V-31				V-32		
	127	128	129	130	131	132	133	134	135
1	227:04	227:04	227:07	227:07	227:07	227:07	227:10	227:10	227:10
2	16:25.4	16:35.9	54:37.3	54:48.5	55:00.0	55:11.6	54:16.1	54:35.5	54:55.5
3	213	210	230	234	237	240	103	105	106
4	-274	-272	290	292	295	298	66	73	81
5	-41.19	-40.66	48.26	48.82	49.39	49.96	11.42	12.52	13.66
6	-11.66	-11.58	-3.99	-3.88	-3.77	-3.66	-10.06	-9.97	-9.87
7	3.99	3.46	6.78	7.09	7.44	7.82	11.11	11.09	11.19
8	184.14	183.73	65.38	61.63	58.14	54.98	271.20	276.89	282.69
9	87.89	87.54	327.62	323.76	320.17	316.88	176.61	182.38	188.28
10	83.71	83.77	81.12	80.93	80.72	80.50	85.57	85.79	86.01
11	79.82	79.85	107.84	108.15	108.47	108.80	92.19	92.59	93.00
12	80.88	80.71	73.06	73.16	73.26	73.37	72.18	72.14	72.11
13	4.48	3.87	7.69	8.05	8.46	8.91	11.78	11.77	11.88
14	79.80	79.80	78.87	78.87	78.87	78.87	60.41	60.41	60.41
15	1.06	0.89	-5.88	-5.80	-5.72	-5.63	11.78	11.73	11.69
16	0.119	0.119	0.098	0.098	0.098	0.098	0.093	0.093	0.093
17	0.04	0.04	0.04	0.04	0.04	0.04	0.02	0.02	0.02
18	-41.21	-40.62	49.16	49.80	50.46	51.13	11.64	12.82	14.03
19	-13.32	-13.20	-4.72	-4.62	-4.52	-4.41	-11.41	-11.33	-11.25
20	-41.49	-40.89	48.76	49.39	50.04	50.70	11.53	12.71	13.92
21	-9.99	-9.94	-0.53	-0.31	-0.08	0.17	-10.11	-10.01	-9.90
22	-42.13	-41.51	48.06	48.68	49.32	49.97	11.23	12.40	13.61
23	-10.05	-10.00	-0.74	-0.53	-0.31	-0.08	-10.13	-10.03	-9.93
24	-41.85	-41.24	48.48	49.12	49.77	50.42	11.32	12.49	13.70
25	-13.45	-13.32	-4.84	-4.75	-4.65	-4.54	-11.43	-11.35	-11.28
26	2.86	2.90	2.63	2.59	2.55	2.51	5.79	5.72	5.64
27	42.56	36.83	72.54	75.91	79.68	83.77	119.79	119.60	120.66
28	-38.95	-38.38	51.63	52.32	53.04	53.77	12.86	14.06	15.31
29	-14.98	-14.84	-7.04	-7.02	-7.00	-6.98	-12.27	-12.22	-12.18
30	-39.54	-38.96	50.85	51.52	52.20	52.89	12.43	13.62	14.85
31	-7.71	-7.70	3.42	3.81	4.22	4.66	-9.30	-9.18	-9.05
32	-44.48	-43.82	45.37	45.96	46.57	47.18	10.22	11.38	12.58
33	-7.92	-7.94	1.27	1.50	1.75	2.00	-9.48	-9.37	-9.26
34	-43.80	-43.16	46.50	47.11	47.74	48.38	10.23	11.40	12.60
35	-16.21	-15.99	-7.57	-7.53	-7.50	-7.46	-12.48	-12.40	-12.32
36	0.38	0.38	0.34	0.34	0.33	0.33	0.76	0.75	0.74
37	5.58	4.83	9.51	9.96	10.45	10.99	15.71	15.69	15.82
38	-41.68	-41.07	48.63	49.27	49.92	50.58	11.43	12.61	13.81
39	-11.71	-11.62	-2.75	-2.59	-2.43	-2.26	-10.75	-10.66	-10.57
40	213	210	232	236	239	243	105	107	108

LINE	SITE NUMBER	V-32	V-33*	V-34 *			
	FRAME NUMBER	136	137	138	139	140	141
	EXPOSURE TIME (GMT)						
1	Day: Hour	227:10	227:17	227:20	227:20	227:20	227:20
2	Minute: Second	55:16.6	14:49.7	21:47.3	21:52.1	21:56.9	22:01.7
	S/C POSITION						
3	Altitude (km)	108	99	104	104	103	103
4	Altitude Rate (m/sec)	89	31	-66	-65	-63	-61
5	Latitude (deg)	14.86	6.41	-7.53	-7.25	-6.98	-6.71
6	Longitude (deg)	-9.76	-13.98	-16.83	-16.81	-16.78	-16.76
	S/C ORIENTATION						
7	Tilt Angle (deg)	11.41	13.19	1.46	1.22	1.00	0.81
8	Tilt Azimuth (deg)	288.64	277.02	157.73	151.85	143.26	130.33
9	Swing Angle (deg)	194.32	182.57	63.11	57.24	48.65	35.71
10	North Deviation (deg)	86.24	85.84	85.39	85.39	85.39	85.39
	PHOTOGRAPHY						
	ILLUMINATION						
11	Sun Azimuth (deg)	93.44	90.51	86.26	86.34	86.42	86.50
12	Incident Angle (deg)	72.08	72.84	73.70	73.66	73.62	73.58
13	Emission Angle (deg)	12.13	13.96	1.54	1.29	1.06	0.86
14	Phase Angle (deg)	60.41	58.97	74.20	74.20	74.20	74.20
15	Alpha (deg)	11.65	13.86	-0.50	-0.54	-0.58	-0.62
16	QUAL Albedo	0.093	0.077	0.093	0.093	0.093	0.093
17	Shutter Speed (sec)	0.02	0.04	0.04	0.04	0.04	0.04
	PHOTOGRAPHS						
	TELEPHOTO						
	CORNER COORD. (deg)						
18	A: Latitude	15.32	6.72	-7.40	-7.11	-6.82	-6.53
19	A: Longitude	-11.18	-15.39	-17.40	-17.37	-17.35	-17.32
20	B: Latitude	15.20	6.61	-7.50	-7.21	-6.92	-6.63
21	B: Longitude	-9.79	-14.14	-16.16	-16.14	-16.12	-16.10
22	C: Latitude	14.88	6.31	-7.81	-7.52	-7.23	-6.94
23	C: Longitude	-9.82	-14.16	-16.18	-16.16	-16.14	-16.12
24	D: Latitude	14.97	6.40	-7.71	-7.42	-7.13	-6.84
25	D: Longitude	-11.20	-15.42	-17.43	-17.40	-17.37	-17.35
26	Scale Factor ( $\times 10^6$ )	5.54	5.97	5.86	5.88	5.90	5.92
27	Tilt Distance (mm)	123.13	142.98	15.51	12.97	10.63	8.66
	WIDE ANGLE						
	CORNER COORD. (deg)						
28	A: Latitude	16.63	7.93	-6.33	-6.04	-5.75	-5.46
29	A: Longitude	-12.15	-16.26	-18.09	-18.06	-18.04	-18.01
30	B: Latitude	16.16	7.47	-6.54	-6.25	-5.96	-5.67
31	B: Longitude	-8.91	-13.37	-15.29	-15.27	-15.25	-15.23
32	C: Latitude	13.84	5.35	-8.92	-8.63	-8.33	-8.03
33	C: Longitude	-9.14	-13.54	-15.45	-15.44	-15.42	-15.41
34	D: Latitude	13.86	5.33	-8.68	-8.39	-8.09	-7.79
35	D: Longitude	-12.25	-16.44	-18.31	-18.28	-18.25	-18.22
36	Scale Factor ( $\times 10^6$ )	0.73	0.78	0.77	0.77	0.77	0.78
37	Tilt Distance (mm)	16.15	18.75	2.03	1.70	1.39	1.14
	PRINCIPAL POINT						
38	Latitude (deg)	15.09	6.51	-7.61	-7.32	-7.03	-6.74
39	Longitude (deg)	-10.47	-14.75	-16.79	-16.77	-16.75	-16.72
40	Slant Distance (km)	110	102	104	104	103	103

\*AAP

LINE	V-35 *				V-36				V-37*
	142	143	144	145	146	147	148	149	150
1	227:23	227:23	227:23	227:23	228:02	228:02	228:02	228:02	228:05
2	38:40.2	38:59.8	39:19.8	39:40.4	47:50.4	47:55.2	48:00.0	48:04.4	59:37.4
3	106	107	109	111	100	100	101	101	102
4	74	81	89	97	30	32	34	36	49
5	12.68	13.79	14.93	16.10	6.44	6.71	6.99	7.24	9.18
6	-16.95	-16.85	-16.76	-16.66	-19.17	-19.15	-19.13	-19.11	-20.69
7	8.57	8.56	8.69	8.98	15.53	15.53	15.54	15.55	5.51
8	99.04	91.63	84.19	76.91	94.49	93.50	92.51	91.61	98.49
9	4.19	356.67	349.12	341.72	359.73	358.70	357.67	356.73	3.59
10	85.14	84.93	84.71	84.48	85.32	85.24	85.15	85.08	85.09
11	92.75	93.18	93.61	94.07	90.62	90.72	90.82	90.92	91.47
12	71.45	71.40	71.36	71.32	71.49	71.47	71.45	71.43	72.03
13	9.09	9.09	9.24	9.56	16.45	16.46	16.47	16.48	5.84
14	80.48	80.48	80.48	80.48	87.91	87.91	87.91	87.91	77.82
15	-9.04	-9.09	-9.13	-9.18	-16.42	-16.44	-16.46	-16.48	-5.80
16	0.096	0.096	0.096	0.096	0.077	0.077	0.077	0.077	0.109
17	0.04	0.04	0.04	0.04	0.04	0.04	0.04	0.04	0.02
18	12.80	13.99	15.20	16.45	6.56	6.86	7.15	7.41	9.33
19	-17.04	-16.94	-16.84	-16.74	-18.85	-18.83	-18.80	-18.78	-20.96
20	12.70	13.88	15.09	16.34	6.47	6.76	7.05	7.32	9.23
21	-15.73	-15.60	-15.47	-15.33	-17.55	-17.53	-17.50	-17.47	-19.72
22	12.37	13.55	14.76	15.99	6.14	6.44	6.73	6.99	8.92
23	-15.76	-15.64	-15.51	-15.37	-17.58	-17.56	-17.53	-17.51	-19.74
24	12.50	13.68	14.88	16.12	6.27	6.56	6.85	7.12	9.03
25	-17.07	-16.97	-16.87	-16.76	-18.88	-18.85	-18.83	-18.81	-20.98
26	5.71	5.63	5.54	5.44	5.85	5.84	5.83	5.82	5.93
27	91.89	91.78	93.28	96.44	169.52	169.56	169.66	169.79	58.87
28	13.85	15.06	16.30	17.57	7.53	7.83	8.12	8.39	10.37
29	-17.71	-17.63	-17.55	-17.47	-19.47	-19.45	-19.43	-19.41	-21.62
30	13.75	14.96	16.19	17.47	7.57	7.87	8.16	8.44	10.22
31	-14.70	-14.53	-14.36	-14.17	-16.44	-16.40	-16.37	-16.33	-18.78
32	11.14	12.32	13.51	14.74	4.87	5.16	5.45	5.72	7.78
33	-14.93	-14.81	-14.68	-14.54	-16.68	-16.66	-16.63	-16.61	-18.99
34	11.57	12.74	13.94	15.17	5.42	5.71	6.00	6.27	8.12
35	-17.91	-17.83	-17.74	-17.65	-19.65	-19.62	-19.60	-19.58	-21.81
36	0.75	0.74	0.73	0.71	0.77	0.77	0.76	0.76	0.78
37	12.05	12.04	12.23	12.65	22.23	22.24	22.25	22.27	7.72
38	12.60	13.78	14.98	16.23	6.37	6.66	6.95	7.21	9.13
39	-16.42	-16.31	-16.19	-16.07	-18.25	-18.23	-18.20	-18.18	-20.36
40	107	108	110	112	104	104	105	105	103

\*AAP



LINE	SITE NUMBER	V-37 *					
	FRAME NUMBER	151	152	153	154	155	156
	EXPOSURE TIME (GMT)						
1	Day: Hour	228:05	228:05	228:05	228:05	228:06	228:06
2	Minute: Second	59:42.2	59:47.0	59:51.8	59:56.6	00:01.4	00:06.1
	S/C POSITION						
3	Altitude (km)	103	103	103	103	104	104
4	Altitude Rate (m/sec)	51	53	55	57	58	60
5	Latitude (deg)	9.45	9.73	10.00	10.28	10.55	10.82
6	Longitude (deg)	-20.67	-20.64	-20.62	-20.60	-20.58	-20.55
	S/C ORIENTATION						
7	Tilt Angle (deg)	5.50	5.50	5.52	5.55	5.59	5.65
8	Tilt Azimuth (deg)	95.64	92.79	89.95	87.13	84.35	81.68
9	Swing Angle (deg)	0.73	357.86	355.00	352.17	349.37	346.68
10	North Deviation (deg)	85.06	85.03	84.99	84.96	84.92	84.89
	PHOTOGRAPHY						
	ILLUMINATION						
11	Sun Azimuth (deg)	91.57	91.66	91.76	91.86	91.96	92.06
12	Incident Angle (deg)	72.01	71.99	71.98	71.96	71.94	71.93
13	Emission Angle (deg)	5.83	5.83	5.85	5.88	5.93	5.99
14	Phase Angle (deg)	77.82	77.82	77.82	77.82	77.82	77.82
15	Alpha (deg)	-5.81	-5.83	-5.85	-5.86	-5.88	-5.90
16	QUAL Albedo	0.109	0.109	0.109	0.109	0.109	0.109
17	Shutter Speed (sec)	0.02	0.02	0.02	0.02	0.02	0.02
	PHOTOGRAPHS						
	TELEPHOTO						
	CORNER COORD. (deg)						
18	A: Latitude	9.62	9.92	10.21	10.50	10.79	11.07
19	A: Longitude	-20.93	-20.91	-20.89	-20.86	-20.84	-20.82
20	B: Latitude	9.52	9.81	10.10	10.40	10.69	10.97
21	B: Longitude	-19.69	-19.66	-19.64	-19.61	-19.58	-19.55
22	C: Latitude	9.21	9.50	9.79	10.08	10.37	10.65
23	C: Longitude	-19.72	-19.69	-19.66	-19.64	-19.61	-19.58
24	D: Latitude	9.32	9.61	9.90	10.19	10.48	10.77
25	D: Longitude	-20.96	-20.94	-20.91	-20.89	-20.87	-20.85
26	Scale Factor ( $\times 10^6$ )	5.91	5.90	5.88	5.87	5.85	5.83
27	Tilt Distance (mm)	58.75	58.78	58.95	59.27	59.73	60.32
	WIDE ANGLE						
	CORNER COORD. (deg)						
28	A: Latitude	10.66	10.96	11.25	11.55	11.85	12.14
29	A: Longitude	-21.60	-21.58	-21.56	-21.54	-21.52	-21.50
30	B: Latitude	10.52	10.81	11.11	11.40	11.70	11.99
31	B: Longitude	-18.74	-18.71	-18.67	-18.64	-18.60	-18.57
32	C: Latitude	8.07	8.36	8.64	8.93	9.22	9.51
33	C: Longitude	-18.97	-18.94	-18.92	-18.89	-18.86	-18.84
34	D: Latitude	8.41	8.70	8.99	9.28	9.57	9.85
35	D: Longitude	-21.79	-21.77	-21.74	-21.72	-21.70	-21.68
36	Scale Factor ( $\times 10^6$ )	0.78	0.77	0.77	0.77	0.77	0.77
37	Tilt Distance (mm)	7.71	7.71	7.73	7.77	7.83	7.91
	PRINCIPAL POINT						
38	Latitude (deg)	9.42	9.71	10.00	10.29	10.58	10.87
39	Longitude (deg)	-20.34	-20.31	-20.29	-20.26	-20.24	-20.21
40	Slant Distance (km)	103	103	104	104	104	105

\*AAP

LINE	V-37*	V-38 *				V-40 *			
	157	159	160	161	162	164	165	166	167
1	228:06	228:12	228:12	228:12	228:12	229:01	229:01	229:01	229:01
2	00:10.9	28:16.8	28:24.0	28:31.5	28:39.3	06:25.2	06:30.2	06:35.1	06:40.0
3	104	153	154	156	157	107	107	108	108
4	62	196	198	201	203	69	71	73	75
5	11.09	31.57	31.96	32.37	32.79	12.45	12.73	13.01	13.29
6	-20.53	-22.17	-22.13	-22.08	-22.04	-30.96	-30.94	-30.91	-30.89
7	5.72	2.13	2.52	2.93	3.35	0.52	0.78	1.05	1.32
8	79.01	5.11	5.17	5.23	5.27	333.10	344.22	349.65	352.86
9	343.99	269.52	269.56	269.59	269.61	238.30	249.42	254.84	258.05
10	84.86	84.39	84.37	84.34	84.31	85.20	85.20	85.20	85.19
11	92.16	99.30	99.45	99.62	99.79	92.34	92.44	92.54	92.64
12	71.91	72.75	72.78	72.81	72.85	73.03	73.01	73.00	72.99
13	6.06	2.32	2.74	3.19	3.65	0.56	0.83	1.11	1.40
14	77.82	72.60	72.60	72.60	72.60	72.76	72.76	72.76	72.76
15	-5.91	0.14	0.16	0.19	0.21	0.27	0.26	0.24	0.23
16	0.109	0.063	0.063	0.063	0.063	0.077	0.077	0.077	0.077
17	0.02	0.04	0.04	0.04	0.04	0.04	0.04	0.04	0.04
18	11.36	32.07	32.50	32.95	33.41	12.69	12.99	13.29	13.59
19	-20.80	-23.19	-23.16	-23.13	-23.10	-31.61	-31.59	-31.57	-31.54
20	11.26	31.89	32.32	32.76	33.23	12.58	12.89	13.18	13.48
21	-19.53	-21.06	-21.00	-20.93	-20.86	-30.31	-30.29	-30.26	-30.23
22	10.94	31.44	31.86	32.30	32.76	12.27	12.57	12.86	13.16
23	-19.56	-21.12	-21.06	-21.00	-20.93	-30.34	-30.31	-30.29	-30.26
24	11.06	31.62	32.04	32.48	32.94	12.37	12.67	12.97	13.26
25	-20.82	-23.24	-23.20	-23.17	-23.14	-31.64	-31.61	-31.59	-31.57
26	5.82	3.99	3.95	3.91	3.87	5.70	5.68	5.66	5.64
27	61.06	22.68	26.85	31.19	35.69	5.58	8.31	11.14	14.04
28	12.43	33.72	34.17	34.64	35.13	13.82	14.13	14.43	14.74
29	-21.49	-24.46	-24.46	-24.45	-24.45	-32.36	-32.35	-32.33	-32.31
30	12.28	33.30	33.74	34.21	34.69	13.57	13.88	14.18	14.48
31	-18.53	-19.43	-19.34	-19.24	-19.13	-29.39	-29.35	-29.31	-29.28
32	9.79	29.82	30.23	30.66	31.10	11.14	11.44	11.74	12.03
33	-18.81	-20.00	-19.93	-19.85	-19.78	-29.62	-29.59	-29.56	-29.53
34	10.14	30.21	30.63	31.06	31.51	11.38	11.68	11.97	12.27
35	-21.66	-24.71	-24.69	-24.67	-24.66	-32.55	-32.53	-32.51	-32.49
36	0.76	0.52	0.52	0.51	0.51	0.75	0.74	0.74	0.74
37	8.01	2.97	3.52	4.09	4.68	0.73	1.09	1.46	1.84
38	11.16	31.76	32.18	32.63	33.09	12.48	12.78	13.08	13.37
39	-20.19	-22.15	-22.11	-22.06	-22.01	-30.98	-30.95	-30.92	-30.90
40	105	153	155	156	158	107	107	108	108

\*AAP

LINE	SITE NUMBER	V-41	V-43.2				V-45.1*
	FRAME NUMBER	168	177	178	179	180	182
	EXPOSURE TIME (GMT)						
1	Day: Hour	229:04	229:13	229:13	229:13	229:13	229:23
2	Minute: Second	04:40.5	41:07.0	41:30.9	41:54.0	42:16.8	29:47.5
	S/C POSITION						
3	Altitude (km)	167	129	126	122	120	165
4	Altitude Rate (m/sec)	-216	-145	-136	-128	-119	212
5	Latitude (deg)	-30.37	-18.77	-17.44	-16.15	-14.88	34.60
6	Longitude (deg)	-36.52	-40.61	-40.49	-40.38	-40.26	-40.96
	S/C ORIENTATION						
7	Tilt Angle (deg)	9.64	6.93	6.25	5.82	5.66	5.69
8	Tilt Azimuth (deg)	255.33	130.31	120.27	108.68	95.97	299.33
9	Swing Angle (deg)	159.02	35.62	25.56	13.94	1.20	203.82
10	North Deviation (deg)	82.92	85.69	85.59	85.48	85.36	84.97
	PHOTOGRAPHY						
	ILLUMINATION						
11	Sun Azimuth (deg)	82.60	83.88	84.17	84.46	84.76	99.26
12	Incident Angle (deg)	80.45	77.04	76.78	76.53	76.30	74.57
13	Emission Angle (deg)	10.58	7.44	6.71	6.23	6.05	6.23
14	Phase Angle (deg)	69.94	82.23	82.23	82.23	82.23	68.72
15	Alpha (deg)	10.50	-5.25	-5.48	-5.71	-5.94	5.84
16	QUAL Albedo	0.085	0.090	0.090	0.090	0.090	0.080
17	Shutter Speed (sec)	0.04	0.04	0.04	0.04	0.04	0.04
	PHOTOGRAPHS						
	TELEPHOTO						
	CORNER COORD. (deg)						
18	A: Latitude	-30.22	-18.85	-17.43	-16.05	-14.68	35.21
19	A: Longitude	-38.75	-40.98	-40.83	-40.70	-40.57	-42.74
20	B: Latitude	-30.47	-18.97	-17.54	-16.16	-14.79	35.01
21	B: Longitude	-36.40	-39.35	-39.26	-39.18	-39.09	-40.33
22	C: Latitude	-30.96	-19.37	-17.93	-16.53	-15.16	34.53
23	C: Longitude	-36.46	-39.37	-39.29	-39.21	-39.12	-40.39
24	D: Latitude	-30.74	-19.23	-17.79	-16.41	-15.04	34.70
25	D: Longitude	-38.84	-41.01	-40.87	-40.73	-40.60	-42.78
26	Scale Factor ( $\times 10^6$ )	3.59	4.70	4.83	4.95	5.07	3.67
27	Tilt Distance (mm)	103.61	74.11	66.84	62.18	60.42	60.73
	WIDE ANGLE						
	CORNER COORD. (deg)						
28	A: Latitude	-28.26	-17.58	-16.17	-14.82	-13.47	37.08
29	A: Longitude	-40.09	-41.81	-41.65	-41.50	-41.35	-44.33
30	B: Latitude	-29.05	-17.74	-16.33	-14.97	-13.62	36.48
31	B: Longitude	-34.90	-38.19	-38.12	-38.05	-37.98	-38.60
32	C: Latitude	-32.70	-20.86	-19.36	-17.91	-16.49	32.85
33	C: Longitude	-35.23	-38.29	-38.26	-38.23	-38.20	-39.19
34	D: Latitude	-32.43	-20.42	-18.93	-17.51	-16.10	33.10
35	D: Longitude	-40.98	-42.16	-41.96	-41.77	-41.60	-44.52
36	Scale Factor ( $\times 10^6$ )	0.47	0.62	0.63	0.65	0.66	0.48
37	Tilt Distance (mm)	13.59	9.72	8.77	8.15	7.92	7.96
	PRINCIPAL POINT						
38	Latitude (deg)	-30.61	-19.11	-17.67	-16.29	-14.92	34.87
39	Longitude (deg)	-37.57	-40.20	-40.08	-39.97	-39.86	-41.54
40	Slant Distance (km)	170	130	126	123	120	166

\*AAP

LINE	V-45.1 *			V-46					
	183	184	185	186	187	188	189	190	191
1	229:23	229:23	229:23	230:02	230:02	230:02	230:02	230:02	230:02
2	29:55.4	30:03.3	30:11.2	37:57.9	38:04.2	38:10.6	38:16.9	38:23.3	38:29.7
3	167	168	170	134	135	136	137	138	140
4	214	217	219	156	159	161	163	165	167
5	35.02	35.44	35.86	25.47	25.81	26.17	26.51	26.86	27.22
6	-40.91	-40.85	-40.80	-43.76	-43.72	-43.68	-43.65	-43.61	-43.57
7	5.87	6.07	6.30	0.90	1.24	1.58	1.93	2.28	2.63
8	303.15	306.72	310.04	346.68	351.89	354.90	356.82	358.17	359.17
9	207.63	211.19	214.50	251.28	256.48	259.48	261.38	262.72	263.70
10	84.98	85.00	85.01	84.62	84.60	84.59	84.57	84.55	84.53
11	99.42	99.58	99.73	96.30	96.42	96.55	96.68	96.81	96.94
12	74.61	74.64	74.68	73.86	73.87	73.87	73.88	73.89	73.90
13	6.43	6.66	6.91	0.97	1.33	1.71	2.08	2.46	2.84
14	68.72	68.72	68.72	73.53	73.53	73.53	73.53	73.53	73.53
15	5.87	5.90	5.93	0.32	0.33	0.33	0.34	0.34	0.34
16	0.080	0.080	0.080	0.075	0.075	0.075	0.075	0.075	0.075
17	0.04	0.04	0.04	0.04	0.04	0.04	0.04	0.04	0.04
18	35.67	36.14	36.61	25.81	26.18	26.57	26.94	27.33	27.71
19	-42.71	-42.68	-42.65	-44.64	-44.61	-44.58	-44.55	-44.52	-44.59
20	35.48	35.94	36.41	25.66	26.03	26.41	26.79	27.17	27.55
21	-40.26	-40.19	-40.12	-42.87	-42.82	-42.77	-42.73	-42.67	-42.62
22	34.99	35.45	35.91	25.26	25.63	26.01	26.38	26.76	27.14
23	-40.32	-40.26	-40.19	-42.92	-42.87	-42.82	-42.77	-42.73	-42.68
24	35.17	35.63	36.09	25.41	25.78	26.16	26.54	26.92	27.30
25	-42.75	-42.72	-42.69	-44.67	-44.64	-44.61	-44.58	-44.56	-44.53
26	3.64	3.60	3.56	4.54	4.50	4.47	4.44	4.40	4.37
27	62.67	64.87	67.29	9.61	13.18	16.87	20.53	24.26	28.00
28	37.58	38.07	38.57	27.24	27.63	28.03	28.43	28.83	29.23
29	-44.34	-44.35	-44.36	-45.67	-45.65	-45.64	-45.63	-45.61	-45.60
30	36.97	37.46	37.94	26.89	27.27	27.67	28.06	28.45	28.85
31	-38.50	-38.39	-38.28	-41.57	-41.50	-41.43	-41.36	-41.29	-41.21
32	33.30	33.74	34.19	23.83	24.20	24.57	24.93	25.30	25.67
33	-39.11	-39.03	-38.95	-41.96	-41.90	-41.86	-41.80	-41.75	-41.69
34	33.55	34.00	34.45	24.16	24.53	24.90	25.27	25.64	26.02
35	-44.51	-44.50	-44.49	-45.91	-45.89	-45.87	-45.85	-45.83	-45.81
36	0.48	0.47	0.47	0.60	0.59	0.59	0.58	0.58	0.57
37	8.22	8.51	8.83	1.26	1.73	2.21	2.69	3.18	3.67
38	35.33	35.79	36.26	25.53	25.91	26.29	26.66	27.05	27.43
39	-41.49	-41.44	-41.39	-43.77	-43.73	-43.70	-43.66	-43.62	-43.58
40	168	170	171	134	135	136	138	139	140

\*AAP

LINE	SITE NUMBER	V-46		V-48			
	FRAME NUMBER	192	193	194	195	196	197
	EXPOSURE TIME (GMT)						
1	Day: Hour	230:02	230:02	230:08	230:08	230:08	230:08
2	Minute: Second	38:36.3	38:42.8	58:44.4	58:50.1	58:55.9	59:01.8
	S/C POSITION						
3	Altitude (km)	141	142	125	126	127	127
4	Altitude Rate (m/sec)	170	172	133	135	137	139
5	Latitude (deg)	27.58	27.93	21.86	22.18	22.50	22.83
6	Longitude (deg)	-43.53	-43.50	-47.61	-47.58	-47.54	-47.51
	S/C ORIENTATION						
7	Tilt Angle (deg)	2.99	3.35	1.04	1.32	1.61	1.93
8	Tilt Azimuth (deg)	359.95	0.57	39.44	31.67	26.58	23.06
9	Swing Angle (deg)	264.47	265.06	304.02	296.23	291.14	287.59
10	North Deviation (deg)	84.51	84.49	84.56	84.54	84.52	84.50
	PHOTOGRAPHY						
	ILLUMINATION						
11	Sun Azimuth (deg)	97.07	97.20	95.02	95.13	95.25	95.36
12	Incident Angle (deg)	73.91	73.92	74.02	74.01	74.01	74.01
13	Emission Angle (deg)	3.23	3.62	1.12	1.41	1.73	2.07
14	Phase Angle (deg)	73.53	73.53	74.65	74.65	74.65	74.65
15	Alpha (deg)	0.35	0.35	-0.64	-0.64	-0.64	-0.65
16	QUAL Albedo	0.075	0.075	0.154	0.154	0.154	0.154
17	Shutter Speed (sec)	0.04	0.04	0.02	0.02	0.02	0.02
	PHOTOGRAPHS						
	TELEPHOTO						
	CORNER COORD. (deg)						
18	A: Latitude	28.11	28.50	22.18	22.52	22.87	23.22
19	A: Longitude	-44.46	-44.43	-48.33	-48.31	-48.28	-48.25
20	B: Latitude	27.95	28.33	22.04	22.38	22.73	23.08
21	B: Longitude	-42.57	-42.52	-46.74	-46.70	-46.65	-46.61
22	C: Latitude	27.53	27.91	21.66	22.00	22.35	22.70
23	C: Longitude	-42.62	-42.57	-46.78	-46.74	-46.70	-46.66
24	D: Latitude	27.69	28.07	21.81	22.15	22.49	22.84
25	D: Longitude	-44.49	-44.46	-48.37	-48.34	-48.31	-48.28
26	Scale Factor ( $\times 10^6$ )	4.33	4.29	4.88	4.85	4.82	4.78
27	Tilt Distance (mm)	31.86	35.66	11.09	14.03	17.20	20.51
	WIDE ANGLE						
	CORNER COORD. (deg)						
28	A: Latitude	29.64	30.05	23.50	23.86	24.22	24.59
29	A: Longitude	-45.59	-45.58	-49.25	-49.23	-49.22	-49.20
30	B: Latitude	29.25	29.66	23.19	23.54	23.90	24.26
31	B: Longitude	-41.14	-41.06	-45.55	-45.50	-45.44	-45.38
32	C: Latitude	26.06	26.43	20.33	20.66	21.00	21.35
33	C: Longitude	-41.63	-41.57	-45.90	-45.86	-45.81	-45.77
34	D: Latitude	26.40	26.78	20.66	21.00	21.34	21.68
35	D: Longitude	-45.79	-45.77	-49.48	-49.46	-49.44	-49.42
36	Scale Factor ( $\times 10^6$ )	0.57	0.56	0.64	0.64	0.63	0.63
37	Tilt Distance (mm)	4.18	4.68	1.45	1.84	2.26	2.69
	PRINCIPAL POINT						
38	Latitude (deg)	27.82	28.21	21.92	22.26	22.61	22.96
39	Longitude (deg)	-43.54	-43.49	-47.56	-47.52	-47.49	-47.45
40	Slant Distance (km)	141	142	125	126	127	127

LINE	V-48				V-49				V-50*
	198	199	200	201	202	203	204	205	206
1	230:08	230:08	230:08	230:08	230.12	230:12	230:12	230:12	230:18
2	59:07.7	59:13.6	59:19.5	59:25.6	10:29.4	10:36.0	10:42.5	10:48.9	33:07.1
3	128	129	130	131	132	133	134	135	140
4	141	143	146	148	151	153	155	157	167
5	23.16	23.49	23.82	24.15	24.55	24.92	25.28	25.63	27.11
6	-47.48	-47.45	-47.41	-47.38	-49.09	-49.05	-49.01	-48.97	-52.30
7	2.24	2.56	2.88	3.21	6.01	6.13	6.27	6.43	5.84
8	20.52	18.62	17.15	15.94	293.87	297.12	300.19	303.07	294.83
9	285.05	283.13	281.64	280.42	198.69	201.95	205.01	207.89	199.62
10	84.48	84.46	84.44	84.42	85.15	85.17	85.20	85.22	85.14
11	95.48	95.60	95.71	95.83	95.66	95.78	95.90	96.03	96.36
12	74.01	74.01	74.01	74.01	74.61	74.62	74.63	74.63	74.88
13	2.41	2.75	3.10	3.46	6.47	6.60	6.76	6.93	6.31
14	74.65	74.65	74.65	74.65	68.48	68.48	68.48	68.48	68.90
15	-0.65	-0.66	-0.66	-0.67	6.13	6.13	6.13	6.13	5.97
16	0.154	0.154	0.154	0.154	0.079	0.079	0.079	0.079	0.065
17	0.02	0.02	0.02	0.02	0.04	0.04	0.04	0.04	0.04
18	23.58	23.93	24.29	24.65	25.01	25.41	25.80	26.18	27.60
19	-48.22	-48.19	-48.16	-48.13	-50.42	-50.39	-50.37	-50.34	-53.72
20	23.43	23.79	24.14	24.50	24.86	25.26	25.65	26.03	27.44
21	-46.57	-46.52	-46.48	-46.43	-48.67	-48.63	-48.58	-48.54	-51.84
22	23.05	23.40	23.75	24.11	24.48	24.87	25.25	25.63	27.03
23	-46.61	-46.57	-46.52	-46.48	-48.72	-48.67	-48.63	-48.58	-51.88
24	23.20	23.55	23.90	24.26	24.61	25.00	25.39	25.77	27.17
25	-48.26	-48.23	-48.20	-48.17	-50.45	-50.42	-50.40	-50.37	-53.75
26	4.75	4.72	4.69	4.65	4.59	4.55	4.52	4.48	4.35
27	23.88	27.28	30.70	34.26	64.19	65.53	67.06	68.74	62.36
28	24.95	25.32	25.69	26.07	26.51	26.92	27.33	27.74	29.18
29	49.18	-49.17	-49.15	-49.14	-51.54	-51.53	-51.53	-51.52	-54.93
30	24.63	24.99	25.36	25.73	26.04	26.45	26.85	27.25	28.68
31	-45.32	-45.25	-45.19	-45.12	-47.47	-47.40	-47.34	-47.28	-50.53
32	21.70	22.04	22.38	22.74	23.14	23.53	23.91	24.28	25.62
33	-45.72	-45.67	-45.62	-45.57	-47.83	-47.78	-47.73	-47.68	-50.93
34	22.03	22.38	22.72	23.08	23.32	23.71	24.09	24.47	25.81
35	-49.40	-49.38	-49.35	-49.33	-51.73	-51.71	-51.69	-51.67	-55.13
36	0.62	0.62	0.61	0.61	0.60	0.60	0.59	0.59	0.57
37	3.13	3.58	4.03	4.49	8.42	8.59	8.79	9.01	8.18
38	23.32	23.67	24.02	24.39	24.74	25.13	25.52	25.90	27.31
39	-47.42	-47.38	-47.34	-47.30	-49.55	-49.51	-49.48	-49.44	-52.78
40	128	129	130	131	133	134	135	136	140

\*AAP

LINE	SITE NUMBER	V-50 *			V-51 *		
	FRAME NUMBER	207	208	209	210	211	212
	EXPOSURE TIME (GMT)						
1	Day: Hour	230:18	230:18	230:18	230:21	230:21	230:21
2	Minute: Second	33:13.5	33:19.1	33:26.8	39:42.2	39:47.3	39:52.4
	S/C POSITION						
3	Altitude (km)	141	142	143	108	109	109
4	Altitude Rate (m/sec)	169	171	174	71	73	75
5	Latitude (deg)	27.46	27.77	28.19	12.53	12.82	13.10
6	Longitude (deg)	-52.26	-52.23	-52.18	-55.49	-55.47	-55.44
	S/C ORIENTATION						
7	Tilt Angle (deg)	5.96	6.08	6.28	9.60	9.61	9.63
8	Tilt Azimuth (deg)	298.03	300.73	304.24	275.71	277.43	279.15
9	Swing Angle (deg)	202.83	205.52	209.03	180.87	182.61	184.34
10	North Deviation (deg)	85.16	85.18	85.21	85.38	85.43	85.48
	PHOTOGRAPHY						
	ILLUMINATION						
11	Sun Azimuth (deg)	96.48	96.58	96.73	91.82	91.90	91.99
12	Incident Angle (deg)	74.89	74.90	74.91	75.48	75.46	75.45
13	Emission Angle (deg)	6.45	6.58	6.79	10.21	10.22	10.24
14	Phase Angle (deg)	68.90	68.90	68.90	65.30	65.30	65.30
15	Alpha (deg)	5.97	5.98	5.99	10.18	10.17	10.15
16	QUAL Albedo	0.065	0.065	0.065	0.060	0.060	0.060
17	Shutter Speed (sec)	0.04	0.04	0.04	0.04	0.04	0.04
	PHOTOGRAPHS						
	TELEPHOTO						
	CORNER COORD. (deg)						
18	A: Latitude	27.98	28.31	28.77	12.81	13.12	13.43
19	A: Longitude	-53.69	-53.67	-53.64	-56.80	-56.77	-56.75
20	B: Latitude	27.82	28.15	28.61	12.69	13.00	13.31
21	B: Longitude	-51.79	-51.75	-51.69	-55.44	-55.41	-55.39
22	C: Latitude	27.41	27.74	28.19	12.37	12.68	12.99
23	C: Longitude	-51.84	-51.80	-51.74	-55.47	-55.44	-55.41
24	D: Latitude	27.55	27.88	28.34	12.47	12.78	13.09
25	D: Longitude	-53.73	-53.70	-53.67	-56.82	-56.80	-56.78
26	Scale Factor ( $\times 10^6$ )	4.31	4.28	4.24	5.55	5.53	5.51
27	Tilt Distance (mm)	63.70	65.03	67.08	103.21	103.28	103.45
	WIDE ANGLE						
	CORNER COORD. (deg)						
28	A: Latitude	29.58	29.93	30.41	14.07	14.39	14.70
29	A: Longitude	-54.93	-54.93	-54.92	-57.68	-57.67	-57.66
30	B: Latitude	29.08	29.43	29.90	13.63	13.95	14.26
31	B: Longitude	-50.46	-50.40	-50.31	-54.57	-54.54	-54.50
32	C: Latitude	25.99	26.31	26.76	11.30	11.61	11.91
33	C: Longitude	-50.87	-50.83	-50.76	-54.78	-54.75	-54.72
34	D: Latitude	26.19	26.51	26.96	11.36	11.67	11.97
35	D: Longitude	-55.11	-55.09	-55.08	-57.89	-57.87	-57.84
36	Scale Factor ( $\times 10^6$ )	0.57	0.56	0.56	0.73	0.73	0.72
37	Tilt Distance (mm)	8.35	8.53	8.80	13.54	13.55	13.57
	PRINCIPAL POINT						
38	Latitude (deg)	27.69	28.02	28.48	12.59	12.89	13.20
39	Longitude (deg)	-52.74	-52.71	-52.67	-56.11	-56.08	-56.06
40	Slant Distance (km)	141	142	144	110	110	111

\*AAP



LINE	V-51 *								
	213	214	215	216	217				
1	230:21	230:21	230:21	230:21	230:21				
2	39:57.4	40:02.5	40:07.7	40:13.0	40:18.4				
3	109	110	110	111	111				
4	77	79	81	83	85				
5	13.39	13.68	13.97	14.27	14.58				
6	-55.41	-55.39	-55.36	-55.33	-55.30				
7	9.65	9.68	9.72	9.77	9.84				
8	280.82	282.52	284.24	285.98	287.72				
9	186.04	187.76	189.49	191.25	193.01				
10	85.53	85.57	85.62	85.67	85.72				
11	92.07	92.16	92.25	92.34	92.43				
12	75.44	75.42	75.41	75.40	75.38				
13	10.26	10.30	10.35	10.40	10.47				
14	65.30	65.30	65.30	65.30	65.30				
15	10.13	10.12	10.10	10.08	10.07				
16	0.060	0.060	0.060	0.060	0.060				
17	0.04	0.04	0.04	0.04	0.04				
18	13.73	14.04	14.35	14.67	15.00				
19	-56.73	-56.71	-56.69	-56.67	-56.64				
20	13.61	13.92	14.23	14.55	14.88				
21	-55.36	-55.33	-55.30	-55.27	-55.24				
22	13.29	13.60	13.91	14.23	14.55				
23	-55.39	-55.36	-55.33	-55.30	-55.27				
24	13.39	13.70	14.01	14.33	14.65				
25	-56.76	-56.74	-56.71	-56.69	-56.67				
26	5.49	5.47	5.45	5.43	5.40				
27	103.71	104.07	104.52	105.09	105.77				
28	15.01	15.33	15.66	15.99	16.32				
29	-57.64	-57.63	-57.62	-57.61	-57.60				
30	14.57	14.88	15.20	15.53	15.86				
31	-54.47	-54.44	-54.40	-54.36	-54.32				
32	12.21	12.52	12.83	13.14	13.47				
33	-54.69	-54.66	-54.63	-54.60	-54.57				
34	12.27	12.58	12.89	13.21	13.53				
35	-57.82	-57.80	-57.78	-57.76	-57.74				
36	0.72	0.72	0.71	0.71	0.71				
37	13.60	13.65	13.71	13.78	13.87				
38	13.50	13.81	14.12	14.44	14.77				
39	-56.03	-56.01	-55.98	-55.96	-55.93				
40	111	112	112	112	113				

\*AAP

LINE	SITE NUMBER	V-A 1					
	FRAME NUMBER	5	6	7	8	9	10
	EXPOSURE TIME (GMT)						
1	Day: Hour	218:11	218:11	218:11	218:11	218:11	218:11
2	Minute: Second	22:02.7	22:05.4	22:08.1	22:10.8	22:13.5	22:16.1
	S/C POSITION						
3	Altitude (km)	2642	2644	2646	2647	2649	2651
4	Altitude Rate (m/sec)	660	660	660	660	659	659
5	Latitude (deg)	59.01	58.98	58.95	58.92	58.89	58.86
6	Longitude (deg)	-81.41	81.40	-81.39	-81.38	-81.37	-81.36
	S/C ORIENTATION						
7	Tilt Angle (deg)	9.22	9.20	9.19	9.17	9.16	9.15
8	Tilt Azimuth (deg)	287.40	287.24	287.08	286.91	286.75	286.59
9	Swing Angle (deg)	91.42	91.25	91.08	90.90	90.73	90.56
10	North Deviation (deg)	8.53	8.44	8.35	8.26	8.18	8.09
	PHOTOGRAPHY						
	ILLUMINATION						
11	Sun Azimuth (deg)	260.64	260.71	260.79	260.86	260.94	261.01
12	Incident Angle (deg)	82.99	83.01	83.04	83.07	83.10	83.12
13	Emission Angle (deg)	23.80	23.77	23.75	23.72	23.69	23.66
14	Phase Angle (deg)	106.79	106.79	106.79	106.79	106.79	106.79
15	Alpha (deg)	-23.80	-23.77	-23.74	-23.72	-23.69	-23.66
16	QUAL Albedo	0.099	0.099	0.099	0.099	0.099	0.099
17	Shutter Speed (sec)	0.04	0.04	0.04	0.04	0.04	0.04
	PHOTOGRAPHS						
	TELEPHOTO						
	CORNER COORD. (deg)						
18	A: Latitude	77.22	77.16	77.10	77.03	76.97	76.91
19	A: Longitude	-107.24	-107.05	-106.85	-106.66	-106.47	-106.30
20	B: Latitude	44.14	44.06	43.97	43.88	43.79	43.71
21	B: Longitude	-102.04	-102.01	-101.98	-101.94	-101.91	-101.88
22	C: Latitude	42.12	42.04	41.96	41.87	41.79	41.70
23	C: Longitude	-114.65	-114.61	-114.57	-114.53	-114.49	-114.45
24	D: Latitude	74.10	74.07	74.04	74.02	73.99	73.96
25	D: Longitude	-144.19	-143.92	-143.64	-143.37	-143.10	-142.84
26	Scale Factor ( $\times 10^6$ )	0.22	0.22	0.22	0.22	0.22	0.22
27	Tilt Distance (mm)	98.99	98.83	98.68	98.52	98.36	98.22
	WIDE ANGLE						
	CORNER COORD. (deg)						
28	A: Latitude	48.93	49.14	49.34	49.52	49.69	49.85
29	A: Longitude	39.82	39.53	39.25	38.98	38.71	38.46
30	B: Latitude	3.71	3.23	2.72	2.19	1.63	1.06
31	B: Longitude	-74.82	-74.78	-74.75	-74.70	-74.66	-74.62
32	C: Latitude	(OFF)	(OFF)	(OFF)	(OFF)	(OFF)	(OFF)
33	C: Longitude	(LIMB)	(LIMB)	(LIMB)	(LIMB)	(LIMB)	(LIMB)
34	D: Latitude	67.54	67.72	55.69	55.75	54.97	55.21
35	D: Longitude	85.51	85.37	100.16	100.38	100.64	100.84
36	Scale Factor ( $\times 10^6$ )	0.03	0.03	0.03	0.03	0.03	0.03
37	Tilt Distance (mm)	12.98	12.96	12.94	12.92	12.90	12.88
	PRINCIPAL POINT						
38	Latitude (deg)	60.28	60.21	60.15	60.08	60.01	59.95
39	Longitude (deg)	-110.41	-110.33	-110.26	-110.18	-110.10	-110.03
40	Slant Distance (km)	2733	2735	2737	2738	2740	2741

LINE	V-A1		V-A2						
	11	12	13	14	15	16	17	18	19
1	218:11	218:11	218:13	218:13	218:13	218:13	218:13	218:13	218:13
2	22:18.7	22:21.5	33:25.1	33:27.8	33:30.5	33:33.2	33:35.9	33:38.6	33:41.2
3	2653	2655	5752	5753	5753	5754	5754	5754	5755
4	659	659	166	166	165	165	165	165	165
5	58.83	58.79	11.15	11.14	11.13	11.12	11.11	11.10	11.09
6	-81.35	-81.34	-74.85	-74.85	-74.85	-74.85	-74.85	-74.85	-74.85
7	9.13	9.12	7.74	7.74	7.73	7.73	7.73	7.73	7.72
8	286.43	286.26	277.13	277.06	276.98	276.90	276.82	276.75	276.67
9	90.39	90.20	90.11	90.04	89.96	89.88	89.80	89.72	89.65
10	8.01	7.92	359.26	359.23	359.20	359.17	359.15	359.12	359.09
11	261.08	261.16	270.72	270.72	270.73	270.73	270.74	270.74	270.74
12	83.15	83.18	86.53	86.54	86.55	86.56	86.57	86.58	86.59
13	23.63	23.60	35.46	35.45	35.44	35.43	35.43	35.42	35.41
14	106.79	106.79	121.99	121.99	121.99	121.99	121.99	121.99	121.99
15	-23.64	-23.61	-35.46	-35.45	-35.44	-35.44	-35.43	-35.42	-35.41
16	0.099	0.099	0.110	0.110	0.110	0.110	0.110	0.110	0.110
17	0.04	0.04	0.04	0.04	0.04	0.04	0.04	0.04	0.04
18	76.85	76.78	53.93	53.86	53.79	53.72	53.65	53.58	53.51
19	-106.12	-105.93	-99.41	-99.36	-99.30	-99.24	-99.19	-99.13	-99.08
20	43.62	43.53	-27.60	-27.68	-27.75	-27.83	-27.91	-27.98	-28.05
21	-101.84	-101.81	-101.99	-102.01	-102.04	-102.06	-102.09	-102.11	-102.14
22	41.62	41.53	-26.62	-26.78	-26.95	-27.13	-27.32	-27.54	-27.78
23	-114.41	114.37	-138.04	-138.34	-138.67	-139.04	-139.45	-139.93	-140.49
24	73.93	73.90	48.08	48.03	47.98	47.93	47.88	47.82	48.27
25	-142.58	-142.31	-151.98	-151.23	-150.58	-149.98	-149.43	-148.92	-154.33
26	0.22	0.22	0.10	0.10	0.10	0.10	0.10	0.10	0.10
27	98.07	97.91	82.88	82.86	82.83	82.81	82.78	82.76	82.74
28	50.00	50.16	26.58	26.53	26.49	26.45	26.40	26.36	26.31
29	38.21	37.95	-8.45	-8.50	-8.56	-8.62	-8.67	-8.73	-8.78
30	0.44	-0.27	-27.31	-27.42	-27.52	-27.63	-27.74	-27.84	-27.95
31	-74.57	-74.52	-22.36	-22.24	-22.11	-21.97	-21.84	-21.70	-21.57
32	(OFF)	(OFF)	-4.16	-4.22	-4.27	-4.32	-4.37	-4.43	-4.48
33	(LIMB)	(LIMB)	-30.35	-30.33	-30.31	-30.29	-30.27	-30.25	-30.23
34	(OFF)	(OFF)	9.58	9.53	9.48	9.44	9.39	9.34	9.30
35	(LIMB)	(LIMB)	-27.16	-27.16	-27.16	-27.15	-27.15	-27.15	-27.14
36	0.03	0.03	0.01	0.01	0.01	0.01	0.01	0.01	0.01
37	12.86	12.84	10.87	10.87	10.86	10.86	10.86	10.85	10.85
38	59.89	59.82	13.17	13.13	13.08	13.04	12.99	12.95	12.90
39	-109.96	-109.88	-103.16	-103.15	-103.14	-103.13	-103.12	-103.11	-103.11
40	2743	2744	6006	6007	6007	6007	6008	6008	6008

LINE	SITE NUMBER	V-A2	V-A3	V-A4	V-A6	V-A7.1	V-A8
	FRAME NUMBER	20	21	22	24	25	26
	EXPOSURE TIME (GMT)						
1	Day: Hour	218:13	218:17	219:00	219:13	219:20	220:01
2	Minute: Second	33:43.9	17:6.4	34:59.7	50:51.4	50:19.4	42:05.1
	S/C POSITION						
3	Altitude (km)	5755	3343	5107	5006	2549	5067
4	Altitude Rate (m/sec)	165	-575	-312	341	690	-330
5	Latitude (deg)	11.08	-50.70	-25.64	24.03	58.74	-25.61
6	Longitude (deg)	-74.85	-69.31	-77.30	-89.35	-99.81	-90.85
	S/C ORIENTATION						
7	Tilt Angle (deg)	7.72	16.99	10.08	8.49	9.28	9.88
8	Tilt Azimuth (deg)	276.60	188.71	258.84	281.19	284.47	258.84
9	Swing Angle (deg)	89.57	26.77	90.25	89.70	89.62	89.83
10	North Deviation (deg)	359.06	282.50	355.89	0.90	8.26	355.81
	PHOTOGRAPHY						
	ILLUMINATION						
11	Sun Azimuth (deg)	270.75	346.87	275.57	268.57	260.73	275.32
12	Incident Angle (deg)	86.60	85.52	82.50	83.78	82.85	82.99
13	Emission Angle (deg)	35.40	58.67	43.55	34.97	23.42	42.23
14	Phase Angle (deg)	121.99	119.84	126.06	118.75	106.28	125.22
15	Alpha (deg)	-35.40	-36.75	-43.55	-34.97	-23.43	-42.23
16	QUAL Albedo	0.110	0.109	0.108	0.109	0.100	0.099
17	Shutter Speed (sec)	0.04	0.04	0.04	0.04	0.04	0.04
	PHOTOGRAPHS						
	TELEPHOTO						
	CORNER COORD. (deg)						
18	A: Latitude	53.44	-62.57	8.66	60.50	75.63	7.91
19	A: Longitude	-99.02	-83.47	-110.18	-113.91	-124.22	-122.12
20	B: Latitude	-28.13	-75.08	-63.08	-7.96	43.80	-62.84
21	B: Longitude	-102.16	101.52	-119.30	-115.03	-119.53	-130.80
22	C: Latitude	-28.11	-71.29	-45.36	-15.84	41.85	-47.41
23	C: Longitude	-141.31	149.53	-167.41	-144.98	-131.59	-172.88
24	D: Latitude	48.23	-62.24	8.99	56.64	73.01	6.42
25	D: Longitude	-153.09	-107.72	-142.61	-171.58	-156.73	-149.80
26	Scale Factor ( $\times 10^6$ )	0.10	0.15	0.11	0.12	0.23	0.11
27	Tilt Distance (mm)	82.71	186.37	108.40	91.10	99.65	106.28
	WIDE ANGLE						
	CORNER COORD. (deg)						
28	A: Latitude	26.27	-29.14	31.22	38.16	58.18	30.36
29	A: Longitude	-8.84	-50.67	-49.86	-3.45	12.53	-62.56
30	B: Latitude	-28.06	(OFF)	-46.24	-36.59	6.62	-46.02
31	B: Longitude	-21.42	(LIMB)	-2.51	-50.07	-92.86	-14.17
32	C: Latitude	-4.53	(OFF)	-22.39	7.78	(OFF)	-22.54
33	C: Longitude	-30.20	(LIMB)	-45.32	-56.78	(LIMB)	-58.23
34	D: Latitude	9.25	-16.02	-11.44	18.71	(OFF)	-11.66
35	D: Longitude	-27.14	-141.85	-50.03	-52.01	(LIMB)	-62.92
36	Scale Factor ( $\times 10^6$ )	0.01	0.02	0.01	0.02	0.03	0.01
37	Tilt Distance (mm)	10.85	24.44	14.22	11.95	13.07	13.94
	PRINCIPAL POINT						
38	Latitude (deg)	12.86	-83.88	-27.21	26.32	59.38	-27.30
39	Longitude (deg)	-103.10	-178.75	-114.78	-118.55	-127.50	-127.05
40	Slant Distance (km)	6009	3955	5480	5246	2636	5418

LINE	V-A10	V-A11.2	V-A12	V-A13	V-A14	V-A15	V-A16	V-A17.1	V-A18.1
	28	29	30	31	32	39	43	53	65
1	220:14	220:21	221:02	221:09	221:15	222:10	223:03	223:18	224:11
2	52:20.1	51:31.5	43:35.0	32:18.9	57:41.3	52:51.5	58:21.3	40:05.8	49:22.2
3	5010	2546	5067	1361	1395	1250	1189	1188	1190
4	340	691	-330	188	164	250	-277	278	-277
5	24.23	59.09	-25.32	26.15	22.70	37.17	-44.87	42.59	-44.68
6	-103.16	-113.56	-104.74	-113.59	-116.75	-128.86	-129.45	-147.00	-147.26
7	8.45	10.38	9.81	21.59	20.96	26.24	20.23	25.01	20.92
8	280.53	284.33	259.84	280.48	280.31	282.17	251.66	297.10	252.91
9	89.45	90.23	90.16	89.06	90.19	88.98	90.00	107.25	89.94
10	1.17	11.90	355.77	358.69	358.78	2.99	1.92	12.41	0.36
11	268.16	256.57	275.50	270.97	271.45	264.38	267.39	262.47	269.28
12	82.94	80.44	82.36	88.70	89.66	80.64	94.34	81.51	92.63
13	34.78	26.36	41.84	41.01	40.14	49.48	35.61	45.37	36.98
14	117.73	106.81	124.20	129.71	129.81	130.12	129.95	125.32	129.62
15	-34.78	-26.36	-41.84	-41.01	-40.14	-49.47	-35.61	-44.01	-36.98
16	0.099	0.108	0.108	0.108	0.120*	0.108	0.108	0.108	0.100*
17	0.04	0.04	0.04	0.04	0.04	0.04	0.04	0.04	0.04
18	60.38	75.66	8.68	37.07	33.98	47.53	-39.78	57.84	-39.28
19	-127.93	-146.76	-135.45	-132.03	-134.42	-155.64	-149.23	-175.65	-167.62
20	-8.10	43.94	-61.98	18.77	15.34	29.64	-55.31	40.97	-54.98
21	-128.53	-135.52	-143.85	-133.11	-135.41	-154.57	-147.33	-169.06	-166.51
22	-16.17	41.34	-47.12	18.01	14.68	27.69	-56.05	39.90	-55.55
23	-158.37	-147.83	-176.52	-140.08	-142.23	-163.34	-156.28	-176.36	-175.69
24	55.84	71.75	6.98	37.97	34.95	47.61	-39.37	57.57	-38.68
25	162.80	-177.88	-162.64	-140.24	-142.39	-167.15	-155.82	170.46	-174.33
26	0.12	0.23	0.11	0.39	0.38	0.39	0.46	0.43	0.45
27	90.62	111.74	105.46	241.42	233.66	300.71	224.77	284.53	233.20
28	37.95	61.49	31.56	44.61	42.06	54.91	-29.60	67.76	-29.41
29	-15.41	0.47	-74.84	-111.61	-114.52	-131.80	-136.24	-145.29	-154.20
30	-35.21	10.59	-46.21	7.65	4.02	20.62	-60.26	33.28	-60.45
31	-64.01	-108.04	-28.27	-119.53	-121.77	-139.06	-121.07	-153.35	-140.51
32	7.96	(OFF)	-22.36	0.99	-10.79	3.44	-65.24	18.77	-64.16
33	-70.27	(LIMB)	-71.90	-145.23	-161.90	-174.02	139.40	166.08	121.55
34	18.93	(OFF)	-11.40	56.88	51.50	61.48	-14.82	70.55	-14.06
35	-65.56	(LIMB)	-76.43	-179.50	-150.76	167.41	-177.92	115.55	165.19
36	0.02	0.03	0.01	0.05	0.05	0.05	0.06	0.06	0.06
37	11.88	14.65	13.83	31.66	30.64	39.44	29.48	37.32	30.58
38	26.22	59.27	-26.57	28.03	24.75	38.42	-47.68	48.69	-47.19
39	-132.25	-145.04	-140.45	-135.32	-137.60	-158.35	-151.41	-174.98	-170.17
40	5247	2656	5411	1570	1597	1551	1333	1431	1347

\* ALBEDO ARRIVED AT BY STOCHASTIC METHODS

L <sub>INE</sub>	SITE NUMBER	V-A19	V-A20	V-A21	V-A22	V-A23	V-A24
	FRAME NUMBER	79	85	103	124	158	163
	EXPOSURE TIME (GMT)						
1	Day: Hour	225:02	225:18	226:10	227:02	228:10	228:19
2	Minute: Second	34:32.3	29:40.0	24:50.7	20:03.9	10:05.7	42:58.5
	S/C POSITION						
3	Altitude (km)	1242	1237	1234	1234	1230	1228
4	Altitude Rate (m/sec)	254	256	257	257	256	257
5	Latitude (deg)	37.80	37.84	37.88	37.84	37.80	37.75
6	Longitude (deg)	-163.83	-172.42	178.77	170.04	152.70	147.31
	S/C ORIENTATION						
7	Tilt Angle (deg)	25.42	25.24	24.85	24.42	23.64	23.70
8	Tilt Azimuth (deg)	281.04	280.84	280.55	280.20	279.49	278.93
9	Swing Angle (deg)	89.48	89.62	89.82	89.90	89.95	89.71
10	North Deviation (deg)	3.93	4.06	4.23	4.30	4.38	4.49
	PHOTOGRAPHY						
	ILLUMINATION						
11	Sun Azimuth (deg)	263.62	263.58	263.57	263.63	263.74	263.45
12	Incident Angle (deg)	79.81	79.78	79.76	79.80	79.89	79.45
13	Emission Angle (deg)	47.40	46.87	45.93	44.99	43.23	43.30
14	Phase Angle (deg)	127.22	126.65	125.70	124.79	123.12	122.76
15	Alpha (deg)	-47.40	-46.87	-45.93	-44.99	-43.23	-43.30
16	QUAL Albedo	0.108	0.10*	0.10*	0.10*	0.108	0.10*
17	Shutter Speed (sec)	0.04	0.04	0.04	0.04	0.04	0.04
	PHOTOGRAPHS						
	TELEPHOTO						
	CORNER COORD. (deg)						
18	A: Latitude	47.64	47.57	47.48	47.32	47.01	46.78
19	A: Longitude	170.41	162.19	153.99	145.90	129.78	124.36
20	B: Latitude	30.14	30.21	30.29	30.24	30.18	29.97
21	B: Longitude	171.95	163.78	155.63	147.54	131.38	126.03
22	C: Latitude	28.33	28.46	28.61	28.64	28.71	28.46
23	C: Longitude	163.84	155.84	147.94	140.07	124.29	118.95
24	D: Latitude	47.59	47.52	47.43	47.28	46.97	46.70
25	D: Longitude	159.67	151.68	143.81	136.03	120.47	115.11
26	Scale Factor ( $\times 10^6$ )	0.40	0.41	0.41	0.41	0.42	0.42
27	Tilt Distance (mm)	289.95	287.54	282.45	276.96	267.07	267.71
	WIDE ANGLE						
	CORNER COORD. (deg)						
28	A: Latitude	55.40	55.37	55.36	55.26	55.03	54.86
29	A: Longitude	-166.49	-174.98	176.50	168.13	151.42	145.79
30	B: Latitude	21.38	21.52	21.62	21.57	21.51	21.37
31	B: Longitude	-172.77	178.94	170.64	162.41	145.97	140.64
32	C: Latitude	9.80	10.68	11.71	12.33	3.38	3.50
33	C: Longitude	158.89	151.54	144.41	137.04	109.58	104.87
34	D: Latitude	61.14	60.99	60.81	60.58	57.72	57.48
35	D: Longitude	138.92	132.10	125.74	119.40	72.44	68.63
36	Scale Factor ( $\times 10^6$ )	0.05	0.05	0.05	0.05	0.06	0.06
37	Tilt Distance (mm)	38.03	37.71	37.04	36.32	35.03	35.11
	PRINCIPAL POINT						
38	Latitude (deg)	38.68	38.68	38.67	38.57	38.40	38.17
39	Longitude (deg)	168.09	159.94	151.83	143.79	127.75	122.37
40	Slant Distance (km)	1515	1503	1488	1477	1453	1451

LINE	V-A25			V-A9					
	181			27					
1	229.17			220:09					
2	56:42.4			05:00.2					
3	1179			5871					
4	278			-140					
5	41.62			-11.22					
6	134.25			-96.46					
7	22.95			--					
8	278.04			--					
9	89.41			--					
10	5.53			--					
11	262.20			--					
12	79.20			--					
13	40.88			--					
14	120.09			--					
15	-40.88			--					
16	0.108			--					
17	0.04			0.01					
18	49.79			EARTH PHOTO					
19	111.89								
20	33.90								
21	113.95								
22	32.47								
23	107.32								
24	49.53								
25	103.10								
26	0.44								
27	258.36								
28	57.74								
29	133.31								
30	25.77								
31	128.40								
32	11.49								
33	96.55								
34	59.94								
35	69.57								
36	0.06								
37	33.88								
38	41.62								
39	110.19								
40	1372								





## 6.0 Photographic Operations

### 6.1 MISSION PLANNING SUMMARY

Mission design required acquisition of 213 frames of photography from three different lunar ellipses. In this respect, the design differed from all previous Lunar Orbiter missions. To accomplish the desired photography, the spacecraft was to be injected into an initial ellipse having a 6,000-kilometer apolune and a 200-kilometer perilune. A total of 19 frames was scheduled for the initial ellipse, 17 of which were to cover areas of the farside, the remaining two to satisfy the film-set constraint. A transfer maneuver was then to be performed to reduce perilune altitude to 100 kilometers. In this intermediate ellipse, six additional frames of farside photography were to be taken and one frame for film-set constraint. A second transfer maneuver was then to be performed to place the spacecraft in a final ellipse having a 1,500-kilometer apolune and a 100-kilometer perilune altitude. Photography of the 45 selected nearside targets using the 187 remaining frames was to be accomplished from the final ellipse.

Priority readout was to be conducted between photo exposures to provide information and data for mission control purposes. Complete readout of the first 38 frames was planned for priority readout. Final readout was to follow exposure and processing of the 213 planned photographs.

Table 6-1 consists of a summary of the primary orbital parameters of the three Mission V ellipses and, for comparison, of the four earlier missions.

### 6.2 MISSION CONDUCT

The photographic portion of Mission V progressed as planned; no significant deviations from the flight plan were required. Small changes to the flight plan were effected in real time, primarily to ensure adherence to the planned flight profile. No special workaround procedures were required, since no significant spacecraft problems developed prior to completion of final readout.

The only significant anomaly experienced during the mission occurred after completion of the photographic phase. During film rewind for final repositioning following completion of photography, the leader parted approximately 1 foot from the splice to the film. This failure precluded any additional readout during the extended-mission phase.

#### 6.2.1 Initial Ellipse

The parameters of the initial orbit were: perilune altitude, 202.0 kilometers; apolune altitude, 6,030.3 kilometers; period, 505 minutes; and inclination, 85.1 degrees.

Table 6-1: Primary Orbital Parameters—Lunar Orbiter Missions

Parameter		L.O.V			L.O.	L.O.	L.O.	L.O.
		Initial	Inter.	Final	IV	III	II	I
Orbit period	(hrs)	8	8	3	12	3	3	3
	(min)	30	22	11	1	28	28	26
	(sec)	29.1	40	14	—	—	34	21
Inclination	(deg)	85	85	85	85	21	12	12
Perilune altitude	(km)	200	100	100	2700	55	50	50
Apolune altitude	(km)	6,092	6,092	1,500	6,110	1,850	1,850	1,850
Time in sunlight	(%)	100	100	100	100	75	75	75
Earth occultation	(%)	2	0	15	0	29	29	29

Shortly after injecting into lunar orbit, the TWTA was turned on, and at 18:24 on August 5 the Goldstone test film was read out. All parameters were normal except for unexplained momentary loss of scan lines that caused occasional random loss of seven scan lines.

The first site was photographed at 11:22 on August 6, and subsequent photography in this ellipse was conducted according to plan. Four farside sites, exposing 18 frames, were photographed. All camera pointing maneuvers were two-axis (H roll - pitch) and were chosen so that the camera window was shaded by the thermal door. Sites and frames exposed are listed in Table 6-2.

**Table 6-2: Initial-Ellipse Photography**

<u>Site</u>	<u>Orbit</u>	<u>Frame Numbers</u>
VA-1	2	5 - 12
VA-2	2	13 - 20
VA-3	3	21
VA-4	4	22
VA-5	4	23 (blank; film-set)

Transfer from initial to intermediate ellipse was executed at 08:43:48.7 GMT on August 7 following 40 hours in the initial ellipse.

### 6.2.2 Intermediate Ellipse

The first orbit determination after transfer to the intermediate ellipse indicated that the maneuver was near nominal. Table 6-3 shows a comparison of planned and achieved orbital elements.

During the intermediate orbit, photography consisted of six additional farside photographs from near apolune and one photograph of the Earth. All exposures were taken as single frames. As in the initial ellipse, the camera was pointed using a two-axis maneuver (H roll - pitch). The camera window was shaded by the open thermal door for all farside photographs. For the Earth

**Table 6-3: Comparison of Designed and Achieved Intermediate-Ellipse Elements**

<u>Element</u>	<u>Design Value</u>	<u>Achieved Value</u>
Perilune altitude	101.33 kilometers	100.4 kilometers
Apolune altitude	6,065.64 kilometers	6,066.8 kilometers
Inclination	84.62 degrees	84.61 degrees
Argument of perilune	1.38 degrees	1.34 degrees
Longitude of ascending node	95.90 degrees	95.90 degrees

photograph, the camera window was on the shaded side of the spacecraft. Table 6-4 summarizes photography from the intermediate ellipse.

Periodic processing and two readout sequences were conducted during this ellipse as planned. All data indicated continued good-quality photographs, although sporadic scan-line dropouts occurred, as shown in later readouts.

**Table 6-4: Intermediate-Ellipse Photography**

<u>Site</u>	<u>Orbit</u>	<u>Frame Numbers</u>
VA-6	5	24
VA-7.1	6	25
VA-8	7	26
VA-9 (Earth)	8	27
VA-10	8	28
VA-11.2	9	29
VA-12	10	30

Transfer from intermediate to final ellipse was made August 9 after the spacecraft had been in the intermediate orbit nearly 2 days.

### 6.2.3 Final Ellipse

Transfer from the intermediate ellipse took place on August 9, starting at 05:08:32.65 GMT. Comparison of predicted and observed transfer doppler tracking data indicated that the transfer was near nominal. The first orbit determination after transfer confirmed this estimate. A comparison of planned and obtained orbit elements after transfer is shown in Table 6-5.

During the mission, orbital elements undergo some change caused by characteristics of the lunar gravitational field. Changes in perilune altitude, inclination, ascending node longitude, and perilune argument are plotted in Figures 6-1 through 6-4.

#### 6.2.3.1 Photographic Coverage Design

A total of 41 nearside sites was covered during 50 photographic passes in the final ellipse. Five sites were photographed by multiple-pass coverage to obtain telephoto stereo coverage, or broader areal coverage including stereo. In addition, 12 farside photographs were taken from near apolune.

Spacecraft maneuvers for nearside photography were based on the requirements that the camera axis must point directly at the specified target position at the midpoint of a sequence of exposures, and that image motion compensation

be provided by aligning the spacecraft X-axis in the direction of travel. One exception was made for Site V-25, the Alpine Valley, for which the frame orientation was designed so that the long axis of the telephoto frame was parallel to the valley.

Timing of the photographs was constrained by three ground rules:

- Spacecraft was to be at the point where the ground track was closest to the target for all but the westerly oblique photographs and Site V-25;
- Site V-25 was to be taken when the spacecraft crossed the extension of the valley axis;
- Westerly oblique photographs were to be taken when the spacecraft was at the latitude of the target.

Farside photographs required roll-pitch maneuvers to point the camera at the specified target position. Exposures were to be made when spacecraft was at a specified latitude.

#### 6.2.3.2 Photographic Phase

Site photography was conducted on almost every orbit of the final ellipse, beginning with Orbit II 4.5 hours after the second transfer. All planned photography was accomplished, the film processing schedule was maintained, and

**Table 6-5: Comparison of Designed and Achieved Final-Ellipse Elements**

Element	Values		
	Design	First Estimate	Best Estimate
Perilune altitude (km)	99.1	98.51	98.93
Apolune altitude (km)	1,501.9	1,499.0	1,499.4
Inclination (deg)	84.76	84.74	84.76
Longitude of ascending node (deg)	71.40	71.39	71.38
Argument of perilune (deg)	1.61	1.80	1.88
Period (min)	191.0	—	190.9

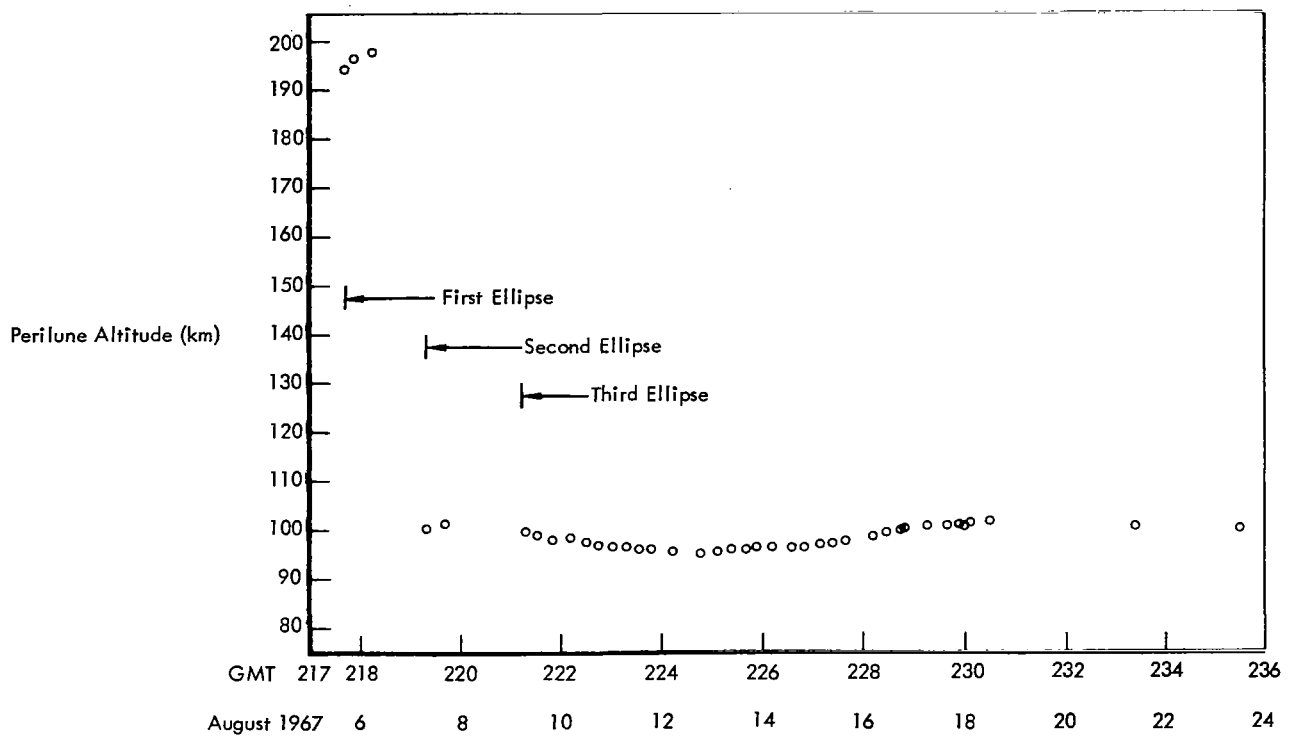


Figure 6-1: Perilune Altitude vs Time

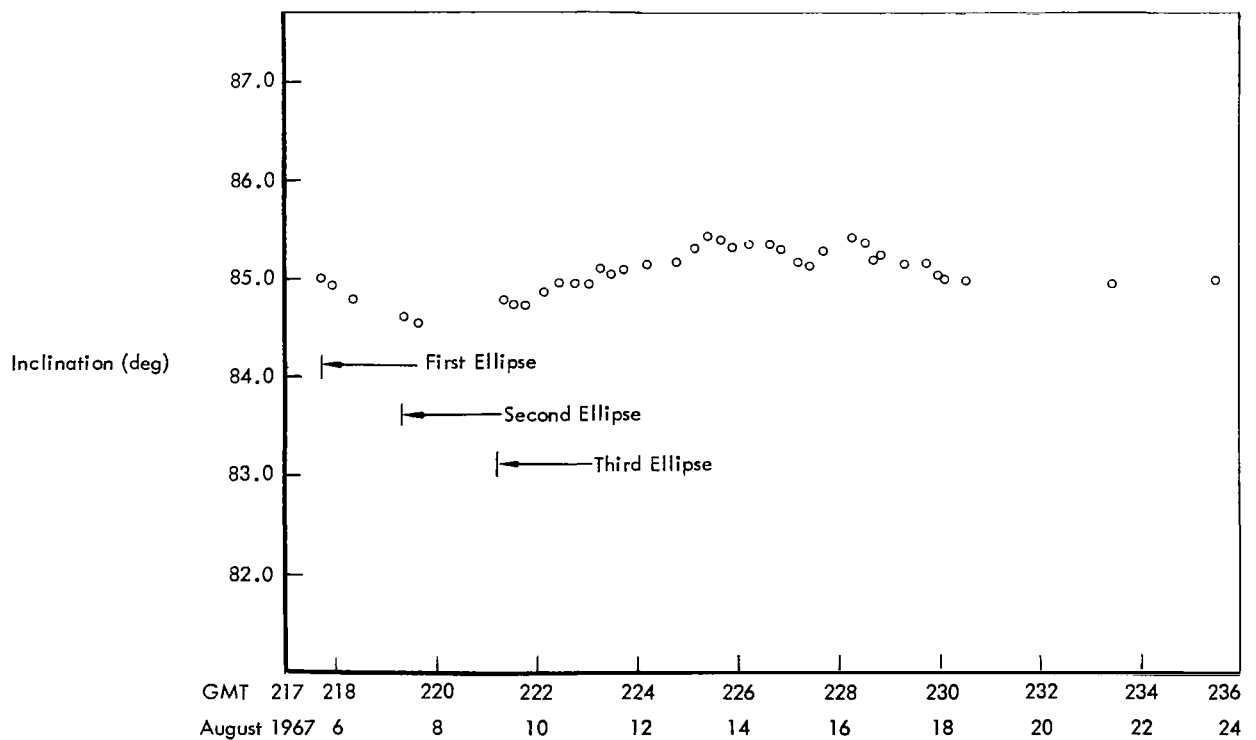


Figure 6-2: Orbit Inclination vs Time

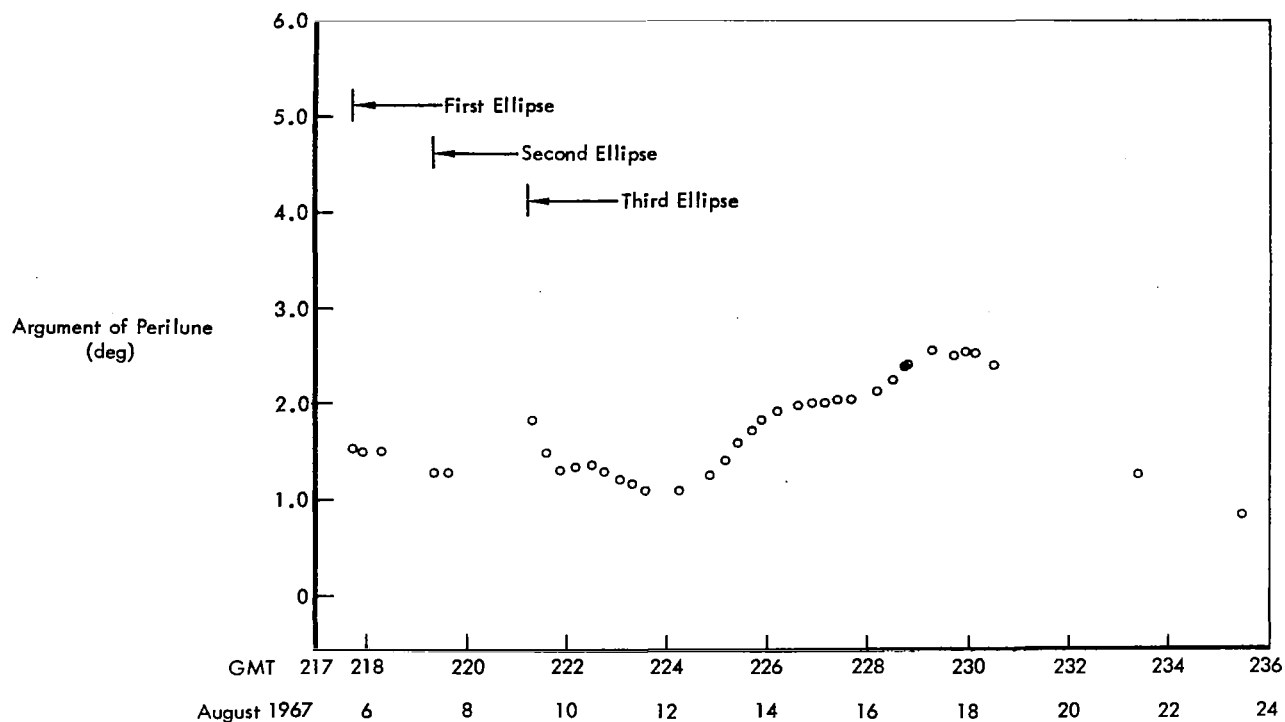


Figure 6-3: Argument of Perilune History

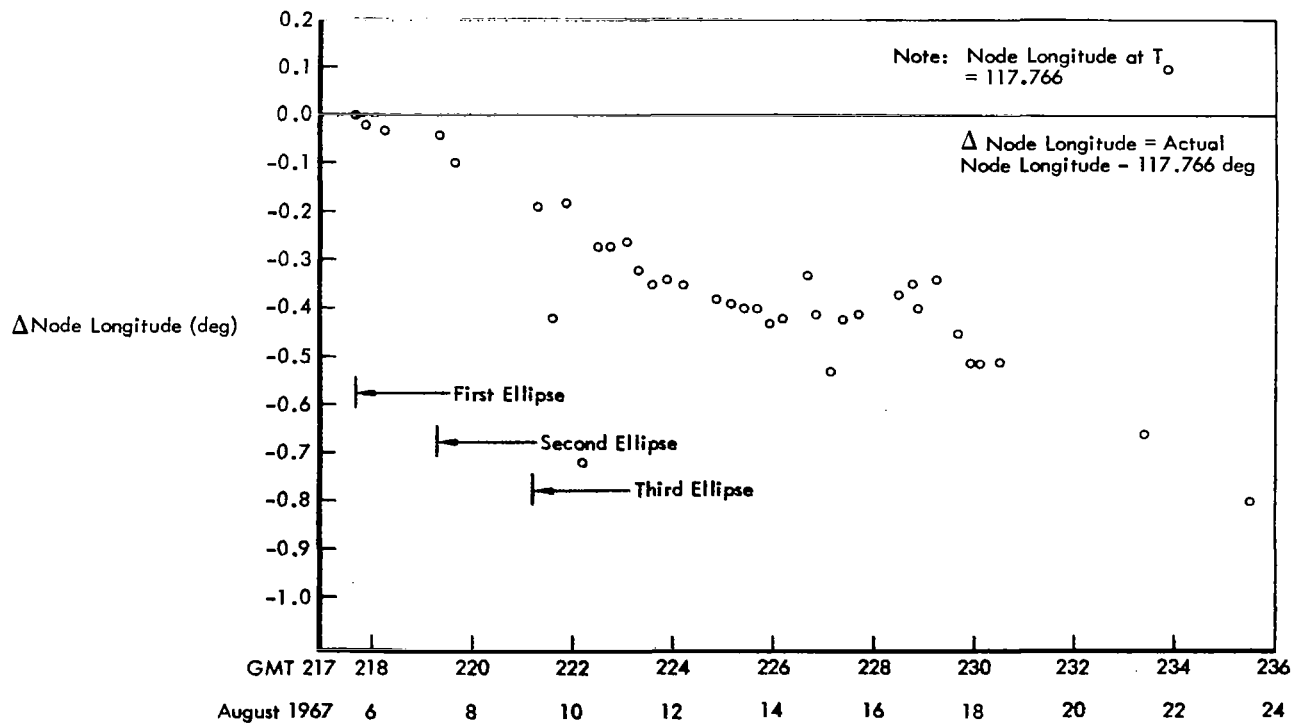


Figure 6-4: Ascending-Node Longitude History

a modified priority readout schedule was met. The readout schedule was modified during mission operations to eliminate readout of redundant data and scheduled readout periods of less than 10 minutes duration.

Photography of the last site, Site V-51, was completed in Orbit 83 as scheduled. It was decided to delay cutting the Bimat until after readout of some data from Sites V-48 and -49. The processing and readout schedule was modified to obtain this additional priority readout during Orbits 83 and 84, and the cut-Bimat sequence rescheduled for Orbit 85. The cut-Bimat sequence was initiated in a normal manner by starting processing and loading a "Bimat-cut" command in the programmer to be executed 34 minutes later. Seven minutes before the Bimat-cut sequence was to occur, a Bimat-clear signal was received by telemetry, indicating that the Bimat supply was exhausted. It was found, subsequently, that the supply of Bimat loaded prior to launch was about 5 feet less than that required. Because of the short Bimat, Wide-Angle Frame 217 was not processed and Wide-Angle Frame 216 was degraded. No telephoto frames were lost. Very little data was lost, since Site V-51 was photographed as an eight-frame sequence in the fast mode.

#### 6.2.3.3 Final Readout

Final readout was started in Orbit 85 and continued normally until completion. A readout of about 2.5 hours' duration during each orbit was scheduled. By Orbit 137, final readout reached the point where priority readout had provided complete recovery and thus all photography had been reconstructed. Final readout was continued, however, to reposition all film on the film supply reel for permanent storage, preserve readout capability, and move the splice onto the reel to remove tension on the splice. Before this operation was completed, the leader apparently parted in or near the readout gate about a foot from the splice. This failure eliminated the possibility of later rereading out the film, but had no effect on the success of the mission.

### 6.3 PHOTOGRAPHIC CONTROL

Exposure and photo subsystem control pro-

cedures were basically the same as those used during Mission III. Site photography followed the mission plan with only a few minor changes.

#### 6.3.1 Exposure Control

Exposure control for Mission V photography was accomplished by careful selection of shutter speeds, together with premission studies relating site illumination, site location, and orbit characteristics that established the best opportunity for photography of each site. Selection of the shutter speed was based on the results of a computer evaluation, Photo Quality Prediction Program (QUAL). Spacecraft film density predictions obtained from QUAL were the prime data for making shutter speed selections. The basic data and photo subsystem parameters used as input to the program are listed in Table 6-6.

**Table 6-6:**  
**Exposure Control Data for QUAL Input**

Transmissivity of telephoto lens and folding mirror	0.66
Transmissivity of wide-angle lens	0.91
80-mm neutral-density-filter density	0.18
Shutter speed (second)	
	0.036
Focal-plane (610-mm lens)	0.019
	0.010
	0.04
80-mm lens assumed nominal	0.02
	0.01

#### Notes:

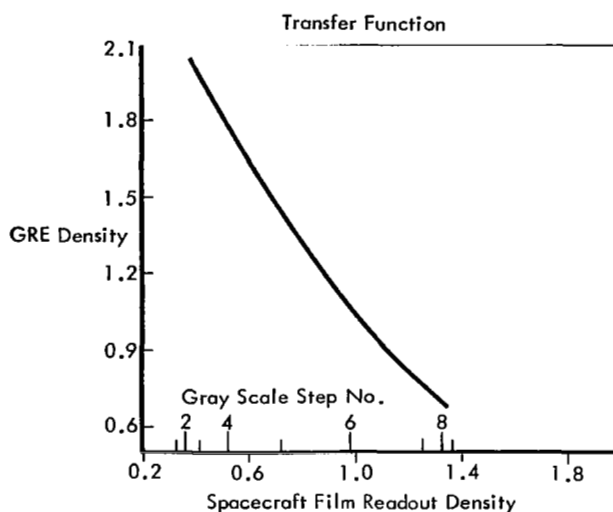
Illumination and observational geometry computed from ephemeris and orbital data.  
Site albedo data supplied by USGS  
Film sensitometric data from preflight calibration (Section 3.3).

Transmission of the optical windows was estimated to be 92%, but this was considered close enough to 100% to have no significance in the computations. For photography through Site V-14 (Frames 5 to 69), a value of 74.5% was used for the 610-mm-lens transmissivity. It was then realized that this value did not include the reflectance of the folding mirror. A value of 0.66 was then used for the 610-mm-lens transmission to account for the combined loss. The change, however, would not have affected the decision on shutter speed for the earlier photographs.

Data on albedo and albedo distribution of each nearside site were supplied by the USGS, as was done for prior missions. On the basis of experience gained on those earlier missions, the albedo values provided by USGS were reduced by a factor of 1.3 for use in the QUAL computations. In marginal cases, where density predictions did not clearly indicate a particular shutter speed but rather a choice of two, discussions with advisors from the USGS and NASA resolved the decision on the basis of the character of the principal feature and type of terrain. Pre-mission studies frequently permitted prediction of potential marginal cases and provided an opportunity to resolve the exposure decision well before the photography was scheduled. The validity of such "predictive decisions" was enhanced by the very nearly nominal character of the mission.

Throughout mission photography, accuracy of the exposure predictions was verified by examination of the reconstructed record. Density measurements were made on the image in areas showing flat (or as nearly flat as could conveniently be found) lunar surface in the frames read out in priority readout. Density values obtained from the GRE film were converted to equivalent spacecraft film densities, using appropriate transfer functions obtained from the QUAL computer program. Figure 6-5 is an example of the transfer function plots. It is for an Apollo site (V-11a) that is quite flat and measured densities showed good agreement with the

predicted values. However, at sites having mountainous topography, measured densities



Edge No.	Measured GRE Density	Spacecraft Film Density	Frame No.
872	1.36	0.82	55W Wide Angle
871	1.42	0.78	
870	1.32	0.84	
869	1.56	0.70	
868	1.51	0.72	
867	1.57	0.70	
930	1.86	0.52	57T Telephoto Note: Predicted telephoto spacecraft film density was 0.68
929	1.82	0.54	
928	1.78	0.57	
927	1.77	0.57	
926	1.80	0.55	
925	1.72	0.60	

Figure 6-5: Transfer Function Plot for Site V11a

did not show as good agreement with predicted values because of the difficulty of locating an image area showing a flat, level surface.

Lunar scene image densities were monitored during the mission for exposure control. Predicted spacecraft film densities are shown in Table 6-7, together with measured image densities for the Apollo sites only. These values show good agreement. The mean density difference (predicted minus measured) for the 16

**Table 6-7: Mission V Predicted Spacecraft Film Densities**

Apollo Site	Mission V Site	Shutter Speed	Telephoto Frame Predicted Density	Apollo Site Scene Density	Apollo Site	Mission V Site	Shutter Speed	Telephoto Frame Predicted Density	Apollo Site Scene Density
IP-1 oblique	V-1	1/50	0.67	0.95	IIP-8	V-26.1	1/25	0.81	0.48
	V-2.1	1/50	0.73	0.64		V-27a	1/50	0.57	
	V-3	1/100	1.16	0.81		V-27b	1/25	0.54	
	V-4	1/50	0.68	1.11		V-28	1/25	0.55	
	V-5.1	1/100	1.00			V-29	1/25	0.56	
IP-1	V-6	1/100	0.95		IIP-2 oblique	V-30	1/25	0.59	
	V-8a	1/50	0.67	0.53		V-31	1/25	0.75	
IP-1	V-8b	1/25	0.57	0.93		V-32	1/50	0.63	
IIP-2 oblique	V-9.1	1/100	0.93	0.76		V-33	1/25	0.90	
	V-10	1/100	0.90			V-34	1/25	0.72	
IIP-2	V-11a	1/50	0.68			V-35	1/25	0.79	
	V-11b	1/25	0.70	0.86		V-36	1/25	0.53	
	V-12	1/50	0.59			V-37	1/50	0.61	
	V-13	1/100	0.90			V-38	1/25	0.55	
	V-14	1/50	0.58			V-40	1/25	0.71	
IIP-6	V-15.1	1/50	0.65	0.77	IIP-11	V-41	1/25	0.53	0.60
	V-16a	1/50	0.61	0.52		V-42a	1/25	0.62	
	V-16b	1/25	0.56	0.98		V-42b	1/25	0.43	
	V-18	1/50	0.45	0.67		V-43.2	1/25	0.56	
	V-19	1/50	0.78			V-45.1	1/25	0.73	
IIP-6	V-21	1/50	0.68	0.82		V-46	1/25	0.64	
	V-22	1/25	0.77			V-48	1/50	0.70	
	V-23.1	1/50	0.77			V-49	1/25	0.72	
	V-24	1/50	0.75			V-50	1/25	0.57	
	V-25	1/50	0.72			V-51	1/25	0.56	



values was  $\pm 0.13$  in spacecraft film density. Image densities for the other nearside sites showed considerable scatter due to terrain effects, but the exposures were considered generally satisfactory. A comparison of densities of corresponding telephoto and wide-angle photographs confirmed the expected exposure match between cameras.

### 6.3.2 Camera-On Time Bias

Corrections to the commanded camera-on time are necessary so that shutter actuation occurs at the instant the camera axis intercepts the point target. The correction is affected by normal camera actuation delay, the number of photographs to be taken in a multiple-frame sequence, and the sequencing mode, and whether or not the V/H sensor for image motion compensation is to be used.

Correction for the multiple-frame sequences is normally made to place the point target at or near the center of the sequence coverage. Data on the sequencing rate established by the V/H ratio and mode determine the proper time for the first exposure of a sequence. For photography with the V/H sensor on, a bias for camera-on time was introduced to obtain a uniform distribution of actual exposure times before and after the time computed for the target position. The bias was adjusted to minimize camera-on time uncertainty caused by the V/H sensor cycle and to correct for known camera actuation delays. Bias was calculated using the predicted V/H ratio, and was computed as

$$-\left[0.1 + \left(\frac{0.50}{\text{V/H ratio}}\right)\right] \text{ Observed deviations from}$$

the scheduled times are shown in Figure 6-6, in which  $\Delta t$  is the actual exposure time as read from the time code minus the median predicted exposure time. When photographs were to be taken without image motion compensation (V/H sensor off), the standard bias of  $-0.9$  second for camera-on time was used for the normal camera actuation delay. As data were received from priority readout, a comparison of actual and predicted exposure time indicated that a standard bias of  $-1.0$  second would result in a more exact exposure time. Use of the revised bias started with Site V-25 (Frame 102).

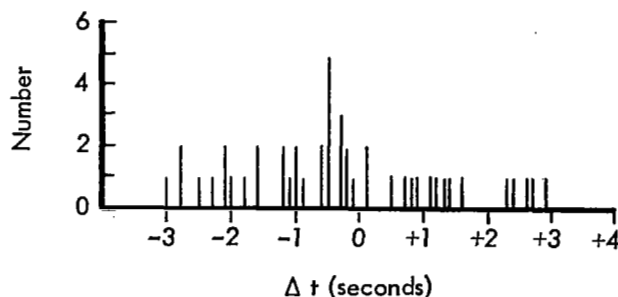


Figure 6-6: Distribution of First Exposure Time Deviations

A comparison of predicted and actual photographic coverage of sites, made from priority readout, indicated the presence of a significant downtrack error (that is, photographs were being taken too late). To compensate for this apparent error in targeting, an additional  $-3.0$ -second bias was introduced beginning with Site V-26.1 (Frame 104) to obtain the correct camera-on time for the flight programmer.

## 6.4 PHOTO SUBSYSTEM PERFORMANCE

### 6.4.1 Film Budget and Photo Data Summary

The Mission V film budget, as actually performed, is summarized in Table 6-8. Data included are film advance through the camera, processing, and readout through Bimat-cut on an orbit-by-orbit basis. Farside sites photographed from apolune are designated by an "A" prefix on the site number.

Mission photography is summarized, frame by frame, in Table 6-9. Included are site numbers, orbit, readout sequences, framelet numbers identifying frame edges and time-code location, and the GMT time of exposure obtained by conversion of spacecraft time shown by the time code.

Priority readout accomplished during the course of mission photography is diagrammed in Figure 6-7.

### 6.4.2 Camera

#### 6.4.2.1 Camera Film Handling

The amount of film advanced for each dual frame or pair of telephoto and wide-angle

**Table 6-8: Actual Mission V Film Budget**

Table 6-8: Actual Mission V Film Budget												
Initial Ellipses												
*	Site No.	Orbit No.	Event (frames)			Total Frames Accumulated			Frame Numbers			Site Number Readout
			Take	Process	Readout	Readout	Extra In Storage Loop	Bimat Thru Processor	Exposed	Wide-Angle and Time Code Readout	Telephoto Readout	
		1										
		2	12	0	0	0	12	0	Film Adv.			
	A-1	2	8	12	0	0	8	1.7	5-12			
	A-2	2	8	14.7	0	0	1.3	16.4	13-20			
	A-3	3	1	2.0	0	0	0.3	18.4	21			
	A-4	4	1	0	0	0	1.3	18.4	22			
	A-5	4	1(FS)	2.0	0	0	0.3	20.4	23			
	A-6	5	1	0	1.7	1.7	1.3	20.4	24	4 (Blank)	6,5	A-1
	A-7	6	1	2.0	2	3.7	0.3	22.4	25	6,5	8,7	A-1
	A-8	7	1	0	0	3.7	1.3	22.4	26	—	—	
	A-9	8	1	2.2	0	3.7	0.1	24.6	27	—	—	
	A-10	8	1	0	0	3.7	1.1	24.6	28	—	—	
	A-11.2	9	1	0	0	3.7	2.1	24.6	29	—	—	
	A-12	10	1	2.0	0	3.7	1.1	26.6	30	—	—	

Final Ellipse												
	A-13	11	1	0	1.1	4.8	2.1	26.6	31	11 <sup>⊕</sup> 10	12	
		12	0	0	0	4.8	2.1	26.6	—	—	—	
	A-14	13	1	2.0	0	4.8	1.1	28.6	32	—	—	
		14	0	0	0	4.8	1.1	28.6	—	—	—	
	1	15	4F	0	1.5	6.3	5.1	28.6	33-36	13 <sup>⊕</sup> 12	14, 13 <sup>⊕</sup>	A-2
		16	0	2.0	0.4	6.7	3.1	30.6	—	11 <sup>⊕</sup>	13 <sup>⊗</sup>	A-2
	2.1	17	1	0	2.1	8.8	4.1	30.6	37	14, 13	16, 15	A-2
		18	0	0	0	8.8	4.1	30.6	—	—	—	
	3		1							—	—	
	A-15	19	1	2.0	0	8.8	4.1	32.6	38, 39	—	—	
	4	20	1	0	0	8.8	5.1	32.6	40	—	—	

\*Notes: (By Orbit Number)

2. Eight frames of Estar leader and four frames of SO-243 film are advanced through the camera but not exposed. Twelve frames of film leader are "processed" with 10.3 frames of dry and 1.7 frames of wet Bimat.
4. Transfer from first to second ellipse at apolune following Orbit 4.
8. Earth photo taken.
10. Transfer from second to third ellipse at perilune of Orbit 10.

General — <sup>⊕</sup> Indicates partial frame readout

Final Ellipse													
	Site No.	Orbit No.	Event (frames)			Total Frames Accumulated			Frame Numbers			Site Number Readout	
			Take	Process	Readout	Readout	Extra In Stor- age Loop	Bimat Thru Processor	Exposed	Wide-Angle and Time Code Readout	Telephoto Readout		
	5.1	21	1	2.0	0	8.8	4.1	34.6	41	-	-		
		22	0	0	2.0	10.8	4.1	34.6	-	19 <sup>⊕</sup> , 18	20, 19	A-2	
	6	23	1	2.0	0	12.8	3.1	36.6	42	-	-		
		24	0	0	0	12.8	3.1	36.6	-	-	-		
	A-16.1	25	1	2.0	2.1	14.9	2.1	38.6		20, 19	22, 21	A-3	A-4
	8A	26	4F	0	2.1	17.0	6.1	38.6	43-47	22, 21	24, 23	A-5	A-6
	8B	27	4F	2.0	2.0	19.0	8.1	40.6	48-51	24, 23	26, 25	A-7	A-8
	9.1	28	1	2.0	2.0	21.0	7.1	42.6	52	26, 25	28, 27	A-9	A-10
①	A-17.1	29	1	2.0	2.2	23.2	6.1	44.6	53	28, 27	30, 29	A-11.2	A-12
①	10	30	1	2.0	2.1	25.3	5.1	46.6	54	30, 29	32, 31	A-13	A-14
①	11A	31	4F	2.0	2.0	27.3	7.1	48.6	55-58	32, 31	34, 33	1	
	11B	32	4F	4.0	1.4	28.7	7.1	52.6	59-62	35 <sup>⊕</sup> , 34	36, 35 <sup>⊕</sup>	1	
	12	33	1	2.0	1.8	30.5	6.1	54.6	63	37 <sup>⊕</sup> , 36	38, 37	2.1	3
	13 A-18	34	1	2.0	1.9	32.4	5.1	56.6	64	39 <sup>⊕</sup> , 38	40, 39	4	A-15
	14	35	4F	2.0	1.2	33.6	8.1	58.6	66-69	41 <sup>⊕</sup> , 40	42	6	
	15.1	36	1	3.0	1.8	35.4	6.1	61.6	70	43 <sup>⊕</sup> , 42	44, 43	8A	
	16A	37	4F	0	1.7	37.1	10.1	61.6	71-74	46 <sup>⊕</sup> , 45	47, 46 <sup>⊕</sup>	8A	
①	16B	38	4F	2.9	1.7	38.8	11.2	64.5	75-78	49 <sup>⊕</sup> , 48	50, 49	8B	
①	A-19	39	1	2.1	2.1	40.9	10.1	66.6	79	51 <sup>⊕</sup> , 50, 49 <sup>⊕</sup>	52, 51	9.1	8B
		40	0	2.0	1.7	42.6	8.1	68.6	-	53 <sup>⊕</sup> , 52	54, 53 <sup>⊕</sup>	10	A-17.1
	18	41	4F	2.0	1.5	44.1	10.1	70.6	80-83	55 <sup>⊕</sup> , 54	56, 55 <sup>⊕</sup>	11A	
	19	42	1	2.0	2.0	46.1	9.1	72.6	84	57 <sup>⊕</sup> , 56, 55	58, 57	11A	
		43	0	2.0	1.8	47.9	7.1	74.6	-	58	60, 59	11B	
	A-20	44	1	4.0	1.1	49.0	4.1	78.6	85	62	64	13	
	21	45	4F	4.1	1.4	50.4	4.0	82.7	86-89	64	66, 65 <sup>⊕</sup>	14	A-18
	22	46	4F	2.0	1.5	51.9	6.0	84.7	90-93	67, 66	68, 67 <sup>⊕</sup>	14	
	23.2	47	4F	2.0	1.5	53.4	8.0	86.7	94-97	69, 68	70, 69 <sup>⊕</sup>	14	15.1
	24 25	48	4F <sub>1</sub>	3.0	1.4	54.8	9.0	89.7	98-101	71 <sup>⊕</sup> , 70	72, 71 <sup>⊕</sup>	16A	
	A-21	49	1	0	0.8	55.6	11.0	89.					

① In the Event/Readout column, readout for this orbit is broken into two or three periods, one of which may begin early in the following orbit.

Final Ellipse												
	Site No.	Orbit No.	Event (frames)			Total Frames Accumulated			Frame Numbers			Site Number Readout
			Take	Process	Readout	Readout	Extra in Storage	Bimat Thru Processor	Exposed	Wide Angle And Time Code Readout	Telephoto Readout	
②	33	58	0	6.0	1.9	66.9	13.0	120.7	—	102, 101	103, 102	A-21 25
	34	59	1	3.0	1.6	68.5	11.0	123.7	137	104	106, 105 <sup>⊕</sup>	26
①	35	60	4F	3.0	1.6	70.1	12.0	126.7	138-141	107	109, 108 <sup>⊕</sup>	27A
	36	61	4S	4.0	1.5	71.6	12.0	130.7	142-145	110	112, 111 <sup>⊕</sup>	27B 27A
①	37	62	4F	0	1.8	73.4	16.0	130.7	146-149	115 <sup>⊕</sup> , 114	116, 115	28 27B
	38	63	8F	4.4	2.5	75.9	19.6	135.1	150-157	119, 118, 117	121 <sup>⊕</sup> , 120, 119	29 28
①	A-23	64	1	3.7	0.9	76.8	16.9	138.8	158	123 <sup>⊕</sup>	124	A-22
	38	65	4F	2.0	2.7	79.5	18.9	140.8	159-162	124, 123	126, 125	30
①	A-24	66	—	3.0	3.1	82.6	15.9	143.8	—	127, 126, 125	129, 128, 127	31 30
	40	67	1	4.0	2.6	85.2	12.9	147.8	163	131, 130	133, 132, 131 <sup>⊕</sup>	32 31
①	41	68	—	4.0	3.7	88.9	8.9	151.8	—	135, 134, 133	137, 136, 135, 134	33 32
	42A	69	4F	3.0	2.7	91.6	9.9	154.8	164-167	138, 137	140, 139, 138	34
①	42B	70	1	3.0	3.0	94.6	7.9	157.8	168	141, 140, 139	143, 142, 141	34 35
	43.1	71	4F	3.0	2.6	97.2	8.9	160.8	169-172	144, 143	146, 145, 144 <sup>⊕</sup>	36 35
①	44	72	4F	3.0	3.0	100.2	9.9	163.8	173-176	147, 146, 145	149, 148, 147	36
	45.1	73	4S	3.1	3.4	103.6	10.8	166.9	177-180	151, 150 <sup>⊕</sup> , 149, 148	152, 151, 150	37
①	A-25	74	1	3.0	2.5	106.1	8.8	169.9	181	154 <sup>⊕</sup> , 153, 152	155, 154, 153 <sup>⊕</sup>	37
	46	75	0	4.0	3.7	109.8	4.8	173.9	—	158 <sup>⊕</sup> , 157, 156, 155	159, 158, 157, 156 <sup>⊕</sup>	37 A-23 38
①	47	76	4F	3.0	3.0	112.8	5.8	176.9	182-185	161, 160, 159	162, 161, 160	38
	48	77	8F	3.0	2.7	115.5	10.8	179.9	186-193	163, 162	165, 164, 163 <sup>⊕</sup>	A-24 40
①	49	78	—	4.0	3.7	119.2	6.8	183.9	—	167, 166, 165	169, 168, 167, 166	42A, 41 40
	50	79	8F	3.0	2.6	121.8	11.8	186.9	194-201	170, 169	172, 171, 170	42A
①	51	80	4F	6.2	3.2	125.0	9.6	193.1	202-205	177, 176, 175, 174	178, 177, 176	43.1 42B
	52	81	—	4.0	3.7	128.7	5.6	197.1	—	180, 179	182, 181, 180	45.1, A-25
①	53	82	4F	5.3	2.0	130.8	4.3	202.4	206-209	186, 185	187, 186	46
	54	83	8F	10.0	2.0	132.8	2.3	212.4	210-217	196, 195	197, 196	48
①	F.A.	84	16	6.0	2.3	135.1	12.3	218.4	—	202, 201, 200	203, 202	49
	55	85	—	5.7			6.6	224.1	—			

\* Notes: (By Orbit Number)

② In the Event/Process column, processing for this orbit continues into the next orbit.

84 F.A. - Film Advance

85 Bimat supply exhausted after 224.1 frames of Bimat

86 Begin Final Readout

Table 6-9: Photography Operational Data Summary

Frame	Photo Site	Photo Orbit	Shut-ter Speed	Proc Orbit (index)	R/O Seq. T	R/O Seq. WA	R/O Orbit	WA Edge No.s	TC Frmlt	Tele Edge No.s	S/C Time	Exposure GMT	*
1				2									
2													
3													
4													
5	A-1	2	1/25		2/148	3/148	6/145	332 303	301	168 067	77349.4	218:11:22:02.74	
6					2 3	3/148	6/145	463 431	430	299 202	77352.1	218:11:22:05.44	
7					3	147	6/145	594 565	564	428 335	77354.8	218:11:22:08.14	
8					3/148	147	6/144	724 694	693	561 465	77357.5	218:11:22:10.84	
9					147	147	144	855 826	826	693 597	77360.2	218:11:22:13.54	
10						4/146	12/144	987 958	957	825 729	77362.8	218:11:22:16.14	
11					4/147	4/6	12/6	118 090	089	957 860	77365.4	218:11:22:18.74	
12	A-1	2	1/25	(12.06)	4/146	5/146	12/5	250 221	220	088 991	77368.2	218:11:22:21.54	
13	A-2	2	1/25	3	5 6	5/ 7	15/6/ 7	379 352	351	218 122	85231.8	218:13:33:25.13	
14				(14.06)	5/146	7	15/ 17	505 488	480	348 252	85234.5	218:13:33:27.83	
15				4	7/145	7/145	17/142	642 614	612	480 383	85237.2	218:13:33:30.53	
16				(16.36)	7/145	144	17/141	773 744	743	611 515	85239.9	218:13:33:33.23	
17				6	145	8/144	22/141	904 876	875	743 646	85242.6	218:13:33:35.93	
18				(18.36)	144	8/144	22/141	039 013	005	873 777	85245.3	218:13:33:38.63	
19				8	8/144	8/ 9	22/5	166 140	139	006 910	85247.9	218:13:33:41.23	
20	A-2	2	1/25	(20.51)	8/9	9/143	22/5	297 271	270	138 042	85250.6	218:13:33:43.9	
21	A-3	3	1/25	10	9/143	9/10	25/6	432 404	401	267 170	98653.1	218:17:17:6.4	
22	A-4	4	1/25	(22.20)	9/143	10/143	25/6	560 533	530	398 301	20068.8	219:0:34:59.7	
23	A-5	4	1/25	11	10/143	10/1	26/7	692 663	662	530 434	39614.9	219:06:0:45.8	1
24	A-6	5	1/25	(24.20)	10/143	11	26/7	821 794	793	661 564	67820.5	219:13:50:51.4	
25	A-7.1	6	1/25	16	11/142	11/2	27/8	951 924	924	791 695	92988.5	219:20:50:19.4	
R/O Seq	Framelets		R/O Seq	Framelets				*COMMENTS: 1. Film set - door closed 2. The final R/O Sequence is not always noted above since Final R/O is continuous except for two framelets lost in Frame 217T.					
002	289/067		142	933/599									
003	546/284		143	598/161									
004	099/950		144	160/744									
005	356/158		145	743/344									
006	157/109		146	343/921									
007	623/349		147	920/499									
008	146/888		148	498/065									
009	412/136												
010	674/398												
011	937/675												

**Table 6-9 (Continued)**

Frame	Photo Site	Photo Orbit	Shut-ter Speed	Proc Orbit (Index)	R/O Seq. T	R/O Seq. WA	R/O Orbit	WA Edge No.s	TC Frmlt	Tele Edge No.s	S/C Time	Exposure CMT	*
26	A-8	7	1/25	16 (26.20)	11/142	12/141	27/8	085 056	054	922 826	5636.8	220:01:42:5.09	
27	A-9	8	1/100	19	12/141	12/4	28/9	218 190	186	049 953	32211.7	220:09:05:0.19	1
28	A-10	8	1/25	(28.20)	12/4	13/141	28/9	348 320	315	184 088	53051.6	220:14:52:20.07	
29	A-11.2	9	1/25	21	13	13/140	29/138	479 450	449	317 220	78203.0	220:21:51:31.48	
30	A-12	10	1/25	(30.20)	13/141	15/140	29/137	604 583	579	447 350	95726.5	221:02:43:34.97	
31	A-13	11	1/25	23	15/140	15/6	30/1	739 711	710	578 481	15392.8	221:09:32:18.87	
32	A-14	13	1/25	(32.16)	15	16/139	30/1	871 842	841	709 613	38515.2	221:15:57:41.26	
33	V-1	15	1/50	25	16/140	16	31/136	002 974	972	840 714	56517.2	221:20:57:43.26	
34	↓	↓	↓	(34.16)	16/139	17	31/2	134 105	104	972 876	56523.9	221:20:57:49.96	
35	↓	↓	↓	27	17	17/139	32/136	266 238	236	104 070	56530.4	221:20:57:56.46	
36	V-1	15	1/50	(36.16)	17/139	19/138	32/3	398 369	368	236 139	56536.9	221:20:58:02.96	
37	V-2.1	17	1/50	28	19/138	18/21	33/4	529 500	499	367 271	79577.6	222:03:22:3.64	
38	V-3	19	1/100	(38.16)	18/9	21/138	33/4	659 630	629	498 400	102830.3	222:09:49:36.34	
39	A-15	19	1/25	29	21/138	20/137	34/135	789 761	759	628 531	1767.9	222:10:52:51.53	
40	V-4	20	1/50	(40.16)	20/1	22	34/5	921 893	892	759 663	8904.5	222:12:51:48.13	
41	V-5.1	21	1/100	30	22/137	22/137	35/134	051 024	023	890 794	20882.9	222:16:11:26.52	
42	V-6	23	1/100	(42.16)	22	24/136	35/6	188 155	154	021 925	43845.0	222:22:34:8.60	
43	A-16.1	25	1/25	31	24/137	23	36	315 285	284	150 051	63297.7	223:03:58:21.30	
44	V-8a	26	1/50	(44.20)	23/4	136	36/133	446 418	416	284 188	78241.9	223:08:07:25.50	
45	↓	↓	↓	32	136	26/135	37	577 548	548	415 319	78245.2	223:8:7:28.80	
46	↓	↓	↓	(46.20)	26/136	25	37	709 681	679	547 451	78249.6	223:8:7:33.20	
47	V-8a	26	1/50	33	25/6	135	37	841 813	812	679 583	78253.8	223:08:07:37.40	
48	V-8b	27	1/25	(48.20)	135	28/135	38/132	974 945	944	811 715	89711.6	223:11:18:35.19	
49	↓	↓	↓	34	28/135	27/9	38/9	102 074	072	940 845	89716.4	223:11:18:39.99	
50	↓	↓	↓	(50.16)	27/8	29/134	38/9	234 205	204	072 976	89721.4	223:11:18:44.99	
R/O Seq	Framelets	R/O Seq	Framelets	R/O Seq	Framelets	*COMMENTS: 1. Earth Photo							
012	200/933	021	695/527	134	433/993								
013	463/270	022	035/885	135	992/548								
014	269/182	023	293/211	136	547/106								
015	725/453	024	210/060	137	105/692								
016	987/725	025	688/636	138	691/249								
017	250/070	026	634/472	139	248/815								
018	508/437	027	080/050	140	814/377								
019	436/268	028	049/853	141	376/934								
020	774/696	029	358/089										

Table 6-9 (Continued)

Frame	Photo Site	Photo Orbit	Shut-ter Speed	Proc Orbit (Index)	R/O Seq. T	R/O Seq. WA	R/O Orbit	WA Edge No.s	TC Frmlt	Tele Edge No.s	S/C Time	Exposure GMT	*
51	V-8b	27	1/25	34	29/134	29/134	39/131	367 338	335	205 108	89726.2	223:11:18:49.79	
52	V-9.1	28	1/100	(52.16)	29/134	30/133	39/40/130	498 470	469	336 240	101248.8	223:14:30:52.19	
53	A-17.1	29	1/25	35	30/133/4	30/133	40/131	628 599	598	466 370	11344.6	223:18:40:5.79	
54	V-10	30	1/100	(54.16)	30/133	31/133	41/130	760 730	729	597 501	18875.7	223:20:45:36.89	
55	V-11a	31	1/50	36	31/133	31/132	41/3	890 862	860	729 633	30779.0	224:00:04:0.19	
56					31/133	32/3/132	41/2	022 993	992	860 764	30783.5	224:00:04:4.7	
57				(57.16)	32	32/132	42/3	155 126	124	992 896	30787.9	224:00:04:9.09	
58	V-11a	31	1/50	38	32/3/132	34/132	42/3	285 258	255	124 028	30792.4	224:00:04:13.59	
59	V-11b	32	1/25		34/132	34/131	43/128	418 390	388	255 159	42247.6	224:03:15:8.79	
60				(60.06)	34/131	131	43/128	547 518	517	385 289	42252.4	224:03:15:13.59	
61				39	131	131	128	679 650	649	517 421	42257.2	224:03:15:18.39	
62	V-11b	32	1/25	(62.16)	131	35/130	44/127	810 781	780	648 552	42265.2	224:03:15:23.3	
63	V-12	33	1/50	40	35/131	35/130	44/127	943 914	913	780 685	53669.5	224:06:25:30.68	
64	V-13	34	1/100	(64.16)	35/130	37/130	44/5	074 043	043	910 814	65152.2	224:09:36:53.38	
65	A-18.1	35	1/25	41	37/130	36/130	45/127	204 175	174	041 945	73101.0	224:11:49:22.17	
66	V-14	35	1/50	(66.16)	36	39/129	45/6	334 307	304	173 077	76979.7	224:12:54:0.87	
67				42	39/7/129	38/129	46/126	466 437	436	304 208	76985.4	224:12:54:6.57	
68				(68.16)	38/9/129	40/129	46/7	597 570	568	436 340	76991.3	224:12:54:12.47	
69	V-14	35	1/50	43	40/129	40/128	47/125	729 700	699	567 471	76997.0	224:12:54:18.17	
70	V-15.1	36	1/50	(70.16)	40/128	41/128	47/8	860 832	831	699 603	88368.0	224:16:03:49.16	
71	V-16a	37	1/50	44	41/128	41/128	48/125	992 963	961	829 732	99541.1	224:19:10:2.26	
72					41/128	127	48/125	123 093	092	961 861	99545.5	224:19:10:6.66	
73					128	127/28	124/25	254 225	225	092 996	99545.9	224:19:10:11.06	
74	V-16a	37	1/50	(74.16)	127	42/127	124	386 357	356	224 128	99554.3	224:19:10:15.46	
75	V-16b	38	1/25	45	42/127	127	124	517 489	488	355 259	6150.3	224:22:21:9.06	
R/O Seq	Framelets	R/O Seq	Framelets	R/O Seq	Framelets	*COMMENTS:							
029	358/089	036	176/119	127	574/119								
030	609/391	037	118/996	128	118/665								
031	869/667	038	465/410	129	664/214								
032	132/961	039	409/265	130	213/757								
033	960/865	040	716/527	131	756/317								
034	396/165	041	977/793	132	316/865								
035	915/773	042	368/269	133	864/434								

Table 6-9 (Continued)

Frame	Photo Site	Photo Orbit	Shut-ter Speed	Proc Orbit (Index)	R/O Seq. T	R/O Seq. WA	R/O Orbit	WA Edge No.s	TC Fmult	Tele Edge No.s	S/C Time	Exposure GMT	*
76	V-16b	38	1/25	(76.17)	127	126	123/4	648 619	618	486 390	6155.1	224:22:21:13.86	
77	V-16b	38	1/25	46	126	43/126	50/123	779 750	749	520	6160.0	224:22:21:18.76	
78	V-16b	38	1/25	(78.26)	43/126	43/126	50/123	911 882	881	749 652	6165.0	224:22:21:23.76	
79	A-19	39	1/25	47	43/126	44/125/6	50/51 122/3	042 013	012	881 784	21353.5	225:02:34:32.25	
80	V-18	41	1/50	(80.32)	126	44/125	51/122/3	172 144	143	010 914	40576.8	225:07:54:55.55	
81	V-18	41	1/50	48	44/125	45/125	51/52 122	303 274	273	140 044	40581.3	225:07:55:0.05	
82	V-18	41	1/50	(82.32)	125	45/125	52/122	436 407	406	274 177	40585.8	225:07:55:4.55	
83	V-18	41	1/50	49	45/125	124	52/121/2	567 538	537	404 308	40590.3	225:07:55:09.05	
84	V-19	42	1/50	49	124/5	124	121/2	699 670	669	537 440	51738.8	225:11:00:57.55	
85	A-20	44	1/25	(85.32)	124	46/124	53/121	828 800	799	666 570	78661.3	225:18:29:40.04	
86	V-21	45	1/50	50	46/124	46/123/4	53/120/1	960 931	930	798 702	87063.7	225:20:49:42.43	
87	V-21	45	1/50	50	46/124	123	53/120/1	091 063	062	929 833	87072.1	225:20:49:50.83	
88	V-21	45	1/50	50	123	123	120	223 195	194	061 965	87080.6	225:20:49:59.33	
89	V-21	45	1/50	(89.32)	123	47/123	54/120	355 326	324	193 097	87089.2	225:20:50:07.93	
90	V-22	46	1/25	51	47/123	122	54/119 20	487 454	458	324 229	98206.8	225:23:55:23.53	
91	V-22	46	1/25	(91.32)	122/3	122	119/120	616 587	586	454 358	98212.3	225:23:55:31.03	
92	V-22	46	1/25	52	122	48/122	55/119	720 720	718	586 490	98217.9	225:23:55:36.63	
93	V-22	46	1/25	(93.32)	48/122	122	55/119	879 851	850	718 621	98223.6	225:23:55:42.33	
94	V-23.1	47	1/50	53	122	49/121	56/117/9	012 984	981	850 754	4585.4	226:03:02:41.73	
95	V-23.1	47	1/50	53	49/121/2	49/121	56/117/9	112	111	978 883	4590.2	226:03:02:46.53	
96	V-23.1	47	1/50	53	49/121	121	56/117	274 246	245	112 016	4594.9	226:03:02:51.23	
97	V-23.1	47	1/50	(97.32)	121	121	117	405 377	375	242 146	4599.7	226:03:02:56.03	
98	V-24	48	1/50	53	121	50/120/1	57/116/7	537 509	509	376 279	15835.5	226:06:10:11.83	
99	V-24	48	1/50	53	50/121	50/120	57/116/7	666 638	636	505 408	15840.1	226:06:10:16.43	
100	V-24	48	1/50	(100.32)	50/120	51/120	57/116 58	798 770	769	637 540	15844.6	226:06:10:20.93	
R/O Seq	Framelets	R/O Seq	Framelets	R/O Seq	Framelets	*COMMENTS:							
043	911/713	049	138/958	123	432/955								
044	155/031	050	662/415	124	954/485								
045	425/272	051	033/788	125	484/024								
046	959/788	120	013/540	126	023/575								
047	355/311	121	539/898										
048	742/640	122	897/433										



Table 6-9 (Continued)

Frame	Photo Site	Photo Orbit	Shut-ter Speed	Proc Orbit (Index)	R/O Seq. T	R/O Seq. WA	R/O Orbit	WA Edge No.s	TC Fm/lt	Tele Edge No.s	S/C Time	Exposure GMT	*
101	V-24	48	1/50	55	120	120	116	931 903	902	769 673	15849.1	226:06:10:25.43	
102	V-25	49	1/50		120	119	115/116	063 034	033	901 805	28326.9	226:09:38:23.22	
103	A-21	49	1/25	(103.32)	119/20	119	115/116	192 164	162	030 933	31114.4	226:10:24:50.72	
104	V-26.1	50	1/25	55	119	53/ 119	59/ 115	322 294	292	160 064	39260.1	226:12:40:36.42	
105	↓	↓	↓		53/ 119	52/ 119	59/ 115	454 425	424	292 196	39286.5	226:12:41:02.82	
106	↓	↓	↓	(105.32)	52 /3/119	118	59/ 114	586 557	556	423 328	39311.3	226:12:41:27.62	
107	V-26.1	50	1/25	57	118/	55/ 118	60/ 114	718 690	687	556 460	39336.8	226:12:41:53.12	
108	V-27a	51	1/50		55/ 118	118	60/ 114	850 821	820	687 592	50309.7	226:15:44:46.01	
109	↓	↓	↓		54 5 /118	118	60/ 114	979 951	950	817 721	50314.2	226:15:44:50.51	
110	↓	↓	↓	(110.32)	118	57/ 117	61/ 113	112 083	081	950 853	50318.7	226:15:44:55.01	
111	V-27a	51	1/50	58	57/8	117	61/ 113	244 215	214	081 985	50323.2	226:15:44:59.51	
112	V-27b	52	1/25		56/7	117	61/ 113	375 347	345	213 117	61772.8	226:18:55:49.10	
113	↓	↓	↓	(113.32)	117	116	112/ 113	505 477	476	343 247	61777.5	226:18:55:53.80	
114	↓	↓	↓	59	117	60/ 116	62/ 112	637 608	607	475 379	61782.3	226:18:55:58.60	
115	V-27b	52	1/25		60/ 116	59/ 116	62/ 112	769 740	739	607 511	61787.0	226:18:56:3.30	
116	V-28	53	1/25	(116.32)	59/60	116	62/ 112	900 872	871	738 642	72987.1	226:22:02:43.40	
117	↓	↓	↓	60	116	62/ 115	64/ 111	030 002	000	868 771	72992.5	226:22:02:48.80	
118	↓	↓	↓		115	61/ 115	63/ 111	162 133	132	999 903	72997.9	226:22:02:54.20	
119	V-28	53	1/25	(119.32)	61/2	61/ 115	63/4/ 111	293 265	263	131 035	73003.2	226:22:02:59.50	
120	V-29	54	1/25	61	61/ 115	115	63/ 111	425 397	396	264 167	84913.3	227:01:21:29.60	
121	↓	↓	↓		61/ 115	114	63/ 110	555 526	525	296 284	84918.2	227:01:21:34.5	
122	↓	↓	↓	(122.17)	114/ 15	63/ 114	64/ 110	688 658	658	525 429	84923.1	227:01:21:39.40	
123	V-29	54	1/25	62	114	63/4	64/5 109	819 790	789	657 559	84928.1	227:01:21:44.40	
124	A-22	54	1/25		63/4/5	64/ 113	64/5/6 109	949 921	920	787 691	88427.6	227:02:20:3.90	
125	V-30	55	1/25		64/ 113	64/7	65/7 109	081 053	051	917 820	95388.7	227:04:16:5.00	
R/O Seq	Framelets	R/O Seq	Framelets	*COMMENTS									
052	426/369	061	329/092										
053	376/213	062	090/007										
054	817/782	063	805/686										
055	781/610	064	052/778										
056	210/159	114	029/505										
057	158/027	115	503/981										
058	026/014	116	980/494										
059	753/705	118	992/501										
060	704/515	119	499/014										

Table 6-9 (Continued)

Frame	Photo Site	Photo Orbit	Shut-ter Speed	Proc Orbit (Index)	R/O Seq. T	R/O Seq. WA	R/O Orbit	WA Edge No.s	TC Fmilt	Tele Edge No.s	S/C Time	Exposure GMT	*
126	V-30	55	1/25	62 (126.17)	64/7 113/4	66/113	65/6/7 109/110	212 183	181	049 953	95398.9	227:04:16:15.20	
127	↓	↓	↓	63	66/7/113	66/113	66/7/109	343 316	316	181 085	95409.1	227:04:16:25.40	
128	V-30	55	1/25		66/113	66/113	66/109	476 447	446	313 217	95419.6	227:04:16:35.90	
129	V-31	56	1/25		66/113	112	66/108/9	607 578	578	445 349	3643.4	227:07:54:37.38	
130	↓	↓	↓	(130.57) 64	112/3	68/112	67/108/9	737 709	707	575 479	3654.6	227:07:54:48.48	
131	↓	↓	↓		68/112	68/112	67/108	869 840	839	707 610	3666.1	227:07:54:59.98	
132	V-31	56	1/25		68/112	68/112	67/108	000 972	971	837 741	3677.7	227:07:55:11.58	
133	V-32	57	1/50		68/112	69/111	67/8 107/8	132 103	102	970 873	14422.2	227:10:54:16.09	
134	↓	↓	↓	(134.27) 65	69 111/2	69/111	68/107/8	261 233	231	099 003	14441.6	227:10:54:35.49	
135	↓	↓	↓		69/111	69/111	68/107	394 365	364	232 135	14461.6	227:10:54:55.49	
136	V-32	57	1/50	(136.27) 66	69/111	111	68/107	525 496	495	362 266	14482.7	227:10:55:16.59	
137	V-33	59	1/25		69/111	70/110	68/9/106	657 628	627	495 398	37255.8	227:17:14:49.69	
138	V-34	60	1/25		70/110	70/110	69/106	786 757	756	624 528	48473.4	227:20:21:47.27	
139	↓	↓	↓	(139.27)	70/110	70/1 110	69/70 106	918 889	888	755 659	48478.2	227:20:21:52.07	
140	↓	↓	↓	67	70/110	71/110	69/70 106	050 021	019	888 791	48483.0	227:20:21:56.87	
141	V-34	60	1/25		71/110	71 109	70/105/6	181 153	151	019 922	48487.8	227:20:22:01.67	
142	V-35	61	1/25		71/109 110	109	70/105/6	313 284	283	151 054	60286.3	227:23:38:40.17	
143	↓	↓	↓	(143.27) 68	71/2 109	72 109	70/1/105	443 414	413	281 184	60305.9	227:23:28:59.77	
144	↓	↓	↓		72/109	72/108 109	71/105	575 547	547	413 317	60325.9	227:23:39:19.77	
145	V-35	61	1/25		72/109	73 108	71/2/105	706 677	676	545 418	60346.5	227:23:39:40.37	
146	V-36	62	1/25		72/3 108	73 108	71/2/104	838 809	808	676 580	71636.5	228:02:47:50.37	
147	↓	↓	↓	(147.27) 69	73/108	73 108	72/104	968 939	938	806 710	71641.3	228:02:47:55.17	
148	↓	↓	↓		73/109	74 107	72/3/104	100 072	071	938 842	71646.1	228:02:47:59.97	
149	V-36	62	1/25		73/4 107/8	74 107	72/3 108/4	232 204	202	069 973	71650.5	228:02:48:4.37	
150	V-37	63	1/50	(150.27)	74/107	74 107	73/103	362 334	333	200 104	83143.5	228:05:59:37.37	
R/O Seq	Framelets	R/O Seq	Framelets										
064	052/778	072	673/337										
065	777/698	073	062/667										
066	452/115	074	482/038										
067	114/048	107	546/024										
068	975/639	108	023/555										
069	493/014	109	554/130										
070	893/543	110	129/607										
071	280/888	111	606/081										
		112	080/556										
		113	554/030										
		114	029/505										

Table 6-9 (Continued)

Frame	Photo Site	Photo Orbit	Shut-ter Speed	Proc Orbit (Index)	R/O Seq. T	R/O Seq. WA	R/O Orbit	WA Edge No.s	TC Frnlt	Tele Edge No.s	S/C Time	Exposure GMT	*
151	V-37	63	1/50	70	74/107	74/107	73/103	492 463	463	330 234	83148.3	228:05:59:42.17	
152					74/107	77/106	73/5 102/3	625 596	595	463 367	83153.1	228:05:59:46.97	
153				(153.27)	77 106/7	75/6 106	74/5 106/7	756 728	727	497 497	83157.9	228:05:59:51.77	
154				71	76/7 106	75/8 106	74/5 102	888 859	858	726 630	83162.7	228:05:59:56.57	
155					75 106	78 106	74/5 102	019 990	989	857 761	83167.5	228:06:00:01.37	
156				(156.27)	78 106	78 105	75 101/2	150 122	121	989 892	83172.2	228:06:00:06.07	
157	V-37	63	1/50	72	78 105/6	78 105	75 101/2	282 253	252	120 023	83177.0	228:06:00:10.87	
158	A-23	64	1/25		78 105	79 105	75/6 101	413 384	383	250 154	98171.8	228:10:10:05.67	
159	V-38	65	1/25	(159.27)	78 105	79 105	75/6 101	544 515	514	382 286	1605.3	228:12:28:16.76	
160				73	79 105	79 104	76 100/1	675 646	645	513 417	1612.5	228:12:28:23.96	
161					79 104/5	80 104	76/7 100/1	807 778	777	645 549	1620.0	228:12:28:31.46	
162	V-38	65	1/25	(162.37)	79 104	80 103	76/7 100	938 910	909	776 679	1627.8	228:12:28:39.26	
163	A-24	67	1/25	74	80 103/4	80 103	77 100	070 042	041	908 811	27687.0	228:19:42:58.45	
164	V-40	69	1/25		80 103	81 102	77/8 99/100	200 171	170	037 941	47093.7	229:01:06:25.15	
165				(165.37)	80 102/3	81 102	77/8 99/100	330 302	301	168 072	47098.7	229:01:06:30.15	
166				75	81 102	81 102	78 99	463 434	433	301 204	47103.6	229:01:06:35.05	
167	V-40	69	1/25		81 102	81 102	78 99	594 565	564	432 336	47108.5	229:01:06:39.95	
168	V-41	70	1/25		81 102	82 101	78/9 98/9	726 697	697	564 466	57789.0	229:04:04:40.45	
169	V-42a	71	1/25	(169.37)	81 101/2	82 101	78/9 98/9	857 826	826	694 599	69722.0	229:07:23:33.44	
170				76	82 101	82 101	79 98	987 958	956	824 728	69726.9	229:07:23:38.34	
171					82 101	82 101	79 98	119 090	089	957 861	69731.7	229:07:23:43.14	
172	V-42a	71	1/25	(172.37)	82 101	82 100	79 97/8	251 223	222	089 993	69736.5	229:07:23:47.94	
173	V-42b	72	1/25	77	100/1	100	97/8	383 354	353	221 125	81183.7	229:10:34:35.15	
174					100	83 100	80 97	515 484	484	351 255	81188.7	229:10:34:40.15	
175				(175.37)	83 100	83 99/100	80 96/7	645 615	614	482 385	81193.7	229:10:34:45.15	
R/O Seq	Framelets	R/O Seq	Framelets										
074	482/038	111	606/081										
075	862/743	110	129/607										
076	742/685	109	554/130										
077	683/630	108	023/555										
078	378/887	107	546/024										
079	775/390	106	070/548										
080	163/807	105	591/071										
081	681/195	104	815/592										
082	080/735	103	076/816										
083	877/465	102	602/077										
		101	127/603										
		100	615/128										

**Table 6-9 (Continued)**

Frame	Photo Site	Photo Orbit	Shut-ter Speed	Proc Orbit (Index)	R/O Seq. T	R/O Seq. WA	R/O Orbit	WA Edge No.s	TC Fmult	Tele Edge No.s	S/C Time	Exposure GMT	
176	V-42b	72	1/25	78	83 100	83 99	80 97	775 746	746	613 517	81198.6	229:10:34:50.05	
177	V-43.2	73	1/25		83 99	83 99	80 96	908 877	877	745 649	92375.6	229:13:41:7.04	
178	↓	↓	↓		83 99	84 99	80/1 96	038 009	009	876 780	92399.5	229:13:41:30.94	
179	↓	↓	↓	(179.10) 79	84/99	84/98	81/95/6	170 141	140	008 912	92422.6	229:13:41:54.04	
180	V-43.2	73	1/25		84/98/9	84/98	81/95/6	301 273	272	139 043	92445.4	229:13:42:16.84	
181	A-25	74	1/25		84/98	84/98	81/95	433 404	404	271 175	2853.3	229:17:56:42.35	
182	V-45.1	76	1/25	(182.10)	84 98	97	81/94/5	563 534	532	400 304	22838.5	229:23:29:47.54	
183	↓	↓	↓	80	97/8	97	94/5	693 664	663	532 435	22846.4	229:23:29:55.44	
184	↓	↓	↓		97	97	94	825 796	795	663 567	22854.3	229:23:30:3.34	
185	V-45.1	76	1/25		97	85/97	82/94	957 930	928	795 699	22862.2	229:23:30:11.24	
186	V-46	77	1/25		85/97	85/96/7	82/93/4	089 060	059	927 831	34128.9	230:02:37:57.93	
187	↓	↓	↓		85/97	96	82/93/4	219 190	190	057 961	34135.2	230:02:38:4.23	
188	↓	↓	↓	(188.30)	85/96	96	82/93	351 322	321	189 093	34141.6	230:02:38:10.63	
189	↓	↓	↓	81	96	96	93	483 454	453	321 225	34147.9	230:02:38:16.93	
190	↓	↓	↓		96	95/6	92/3	615 586	585	453 357	34154.3	230:02:38:23.33	
191	↓	↓	↓		96	95	92/3	747 718	717	585 487	34160.7	230:02:38:29.73	
192	↓	↓	↓	(192.30)	95	95	92	878 848	847	715 619	34167.3	230:02:38:36.33	
193	V-46	77	1/25	83	95	95	92	008 979	978	846 750	34173.8	230:02:38:42.83	
194	V-48	79	1/50		95	94/5	95	139 111	110	977 881	56975.3	230:08:58:44.38	
195	↓	↓	↓		95	86/94	83/91/2	269 241	240	107 010	56981.1	230:08:58:50.13	
196	↓	↓	↓		86/94	86/94	83/91	401 373	372	239 143	56986.9	230:08:58:55.93	
197	↓	↓	↓	(197.60)	86/94	94	83/91	534 505	505	372 276	56992.8	230:08:59:1.83	
198	↓	↓	↓	83	86 94	93/4	83 90/1	665 637	635	504 406	56998.7	230:08:59:7.73	
199	↓	↓	↓		94	93	90/1	796 767	766	634 537	57004.6	230:08:59:13.63	
200	↓	↓	↓		93	87/93	84/90	928 899	898	765 669	57010.5	230:08:59:19.53	
R/O Seq	Framelets	R/O Seq	Framelets	R/O Seq	Framelets								
083	877/465	097	084/459										
084	404/917	098	458/103										
085	108/839	099	102/616										
086	407/145												
087	178/880												
088	112/648												
094	647/127												
095	126/601												
960	600/085												

Table 6-9 (Continued)

Frame	Photo Site	Photo Orbit	Shut-ter Speed	Proc Orbit (Index)	R/O Seq. T	R/O Seq. WA	R/O Orbit	WA Edge No.s	TC Frmlt	Tele Edge No.s	S/C Time	Exposure GMT	•
201	V-48	79	1/50	84	87/93	87/93	84/90	060 031	030	897 801	57016.6	230:08:59:25.63	
202	V-49	80	1/25		87/93	87/92	84/89/90	191 162	161	160 933	68480.4	230:12:10:29.41	
203					87/	92/3	84/89/90	321 293	292	160 063	68487.0	230:12:10:36.01	
204					92	92	89	451 423	422	289 193	68493.5	230:12:10:42.51	
205	V-49	80	1/25		92	91/2	88/9	582 554	553	420 325	68499.9	230:12:10:48.91	
206	V-50	82	1/25		92	91	88/9	714 686	685	552 456	91438.1	230:18:33:07.10	
207				(207.60)	91	91	88	845 817	816	683 587	91444.5	230:18:33:13.50	
208				84	91	91	88	977 949	947	815 718	91450.1	230:18:33:19.10	
209	V-50	82	1/25		91	90	87/8	107 080	078	945 849	91457.8	230:18:33:26.80	
210	V-51	83	1/25		90/1	90	87/8	239 211	210	077 981	102633.2	230:21:39:42.20	
211					90	90	87	370 341	340	208 112	102638.3	230:21:39:47.30	
212					89/90	89	86/7	502 474	473	340 244	102643.4	230:21:39:52.40	
213				(213.35)	89	89	86/7	635 606	604	473 376	102648.4	230:21:39:57.40	
214				85	89	89	86	766 738	736	604 507	102653.5	230:21:40:02.50	
215					89	89	86	896 869	867	734 638	102658.7	230:21:40:07.70	
216					88/9	88	85/6	028 999	998	866 770	102664.0	230:21:40:13.00	
217	V-51	83	1/25		88		85/6			998 901			1
218				(218.10)			85			029			
219													
220													
221													
222													
223													
224													
225													
R/O Seq	Framelets	R/O Seq	Framelets	*COMMENTS: 1. 217 W.A. was not processed due to short Bimat roll. 2. Final R/O started with sequence 88 in orbit 85.									
087	178/880												
088	056/930												
089	927/454												
090	453/038												
091	037/580												
092	579/113												
093	112/648												

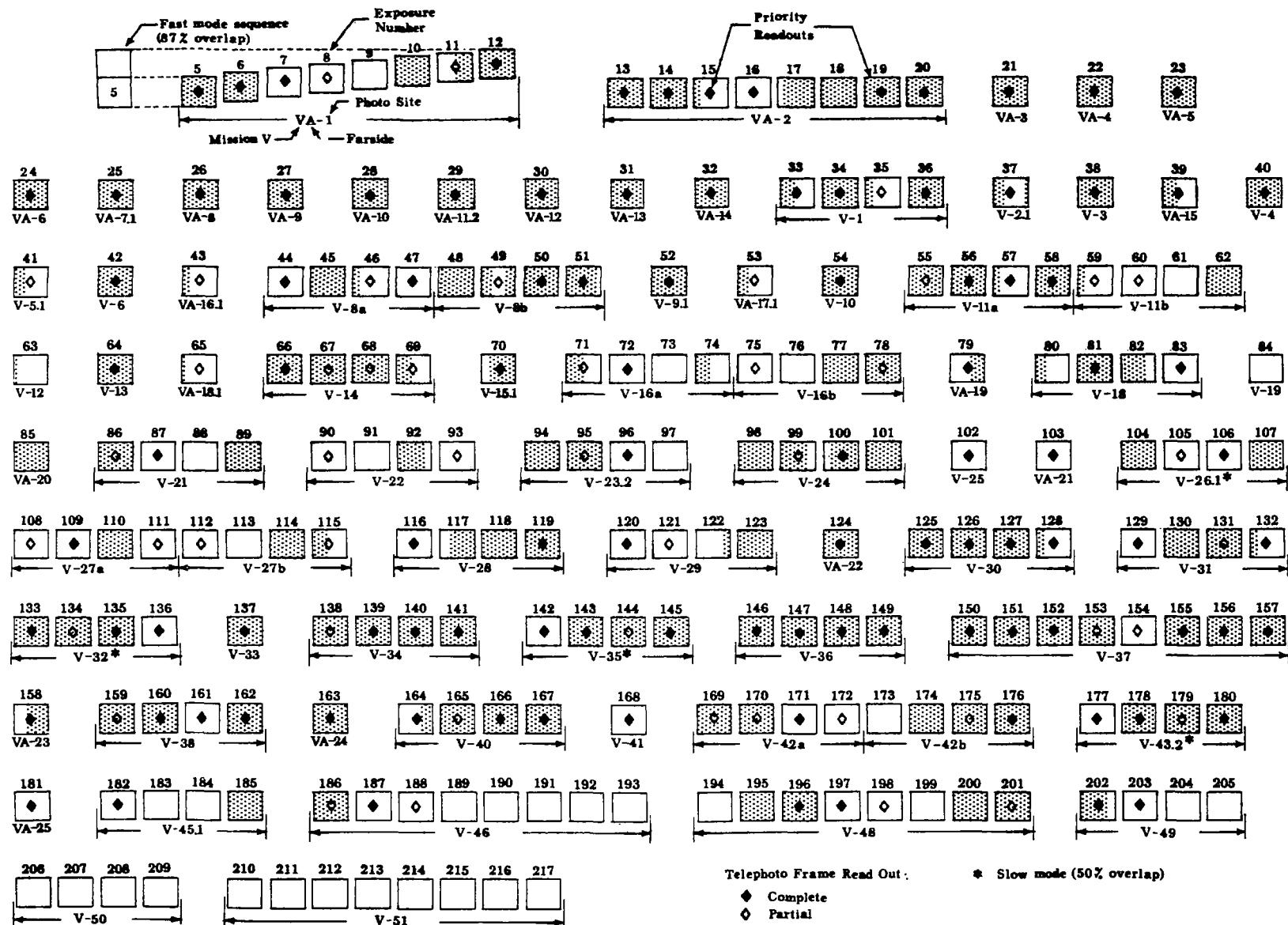


Figure 6-7: Mission V Priority Readout

photographs is determined by the picture formats and the spacing between photographs, including provision for exposure of the time code. The camera specification requires an advance of  $11.690 \pm 0.117$  inches. This may be expressed in terms of the number of edge-data numbers spaced at 0.090 inch along the film. The nominal film advance may thus be stated as 130 plus 3 or minus 2 edge data numbers. This method of indicating spacecraft film length is convenient, and is not affected by readout and reconstruction processes that could influence the spacecraft film-GRE film length relationship.

Film advance for each frame was determined in this manner, and is shown in Figure 6-8. The film advance specified tolerance is shown. Film advances throughout the mission tended to be slightly long, and in a few instances were out of tolerance. The long advances placed the time code near to -- or just on -- the telephoto frame of the next exposure. Over the mission, the actual average film advance was 11.81 inches per frame, which amounted to an additional 2.11 feet of film. This additional film, requiring an equal amount of Bimat for processing, was not sufficient to account for the early exhaus-

tion of Bimat supply discussed in Section 6.2.3.2. Film handling system performance is considered excellent.

#### 6.4.2.2 V/H Ratio Deviation

Some apparent deviation of the telemetered V/H ratio from the predicted V/H ratio was observed. The observed deviations, if real, would have no significant effect on photographic quality, particularly with the cross-track tilts required for most sites. The observed ratio was never larger than the predicted value. The predicted V/H ratio is based on the assumption of a spherical Moon with a radius of 1,738 kilometers. The difference in look-angle between the V/H sensor and the camera, or the effect of major topographic features (mountains or major craters) that would cause errors in V/H ratio, were not taken into account except to disregard sites centered on such features as Aristarchus or Copernicus. In addition, orbit determination is less reliable at  $0^\circ$  longitude when the near-polar orbit is viewed edge-on.

On prior missions, observed low V/H ratios were reported as anomalous V/H sensor performance. It now appears, however, that the

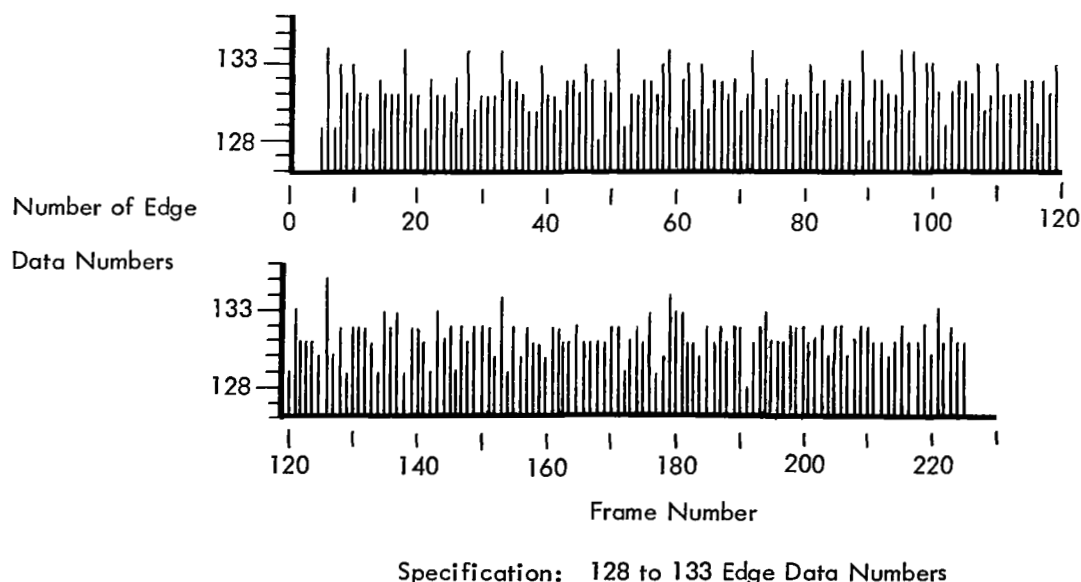


Figure 6-8: Camera Film Advances

effect may quite possibly be the result of the above factors. While a detailed analysis of the V/H ratio data and its relationship to selenodesy is beyond the scope of this report, such a study may well be of significance to the Apollo program.

#### **6.4.2.3 Film Breakage During Rewind**

After final readout had been completed and all photographs successfully recovered, the film was to be wound on the supply spool and only the leader left threaded through the camera. This was to be done to remove the film-leader splice from tension, and to avoid film set so that further readout could be accomplished at a later time if desired. However, before the rewind process was quite complete, the leader apparently parted in or near the readout gate.

Film or leader breakage was indicated when telemetry showed that the readout looper went abruptly to mechanical full and the video-output voltage suddenly increased to its maximum value. The increase in video signal indicated that there was no film in the readout gate. Twenty frames of film were advanced into the camera storage looper from the supply reel. The film did not fill the readout looper, as it should have if the readout looper contents indication had simply been in error. It was concluded, therefore, that the leader had torn about a foot from the splice. No reason for the failure has been indicated.

No loss of data occurred because of this failure. Its only effect was to prevent possible later readout of photographs that had been acquired with complete success.

### **6.4.3 Processor**

#### **6.4.3.1 White Level and Bimat Dryout**

The photo-video chain appeared to function better than on any previous mission. Very few adjustments of the video output gain were required. The Goldstone test film was read out with the video gain set at Step 1. The gain was gradually increased for successive readouts until Sequence 006. At the beginning of that sequence, the gain was increased to Step 5

and was not changed during the remainder of the mission.

The white level remained constant at 5 volts, except during readout of the areas on the spacecraft film where processing was affected by Bimat dryout. Even in these areas, the white level seldom dropped as low as was common during previous missions. During the early portion of the photographic mission, when the photographs were all of farside areas, constraints on the time interval between processing periods were deliberately exceeded to conserve film. In the areas processed by Bimat subjected to extended drying periods, the white level dropped to 4.0 volts. When normal constraints were observed, the white level seldom dropped below 4.5 volts. Plots of white-level variation during two readout sequences are shown in Figures 6-9 and 6-10. The first plot shows the drop in white level during readout of the film section affected by the Bimat dryout occurring during an extended period early in the mission. Figure 6-10 is a similar plot showing the effect of dryout during a period within the normal constraint limit.

Bimat storage life was not exceeded by the time all photography and processing for the mission had been completed. Photography was started earlier in this mission than in others, and temperature was more closely controlled and not excessively high. No long-term changes affecting Bimat characteristics were indicated.

#### **6.4.3.2 Processing Lace Defect**

Throughout the mission, photographs were often affected by a processing defect that has been referred to as "lace" or "freckles," a problem present in varying degrees of severity in all five missions. The exact cause has not been positively identified and no corrective measures have been found during extensive study. The problem has been intermittent, affecting only limited areas along the length of the spacecraft film. Occurrence does not seem to correlate with Bimat life, Bimat dryout, or subsystem operations. The defect appears more frequently on Mission V photographs than on those of previous missions, but it cannot be attributed to any change in hardware, SO-243, or Bimat.



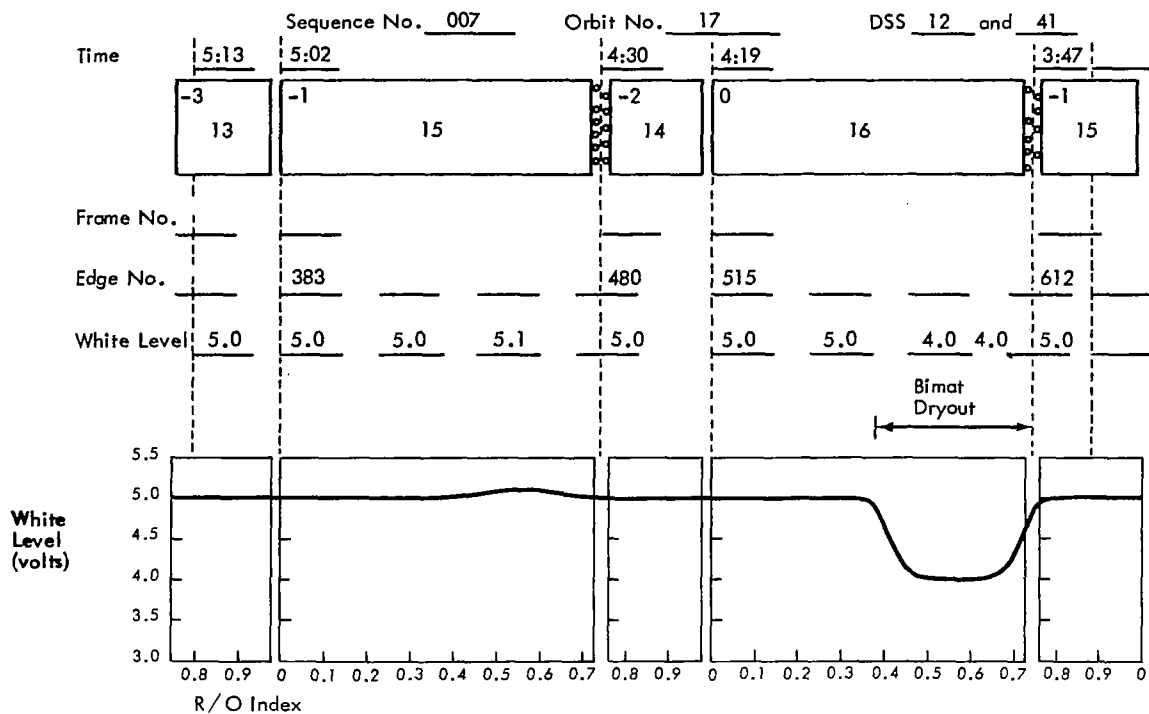


Figure 6-9: White-Level Variation Showing Effect of Extended Bimat Dryout Period

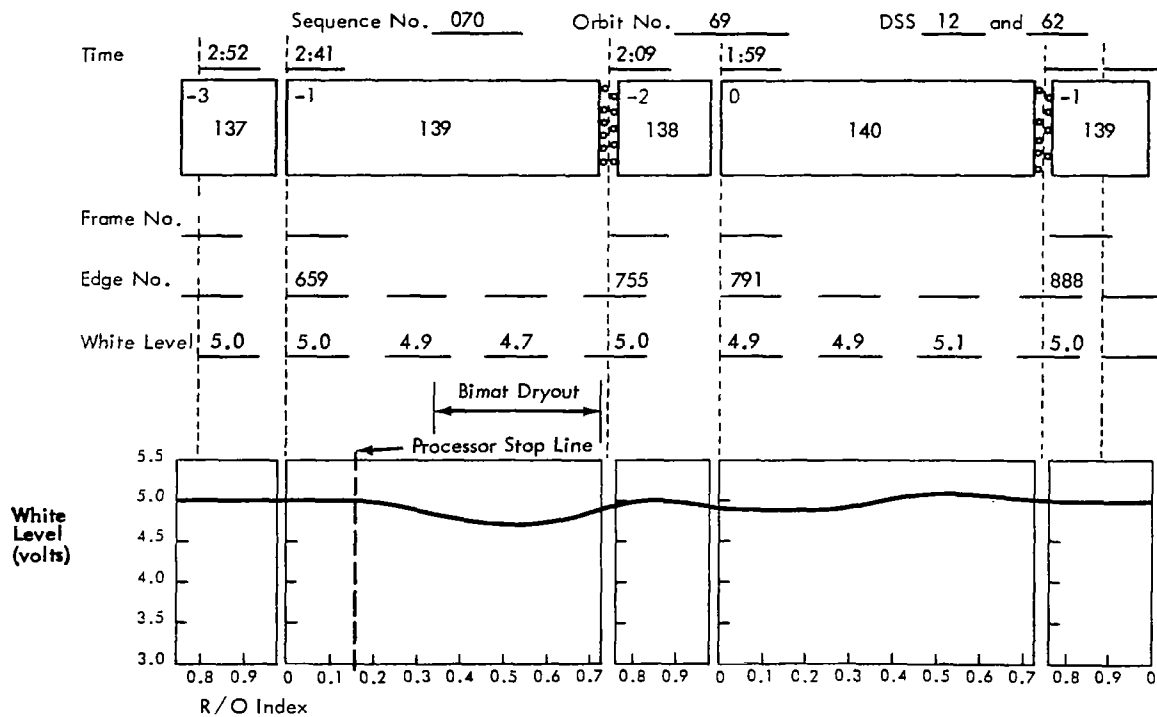


Figure 6-10: White-Level Variation Showing Effect of Normal Bimat Dryout Period

No changes were made in the photo subsystem from the previous two missions, and film and Bimat are the same, within critical manufacturing tolerances.

#### 6.4.4 Readout

Throughout the mission, both priority and final readout progressed without significant difficulty. During final readout, readout sequences of 2.5 hours were scheduled. However, operational requirements resulted in some variation in the duration of the periods, with the maximum being about 3.5 hours. Maximum duration was limited by capacity of the readout looper. Actual readout duration was determined by both the available looper capacity at the start of a readout period and the view period of the recording station. Procedures required during handover from one station to the next made it undesirable to carry out the handover during a readout; therefore, readout was stopped temporarily at these times.

Only two problems affecting readout arose. The first was an intermittent video dropout that occurred during both priority and final readout. The second was a single event that caused loss of two framelets of data.

##### 6.4.4.1 Video Dropout

Video dropout was a phenomenon observed during readout that had not occurred during previous missions. The problem manifested itself when three to six scan lines appeared with no image, followed by another six to eight scans that were distorted as the video returned to normal. Distortion during video recovery often appeared with an "S" pattern. During these events, no GRE sync loss was evident and all operational indications appeared to be normal.

Intermittent video dropout was first observed during readout of the Goldstone test film just prior to the start of mission photography. The first occurrence during readout of a lunar photograph was during Sequence 009. The video dropouts appeared as a narrow white line on the GRE-reconstructed record that obscured very

little image. Even when several dropouts occurred on a single framelet, the relative loss of data is very small considering the over 16,000 scan lines required for each framelet.

Although several framelets read out during final readout had 50 or more of the dropouts, these framelets were recorded during priority readout with no loss. During final readout there were 52 framelets read out with 10 or more dropouts per framelet. Of these, 32 were read out in priority with no loss. All framelets with more than 20 occurrences were read out previously with no dropout. Seven frame-pairs had 50 or more dropouts, but six of these photographs were obtained during priority readout without any loss. Frame 84, obtained only during final readout, had less than 15 dropouts in any one framelet.

An example of the video dropout as it appears on the photograph is shown in Figure 4-97.

##### 6.4.4.2 Framelet Loss

Two framelets of Frame 217 were not recovered during final readout. Readout Sequence 088, the first sequence of final readout, was terminated by a stored-program command, but the readout did not completely terminate. The optical-mechanical scanner stopped in the focus-stop position but scanning and readout electronics did not shut down. In this situation, readout is terminated by a stored-program backup "readout drive on" command. Two framelets are then scanned and readout stops when the optical-mechanical scanner reaches the spot-stop position. Sequence 088 was terminated in this manner. However, a stored-program "acquire Sun" command followed immediately after "readout drive on," thus a real-time "Mode 2 off" command was necessary before "readout drive on" was executed. Two framelets were scanned after "readout drive on," but the information was not transmitted to the ground stations because "Mode 2" was off.

Prior to the next readout, a decision was made to continue readout without retrieving the two lost framelets.

## 7.0 Program Summary

### 7.1 PHOTOGRAPHIC OBJECTIVES

The primary task of the Lunar Orbiter Program as defined by Contract NAS1-3800 was:

"To obtain, from lunar orbit, detailed photographic information of various lunar areas, to assess their suitability as landing sites for Apollo and Surveyor spacecraft, and to improve our knowledge of the Moon."

The landing site portion of the original task for the program, as defined above, was essentially completed by Missions I, II, and III. This permitted broadening the program objectives by planning the use of the remaining two spacecraft to further improve the scientific knowledge of the Moon. Representatives of the scientific community collaborating in the program were near unanimous in asserting that the remainder of the program should consist of:

- Surveying the entire lunar surface at a resolution significantly better than that obtainable from Earth.
- Examining in detail various surface geological processes identified from this survey.

### 7.2 PROGRAM PHOTOGRAPHIC ACCOMPLISHMENTS

#### 7.2.1 Landing Site Photography

The primary task of the Lunar Orbiter program

was essentially completed during the first three missions. Lunar Orbiters I and II accomplished photographic site-search missions of preselected areas grouped in southern and northern latitude bands, respectively, of the established Apollo zone of interest ( $\pm 5^\circ$  latitude,  $\pm 45^\circ$  longitude). Lunar Orbiter III performed a comprehensive site-confirmation mission of the 12 most promising sites selected from the Mission I and II photographs. Mission V provided additional Apollo site coverage to complete the three types of photography – vertical, telephoto convergent stereo, and westerly oblique – required of each of the eight candidate Apollo sites selected on the basis of prior mission photography.

Landing site photography is summarized in Tables 7-1 through -5. The following abbreviations have been used in the above tables:

Mode: "F" Fast sequencing mode  
 "S" Slow sequencing mode  
 Coverage Type: "NV" Near-vertical camera axis  
 "CTS" Convergent telephoto stereo  
 "WO" Westerly oblique  
 "Spec." Specially designed coverage

Table 7-1: Location of Landing Site Photography

Mission I			Mission II			Mission III			Mission V		
Site No.	Lat (deg)	Long. (deg)	Site No.	Lat (deg)	Long. (deg)	Site No.	Lat (deg)	Long. (deg)	Site No.	Lat (deg)	Long. (deg)
IP-1	0.85S	41.90E	IIP-1	4.17N	36.92E	IIIP-1	2.92N	35.25E	V-3.1	0.85S	41.90E
IP-2	0.09N	35.51E	IIP-2	2.75N	34.00E	IIIP-2	0.87S	42.33E	V-6	0.85S	41.90E
IP-3	0.55N	26.16E	IIP-3	4.33N	21.33E	IIIP-3	3.33N	20.25E	V-8	0.85S	41.90E
IP-4	0.01S	13.52E	IIP-4	4.75N	15.75E	IIIP-4	0.62N	27.45E	V-9.1	2.75N	34.00E
IP-5	0.03N	1.52W	IIP-5	2.70N	24.63E	IIIP-5	0.45N	24.52E	V-11	2.75N	34.00E
IP-6	3.88S	2.22W	IIP-6	0.75N	24.17E	IIIP-6	0.33N	21.50E	V-13	0.75N	24.17E

**Table 7-1 (Continued)**

Mission I			Mission II			Mission III			Mission V		
Site No.	Lat (deg)	Long. (deg)	Site No.	Lat (deg)	Long. (deg)	Site No.	Lat (deg)	Long. (deg)	Site No.	Lat (deg)	Long. (deg)
IP-7	3.50S	22.17W	IIP-7	2.17N	2.00W	IIIP-7	0.97N	1.30W	V-16	0.75N	24.17E
IP-8.1	2.98S	36.64W	IIP-8	0.08N	1.00W	IIIP-8	0.83S	19.83W	V-27	0.08N	1.00W
IP-9.2	2.18S	43.58W	IIP-9	1.00N	13.00W	IIIP-9	3.15S	23.18W	V-42	3.28S	36.93W
			IIP-10	3.47N	27.17W	IIIP-10	1.75N	42.00W			
			IIP-11	0.08N	19.92W	IIIP-11	3.28S	36.93W			
			IIP-12	2.42N	34.67W	IIIP-12	2.38S	43.87W			
			IIP-13	1.50N	42.33W						

**Table 7-2: Mission I Landing Site Photography**

Site No.	Sequences			Frame Numbers	Coverage Type*
	No.	Frames Each	Mode		
IP-1	1	16	F	52-67	NV
IP-2	1	16	F	68-83	NV
IP-3	1	16	F	85-100	NV
IP-4	1	8	S	105-112	NV
IP-5	1	16	F	118-133	NV
IP-6	1	8	S	141-148	NV
IP-7	1	16	F	157-172	NV
IP-8.1	1	8	F	176-183	NV
IP-9.2	2	16	F	184-215	NV

\*Wide-angle photography only

### 7.2.2 Broad-Area Coverage

The combined photography of all missions has provided photographic coverage of virtually the entire lunar surface. Coverage of the nearside was accomplished primarily during Mission IV from a relatively high orbit. This photography showed the surface from a near-vertical aspect never before seen except near the center of the disk. Detail was shown at a resolution of about 50 to 150 meters (depending upon altitude), or at least ten times better than possible from Earth.

Farside coverage was obtained on all missions. Because the spacecraft was near apolune and thus at a higher altitude, resolution is not as good as for the nearside but never the less was of the order of 150 to 250 meters for the wide range of operating conditions encountered. The combination of farside photography obtained on each mission has made possible preparation of a preliminary lunar farside chart, LFC-1 at a scale of 1:5,000,000 by the Aeronautical Chart and Information Center. The chart shows the area between 48°N and 48°S latitude on a Mercator projection and the two areas between 48° and 90° N latitude and between 48° and 90° S latitude

**Table 7-3: Mission II Landing Site Photography**

Site Number	Sequences			Frame Numbers	Coverage Type	Remarks
	No	Frames Each	Mode			
IIP-1	1	16	F	5-20	NV	Partial recovery
IIP-2	1	8	F	35-42	NV	
IIP-3	2	8	F	43-58	NV	Successive orbits
IIP-4	1	8	F	59-66	NV	
IIP-5	1	8	F	67-74	NV	Ranger VIII
IIP-6	2	8	F	76-91	NV	Successive orbits
IIP-7	2	8	F	96-111	NV	Successive orbits
IIP-8	3	8	F	113-136	NV	Three successive orbits
IIP-9	1	8	F	138-145	NV	
IIP-10	2	8	F	146-161	NV	Successive orbits
IIP-11	2	8	F	163-178	NV	Successive orbits
IIP-12	2	8	F	179-194	NV	Successive orbits
IIP-13	2	8	F	197-212	NV	Successive orbits

on Polar stereographic projections. These charts, in reduced scale, are shown in Figures 7-1 and -2. The Lunar Orbiter data will support preparation of much more detailed farside charts.

Department of Defense mapping agencies are preparing special photographic charts of candidate Apollo sites and landing ellipses. Scales of 1:100,000, 1:25,000, and 1:12,500 are being used, as appropriate to the application.

Photogrammetry originally was not a requirement for the Lunar Orbiter program. However, refinements including lens calibration, addition of pre-exposed reseau marks on the spacecraft film, and development of computer programs to

provide accurate specification of photograph parameters have added this capability to program accomplishments.

### 7.2.3 Scientific Photography

Prior to Lunar Orbiter Mission V, photography of nearside areas other than the landing sites had been limited to secondary sites using frames that had to be moved to prevent film handling defects and which otherwise would have been blank. Success of the first four missions provided the opportunity to devote Mission V primarily to detailed photography of nearside areas of particular scientific interest and of potential value as possible landable sites for Surveyor and Apollo Applications missions.

**Table 7-4: Mission III Landing Site Photography**

Site Number	Sequences			Frame Numbers	Coverage Type	Remarks
	No	Frames Each	Mode			
IHIP-1	1	16	F	5-20	NV	Successive orbits; retake of IP-1.  Recovery of photography through Site IHIP-6 is incomplete.
IHIP-2	2	8-4	F	25-36	NV	
IHIP-3	1	4	S	40-43	NV	
IHIP-4	1	8	F	44-51	NV	
IHIP-5	2	8	F	52-67	CTS	
IHIP-6	1	4	S	68-71	NV	
IHIP-7	2	8	F	86-101	CTS	
IHIP-8	1	8	F	124-131	NV	
IHIP-9	3	8	F	137-160	Spec. CTS	Coverage designed to ensure including planned Surveyor III site.
IHIP-10	1	8	F	163-170	CTS	CTS to be obtained with Site IIP-13.
IHIP-11	1	8	F	173-180	NV	Retake of IP-8.1 area.
IHIP-12	4	16, 4, 4, 8	F	181-212	Spec.	Coverage specified to ensure coverage of Surveyor I.
IHS-4	1	1	—	39	WO	Site III P-5
IHS-11	1	1	—	84	WO	Site IHIP-7
IHS-21	1	1	—	120	WO	Site IHIP-8
IHS-24	1	1	—	136	WO	Site IHIP-9
IHS-25	1	1	—	161	WO	Site IHIP-10
IHS-27	1	1	—	171	WO	Site IHIP-11
IHS-28	1	1	—	172	WO	Site IHIP-12

Table 7-5: Mission V Landing Site Photography

Site Number	Sequences			Coverage Type	Remarks	Frame Numbers
	No.	Frames Each	Mode			
V-3.1	1	1	—	WO	Oblique of IP-1; includes zero-phase point.	38
V-6	1	1	—	WO	Site IP-1; includes zero-phase point.	42
V-8	2	4	F	CTS	Site IP-1	44-51
V-9.1	1	1	—	WO	Site IIP-2; also photographed as Site IIP-1.	52
V-11	2	4	F	CTS		55-62
V-13	1	1	—	WO	Site IIP-6; also photographed as Sites IP-3 and IIP-5.	64
V-16	2	4	F	CTS		71-78
V-27	2	4	F	CTS	SITE IIP-8	108-115
V-42	2	4	F	CTS	SITE IIP-11	169-176

Particular areas or features of special interest photographed during the first three missions are listed in Table 7-6. Mission V sites are listed in Table 2-2.

#### 7.2.4 Surveyor and Ranger Location

Surveyor I was successfully landed in June 1966, 2 months prior to the launch of Lunar Orbiter I. The landing site was photographed by Lunar Orbiter, but because of problems with the telephoto shutter, location of the Surveyor could not be verified. The area was again photographed by Mission III and the Surveyor I spacecraft was visible on a telephoto frame (Site IIP-12, Telephoto Frame 194, Framelet 248. See Lunar Orbiter III Final Report, *Photography*, NASA CR 984, pages 89 through 91.

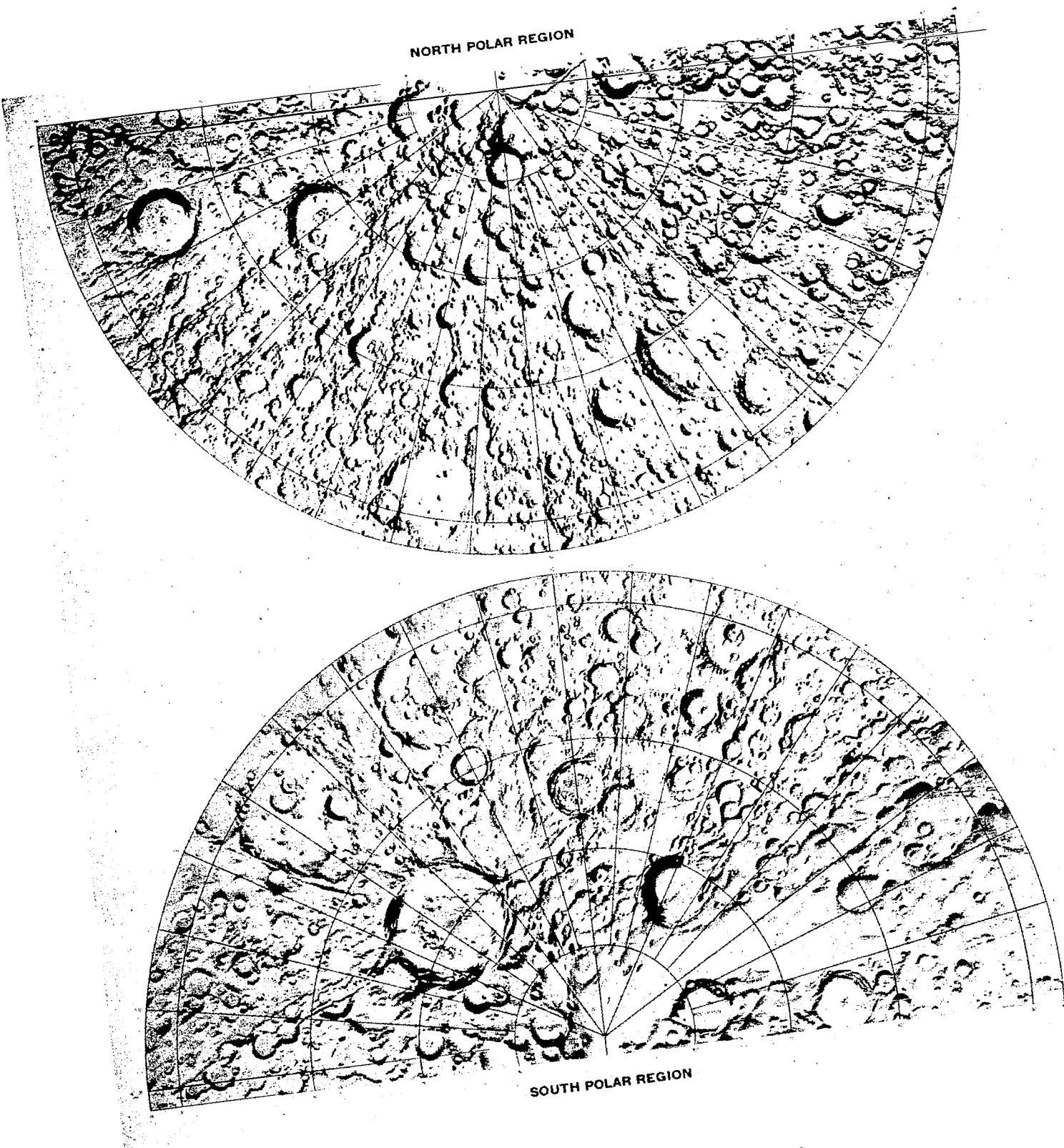
Location of Surveyor III, successfully launched in April 1967, was definitely established by correlating Surveyor photographs and Lunar Orbiter photographs of the predicted landing area. Use of the telephoto frames enabled far more precise location of Surveyor III. (See Lunar Orbiter III Final Report, *Photography*, NASA CR 984, pages 39 through 43. Lunar Orbiter photographs are being used in a similar manner to locate Surveyors V, VI, and VII.

The team concept of Lunar Orbiter providing photography over a large area and Surveyor providing high detail and soil mechanics data over a limited area has been demonstrated to be a powerful tool in the objective of certifying Apollo landing sites and understanding the scientific nature of the Moon.

The probable location of the impact point of Ranger VIII was photographed as Site IIP-5. The impact point was identified by NASA on Telephoto Frame 70 as one of two small, bright craters having diameters of 7 and 15 meters. Ranger VIII did not photograph its impact point; hence, it was not possible to determine which of the two craters was made by its impact. Subsequent intensive study has provided additional evidence that the larger of the two is most likely the Ranger crater.

#### 7.2.5 Earth Photography

Earth was photographed during Missions I and V. The Mission I photographs, Frames 102 and 117, were taken on August 23 and 25, 1966, respectively. (See Lunar Orbiter Final Report, *Photography*, NASA CR847, page 64.) The first telephoto frame shows a crescent Earth and,

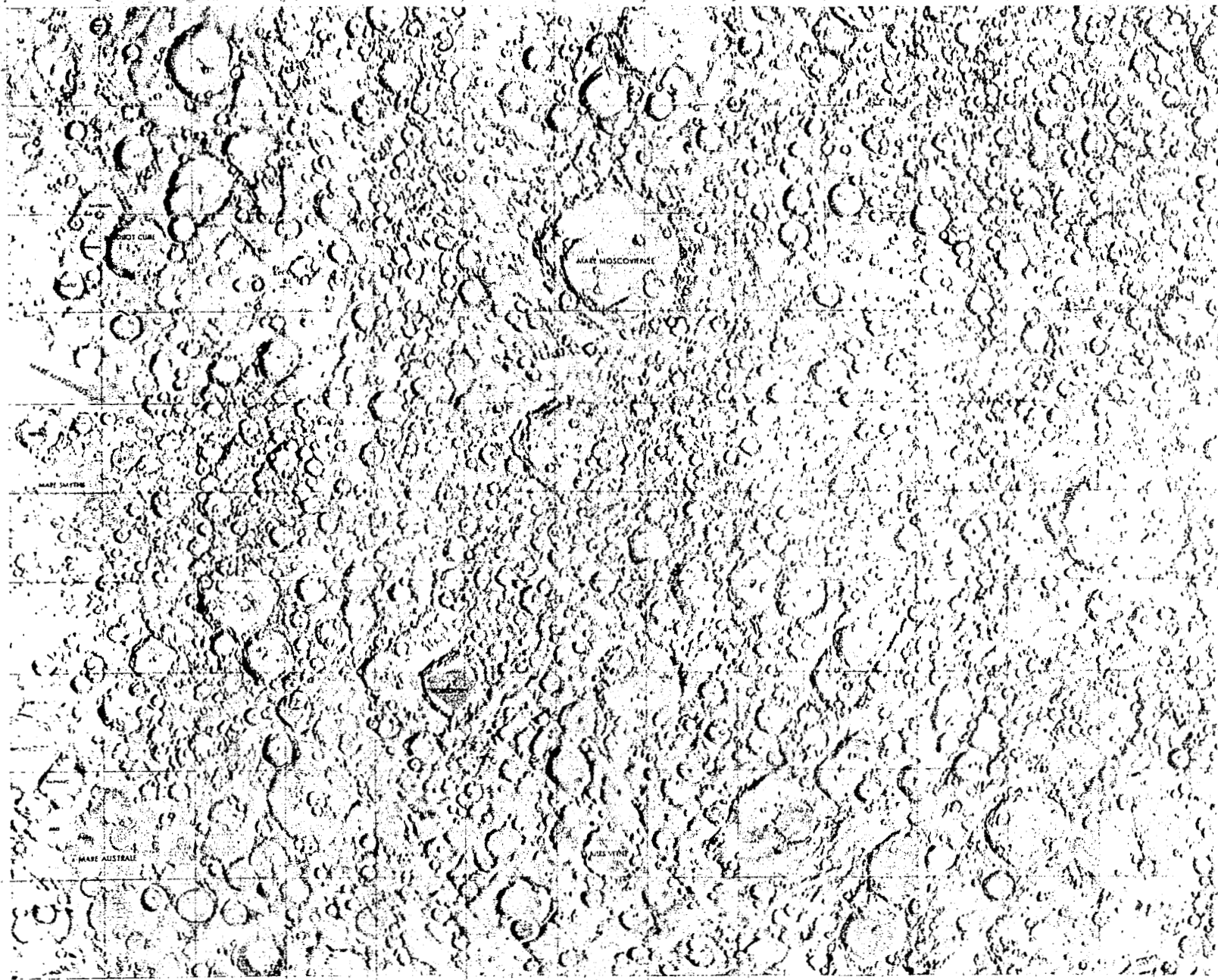


**Figure 7-1: Lunar Farside Chart; Polar Areas**



LFC-1

# LUNAR FARSIDE CHART



## LUNAR FAR SIDE CHART

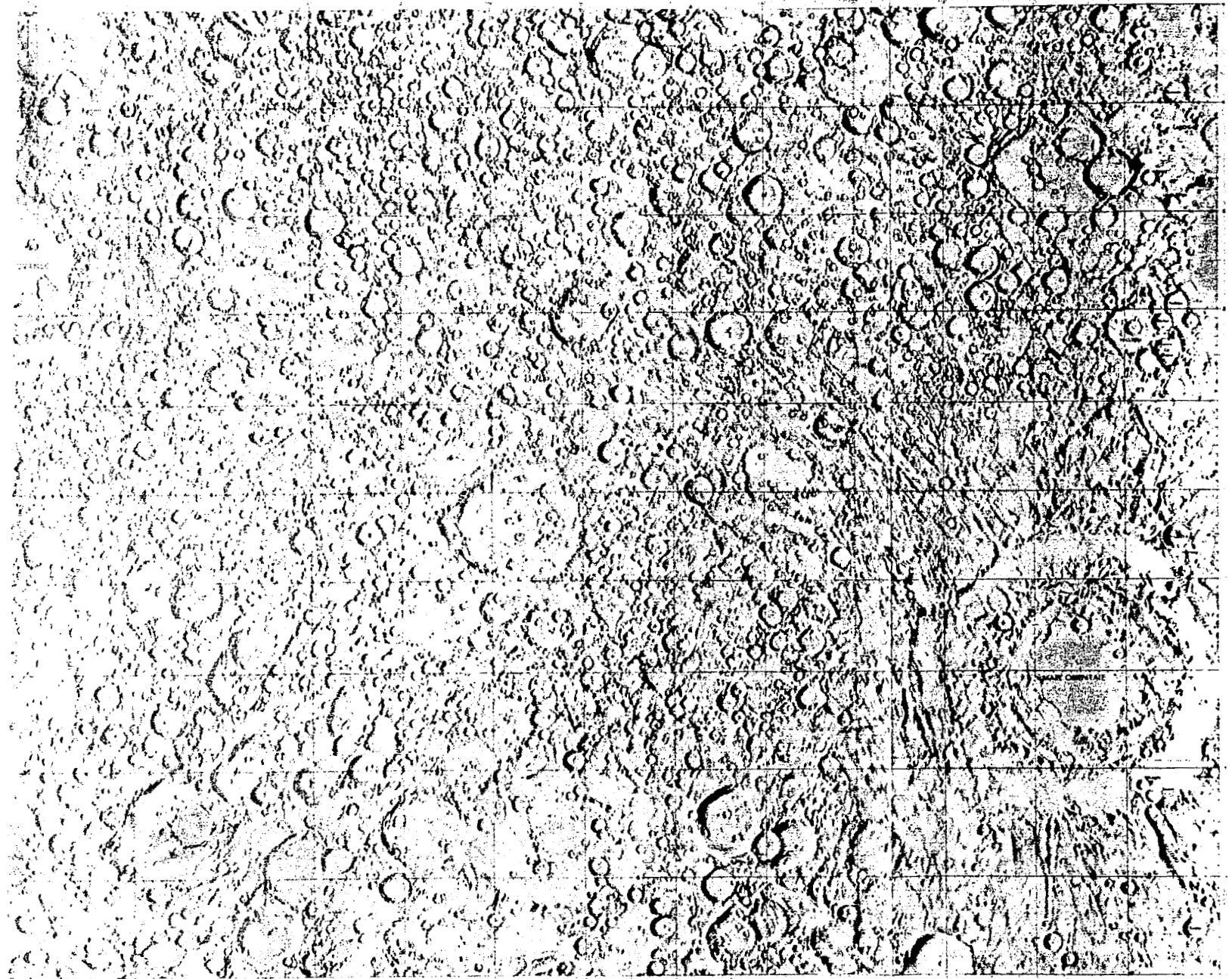


Figure 7-2: Lunar Farside Chart; Mercator

Table 7-6: Special Interest Areas Photographed on Missions I through III

Site	Area or Feature and Type of Photography
I	Farside; 11 frames taken from near apolune.
I Frame 40	Terminator; demonstrates value and feasibility of low sun angle photography.
I Frame 48	Domes near Lansberg; first evidence of their volcanic origin.
I Frame 84	Dionysius; evidence of many different terrain units.
I Frame 41	Taruntius; ejecta and secondary craters.
I Frame 117	Earth and Moon's limb; oblique.
I Frame 149	Chain-craters near Reinhold; first clear evidence of this form.
IIS-6	Rima Triesnecker; slight oblique
IIS-7	Sinus Medii; oblique
IIS-10.2	Gambart C thermal anomaly; vertical
IIS-11	S.W. of Copernicus; near vertical
IIS-12	Northerly oblique of Copernicus
IIS-13	Braided ridge S.W. of Kepler
IIS-15	Northerly oblique of Marius and Marius Hills
IIS-16	Mare area S. of Reiner; vertical
IIS-17	Reiner gamma; oblique

Site	Area or Feature and Type of Photography
IIIS-1	Messier and Messier A; vertical
IIIS-3	Fan-shaped area near Colombo
IIIS-5	Moltke; north oblique
IIIS-6	Rima Hyginus; north oblique
IIIS-7	Vicinity of Dembowski; vertical
IIIS-8	Theophilus; southerly oblique
IIIS-9	Delambre
IIIS-13	Murchison and Pallus; oblique
IIIS-15	Near Schroter; slight oblique
IIIS-16	Mosting; near vertical
IIIS-18	Mosting C; oblique
IIIS-20	Hortensius domes; oblique
IIIS-23	Fra Mauro; oblique
IIIS-26	Kepler; northerly oblique
IIIS-29	Damoiseau; southerly oblique
IIIS-30	Area of Luna 9 landing; oblique
IIIS-31	Floor of Hevelius; near vertical

although cloud cover is extensive, parts of Africa and the Mediterranean Sea are visible. The second photograph, taken 2 days later, included Australia. In addition to Earth, the photographs included a portion of the Moon's limb that demonstrated the value of oblique photography for interpretation of lunar topography. The success of this photography resulted in the decision to take many additional oblique lunar photographs on subsequent missions.

The last Earth photograph was taken on August 8, 1967, during Mission V as Site VA-9. The particular spacecraft-Earth-Sun geometry provided a nearly "full Earth" photograph. The Moon, however, is not included in the scene. A more detailed description will be found in Section 4.6 of this report.

### 7.3 OPERATIONAL SUMMARY

#### 7.3.1 Photographic Problems

The Lunar Orbiter program has been successful in fulfilling all objectives. On occasion, it was necessary during a mission to overcome problems in flight operations affecting photography to achieve that goal. In nearly all cases, techniques, some of which involved nonstandard operational procedures, were developed during flight that enabled the mission to continue and photographs to be obtained.

##### 7.3.1.1 Problems General to Program

The major problems encountered on all missions were those related to film exposure and to the Bimat processing of the SO-243 film aboard the spacecraft. The exposure problem was related principally to the transmissivity differential between the 80-mm wide-angle lens and the 610-mm telephoto lens. The difference was compensated adequately for Missions III, IV, and V by installation of a neutral-density filter on the 80-mm lens.

Throughout the program, a spacecraft film processing defect occurred in varying amounts. It is evident on the photographs as small round or elongated blemishes occasionally present in the form of loops. In some cases, the blemishes appeared in bands longitudinally along the spacecraft film or in isolated groups. This de-

fect has been referred to as "lace" or "freckles." Although considerable analysis and testing were conducted during the program, the cause of the problem could not be established with certainty; thus, no corrective action could be taken. The problem was most evident on Mission V.

Lunar surface characteristics posed an exposure problem because of the extreme luminance range encountered, particularly in areas of rough topography. Spacecraft film density predictions were computed for each shutter speed using the predicted photographic geometry and albedo. These computations were the basis of exposure control and generally were satisfactory. Limited areas of overexposure and underexposure within individual frames were inevitable.

Film exposure control on the spacecraft was a problem, particularly during the first mission because of uncertainty in data regarding the surface characteristics of albedo and the photometric function. However, as experience was gained during the missions, prediction of the most suitable exposure became quite reliable. Data on the albedo of individual sites were prepared by the USGS from Earth-based telescopic observation. They provided data on albedo distribution within the area and a recommended value for each site. Experience acquired during the missions indicated that a reduction of these albedo values by a factor of 1.3 was necessary for proper exposure prediction. These modified values were used in the computer program that generated predicted spacecraft film densities for each shutter speed from the data on illumination and observational geometry, albedo, and camera constants. Shutter speeds were selected on the basis of these predictions to give the most satisfactory film density for the telephoto frame.

Studies involving positional accuracies of the photographs have revealed differences between the computed selenographic coordinates for individual frames and the coordinates of features within the photographed area derived from Earth-based observation. The apparent discrepancies, occurring primarily along the orbit track, were variable during each mission. The discrepancies are the result of a combination

of factors including operational limitations, control accuracies, and uncertainties in critical parameters used for orbital computations. To these must be added the uncertainties in locations derived from Earth-based observation with which the comparisons are made. Computations of the positions for each Lunar Orbiter photograph have been refined on the basis of postmission data analysis. Further refinement of positions is expected from a current study investigating the effects of the lunar gravitational model and orbit-determination computations that have been used.

In general, resolution of the photographs was limited only by the system noise level and met specified requirements except where affected by specific operational requirements such as no IMC or by problems such as the shutter malfunction of Mission I.

#### *7.3.1.2 Problems Related to Specific Missions*

During each mission, problems affecting photography were encountered that were usually unique to that particular mission. These are listed below for each mission.

*Mission I*—The major problem was the malfunction of the telephoto focal-plane shutter. Shutter operation at an incorrect time in the operating sequence caused the telephoto frames to be smeared. This problem was corrected for subsequent flights by appropriate changes in the photo subsystem circuitry and hardware.

*Mission II*—No major operational problems or failures affecting overall mission photography occurred.

Some variations in readout film advance occurred that occasionally resulted in a small amount of incorrect overlap of adjacent framelets. This did not result in any data loss.

Failure of the TWTA terminated final readout before the last eight frames had been readout. Portions of those frames had been recovered by priority readout. Wide-angle coverage was complete because of overlap but some telephoto coverage of Site IIP-1 was lost.

*Mission III*—Problems were encountered with the readout film advance mechanism that occasionally resulted in a framelet being scanned more than once, or the film was not advanced the exact specified amount. This resulted in a redundancy, rather than loss of data read out.

During final readout, a failure occurred that prevented readout of the last 79 frames of photography. Of these frames involved, portions of 36 telephoto and 19 complete and three partial wide-angle frames had been acquired during priority readout. This failure limited coverage, primarily telephoto, of the first six primary sites of the mission.

*Mission IV*—During the first photographic orbit, the camera thermal door failed to open properly for the third site of a sequence of five, but was opened for the last site of that orbit by an alternate procedure. Because the problem reoccurred in the first sequence of the next orbit, the mission was continued with the thermal door open. The consequence of this action was excessive camera window cooling that caused moisture condensation on the inner surface. The resultant diffusion of light from the lunar surface degraded the photographs. An attempt to warm the window by orientation of the spacecraft more directly into the sunlight resulted in a light-leak past baffles, which caused some film fogging. By Orbit 13, emergency operational procedures had been developed sufficiently to successfully command opening and closing the balky thermal door. Condensation was ultimately cleared between Frames 79 and 83. Photography from near apolune, later in the mission, covered most of the lunar area over which the operations problems had occurred.

During a normal processing period in Orbit 35, the readout looper began filling, presumably because an anomalous "readout looper empty" signal originating in the command encoder inhibited the film takeup motor. Processing was terminated and the Bimat was cut. After Bimat-cut, the anomalous signal preventing film takeup was still present. A nonstandard procedure was then devised to inch the last of the processed film past the readout gate so that those frames could be recovered. The emergency technique

was successful and final readout was then initiated.

**Mission V**—Mission V was exceptionally free of operational problems. The only problem, unique to this mission, that affected photographs was an intermittent video signal dropout that for each occurrence affected only a few scan lines of the nearly 17,000 per framelet. During final readout, amounting to 25,000 framelets, only 52 framelets had 10 or more dropouts. Of these 52, 32 were acquired in priority readout with no loss.

### 7.3.2 Program Statistics

Spacecraft ellipse parameters for the five Lunar Orbiter missions are shown in Table 7-7. Depending on the type of mission, photography was performed from varied altitudes depending on ellipse selection and the number of orbits

required to perform each photographic task. Objectives for Missions IV and V required markedly different ellipse designs from those low inclinations used in the first three missions for which the Apollo Zone along the equator was the area of primary interest. Near-polar orbits with inclinations of approximately 85 degrees and more eccentric ellipses were used for the last two missions to enable extended photographic coverage of virtually the entire lunar surface.

Photographic parameters are shown in Table 7-8. Approximately 2,090 photographs were taken in the five missions. Including partial frame readouts, approximately 1,950 of these photographs were recovered. The Lunar Orbiter Project Office has classified 1,668 as "useful," since some photographs were degraded by operational problems mentioned earlier.

Table 7-7: Ellipse Parameters

Function	L.O. I	L.O. II	L.O. III	L.O. IV	L.O. V
<u>Initial Ellipse</u>					
Perilune altitude (km)	* (199) 189	(202) 196	(213) 210	(2701) 2706	(202) 195
Apolune altitude (km)	(1850) 1866	(1850) 1871	(1850) 1802	(6111) 6114	(6050) 6028
Orbit inclination (deg) **	(12.04) 12.16	(11.99) (11.97)	(21.05) 20.94	(85.48) 85.48	(85.05) 85.01
Orbit period (hours:min.)	(3:37) 3:37	(3:37) 3:37	(3:37) 3:37	(12:00) 12:01	(8:30.8) 8:26.9
Number of orbits	43	33	26	48	4
<u>Second Ellipse</u>					
Perilune altitude (km)	(57.9) 56.0	(50.2) 49.7	(54.8) 54.8	N.A.	(101) 100
Apolune altitude (km)	(1855) 1853	(1858) 1853	(1846) 1847		(6066) 6067
Orbit inclination (deg) **	(12.04) 12.05	(11.91) 11.89	(20.87) 20.91		(85.62) 85.61
Orbit period (hours:min.)	(3:29) 3:29	(3:28) 3:28	(3:28) 3:28		(8:23) 8:20.7
Number of orbits	30	146	123		6
<u>Third Ellipse</u>					
Perilune altitude (km)	(40.0) 40.5	N.A.	N.A.	N.A.	(99) 99
Apolune altitude (km)	(1824) 1817				(1502) 1500
Orbit inclination (deg)	(12.03) 12.0				(84.76) 84.76
Orbit period	(3:26) 3:26				(3.11) 3:11.9
Number of orbits	135				136
* Predicted values in parentheses; others are actual values					
** Selenographic-of-date coordinates N.A. - Not applicable					



**Table 7-8: Photographic Parameters**


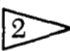

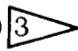
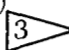
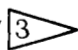

Function	L.O. I	L.O. II	L.O. III	L.O. IV	L.O. V
Dual frames exposed	(212) 1 	(211) 211	(212) 211	(212) 199	(213) 213
First photo date	8-18-66	11-18-66	2-15-67	5-11-67	8-6-67
Last photo date	8-29-66	11-25-66	2-23-67	5-26-67	8-18-67
Telephoto frames read out	(212) 211 2 	(211) 209 3 	170 3 	180	213
Wide-angle frames read out	(212) 211	(211) 208 3 	157 3 	179	212
Final readout started	8-29-66	11-26-66	2-23-67	5-29-67	8-19-67
Last readout completed	9-14-66	12-7-66	3-2-67	6-1-67	8-27-67
Primary Sites Photographed	(10) 10	(13) 13	(12) 12	(176) 147	(41) 41
Frames exposed	(180) 156	(184) 184	(156) 156	(191) 160	(174) 174
Photo sequences	(11) 11	(22) 22	(19) 20	(176) 147	(50) 50
Altitude range (km)	45-54	44-57	45-62	2670-5790	96-248
Secondary Sites Photographed (Nearside)	41	(13) 13	(31) 30	N.A.	N.A.
Frames exposed	(42) 44	(23) 23	(55) 54		
Photo sequences	(42) 41	(14) 14	(31) 30		
Altitude range (km)	46-239	41-51	44-63		
Farside Sites Photographed	7	(4) 4	(1) 1	8	23
Frames exposed	(0) 11	(4) 4	(1) 1	9	37
Photo sequences	(0) 7	(4) 4	(1) 1	8	23
Altitude range (km)	1295-1454	1450-1517	1460	6110-6150	1180-5755
Readout Sequences					
Priority readout	45	53	53	122 4 	86
Final readout	93	73	56	29	61
Total	138	126	109	151	147



Table 7-8 (Continued)

Function	L.O. I	L.O. II	L.O. III	L.O. IV	L.O. V
Types of Site Photography (Frames)					
Vertical	(212) 209	(196) 196	79	190	50
Near vertical	0	(11) 11	80	9	77
High obliques	2	(4) 4	52	0	46
Convergent telephoto stereo	0	(8) 8	36	0	40

- 1 Predicted values in parentheses; others are actual values.
- 2 Telephoto frames smeared because of camera malfunction
- 3 Includes some partially read out frames
- 4 Includes many short readouts during film advance irregularities

N.A. Not applicable

#### 7.4 CONCLUSION

In retrospect, the Lunar Orbiter photographic program has successfully fulfilled its objectives. Those few problems encountered were overcome — even during the missions — by exploiting the operational versatility of the spacecraft and its subsystems. Information vital for successful lunar landings was obtained. The entire Moon has been photographed, and a large number of features of outstanding scientific interest have been photographed in detail. Thus, the program has not only provided data essential to successful initial Apollo landings, but it has also produced a body of lunar data and photographs that will be definitive for many years.

NATIONAL AERONAUTICS AND SPACE ADMINISTRATION  
WASHINGTON, D. C. 20546  
OFFICIAL BUSINESS

FIRST CLASS MAIL

POSTAGE AND FEES PAID  
NATIONAL AERONAUTICS AND  
SPACE ADMINISTRATION

04U 001 56 51 3DS 68150 00903  
AIR FORCE WEAPONS LABORATORY/AFWL/  
KIRTLAND AIR FORCE BASE, NEW MEXICO 87117

ATT MISS MADELINE F. CANCVA, CHIEF TECHN  
LIBRARY /W111/

POSTMASTER: If Undeliverable (Section 158  
Postal Manual) Do Not Return

*"The aeronautical and space activities of the United States shall be conducted so as to contribute . . . to the expansion of human knowledge of phenomena in the atmosphere and space. The Administration shall provide for the widest practicable and appropriate dissemination of information concerning its activities and the results thereof."*

— NATIONAL AERONAUTICS AND SPACE ACT OF 1958

## NASA SCIENTIFIC AND TECHNICAL PUBLICATIONS

**TECHNICAL REPORTS:** Scientific and technical information considered important, complete, and a lasting contribution to existing knowledge.

**TECHNICAL NOTES:** Information less broad in scope but nevertheless of importance as a contribution to existing knowledge.

**TECHNICAL MEMORANDUMS:** Information receiving limited distribution because of preliminary data, security classification, or other reasons.

**CONTRACTOR REPORTS:** Scientific and technical information generated under a NASA contract or grant and considered an important contribution to existing knowledge.

**TECHNICAL TRANSLATIONS:** Information published in a foreign language considered to merit NASA distribution in English.

**SPECIAL PUBLICATIONS:** Information derived from or of value to NASA activities. Publications include conference proceedings, monographs, data compilations, handbooks, sourcebooks, and special bibliographies.

**TECHNOLOGY UTILIZATION PUBLICATIONS:** Information on technology used by NASA that may be of particular interest in commercial and other non-aerospace applications. Publications include Tech Briefs, Technology Utilization Reports and Notes, and Technology Surveys.

*Details on the availability of these publications may be obtained from:*

SCIENTIFIC AND TECHNICAL INFORMATION DIVISION  
NATIONAL AERONAUTICS AND SPACE ADMINISTRATION  
Washington, D.C. 20546